UNIVERSITÀ DEGLI STUDI DI TRIESTE

XXX CICLO DEL DOTTORATO DI RICERCA IN
Scienze della Terra e Meccanica dei Fluidi

3D velocity depth model in the Gulf of Trieste by means of tomographic analysis from multichannel seismic reflection data

Settore scientifico-disciplinare: GEO/11 GEOFISICA APPLICATA

DOTTORANDA/ Ph.D. Student
Michela DAL CIN

COORDINATORE/ Ph.D. Program Coordinator
PROF. Pierpaolo OMARI

SUPERVISORE DI TESI/ Thesis Supervisor
PROF. Angelo CAMERLENGHI

CO-SUPERVISORI DI TESI/ Thesis Co-Supervisors
Dr. Martina BUSETTI
Dr. Gualtiero BÖHM
Dr. Stefano PICOTTI
Dr. Fabrizio ZGUR

ANNO ACCADEMICO 2016/2017

ABSTRACT

The Gulf of Trieste (GT) is a shallow epicontinental basin that is part of the northern Adriatic Sea (Central Mediterranean). It is settled at the proximal southern edge of an active plate boundary, where the convergence between the Adriatic block and the Eurasian plate gave rise to two Meso-Cenozoic Alpine-Himalayan orogens: the Dinarides (NW-SE trending) and the Eastern Alps (E-W oriented). The Gulf of Trieste is the foredeep of the northern External Dinarides and the eastern Alps. Its evolution started from a Mesozoic rifting that generated NE-SW normal faults allowing the aggradation of the Mesozoic-Paleogene Friuli-Dinaric Carbonate Platform. From the Upper Cretaceous to the Oligocene, the Dinaric compression generated NW-SE oriented thrust faults, whose most external elements are located in the GT. Since the Oligocene, the Alpine compression, related to the ongoing N-ward motion of the Adriatic plate, reactivated the tectonic structures with a transpressive kinematics. The GT represents the foot-wall of the Dinaric Karst Thrust, extending along the coast of the Karst Plateau and displacing the carbonates with an important vertical throw. The carbonates lying in the gulf are tilted E and N-wards, due to the weight of the neighbouring chains. They are covered by Eocene turbiditic Flysch, whose top is depicted by an unconformity related to the Messinian erosional phase, that in the eastern part of the gulf was active also during the Pliocene, as proved by the thin package of Quaternary marine and continental deposits covering the surface.

While the geological structure of the onshore areas bounding the gulf have been studied since the 19th Century, the geological characteristics of the offshore remained widely undiscovered until recent time. During the last decade, the National Institute of Oceanography and Experimental Geophysics - OGS, carried out three geophysical surveys in the Gulf of Trieste, collecting 630 km of Multichannel Seismic (MCS) reflection profiles. These data are acquired in the time domain and provide geological information about the investigated subsurface. A focused velocity analysis, encompassing tomographic inversion and depth seismic imaging, is crucial for the reconstruction of detailed and reliable geometries in the depth domain.

In the present work, two main reflectors are considered: the top surface of the flysch and that of the carbonates. Their reflected and refracted events are picked on the prestack seismic data and used as input for the traveltime tomographic inversion. The adopted software detects the three-dimensional seismic velocity field and surface geometries, through an iterative algorithm that minimizes the differences between the modelled and measured traveltimes. The code inverts in sequence the velocity field and updates the reflector structure, until the variations with respect to the previous step become sufficiently small. The obtained model is then improved using an iterative imaging technique involving pre-stack depth migration, residual move-out analysis and grid tomography. The comparison between the results of reflection tomography and refraction analysis allows to gain information on the flysch anisotropy, which can be related to its petrophysical parameters.

The results provide an adequate 3D elastic velocity model in depth of the flysch and carbonates units and of their top surfaces. The top of carbonate platform lies at a maximum depth of around 1.6 km below the seabed, at about 2 km offshore the city of Trieste. This result provides that the vertical displacement of the Karst Thrust is about 1600-1800 m.

The obtained information constitutes a valuable basis for the reliable construction of a 3D geological and structural depth model of the GT. This would, in turn, permit the correlation with the onshore setting and enhance the understanding of the neotectonic evolution of the area.

INDEX

1 INTRODUCTION

The Gulf of Trieste (northern Adriatic Sea) is enclosed by the coastline connecting the outlet of the Tagliamento River (Friuli Venezia Giulia, Italy) to Savudrija (Istria, Croatia). It represents the foredeep of the adjacent External Dinarides and Southern Alpine chains, NW-SE and E-W oriented respectively. Three main tectonic activities were responsible for its present geological setting. During the Mesozoic, a rifting stage affected the Triassic Dolomia Principale Carbonate Platform, generating NE-SW oriented normal faults. In this contest, the aggradation of the Mesozoic-Paleogene Friuli-Dinaric Carbonate Platform took place. From Late Cretaceous to Paleogene, the Outer Dinaric compressional tectonic phase produced a complex fold-thrust system, NW-SE oriented. Its related foredeep migrated progressively SW-wards, involving, in the final stage, the eastern part of the Gulf of Trieste. Here, the carbonate platform was flexured NE-wards and the turbiditic materials of the flysch filled the basin during Eocene. Moreover, the main western-most frontal ramp of the External Dinarides is expressed by the Karst Thrust, running along the Karst coastline. It extends towards NW as the Panzano Line, while it continues SE-wards, in the Slovenian onshore, as the Črni Kal Thrust. This tectonic structure dislocates the carbonates and the flysch with a very important vertical throw. The following Oligocene-Late Cenozoic compression generated the S-wards vergent Southern Alpine belt and caused the deepening of the carbonate platform towards north. Furthermore, this reactivated the Mesozoic-early Cenozoic structures of the gulf with a dextral transcurrent activity. A marine regression, during the Messinian Salinity Crisis, allowed sub-aerial erosion that depicted the upper part of the flysch in valleys and ridges. The successive early Pliocene reflooding involved the western part of the gulf, where it led to the deposition of marine sediments. A further Pliocene sea level drop produced an unconformity characterizing the entire gulf. This is now covered by Plio-Quaternary marine and continental sediments that become thinner from W to E. In these deposits, diffuse presence of fractures and fluids (migrating from the carbonates along main fault strands) indicate neotectonic activity due to the ongoing N-wards movement of the Adria plate.

This geological knowledge of the gulf is relatively recent respect to that of the neighboring onshore. While classical geological investigation begun onland almost two centuries ago, the offshore remained quite undiscovered until the 1950's, when developing geophysical investigation techniques started to be applied also in this offshore. But it is only during the last twelve years that a dense network of multichannel seismic reflection data (630 km) was collected in the gulf. The R/V OGS Explora, of the National Institute of Oceanography and Experimental Geophysics – OGS, conducted three surveys in 2005, 2009 and 2013. These profiles have high potential for the investigation of the deep geological structures buried under the seabed.

The aim of this work is to further analyse these data by means of advanced seismic tomography techniques, in order to achieve a reliable 3D velocity depth model of the main units and surfaces characterising the sedimentary sequence of the gulf. Methods such as tomographic inversion and depth seismic imaging represent a valuable tool for the detection of a detailed velocity field, which is in turn essential for a reliable reconstruction of geometries in the depth domain.

This thesis presents the procedure that utilises the aforementioned methods to gather new geological information from the investigated area. These results are used for a further representation of the relationship with the surrounding onshore. Insights from this type of analysis could further be useful for the detection of the geological structures involved in neotectonic activity. Moreover, they can also provide a contribute in the study of the seismotectonic behaviour of the Gulf of Trieste and its neighbouring region.

2 GEOGRAPHICAL AND GEOMORPHOLOGICAL SETTING

2.1 Geography and Geomorphological Characters of the Gulf of Trieste

2.1.1 Generalities

The study area of the present work is the Gulf of Trieste (GT), that is considered an epicontinental, semi-enclosed shallow marine basin (Biolchi, et al., 2015) located in the North Westernmost part of the Adriatic Sea (Central Mediterranean Sea). The gulf is bounded to the north, east and south by the coastline that connects the outlet of the Tagliamento River (on the eastern border of the Italian Friuli Venezia-Giulia Region) to Rtič Savudrija (Istria, Croatia), and on the west by the imaginary straight line (length of 34 km) that connects the two extreme points of the coastline (Fig. 1). The Italian part of the gulf coastline is approximately 125 km long; the Slovenian coastline is 48 km long, while the Croatian part facing the gulf is about 11 km long; the resulting total shoreline length of the gulf is about 184 km. [1] Therefore, the GT extends over a total area of around 939 km^2 (excluding the surface covered by the internal part of the Grado-Marano Lagoon). From an administrative point of view, this results in about 678 km^2 of the gulf water surface belonging to Italy (northern part), 169 km^2 belonging to Slovenia (south eastern part), 92 km^2 belonging to Croatia (south western part).
The main fresh waters supply into the gulf are given, from W to E in the Italian sector, by the Tagliamento River, the Isonzo River and the Timavo River; while the Rižana River and the Dragonja River inflow into the gulf from the Slovenian and Croatian sectors, respectively.

2.1.2 The Coasts Bordering the Gulf of Trieste

According to (Giorgetti, et al., 1968) (Brambati & Catani, 1988) (Furlani, et al., 2014) and (Biolchi, et al., 2015), in the GT have been identified seven types of coastal morphologies: plunging cliff, sloping coast, shore platform, scree, pocket beach, low-lying and built-up coast (Fig. 4). The average depth is around 20 m bsl, with a wide central-eastern 26 m deep depocenter and with the maximum depth of 38 m bsl near Cape Madona (Mosetti, 1966), (Giorgetti, et al., 1968), (Trobec, et al., 2017) (Trobec, et al., submitted). Along the shoreline of the gulf, several bays are present, such as those (from NW to SE and to SW) of Panzano, Muggia, Koper and Piran.

[1] All values referring to administrative areas and coastline lengths are calculated (considering the Valussi (1973)'s definition) by using, in ArcGis environment (datum: WGS84, projection: UTM33), the official shapefile provided by Friuli Venezia Giulia Regional Agency for Environmental Protection (Italy) and available at the IRDAT geo-database: http://irdat.regione.fvg.it).

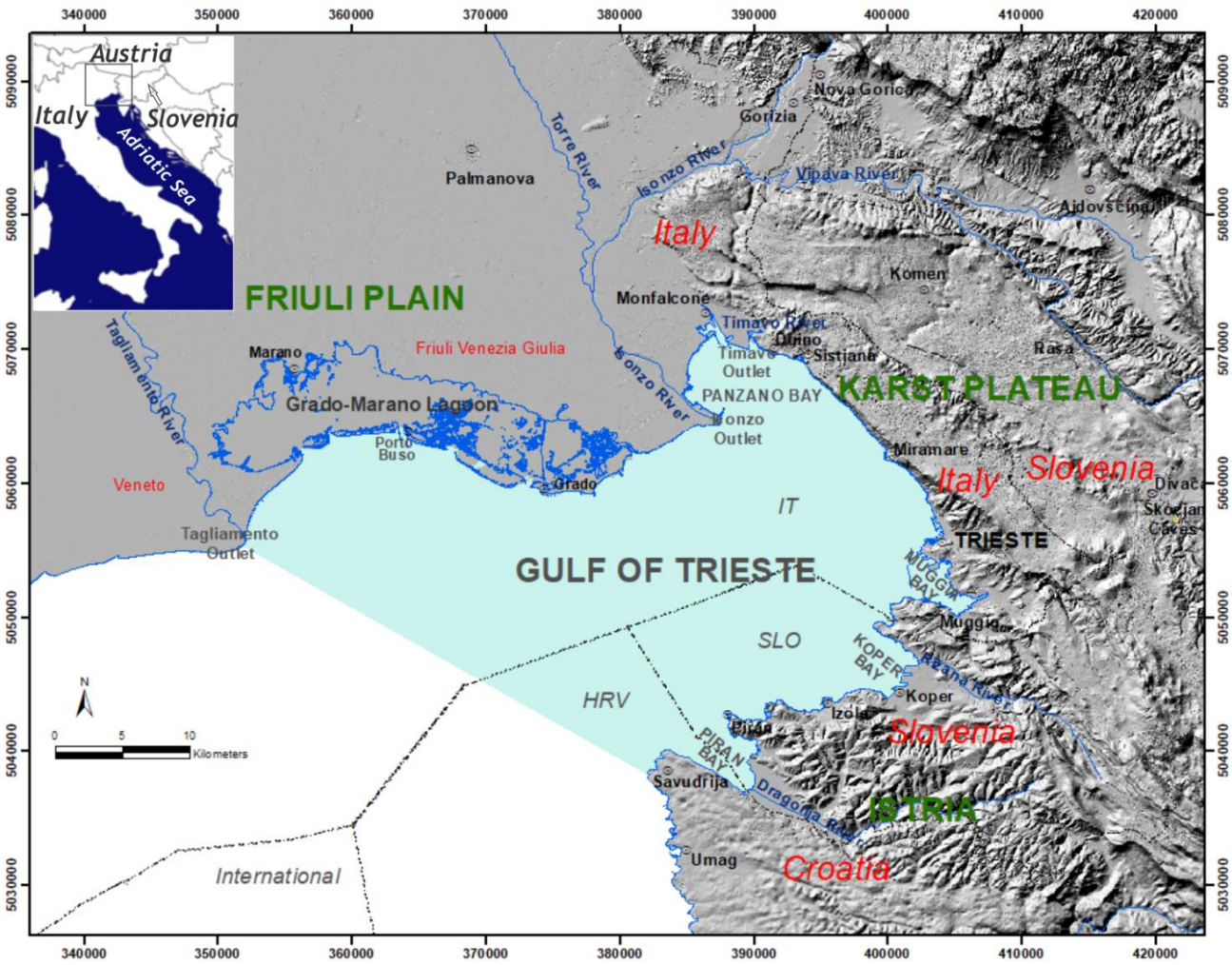

Fig. 1 – Map of the study area Gulf of Trieste (NE Adriatic Sea) and surrounding onshore. The azure area represents the extension of the gulf, enclosed by the coastline connecting the Tagliamento River Outlet and Savudrija. The waters of GT belong to three different Nations: Italy (northern part, from W to E), Slovenia (south-eastern part), Croatia (south-western part). State boundary is represented by black dashed line. Along the different types of shorelines of the gulf, from N to S, are present several bays, known as Panzano, Muggia, Koper and Piran. Map compiled by using ArcGis (ESRI, 2017) software, datum WGS84, projection UTM33. Digital Elevation Model from: (IRDAT-FVG, 2017) for the Italian area, 10 m cell resolution; (EU-DEM, 2017) for the Slovenian and Croatian areas, 20 m cell resolution.

2.1.2.1 The Northern Bound: the Friuli Plain and the Grado – Marano Lagoon

The northern seaboard of the Gulf of Trieste, extending between the Tagliamento (to the W) and the Timavo (to the E) outlets (Fig. 1) is characterized by low-laying and fine sandy to silty-clay shorelines of the Friuli Plain (Brambati & Catani, 1988) (Furlani, et al., 2014) (Biolchi, et al., 2015). The sedimentary terrigenous supply is provided by the Tagliamento and Isonzo Rivers, that built a progradational marine wedge made of pelitic and sandy recent alluvial deposits (Giorgetti, et al., 1968) (Gordini, et al., 2004) (Trobec, et al., submitted). This deltaic sedimentary body appears to be homogeneous within its shallower internal part and extends with a gentle dipping to a depth of about 12-13 m below sea-level (Giorgetti, et al., 1968)(Gordini, et al., 2003). The southeastern Friuli Plain coastline, facing the Panzano Bay between the Isonzo (to the W) and the Timavo (to the E) outlets, represents a low-laying coastal morphology, except from those parts, near the city of Monfalcone, that are built-up(Fig. 4), (Biolchi, et al., 2015).
The Grado and Marano Lagoon extends E-W between the Tagliamento and Isonzo outlets (Fig. 1, Fig. 2) and is the youngest among the lagoons of the Northern Adriatic. It is bounded sea-wards by barrier islands and sandy bars having a total length, from E to W, of about 20 km, and aligned along an arch shape. It covers an area of about 160 km^2 for a length of 32 km and a width of 5 km. From a geographical point of view is subdivided into the Lagoon of Grado (70 km^2) to the east and the Marano Lagoon (90 km^2) to the west and they are separated by the current administrative boundary between the Udine and Gorizia provinces that, within the lagoon, is represented by an imaginary N-S striking line passing through Porto Buso (Fig. 2). This division was settled during the period 1866-1917 and along the coeval boundary between Italy and Austria (Triches, et al., 2011a) (Triches, et al., 2011b).
The origin of the lagoon is related to the last post-glacial transgression and consequent gradual submergence, from W to E, of a deltaic shoreline separated from the sea by offshore bars and dunes, developed thanks to a complex interplay between fluvial sediments, marine currents and wave action (Brambati, 1970) (Giorgetti, et al., 1968) (Marocco, et al., 1984) (Marocco, 1989a) (Marocco, 1989b) (Marocco, 1991). The flooding involved first the area of the Marano Lagoon (4000 years B.P.), when the seal-level was about 6 m lower than the present, with a sedimentary rate ranging between 1.4 and 2.3 mm/year. In the post-roman period the Grado Lagoon begun its evolution due to the change of the Natisone river that had the outlet at the Morgo inlet, became a tributary of the Isonzo river, and then and the eastward disgression of the Isonzo River (Brambati, 1970). Its easternmost part, now artificially reclaimed, is even younger because of the last eastern-wards disgression of the Paleo-Isonzo River between 1000 and 500 years B.P. (Marocco, 1991) (Fig. 3). The young age ascribed to the system is testified by morphological highs made of alluvial deposits and by several archaeological remains (roman platforms, villas and vessels) discovered on the seabed (Auriemma & Maggi, 2012). There is no evidence of a further sea-level rise above the current internal lagoon shoreline (Marocco, et al., 1984).
Morphologically, the internal lagoon is characterised by four different areas: one is composed by the former alluvial plain above mentioned and consisting in sandy and fine graved sediments; another type of area comprises all the lagoon shapes and deposits such as elongated islands emerging few centimetres from the sea-level (*barene*) and covered by vegetation, lagoon channels, tidal flats (*velme*), delta inlets (*fose*) and marshes (*fondao*). A third zone is represented by intertidal and supratidal sandy shoals and eolian dunes. A fourth area is characterised by

anthropic shapes and deposits as embankments and hydraulic constructions (Triches, et al., 2011a)(Triches, et al., 2011b) (Marocco, 1989a) (Marocco, 1989b)(Marocco, 1991).

Fig. 2 – Satellite view of the present Grado and Marano Lagoon, along with the sector of low-lying coast (south-eastern Friuli Plain) facing the Panzano Bay between the Isonzo (to the W) and the Timavo (to the E) outlets. These coastal sectors bound the Gulf of Trieste to the north. The lagoon extends between the Tagliamento (to the W) and the Isonzo (to the E) outlets. Its origin was progressive as started 4000 years B.P., with the onset of the Marano Lagoon system, and successively in post-roman period with the development of the Grado Lagoon. The two parts of the Grado and Marano Lagoon were (and still are) geographically separated along an imaginary N-S striking line that, within the lagoon, passes through Porto Buso: this was the former State boundary between Italy and Austria until a Century ago, while now is the administrative border separating the Udine and Gorizia provinces (Friuli Venezia Giulia). Image taken from Google Earth Pro (Google, 2017) software.

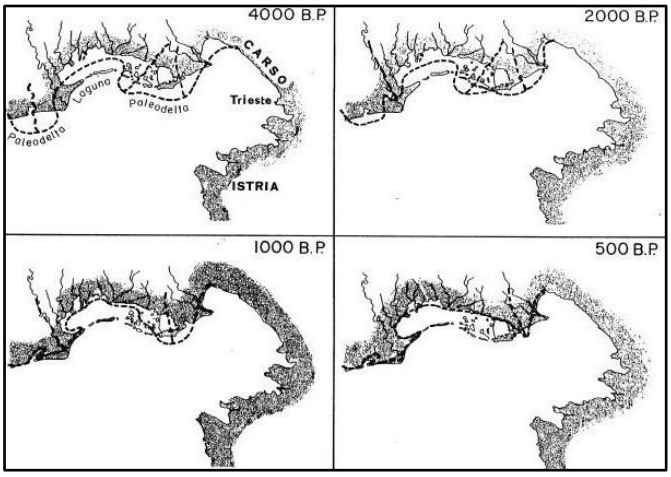

Fig. 3 - Paleogeographic reconstruction of the ancient coastlines in the Gulf of Trieste, between 4000 and 500 years B.P. Dashed lines represent the probable position of the Paleo-Tagliamento (on the W) and Paleo-Isonzo Rivers (on the E). Four scenarii are here shown: in the period from 4000 to 2000 years B.P. (top figure) marine transgression involved firstly the area of the Marano Lagoon and the E-ward migration of the Paleo-Tagliamento delta; between 1000 and 500 years B.P. (lower figure) the flooding progressively moved further E-wards allowing the evolution of the Grado Lagoon in a interplay with the excursions of the Paleo-Isonzo River (Marocco, 1991).

2.1.2.2 The North-Eastern Bound: the Rocky Shoreline of the Classical Karst Plateau

The north-eastern littoral of the Gulf of Trieste, from Duino to Trieste, is characterised by high and rocky coasts represented alternatively by the carbonates of the Meso-Cenozoic Friuli-Dinaric Carbonate Platform of the Classical Karst Plateau and the Eocene turbiditic marls and sandstones of the flysch. Moreover, several different coastal morphologies were identified (Fig. 4) (Giorgetti, et al., 1968) (Morelli & Mosetti, 1968) (Brambati & Catani, 1988) (Furlani, et al., 2009a) (Furlani, et al., 2011a) (Furlani, et al., 2011b) (Fulani, et al., 2011c) (Furlani, et al., 2014) (Biolchi, et al., 2015). In the Panzano Bay (Fig. 1, Fig. 2), a small deltaic wedge is related to the Timavo River. This river flows for few kilometres from its springs near Duino (San Giovanni) after a still unknown path through the Karst where it sinks in correspondence of the Skocjan Caves (San Canziano), after several kilometres of surface flow.
(Furlani, et al., 2014) classified these morphologies, that are typical of the entire Mediterranean sea, as follows:

- sloping coast (Fig. 5a): medium-low slope cliff (5°-45°), without presence of shore platform. This type can be found between the Timavo Outlet and Duino (Cernizza sector, Villaggio del Pescatore) and at Savudrija (north-western Istria);
- plunging cliff (Fig. 5c): vertical or sub-vertical cliff (>45°), plunging into the sea without shore platform at its toe. This type can be found, for example, between Sistiana and Duino;
- scree: high shoreline (Fig. 5e): constituted by weak rock and characterised by the presence of collapsed blocks from the behind cliff. This type can be found, for example, between Sistiana and Miramare;
- pocket beach (Fig. 5d): delimited by bays and inlets. This type can be found, for example, between Sistiana and Duino and along the Flysch shoreline of north-eastern Istria;
- shore platform (Fig. 7): horizontal or sub-horizontal terrace formed thanks to the moving back of the cliff due marine erosion of weak lithology. Type A: gradual and homogeneous slope; type B: changing slope. This type can be found, for example, in the Flysch outcropping along the north-eastern Istria of in the submerged outcrop near Sistiana;
- built-up: has been artificially strongly reshaped in recent times where excavations, embankments, drainages and other constructions were realised.

Moreover, a major part of this shoreline is marked by notches (Fig. 5b) whose depths below sea level increase from Miramare to NW: -0.6 m at Miramare; -1.1 at Marina di Aurisina, -1.6m at Sistiana; -2.8 m at Duino (Furlani, et al., 2009a) (Furlani, et al., 2011b).
Notches are coastal recessions, along marine cliffs, due to mechanical and chemical actions by marine, weathering and biological systems and to lithology level of strength ((Fulani, et al., 2011c) and references therein).
They are considered very important morphological markers, that can provide information on the relative sea level changes (i.e.: (Antonioli, et al., 2004) (Antonioli, et al., 2007a) (Fulani, et al., 2011c).
Hereafter are described the coastal areas of the NE-coast of the gulf, characterised by different lithologies and morphologies (Fig. 4), from NW to SE.

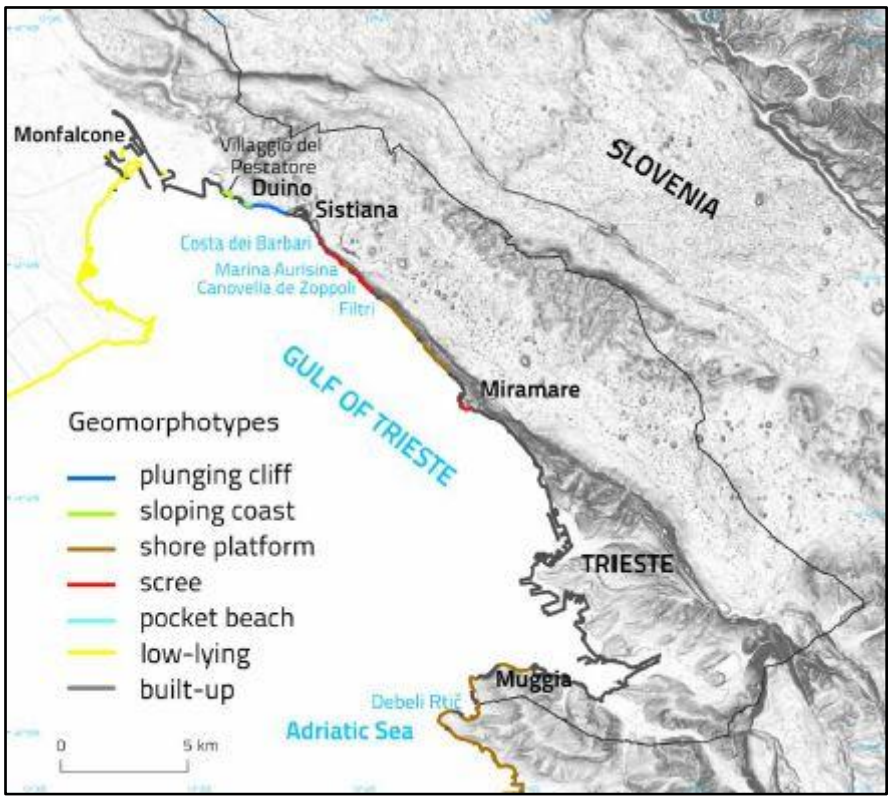

Fig. 4 – Map of the coastal morphologies identified along the eastern and partly northern and southern shoreline of the Gulf of Trieste. (Biolchi, et al., 2015).

2.1.2.2.1The Timavo Outlet – Duino

Along the coastal sector of Cernizza, between Villaggio del Pescatore (just south of the Timavo outlet) and Duino (Fig. 4), 17 fresh water springs are present (Cucchi & Forti, 1983). Sloping coasts (Fig. 5a) made of Cretaceous carbonates (highly fossiliferous Aurisina Limestone) dip about 35° seawards(Marocco, et al., 2008) (Biolchi, et al., 2015). The seabed is very shallow (few meters) and does not allow the recognition of any notch (Furlani, et al., 2009a).
Here, karst morphologies are described by (Furlani, et al., 2011b) as the result of solution from the interaction among fresh, brackish and salty waters. Within the low-tidal zone, the shapes are rounded due to the abrasion by fine sediments; in the inter and supra-tidal zones, the morphologies (i.d. runnels, karrens, cavities, basin-pools; Fig. 6a, b, c, d) have irregular and sharp edges due to action of marine aerosol and bacteria.

2.1.2.2.2The Duino-Sistiana Coast

Between Duino and Sistiana the 70 m high, about 2 km long and E-W trending shoreline plunges almost vertically (70°-110°) into the sea up to -7 m below sea-level (Giorgetti, et al., 1968) (Furlani, et al., 2009a)(Furlani, et al., 2011b) (Biolchi, et al., 2015). The plunging cliffs (Fig. 5a) are represented by Meso-Cenozoic Carbonates of the Friuli-Dinaric Platform (Aurisina Limestone, Liburnica Formation and Alveolinid-Nummulitid Limestone), whose vertical beds dip 85° towards S and strike parallel or sub-parallel to the shoreline. Furthermore, the cliffs are affected by several strike-slip faults with a dominant NW-SE and N-S direction (Cucchi, et al., 2008a) (Marocco, et al.,

2008) (Biolchi, et al., 2015). (Furlani, et al., 2011b) describes these strands as preferential features where karst morphologies like basin pools and grykes form (Fig. 6c, d), due to the action of biological elements and marine spray, where emerged, and to marine mechanical erosion, where submerged. Another element is present in the area: a pocket beach located in the eastern part of the shoreline (Fig. 5d). As concerns the notch carved along the cliff (Fig. 5b), the Authors report a depth below sea level of -1.0 m in the easternmost part, -1.6 m in correspondence of the pocket beach and -2.8 m in the westernmost part.

Along this shoreline the Flysch unit is present only at the submerged base of the carbonate cliff (Morelli & Mosetti, 1968) (Furlani, et al., 2009a). A body of Flysch outcrops, at a depths ranging between -1.5 and -5 m bsl, some tens of meters offshore. It has a width of 45 m and a length of 170 m and it shows mushrooms-like blocks and several eroded fractures. It is partially covered by carbonate blocks (metric size) collapsed from the vertical walls behind. Furthermore, analysis of nanoplankton associations in the silty-marls terms suggested a Lutetian (upper Eocene) age (Furlani, et al., 2009a). According to the Authors, it represents a relict shore platform drowned by the late-Holocene sea-level rise (see section 2.2).

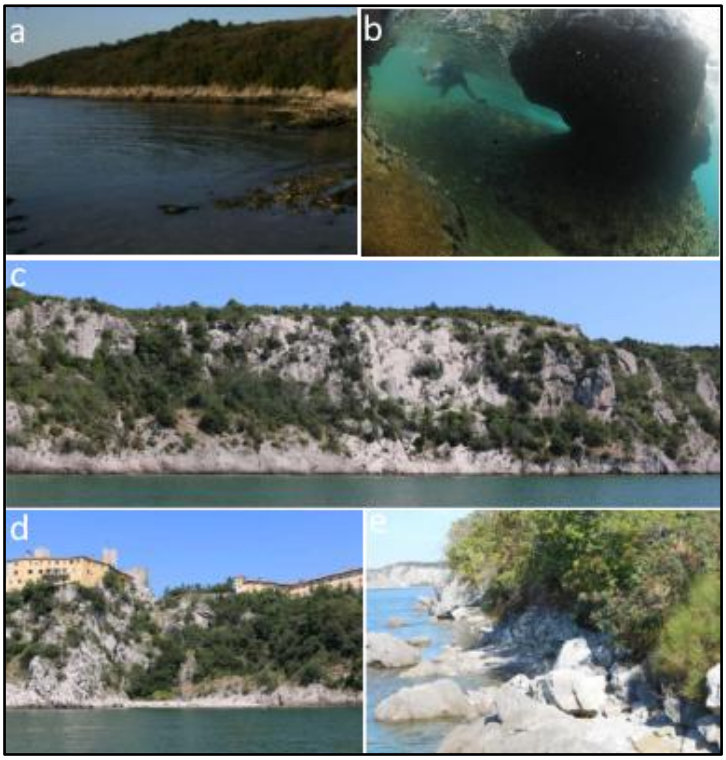

Fig. 5 – Coastal morphologies along the north-eastern cost of the Gulf of Trieste: a) sloping coast at the Cernizza sector between the Timavo Outlet and Duino; b) example of marine notch carved along the carbonates (e.g. Marina di Aurisina); c) vertical plunging cliffs at Duino – Sistiana coastal sector; d) pocket beach between Duino and Sistiana; e) scree at Costa dei Barbari. Figs. a), c), d), e), from (Biolchi, et al., 2015); fig. b) from (Fulani, et al., 2011c).

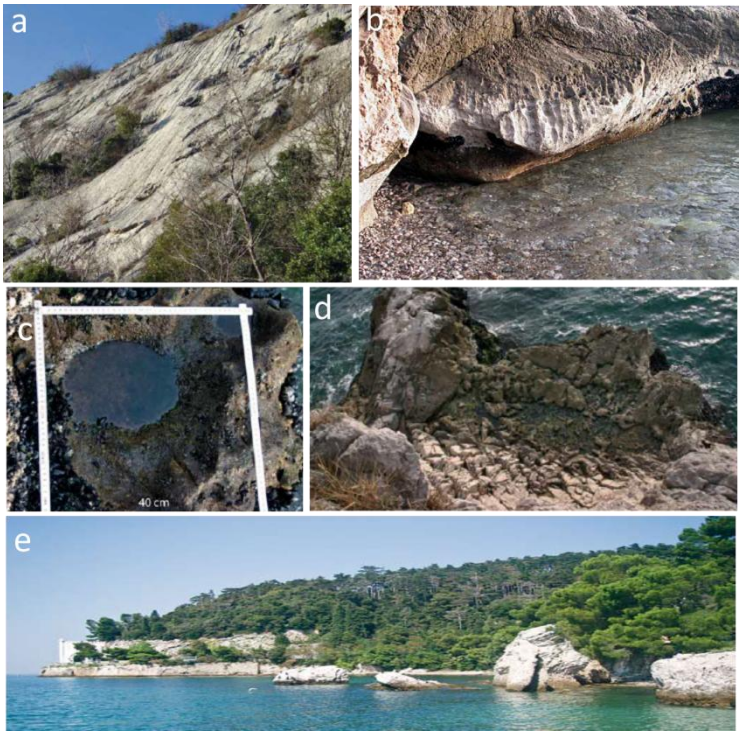

Fig. 6 – Examples of karst morphologies along carbonate shoreline of the north-eastern part of the Gulf of Trieste: a) Karren runnels on the sub-vertical plunging cliff at Duino; b) runnels and cavities on fallen block of the scree at Canovella (south of Sistiana); c) and d) basin-pools and small terrace in correspondence of tectonic joints and fractures at Duino; e) Lower Eocene carbonates olistoliths surrounded by Middle-Upper Flysch at the Miramare promontory. Figs. a), b), c), d) from (Furlani, et al., 2011b); fig. e) from (Odorico, 2010).

2.1.2.2.3The Sistiana – Miramare Coast

From Sistiana to the south, the Flysch formation outcrops with grater continuity, becoming the only lithology of the coast between Miramare and Portorož (near Piran, Istria, Slovenia). Until Miramare the dip of the cliff is very high, while the narrow beach at its toe is made of pebbles-gravel coastal deposits, that make a gentle sloping of the emerged shore, rapidly dipping under the water for 100-200 m seawards (Giorgetti, et al., 1968) (Brambati & Catani, 1988).
The coast connecting Sistiana and Miramare has a NW-SE direction and follows the dinaric Karst thrust. The altitude of carbonates - Flysch contact decreases from the south (300–400 m asl, above sea level) to the north (−1.5 m bsl) at Sistiana. Except from Grignano where the coast is built-up, this shoreline is characterised by the Flysch deposits and at the base developed small beaches of arenaceous and carbonate pebble-gravel. The major part of its length is protected by anthropic walls (Cucchi, et al., 2008a) (Furlani, et al., 2009a).
(Furlani, et al., 2011b) and (Biolchi, et al., 2015) describe this shoreline, where collapsed rocky block are very common. They are made of Meso-Cenozoic carbonates and Quaternary breccias. Sectors where this scree morphological coastal type (Fig. 5e) can be found are Costa dei Barbari, Marina di Aurisina, Canovella de Zoppoli and Filtri (see Fig. 4 for geographic reference of these locations). In particular, at Canovella de Zoppoli, the fallen carbonate blocks (Eocene Alveolinid-Nummulitid Limestone) are affected by incipient karst morphologies (Fig. 6b: small runnels and cavities), probably due to the short time of exposition to weathering and marine action. Well

rounded pebbles are instead present at the sea-level. The marine notch was recognised by (Furlani, et al., 2011b) at a depth of - 1.1 m bsl.
Moreover, at Marina di Aurisina and Filtri, the alternation of sandstone and marlstone has allowed the development of shore platforms, extending some tens of meters offshore (Biolchi, et al., 2015). At Marina di Aurisina, collapsed carbonate blocks (Cretaceous Aurisina limestone and Quaternary breccias) are affected diffuse and intense wave erosion giving rise to mushrooms morphologies. Both the lithologies of the collapsed blocks, present along the ancient coastline, show the marine notch at a depth of -1.2 m bsl (Furlani, et al., 2011b).
At the Miramare promontory, olistoliths (made of the Eocene Alveolinid-Nummulitid Limestone) are included in the sandstone-mudstone matrix of the Flysch of the shore platform (Fig. 6e). (Furlani, et al., 2011b) report that those blocks, facing small beaches, are eroded by marine and biological action. Other blocks are isolated from the sea, but sill are affected by biological dissolution that causes cavities with a diameter of 2 cm. The Authors identified the marine notch on the carbonate olistoliths at depths ranging from -0.6 m to -0.8 m respectively to the south and to the north of the Miramare castle.

2.1.2.2.4The Miramare-Muggia Coast

After Miramare, to the S towards Muggia (through the Trieste harbour, settled south of the city of Trieste in front of the Muggia Bay), the shoreline is now built-up and modified by anthropic structures such as excavations, embankments and drainages (Brambati & Catani, 1988) (Giorgetti, et al., 1968) (Furlani, et al., 2011b) (Biolchi, et al., 2015). These features masked the coast originally composed of Eocene Flysch and alluvial deposits and settled along cliffs and shore platforms (Brambati & Catani, 1988) (Furlani, 2003a) (GeoCGT-FVG, 2013).
The artificial constructions along this sector were realised continuously since the settlement, but in particular more intensively since 1719 when Trieste was declared Free Port. In general, the anthropic structures led to a re-shape of the original coast, now settled on hard-fill materials; the shoreline is now moved of tens, or somewhere even hundreds, meters seawards. For these reasons the sediments of the adjacent seabed have a smaller size respect to those characterising a natural shoreline (Brambati & Catani, 1988).

2.1.2.3 The Southern Bound: Rocky Shoreline of the North-Western Istria

The North-Western Istria coastline bounds the Gulf of Trieste to the south, from Muggia (Italy) to Savudrija for a length of around 69 km. Of these, about 10 km belong to Italy, 48 km belong to Slovenia and 11 km to Croatia. Among the above-listed coastal morphologies, shore platforms extend for a total length of 15 km, while the remaining part of the shoreline is build-up and characterized by the presence of coastal roads, sea walls, landfills and towns (Brambati & Catani, 1988) (Furlani, 2003a)(Furlani, 2003b). (Ambert, 1978) called the area as “Grey Istria”, due to the presence of the thick Eocene Flysch extensively outcropping onshore between Muggia and the Slovenia-Croatia Border, except for the Izola Peninsula that is characterised by a carbonate anticline (Pavšič & Peckmann, 1996) (Placer, et al., 2004) (Placer, et al., 2010). As concerns shore platforms, they are described as erosional surfaces within the actual intertidal zone; while continental shelves are surfaces extending underneath (Trenhaile, 2001). The platform become wide and flat thanks to erosion that seems to be the result of sub-aerial and biological weathering that alternatively protects and attacks intertidal rock, waves that, by removing sediments, exert abrasive action. Moreover, platform width is defined as the area connecting the cliff toe and the

low tidal level of the wave-base (Sunamura, 1992)(Trenhaile, 1987), (Furlani, 2003a), and references therein). (Sunamura, 1992) (Furlani, et al., 2011a) (Furlani, et al., 2009b) evaluated the regression of the Flysch in the order of 0.1 m/y.

2.1.2.3.1The Muggia – Dragonja River Coast

The Muggia-Piran shoreline, crossing the Italy-Slovenia Border, is overall NE-SW oriented. It faces, starting from NE, the Muggia Bay, the Koper Bay (Koprski Zaliv) and the Piran Bay (Piranski Zaliv-Zaljev) that are separated by promontories extending towards the Gulf of Trieste. The promontories are in turn shaped in cliff headlands (Punte) and small bays (Valloni) where pocket beaches developed.
According to (Furlani, 2003a)(Furlani, 2003b), the coastal morphology surrounding headlands is dominated by gently dipping and ramp platforms having 70-80 m and 25-30 m of width respectively. The different extension in width are related by the Authors to the different fetch lengths. These platforms developed on relatively weak Flysch lithology, that allowed the evolution of high cliffs and shore platforms at the base (Fig. 7). The cliff-platform junction is often overbuilt by the coastal road and other harbour structures that narrowed the shore platforms; whereas, in natural condition it can be covered by fallen deposits (cobbles-pebbles-sand) from the cliff, reworked by marine action. In this latter situation, a notch developed in the northern part of the coast. The Authors measured a 2 m high notch, elongated for 15 km and with its roof at 2.8 m a.s.l. Pocket beaches located in the small embayments (e.g. San Bartolomeo) are composed of terrigenous clasts of various shape and size.
Submerged and relict platform are also present and form a continuous morphological structure with the actual ones, reaching an extension up to 300 m.

Fig. 7 – Shore platform along the north-eastern part of the Istria shoreline, where flysch outcrops: the image shows the cliff-platform junction with terrigenous pebbles accumulated in the intertidal zone due to storm wave activity and terrigenous deposits fallen from the cliff at its toe (Furlani, 2003b).

2.1.2.3.2The Dragonja River – Savudrija Coast

The coast between the Dragonja River and Savudrija (the most south-western part on the GT) crosses the border between Slovenia and Croatia. It bounds the Piran Bay (Piranski Zaliv-Zaljev), that is separated by the promontories of Cape Madona (Madona Rtic) and Cape Savudrija (Savudrijski Rtic), to the NE and the NW of the bay respectively.
This coastal sector is characterised by outcropping Early Cretaceous carbonates affected by karst morphologies due to sea level variations and marine processes (Trenhaile, 1987). (Furlani, et al., 2011d) report that this mechanism is developped expecially in coastal areas conditioned by vertical tectonic movements. Moreover, the Authors describe the intertidal zone as gently sloping seawards and made of carbonates where grykes (enlarged solution fissures, sometimes coalescent and hosting waters), channels and small tide-pools occur. The interspaces, at the bottom, are filled by terrigenous deposits ("Terra Rossa").
As occurs for the platforms above described, several factors, like rock weakness, tidal range, marine and weathering processes act in a complex interplay on the genesis and evolution of a gryke (De Waele, et al., 2009)(De Waele & Furlani, 2012). In the case of the grykes present in this part of north-western Istria, they are closely related to the local tide (Fig. 8). Bioerosion is dominant in submerged conditions, while those located above sea level are affected by rainfall and freshwater action.
Shore grykes show elongated forms with origin that should be linked to local tectonics. Since they are closely related to the local tide, those located above sea level are affected by freshwater action, while bioerosion is dominant in submerged conditions. Structures located at higher altitudes are mainly generated by carbonatic dissolution processes, but then grykes can gradually undergo marine processes during tectonic subsidence (Furlani, et al., 2011d).

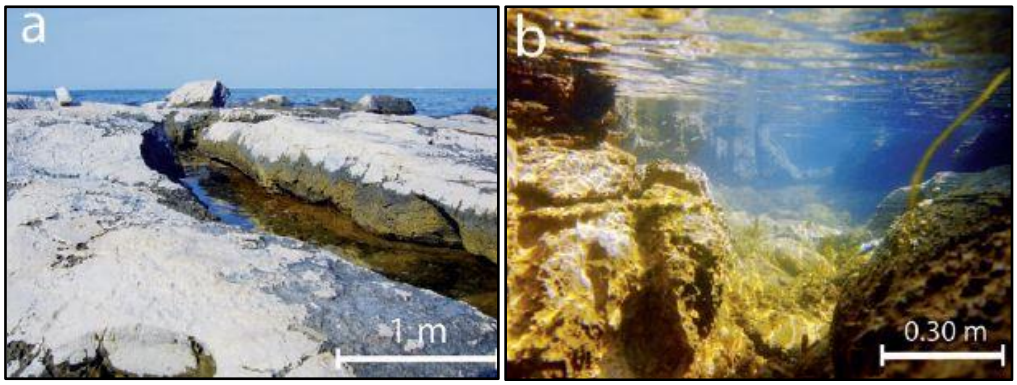

Fig. 8 – Karst morphologies along the north-western Istria coast: shore grykes at Savudrija during low (a) and high (b) tide. (Furlani, et al., 2011d).

2.1.3 Seabed Morphology and Sediments and of the Gulf of Trieste

The Gulf of Trieste is considered an epicontinental, semi-enclosed shallow marine basin, with average depth of 16 m bsl, reaching about 25 m bsl in the central part (Biolchi, et al., 2015) (Trobec, et al., submitted). A morpho-bathymetric depression if present few meters north respect to the coast of Piran (Slovenia), with a maximum depth value of 38 m bsl within the Cape Madona depression (Slavec, 2014) (Trobec, et al., 2017) (Trobec, et al., submitted).

2.1.3.1 The Seabed Morphology

The morphology and the sediments characterising the sea floor of the GT (Fig. 9, Fig. 10, Fig. 11, Fig. 12, Fig. 13) were studied by (Mosetti, 1966) (Giorgetti, et al., 1968) (Brambati & Catani, 1988) (Marocco, 1991) (Gordini, et al., 2003) (Gordini, et al., 2004) (Baradello, et al., 2013) (Slavec, 2014) (Trobec, et al., 2017) (Trobec, et al., submitted), that identified different bathymetric areas, on the basis of the morphologies. According to the above listed works, the morphology of the sea-floor near the shoreline reflects the contribute and distribution of terrigenous sediments provided by the inflowing rivers, especially in the Panzano, Muggia and Koper bays. Whereas, below the Duino-Miramare coast, at just 170 m far from it, the morphology deepens rapidly, reaching a 10 m depth. The northern part (Fig. 9, Fig. 12, Fig. 13a, b) has a surface, deepening from NW to SE, that is constituted by alluvial-deltaic fan (from the Timavo and Isonzo outlets to the Tagliamento delta), reaching a 10-12 m depth at 4 km from the shoreline (Giorgetti, et al., 1968) (Brambati & Catani, 1988) (Gordini, et al., 2003) (Trobec, et al., submitted). This sedimentary wedge represents the final part of the HST (Highstand System Tract) (Trincardi, et al., 2011a)(Trincardi, et al., 2011b). (Gordini, et al., 2003) (GeositiFVG, 2010a) (Trobec, et al., submitted) report the presence, in the north-western part of the gulf, of a series of morphological highs, as the Trezza Grande, Trezza Piccola and the Banco della Mula di Muggia (Fig. 9, Fig. 12, Fig. 13b). These represent the most prominent highs in the entire GT, drowned by the last Holocene marine transgression.
The Trezza Grande trapezoidal body is 6 m high with a surface of 154 sq. km, with and E-W offshore extension similar to that of the Grado and Marano Lagoon. The depths range between -12 and -18 m; the NW irregular side deepens steeply, while the SE one is irregular but less steep and reaches the Croatian and Slovenian sea-floor. The SW slope is characterised by submarine dunes, whereas the NE side is almost flat. It represents a drowned deltaic fan during the last late glacial stage (Gordini, et al., 2002) (Gordini, et al., 2004) (Trincardi, et al., 2011a) (Zecchin, et al., 2015) (Trincardi, et al., 2011b)(Trobec, et al., submitted). (Marocco, 1991) refers to this wedge as made of carbonate fine-medium sand, rich in fossiliferous clasts and re-worked by marine transgression.
(Zecchin, et al., 2015) suggest that the drowning of the Trezza Grande occurred during the latest stage of the post-glacial sea-level rise, when the shoreline shifted near the present day position.
The morphological high “Banco della Mula di Muggia” has a surface of 16 km^2 and is located offshore, south of Grado with a semi-submerged flat area continuously elaborated by wave action. Landwards, the wedge is constituted by clay-mud and sandy deposits, while seawards it connects with the Isonzo fan. To the NW, it extends up to the Grado shore, through submerged sand bars. Above the southern part of the body, some small sandy highs are present between 10 and 16 m bsl (Gordini, et al., 2003). The origin of this high is attributed to one of the deltas created by the paleo-Isonzo River during its E-wards migration, although this hypothesis is still debated

((GeositiFVG, 2010a) and references therein). Moreover, cartographic works, through the last 100 years, testify its evolution in shape and position: its continuous shift towards E suggests a marine transgression (GeositiFVG, 2010a).
The "Trezza Piccola" morphological high is located in the northern part of the gulf, SE of Grado and south of the "Banco della Mula di Muggia". It has a surface of 3.8 km^2 and a depth of 9 to 12 m bsl. It is E-W elongated and rises 1.5 m from the seabed; in the eastern part reaches a depth of 12 m bsl with a submerged sandy bar. The "Trezza Piccola", bounds to the south, the steepening seafloor of the central gulf, around the territorial water boundary (Brambati & Catani, 1988) (Gordini, et al., 2004)(GeositiFVG, 2010a).
(Gordini, et al., 2004) and (Trincardi, et al., 2011b) suggest the sea-bed morphology in the gulf is the result of Late Pleistocene – Holocene processes linked to the interplay between a gradual post-glacial marine transgression and the aggradation of the alluvial coast fed by the Tagliamento and Isonzo paleo-rivers (two of the major rivers in NE Italy, (Marocco, 1991)).
In the northern and central area of the gulf, (Gordini, et al., 2004) identified also 250 rocky outcrops, now known as grebani or trezze (GeositiFVG, 2010b), lye in the sea-floor of the gulf and they are distributed along a NE-SW direction, about 8-9 km far from the external bars of the Grado-Marano Lagoon at depth ranges of 6-24 m bsl. Their density reaches a maximum of about three outcrops per squared kilometres. The Authors recognised planar-tabular morphologies covered by cap reefs. The sandy sediments lying at the base of the trezze are cemented and correspond to the most recent and coarse part of the terrigenous influxes by the neighbouring rivers and by coastal erosion during the HST. Along these outcrops, sub-bottom profiles/Chirp show diffused presence of fluid pockets ((Gordini, et al., 2004)(Gordini, et al., 2010)). Analysis of the chemical composition on seepages revealed that the 81-84% biogenic methane; 15-18% nitrogen and 0.7-1.3% oxygen. These fluids allow, through chemosynthetic bacteria, the solidification of the ground sand leading to the evolution of the trezze in the colonization by calcareous algas, briozoas and serpulidi (Gordini, et al., 2010).
Moreover, (Brambati & Catani, 1988) describe the structure of the central-eastern part as irregular, characterised by thin recent pelagic sediments, limited by marine current action, that allows the outcrop of a relict shore beaches now lying at 25 m bsl. In this area, elongated shapes with steep walls and valleys are inherited morphologies of a hydrological network related to the former sea-level downdrop.
According to (Giorgetti, et al., 1968) (Brambati & Catani, 1988) (Baradello, et al., 2013) (Slavec, 2014) (Trobec, et al., 2017) (Trobec, et al., submitted), the south-eastern part of the gulf's seabed is smoother and deeper than the northern and western one, reaching mean depths of 20-26 m bsl.
In Italian waters, within the Muggia Bay, the seabed morphology (Fig. 10) was reconstructed on the basis of interpretation of a dense network of single-channel seismic reflection profiles/Boomer (Baradello, et al., 2013). The Bay is filled by alternation of marine and continental sediments related to the Late Pleistocene-Holocene glacial-interglacial cycles above the flysch bedrock. The Late-Pleistocene fluvial sediments, recognised in the seismic data, show channel-levee systems oriented along the present-day main axis of the bay. The Holocene (9000 year B.P.) marine transgression led to the deposition of sediments draping the bay, with horizontal stratification. Along the southern part of the bay, a progradational wedge is present with a thickness of 15-20 m and built by the sediments brought by the drainage system of the Muggia peninsula. The northern edge of this body is cut by a side of an anthropic slope realised for a fairway. Furthermore, from the map of Fig. 10 it can be recognised the different sloping gradient between the NE and the SW

sides of the Muggia Bay: the SW one is steeper that the NE one and this is also reflected by the overall onshore morphologies of the Muggia and the Harbour areas, respectively.
Along the Slovenian shoreline, the seabed plunges deeply at 22 m bsl and it decreases with a small degree reaching in the central offshore, at the border with Italian and Slovenian waters, depths of 24-26 m bsl (Fig. 11) (Trobec, et al., 2017) (Trobec, et al., submitted). In Slovenian waters, (Trobec, et al., 2017) highlighted a bathymetry that gently mimics the underlying continental alluvial plain paleo-topography. The Authors identified on the seafloor two trough-like geomorphic features, approximately normal to each other, that were ascribed to two paleo-river thalwegs (Fig. 11 and insets). One is named Paleorižana, located at about 7 km WNW from the present-day Rižana outlet in the Bay of Koper, and extending, for about 10 km, NW-ward towards the Italian waters. The shape of this feauture is slightly sinuous and depressed and it is less than a kilometre wide, lying within sediments at 23-26 m depth bsl. The second is named by the Authors as Paleoreka (referring to a generic river); it has a slightly elevated and sinuous trend, with a central channel-like depression. It is NE-SW oriented and it extends for about 23 km. Moreover, some dune shaped bodies, 22-23 m bls deep, covering an area of few kilometres in the central-western area of the gulf (Slavec, 2014) (Trobec, et al., submitted).
All the major morphological features and trends, that characterise the seabed of the Italian and Slovenian part of the GT, are highlighted in the bathymetric map of Fig. 12 provided by (Trobec, et al., submitted). The surface was modelled by integrating results from analysis of several different investigation methods (multibeam, singlebeam, high resolution single-channel seismic, borehole and core data), with a grid of 50 m x 50 m cells.

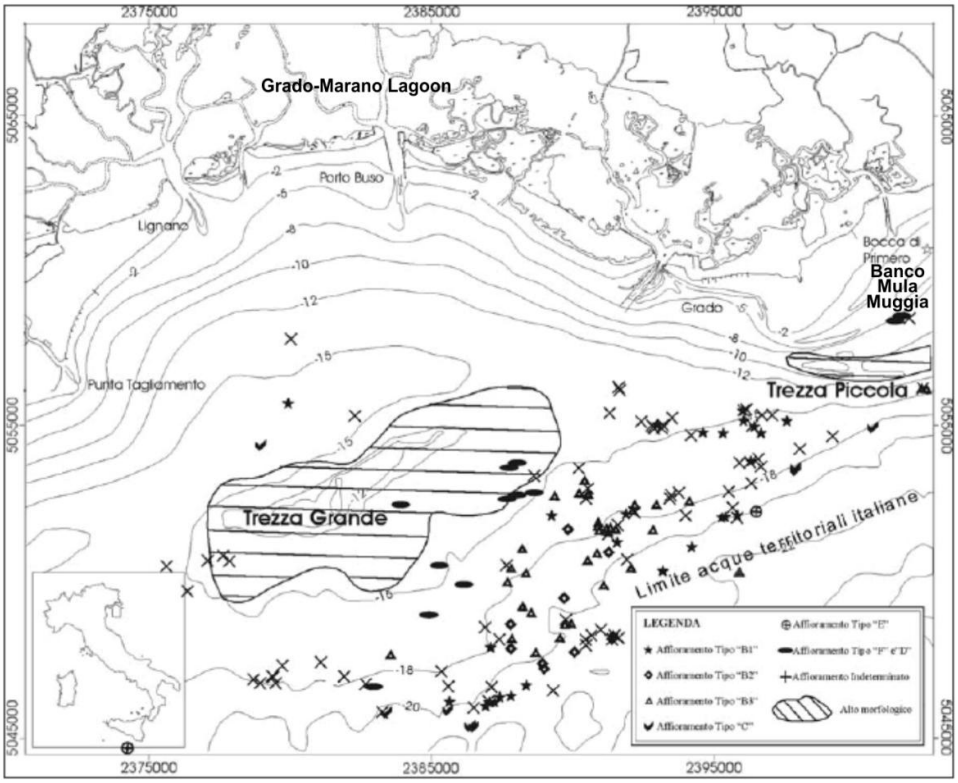

Fig. 9 – Bathymetry (contours in meters) of the Italian north-central part of the Gulf of Trieste where three prominent morphological highs, resulting from Holocene gradual post-glacial marine transgression and Tagliamento and Isonzo paleo-fan aggradation, are indicated: Trezza Grande, Trezza Piccola and Banco della Mula di Muggia. The map shows also the location of the rocky outcrops (grebani or trezze where fluid (80% methane) seepages are present and particular marine biological communities developed. (Gordini, et al., 2004).

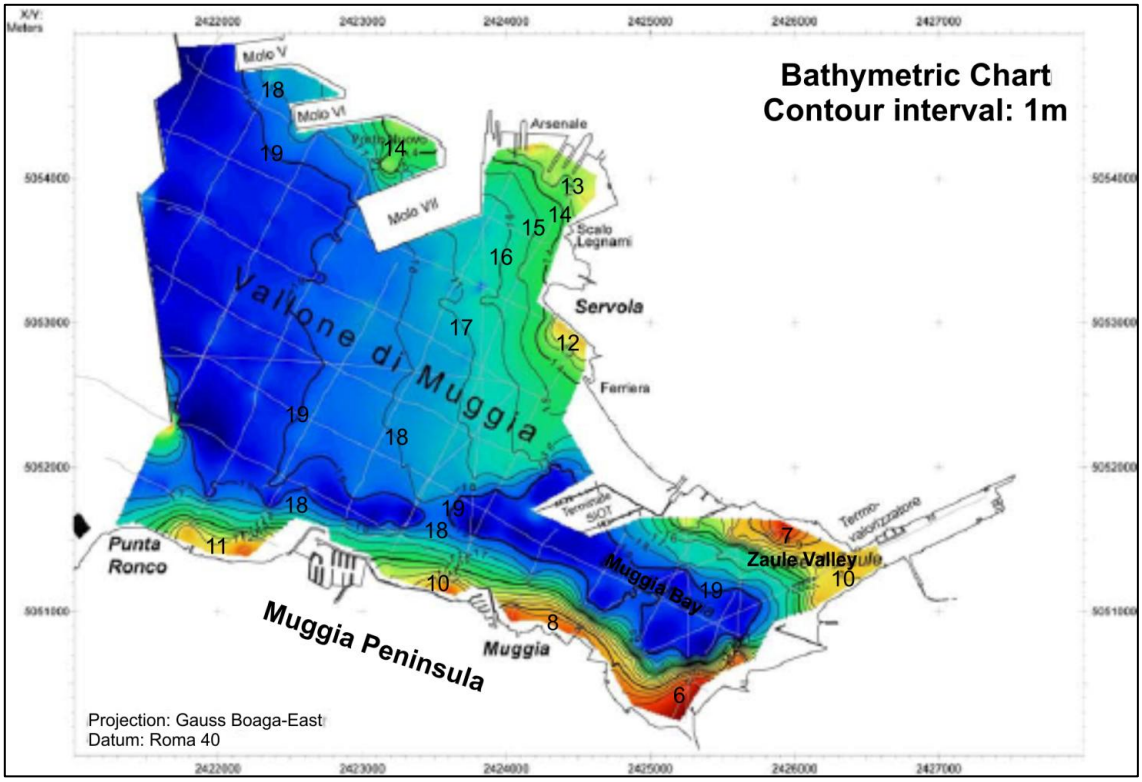

Fig. 10 - Bathymetric map of the Muggia Bay from single-channel seismic data acquired by OGS in 2013 (for location map and details of the seismic survey, refer to Fig.3 and section "Vallone di Muggia (Sito di Interesse Nazionale - SIN) 2013" of the Chapter 2). Contours every 1 m. (Baradello, et al., 2013)

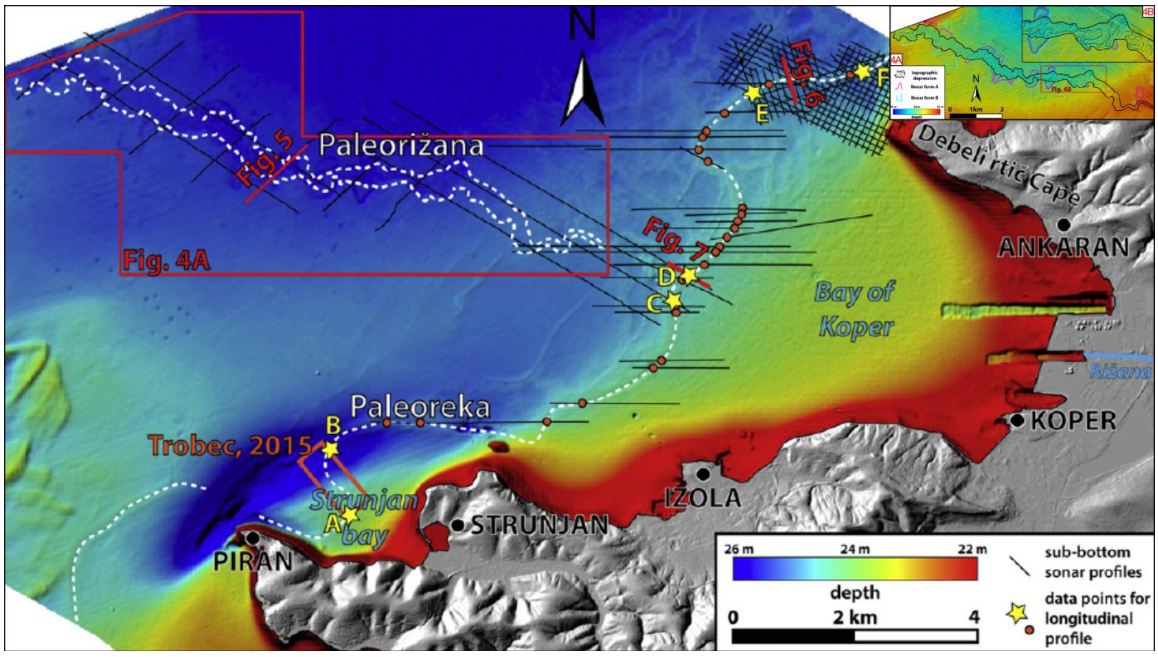

Fig. 11 – Morpho-bathymetric map of the Slovenian waters of the southern Gulf of Trieste. The seabed, surveyed by means multibeam (acquired by Harpha Sea Company, on board of the vessel Lyra), shows major depths ranging between 22 m (right adjacent to the shoreline) and 26 m bsl. In the map are highlighted the features related to the thalwegs of Paleorižana and Paleoreka and the Cape Madona Depression (this latter representing the maximum depth within the gulf with 38 m ((Slavec, 2014) (Trobec, et al., 2017)). Insets on the top-right part focus on details of the bathymetric features related to the Paleorižana. (Trobec, et al., 2017).

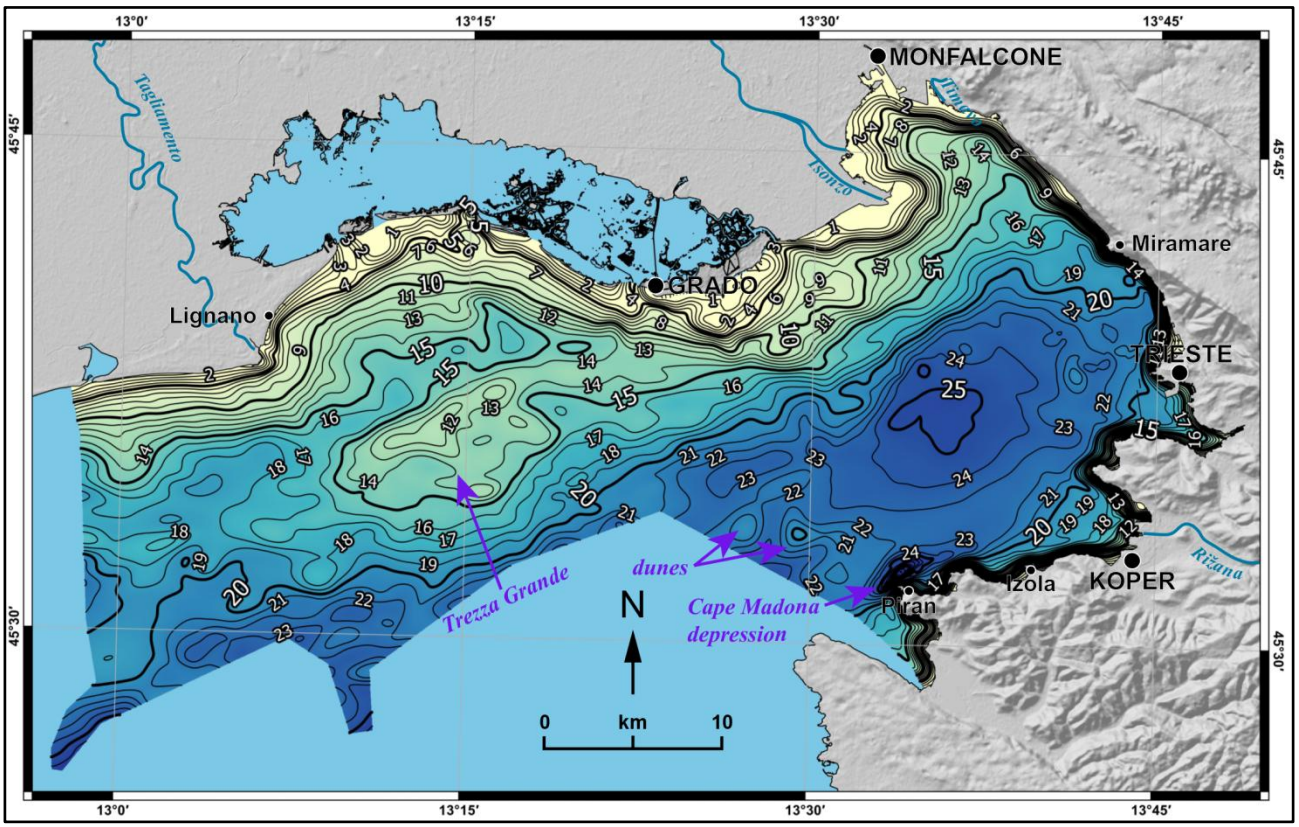

Fig. 12 – Bathymetric map (contour interval: 1m) of the Italian and Slovenian part of the Gulf of Trieste, modelled within a resolution grid of 50 m x 50 m, by means of the integration of geophysical and sedimentological data. The chart shows the main morphological trends, along with the main highs (such as "Trezza Grande" paleo-delta) and depressions (e.g. the wide central-eastern 26 m deep depocenter and "Cape Madona" deepest area of 38 m bsl) of the seabed. (Trobec, et al., submitted).

2.1.3.2 The Sediment of the Seafloor

The pattern of the sediment distribution, along with major chemical components and granulometric characteristics, were identified in the gulf by (Giorgetti, et al., 1968) and (Brambati & Catani, 1988) and in the Grado and Marano Lagoon by. (Marocco, 1989b) on the basis of truth samples. According to (Brambati & Catani, 1988), the main sedimentary processes are the transport and deposition of terrigenous sediments by the main rivers inflowing into the gulf, which provision is continuous and variable depending on the season, and the erosion and deposition locally due to the marine waves and currents (2-10 cm/s), both characterised by moderate action. Furthermore, also precipitation and sedimentation by marine bio-organisms influences the seabed granulometric and sedimentary distribution.
In general, the granulometric distribution in the gulf has a trend in grain size decreasing from the coast to the offshore (Fig. 13b, c). Seawards, main fine sediments are silt, clay and sand; whereas, coarser deposits (pebbles, cobbles, gravel) are distributed mostly along the coast, especially near the cliffs and the river's mouths. The area more affected by fluvial sedimentation is the northern one, where the Tagliamento and Isonzo rivers inflow into the gulf. Especially during floods, turbiditic flows from the Isonzo can also reach the height of Miramare. The Timavo River brings to the sea only fine sediments, since its journey is mostly underground through the base of the karst caves and are then released in the Panzano bay. Coarse deposits are present especially along the high and rocky shoreline (north-eastern and southern parts) of the gulf.
(Brambati & Catani, 1988) summarised the morpho - sedimentological areas of the gulf as follows:

- the fan delta belt of the major rivers flowing into the gulf in the northern part characterised by gravel to silty deposits;
- a part characterised by coarse grain size formed from the erosion of the cliffs especially along the north-eastern (in a sandy-silty matrix) and the southern (in a silty-clay matrix) parts of the gulf;
- a part characterised by human activity, where loose and fine sediments can be found just near the shore, despite that is generally expected in a seabed adjacent to a natural shoreline.

(Giorgetti, et al., 1968) conducted chemical analyses to several samples of sediments collected over the entire gulf. Their results show, for example, that the content of calcium (Fig. 13d) is more dominant within the sediments of the northern part, while the minor contents e distributed in the southern area. This likely reflects the provenance of the deposits: the former from Carbonates, the latter from the Flysch formation.

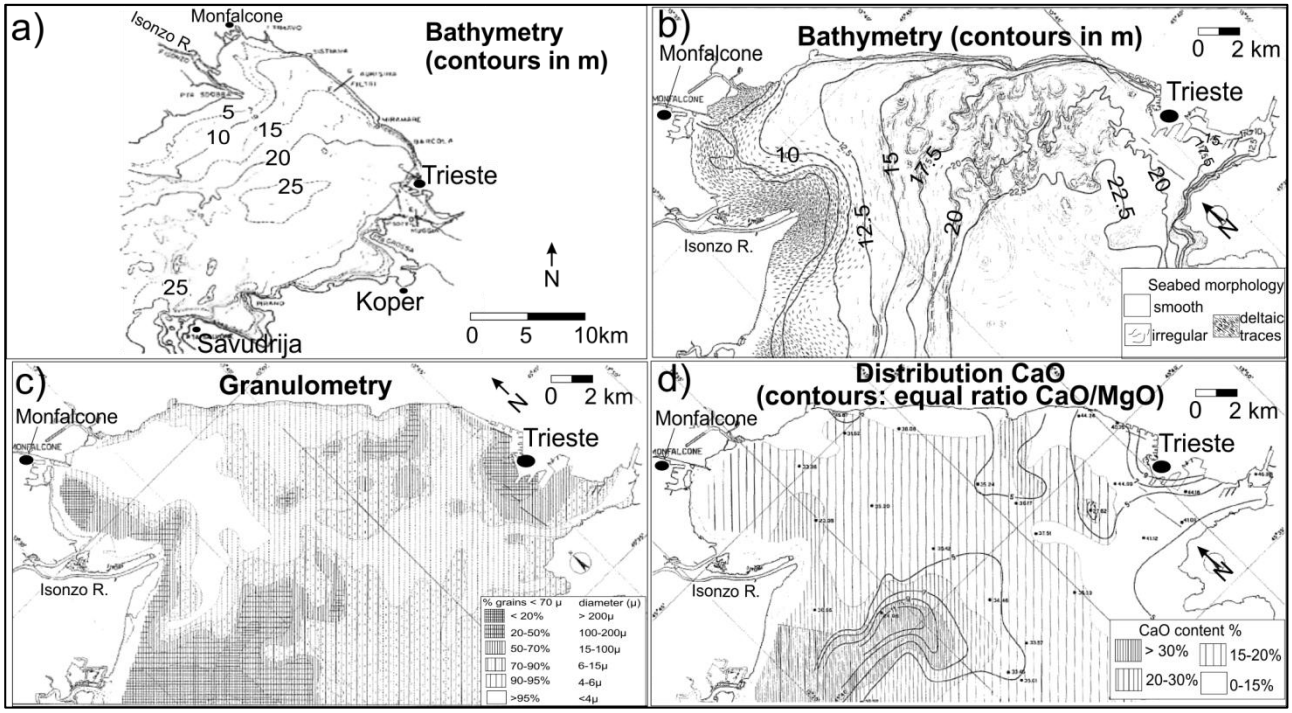

Fig. 13 –Bathymetry and sediment distribution on the seafloor of the Gulf of Trieste. a) Bathymetric map (contours every 5 m), adapted from (Brambati & Catani, 1988); maps, in the eastern part Gulf of Trieste, of: b) bathymetry with indication of some morphological features (contours every 2.5 m), c) granulometric distribution of the sediments on the seabed (different graphical patterns correspond to % of grains having size < 70 micrometers), d) CaO % distribution within the sediments of the seabed, represented by different graphical patterns; while contours refer to equal CaO/MgO ratio. Figs. b) c) d) are adapted from (Giorgetti, et al., 1968).

2.2 Sea Level Change

2.2.1 Definition

Sea level (SL) is the height of the sea surface and it is measured either with respect to the surface of the solid Earth (relative sea level, RSL), or with respect to geocentric reference such as the reference ellipsoid (geocentric sea level). RSL is the more relevant quantity when considering the coastal impacts of sea level change. The Mean Sea Level (MSL) is known as temporal average for a given location, and it is applied to remove shorter period variability. Moreover, it is common to spatially average MSL to define global mean sea level (GMSL). Local RSL change can differ significantly from GMSL because of spatial variability in changes of the sea surface and seafloor height (Church, et al., 2013). The Austrian geologist Eduard Suess, in 1988, used for the first time the term “eustatic”, to refer to global sea level changes and their causes, that are independent from local factors (Suess, 1906). In turn, “eustasy” indicates the global variations of the sea surface with respect to a fixed datum that for instance can be geocentric (Fig. 14 and Fig. 15) or, at present, the fixed orbit of a satellite moving around the Earth.
(Bindoff, et al., 2007) (Church, et al., 2013) summarised the several factors that affect sea level at different scales of time and space, through oscillations with various frequencies and amplitudes.
At global scale, the GMSL fluctuations, for decades or longer time intervals, depend on the following eustatic factors:

- temperature and salinity, influencing the density of the water column (thermal expansion, climate change), Fig. 14;
- exchange of water between oceans and other reservoirs like glaciers, ice caps, ice sheets, land water and atmosphere (climate change) Fig. 14;
- variation in shape and dimension of the ocean basins (geodynamics);
- Earth’s orbit eccentricity relative to the Sun, Earth’s rotation axis oscillations and Earth’s precessions (astronomic factors).

At regional scale, local sea level change, active for short and long time scale periods, can be caused by:

- oceanographic properties, such as changes in ocean circulation, atmospheric pressure, tides, and waves, Fig. 14;
- vertical land movements such as isostatic adjustment, tectonics, subsidence and sedimentation, Fig. 15.

Moreover, there is relative recent contribution in sea level fluctuation, at both large and small time and space scales, from antrophic activities (such as depletion of groundwater for agriculture and other uses, wetland drainage and deforestation, pollution that impact on climate, and others).
Although these local factors do not affect ocean water volume, they have an impact on the GMSL.
The measure of local RSL, and in turns MSL, is obtained by means of tide gauges, since the past few centuries. Anyhow, tide gauges provide information with respect to the land on which they lie. Starting from two decades ago, geocentric sea level is being measured using satellite altimetry (e.g. the Topex/Poseidon and Jason1 satellites (NASA, 2017)). These latter type of data provide independent observation from which it is possible to determine differential coastal and land

movements. GPS measurements were used to validate the method of geocentric evaluating crustal movements. As concerns historical, pre-historical and geological time spans, proxy records from archeology, paleontology, geomorphology and stratigraphy are fundamental for the estimation of the past RSL variations (Douglas, 2001) (Bindoff, et al., 2007)(Antonioli, et al., 2007b) (Antonioli & Silenzi, 2007c) (Antonioli, et al., 2009) (Braitenberg, et al., 2011) (Church, et al., 2013). The effects of sea-level changes are the marine transgressions and regressions. These are directly reflected on the sedimentary dynamics and in turns on the related stratigraphic depositional sequences.

To summarise, the MGSL and MSL variations result from the combined action of sedimentation, tectonics, subsidence, geodynamics, isostasy, astronomic motion of the Earth, ice-sea-land waters exchanges, thermal expansion (Fig. 14 and Fig. 15).

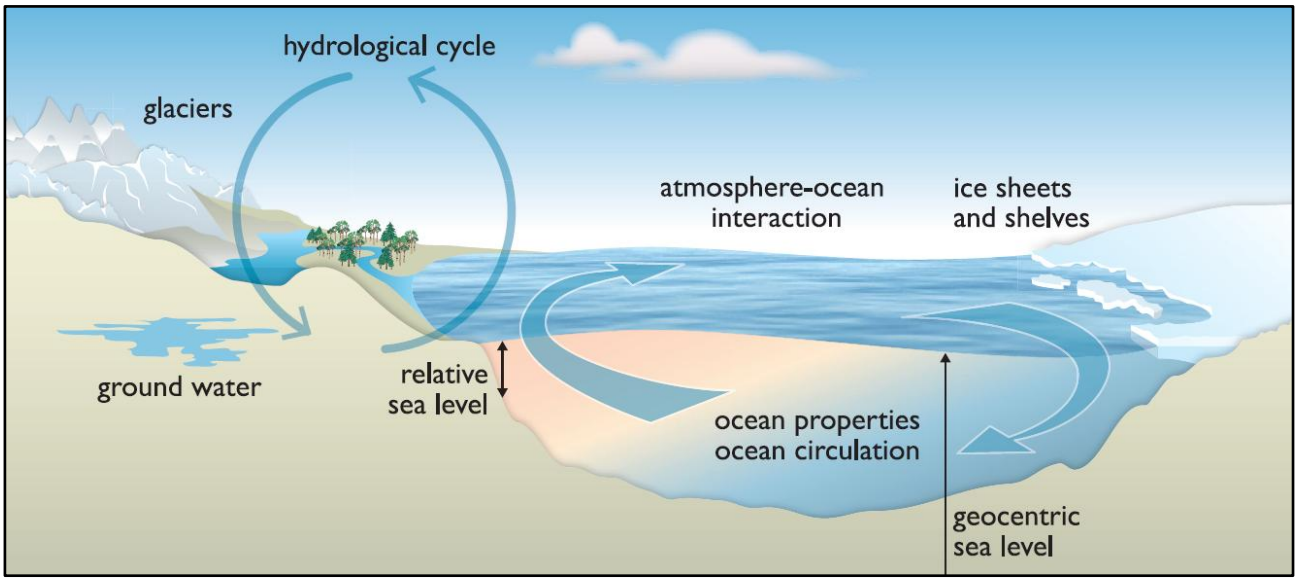

Fig. 14 – Sketch representing the processes, related to climate chances, contributing in global and regional sea-level changes. The term "ocean properties" refers to ocean temperature, salinity and density, which influence and are dependent on ocean circulation. Both relative and geocentric sea level vary with position. The geocenter should be located out of the space represented by the image. Note that other factors influencing global and local sea level changes, such as tectonics, geodynamics, isostasy, subsidence, Earth's astronomic motion, and sedimentation are not displayed in the picture. (Church, et al., 2013).

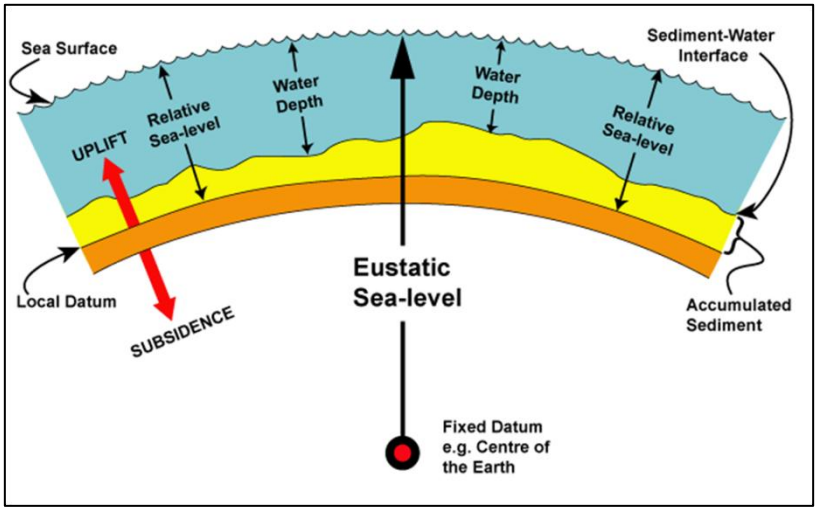

Fig. 15 – Sketch representing sea level height with respect to the geocentric global datum and a local datum. Processes as sedimentation, tectonics and subsidence are represented, as factors that influence relative sea level change. (SEPM, 2017).

2.2.2 Instrumental Present, Future and Past Global Sea Level Change

As said, present day sea level can be measured from orbiting satellites, while tidal gauges, located along coasts, detect local variability (e.g. (Douglas, 2001) (Bindoff, et al., 2007) (Church, et al., 2013)). The geocentric crustal movement rates, then, can be estimated by the differential rate between a tide gauge and the sea surface height observed by satellite altimeter ((Braitenberg, et al., 2011) and references therein). Anyhow, the components contributing in the sea level variations are several; this brings difficulties into the quantitative forecast of the actual and future trends. Despite this, the instrumental records of sea level change (Fig. 16) shows evidence of a global sea level rise since the 19th century with rate of about 1.7 mm yr–1. More accurate satellite measurements, tied for the last two decades, reveal an higher average global rising: 3 mm yr–1, mainly due to glacier melting and sea thermal expansion. This is not uniform around the world: in some regions, rates are up to several times the global mean rise, while in other regions sea level is falling (Fig. 17). These differences are related to non-uniform changes in temperature and salinity and ocean circulation. Projections for global sea level variation during the 21st century, indicate a sea level rising at even higher rate than the actual (Fig. 17). The IPCC (Intergovernmental Panel on Climate Change) Special Report on Emission Scenarios (SRES) aware that by mid-2090s, global sea level will be rising, on average, at about 4 mm/y.

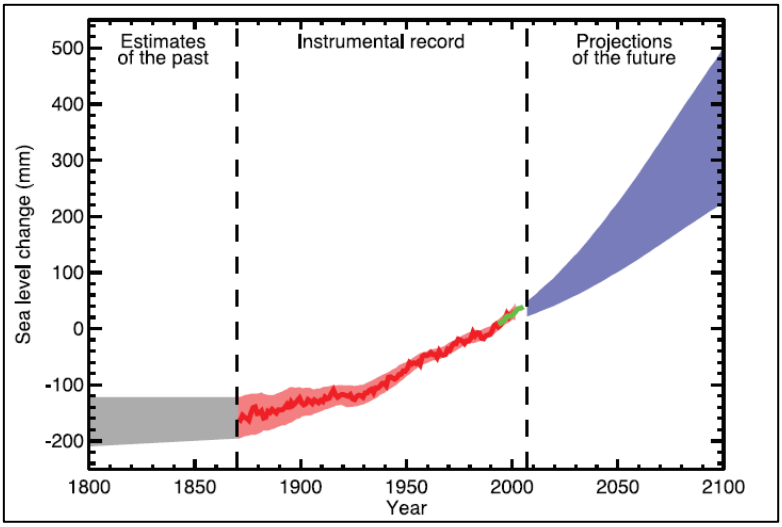

Fig. 16 - Evolution of global mean sea level (deviation from the 1980-1999 mean) in the past two centuries (gray and red shadings and red and green lines) and as projected for the future within the end of the 21 century (blue shading SRES scenario). The grey shading shows the uncertainty in the estimated long-term and past rate variations. The red line is a reconstruction of global mean sea level from tide gauges, with red shading indicating variations from a smooth curve. The green line shows global mean sea level observed from satellite altimetry. The blue shading represents the range of model projections for the SRES scenario for the rest of 21st century. Over many centuries or millennia, sea level could rise by several metres. (Church, et al., 2013).

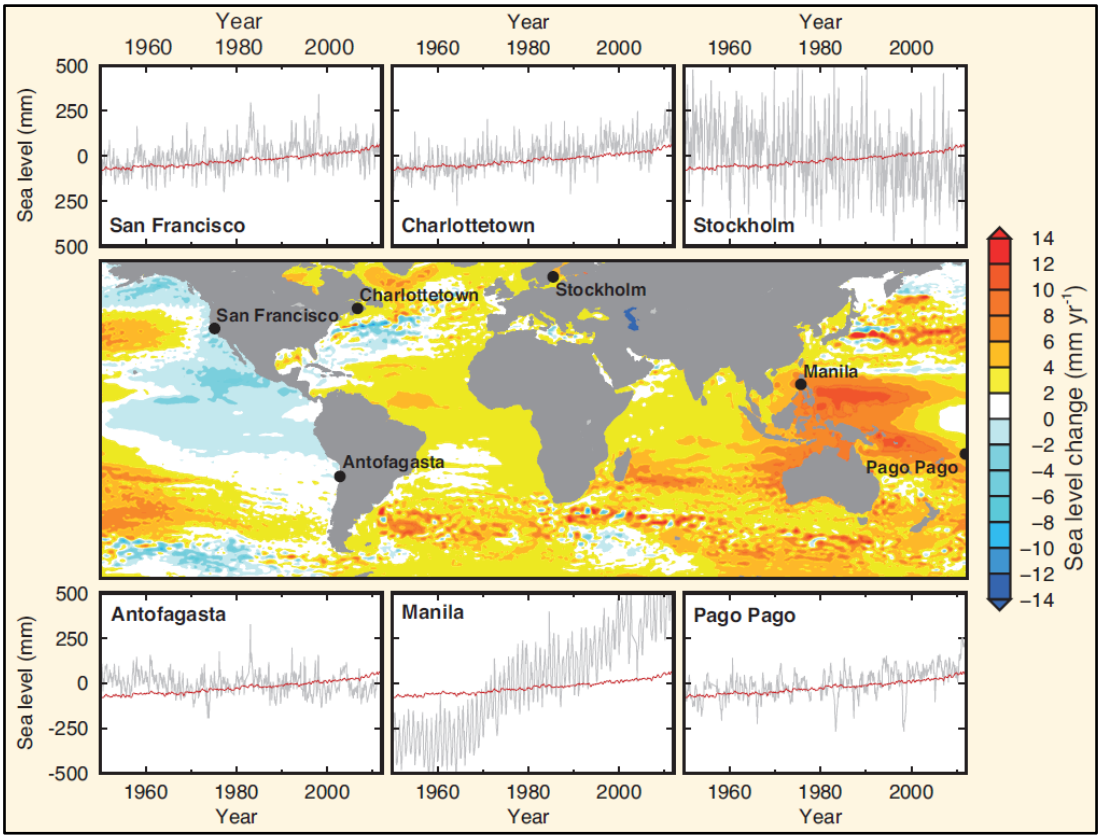

Fig. 17 - Colour map of the changes in sea surface height (referred to geocentric datum) detected by satellite altimetry, in the period 1993-2012. Graphs, referred to some locations, show the global mean sea level variations (red lines) with tide gauge time series (grey lines). The large amplitude and short time (hours to years) span oscillations of the grey lines are ascribed to natural climate variability (e.g. storms). (Church, et al., 2013).

2.2.3 Interpreted Past Sea Level Change

There is general agreement that information about the past sea level fluctuations are useful to detect past climate changes and to better understand and model current and future variation (Lambeck, et al., 2011) (Church, et al., 2013) (Kopp, et al., 2013).
Several studies on Phanerozoic sea-level changes (541 My ago to present), on various time scales, were published in the last decades (e.g. (Mitchum & Vail, 1977) (Vail, 1977), (Hallam & Cohen, 1989) (Coe, 2002), (Haq & Schutter, 2008)) on the basis of geological records (i.e. paleontology, chemiostratigraphy, tectonics, geodynamics, geomorphology) and sequence stratigraphy (the recent branch of stratigraphy that relates eustatic cycles with sedimentary deposits. Sea level has changed over geologic time (Vail, 1977) (Hallam & Cohen, 1989), and over most of geologic history long-term average sea level (Fig. 18) has been significantly higher than today, especially in the Paleozoic. Starting form Cambrian, a gradual raise of sea level occurred until Ordovician, when sea level stabilised. At the end of Ordovician, large glaciations caused important sea drops that stabilised at low stand in Silurian. During Devonian, falling sea level is followed by a gradual rise until the drastic falling stage of the Permian. Through the Mesozoic, a gradual trend of sea rising is marked by high frequency fluctuations of sea level. A new large time scale sea level fall tendency, over tens of millions years, is defined through Paleogene to Neogene, depicted by shorter time span variations. For instance, during middle Pliocene (3.3-3.0 My BP), global mean surface temperatures were 2°-3.5°C warmer than pre-industrial period. GMSL, based on proximal sedimentary records, was about 20 m higher that today due to partly melting of Antarctic and Greenland Ice Sheets (Church, et al., 2013) (Kopp, et al., 2013).

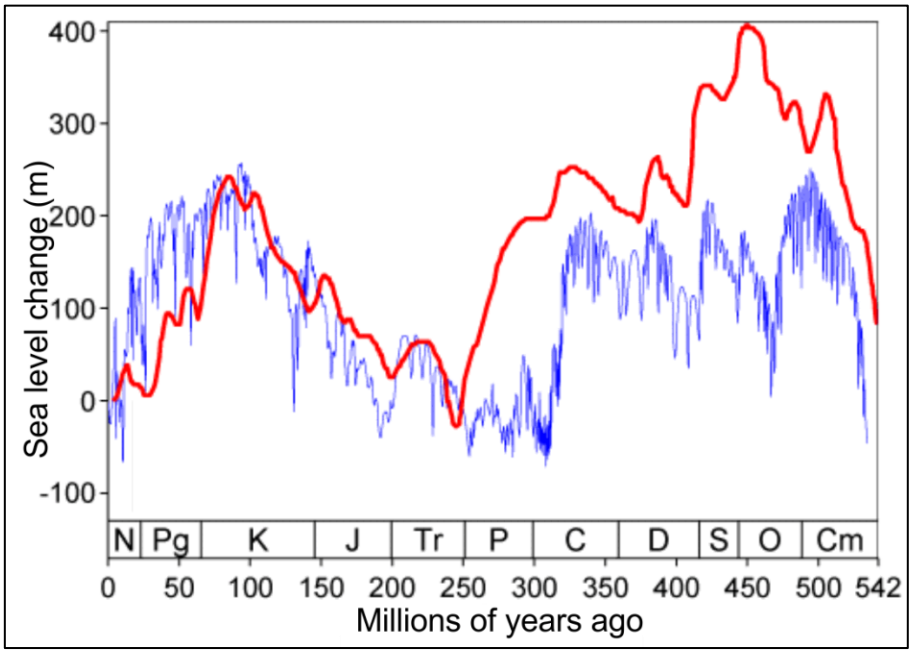

Fig. 18 – Reconstruction of the global sea level fluctuation over the past 550 My. The blue and red curves represent (Vail, 1977) (Exxon Corporation) and (Hallam & Cohen, 1989) estimations, respectively.

During Pliocene and Quaternary, several short time term periods of glacial-interglacial cycles occurred, causing a series of global sea level eustatic oscillations (Fig. 18, Fig. 19, Fig. 20, Fig. 21) (Milankovitch, 1941) (Clark, et al., 2009) (Lambeck, et al., 2011). During glacial periods, the ice

sheet expansion trapped large part of sea water, producing global sea level fall. Whereas, it is assumed that all glacier losses, during interglacial periods, contribute to global sea level rise. Oscillation amplitudes are of the order of around 100 m maximum. The most recent glacial period occurred in Pleistocene, between about 120 and 11.5 ky BP. The glaciations, that occurred during this period, covered many areas of the Northern Hemisphere and have different names, according to their geographic locations (e.g. Würm, Fig. 19 and Fig. 20). Within this interval, the Last Glacial Maximum (LGM), defined as the most recent interval in Earth history when global ice sheets reached their maximum volume, occurred 26.5-19 ky BP (Clark, et al., 2009). Since the Holocene, the Earth has been in an interglacial period. The causes of these fluctuations are explained by the Milancovitch cycles (Fig. 19 and Fig. 21). These are based on the changing in solar irradiation (or solar forcing) received by the Earth. The cycles are affected by 3 fundamental factors: changes in Earth's obliquity, precession and eccentricity, occurring about every 41, 26 and 100 ky, respectively. The combined effects cause the glacial-interglacial periods, over a time span of about 21 ky (Milankovitch, 1941).

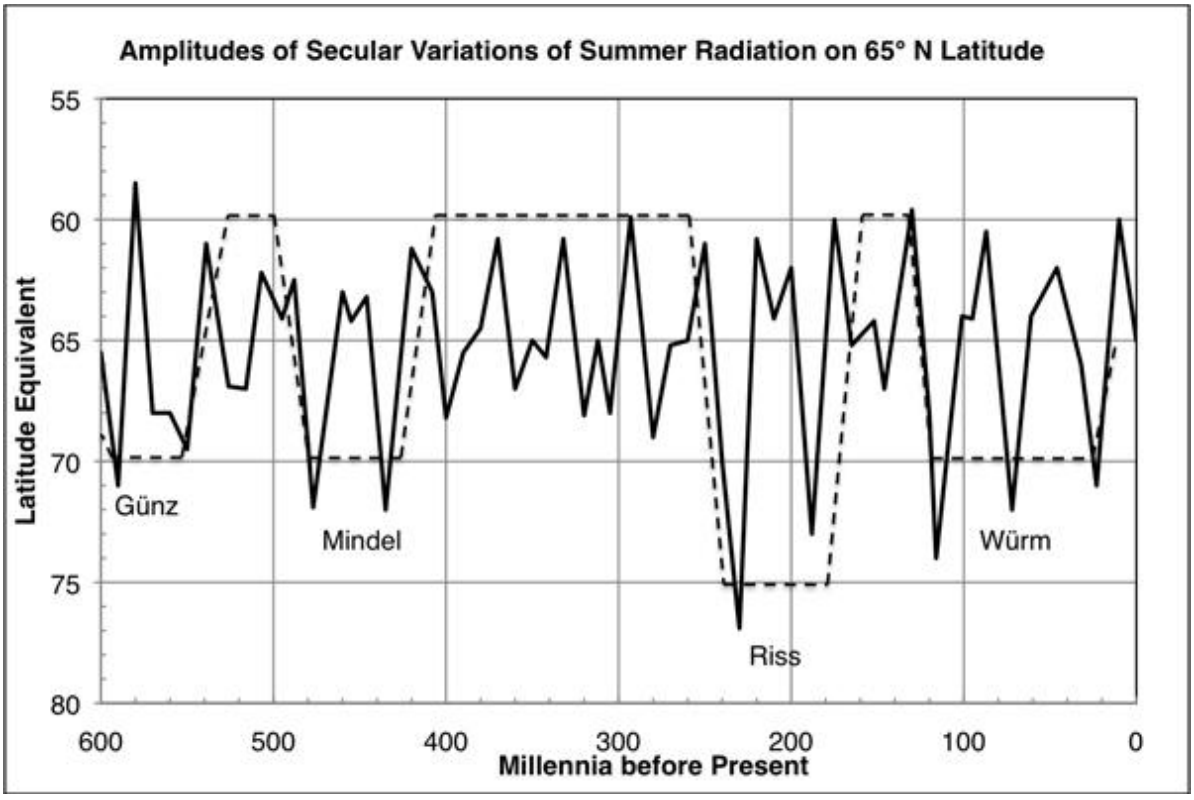

Fig. 19 – The graph shows solar energy receipt, by Earth, during summer at 65°N for the past 600 ky. The solid line indicate variation in insulation relative to the present. A value of 70° shows that at that time in the past, summer insulation at 65° is the same as received at 70° today and, so, colder than the present. A value less than 65° represents warmer conditions than at present. The dashed line is Milankovitch's schematic estimation of these last glaciations (Günz, Mindel, Riss, Würm) and intervening interglacials. (Lee & Cleveland, 2017),adapted from (Milankovitch, 1941).

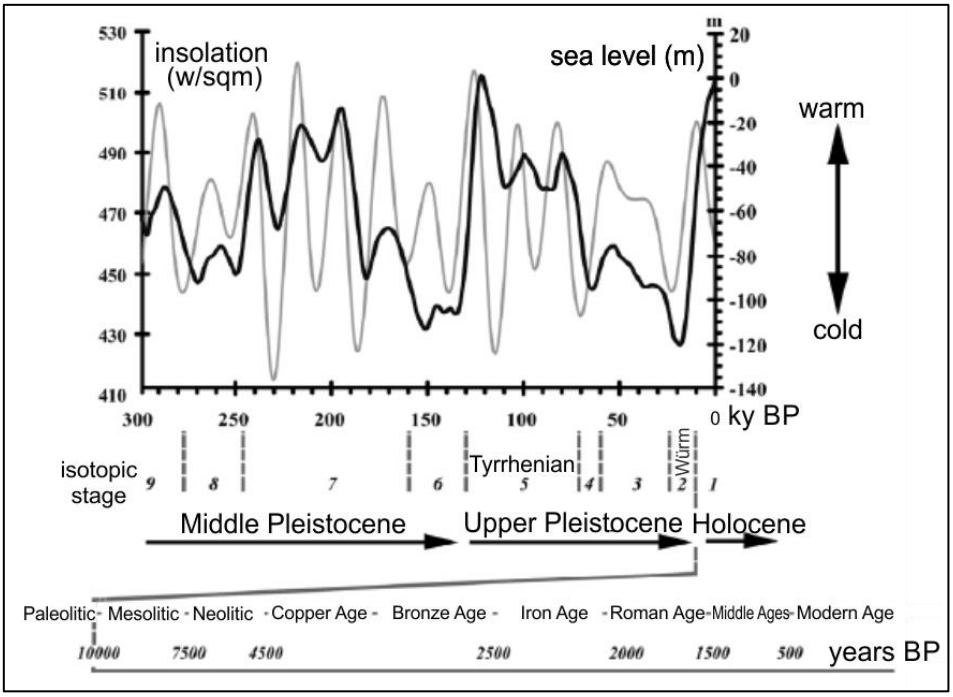

Fig. 20 – Sea level variations (black line) and solar irradiation (grey line) during Middle-Upper Pleistocene and Holocene. Last stage of sea level rising, started after the Würm glaciation and reached about 120 m of rise. Adapted from (Silenzi, et al., 2004).

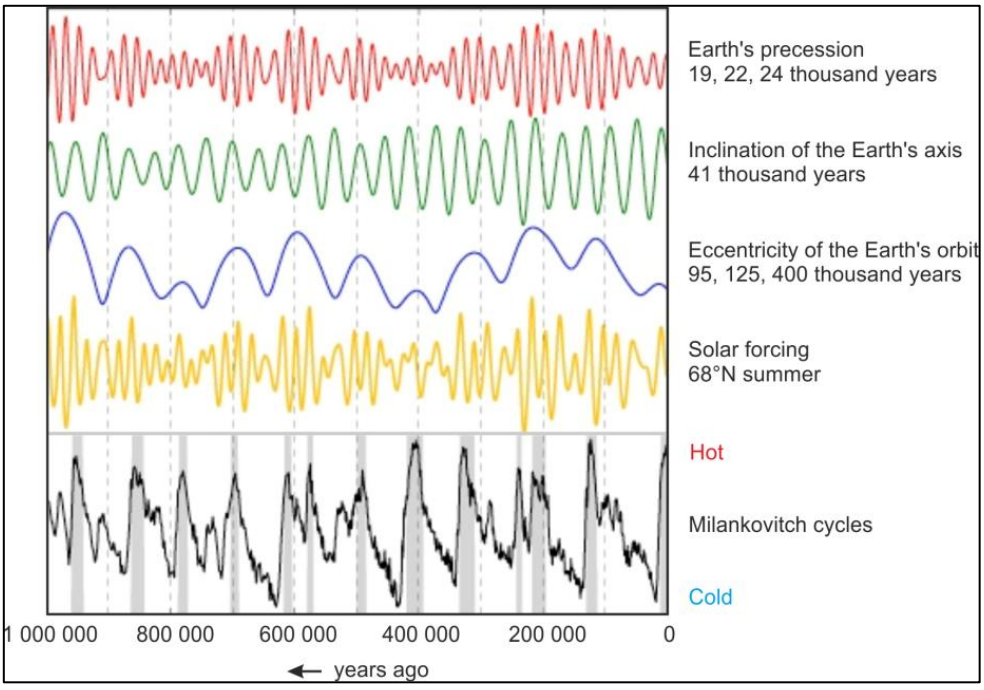

Fig. 21 – Graph showing the periodicity of each of the three processes (precession in red, obliquity in green, eccentricity in blue) that contribute to the Milancovitch cycles (black line), resulting in a recurrence of a cycle of glacial-interglacial every about 21 ky. The yellow line represents the resulting solar irradiation received by Earth at 68°N parallel, trough time, in relation to the three changing movements of the Earth. (Generalic, 2011), adapted from (Milankovitch, 1941).

2.2.4 Sea Level Change and Geology: the Sequence Stratigraphy

The modern stratigraphy proposed a new approach for studying the stratigraphic successions, with the effort to link together the lithological aspects with their relative timing of deposition.
Sequence Stratigraphy, in fact, deals with the order, or sequence, in which depositional related successions were deposited in the available accommodation space. In this way, the concept of timing is introduced by the System Tracts, related to changes in global and local relative sea level. By defining and physically recognising surfaces formed during the sea-level change, associated with deposition and erosion, it is then possible to correlate deposits both at global and local space scales, with a good level of confidence. The relevant aspect of this theory is to give information about lithostratigraphic units, characterising them by the depositional environment (or facies), but also to find a temporal relationship with other different deposits that can be in different places, by defining isochronous surface boundaries. This stands at the basis of their origin, that should be related to the same tectonic and eustatic events. In the late 1970s it was define the Depositional Sequence as a stratigraphic unit composed of a relatively conformable succession of genetically related and bounded at its top and base by unconformities or their correlative conformity (Mitchum & Vail, 1977)(Vail, 1977).
Within a complete cycle of sea level variation (Fig. 22), four phases of relative sea level change can be distinguished (Vail, 1977) (Wilgus, et al., 1988):

1- FSL: falling stage sea level
2- LSL: low stand sea level
3- RSL: rising stage sea level
4- HSL: high stand sea level

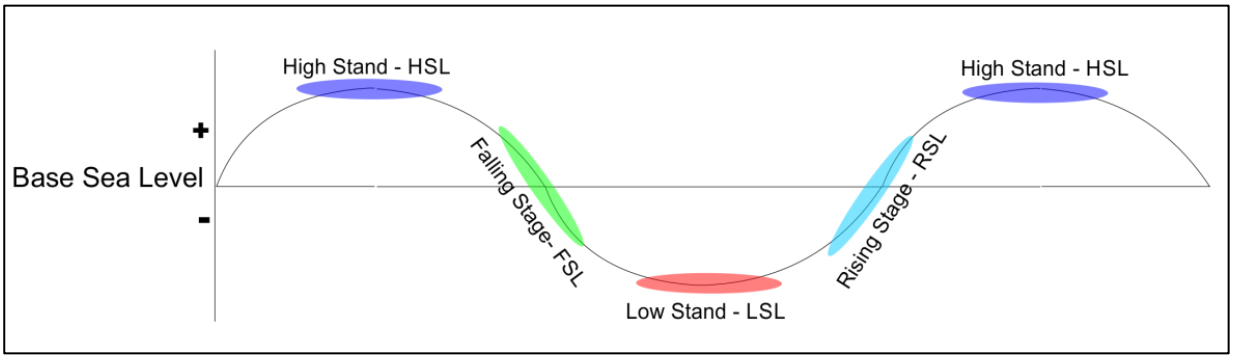

Fig. 22 – Scheme of a complete cycle of sea level variation, according to (Wilgus, et al., 1988): violet, green, red and azure shadows indicate, respectively, the intervals of high stand (HSL), falling stage (FSL), low stand (LSL) and rising stage (RSL) of sea level.

According to (Posamentier, et al., 1988a) (Posamentier & Vail, 1988b) (Van Wagoner, et al., 1988) (Wilgus, et al., 1988), sequence stratigraphy helps the recognition of each cycle phase and provides a nomenclature to define each element (system tract, ST) composing a depositional sequence (Fig. 23). System tracts are composed of all deposits accumulating during one phase of relative sea level change and their boundaries are represented by primary surfaces (Sequence Boundary, SB).

- FSST (Plint & Nummedal, 2000): falling stage/forced regressive system tract; it consists of all the regressional deposits that accumulated after the onset of a relative sea level fall

(FSL). This is the product of a forced regression to be not confused with the sediments deposited during a normal regression. A variety of succession of genetically related beds (parasequences) can be deposited, such as downwards stepping prograding clinoforms and mass flow deposits in distal areas. This system tract is characterised by erosion in proximal sectors, acting at the same time of distal deposition. The FSST lies directly on the sequence boundary (SB), an erosional surfaces that laterally passes to a conformable surface. FSST is placed below the low stand system tract deposits. The areal distribution of these features depends on the depositional profile, the rate of sediments supply and the rate of relative sea level fall.

- LST (Posamentier & Allen, 1999): low stand system tract; it consists of all deposits that accumulated during the early stage of the sea level rise. The LST lies directly above the FSST. It is bounded at its base by a subaerial unconformity or its correlative conformity. At its top, it is depicted by the transgressive surface formed by onlapping sediments on the margin. Backstepping and retrogradational patterns, onlapping beds, aggrading clinoforms up-dip thickening characterise the parasequences of this depositional system tract.
- TS (Van Wagoner, et al., 1988): transgressive surface defined as the surface that lies over the low stand system tract (LST) and the transgressive systems tract (TST).
- TST (Van Wagoner, et al., 1988): transgressive systems tract comprising the deposits that accumulated from the onset of coastal transgression, until the time of maximum transgression of the coast, just prior to the renewed regression of the HST. The TST lies directly on the transgressive surface (TS) formed when the sediments onlap the underlying LST and is overlain by the maximum flooding surface (MFS) formed when marine sediments reach their most landward position. Stacking patterns exhibit backstepping onlapping retrogradational clinoforms that thicken landward. In cases where there is a high sediment supply the parasequences may be aggradational.
- MFS (Posamentier & Allen, 1999): maximum flooding surface defined as surface of deposition at the time the Shoreline is at its maximum landward position.
- HST (Van Wagoner, et al., 1988): High stand system tract consists of all the progradational deposits that formed when sediment accumulation rates exceed the rate of increase in accommodation space. The HST constitutes the upper systems tract of a stratigraphic sequence and lies directly on the maximum flooding surface (MFS) formed when marine sediments reached their most landward position. This systems tract is capped by a sequence boundary (SB). Stacking patterns exhibit prograding aggrading clinoforms that thin upward.

Moreover, (Embry & Johannessen, 1992) defined the Regressive System Tract. It lies above a transgressive systems tract and it is overlain by the initial transgressive surface of the transgressive systems tract.

The sequence boundaries (SB), enveloping the sequence tracts (Fig. 23), are identified as significant erosional unconformities and their correlative conformities. These boundaries are the product of a fall in sea level that eroded the subaerial exposed sediment surface of the earlier sequences. These boundaries are diachronous and depict the top of the previous high stand systems tract and erode the surface of the downstepping sediments deposited during the forced regression associated with the sea level fall (Catuneanu, 2002).

This complete sequence is known as a transgressive-regressive (T-R) sequence.

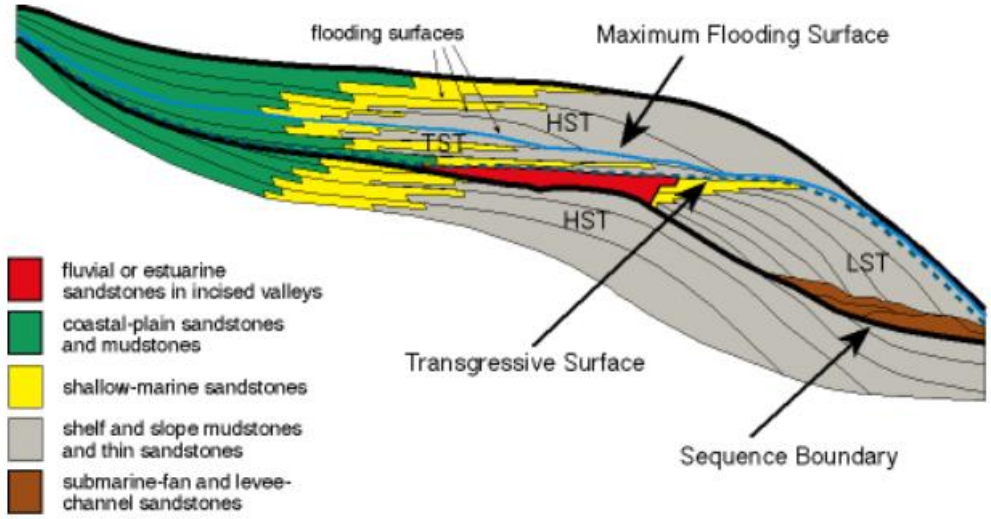

Fig. 23 – Schematic sketch of a "depositional sequence" (or transgressive - regressive sequence, T-R) composed by system tracts (ST, depositional units accumulated during one phase of relative sea level change). It is bounded at its top and base by unconformities or their correlative conformities (SB, Sequence Boundary). The different colours refer to different type of sediments and their depositional environment, highlighting the changing position throughout a complete regressive-transgressive cycle. Internal surfaces (e.g. MFS – Maximum Flooding Surface; TS – Transgressive Surface) are also represented. (Holland, 2016), adapted from (Van Wagoner, et al., 1988).

2.2.5 Sea Level Change in the Northern Adriatic Sea and in Gulf of Trieste

The last transgression in the Adriatic sea occurred in late Holocene, at the end of the LGM Würm (9 ky BP), with a maximum sea level rise of about 120 m (Fig. 20) (Silenzi, et al., 2004). In the Northern Adriatic sea, during Pliocene, Pleistocene and Holocene, several transgressive-regressive cycles occurred and were detected by interpretation of well-core and seismic depositional systems, which revealed alternation of shallow marine and continental deposits (Busetti, et al., 2007) (Romeo, 2009) (Busetti, et al., 2010b) (Cimolino, 2010) (Trincardi, et al., 2011a)(Trincardi, et al., 2011b) (Busetti, et al., 2013) (Zampa, 2014) (Zecchin, et al., 2017). At the end of the LGM, the melting glaciers of the Alpine areas started to feed the large fluvial–glacial systems that led to the alluvial megafans in the Venetian-Friuli plain (Fontana, et al., 2008). Moreover, (Ferranti, et al., 2006) identified, by means of well data, a Late Pleistocene subsiding trend, increasing from the Friulian to the Venetian plain.
In the North Adriatic sea (Zecchin, et al., 2017) identified three main Pliocene-Pleistocene depositional sequences, bounded by regional unconformities:

- The Zanclean Sequence related to the flooding in late Messinian of incised valleys, with southwards sediment progradation of a shelf-slope system probably linked to an Apennine tectonic phase.
- The Piacenzian-Gelasian Sequence that registered a relatively rapid transgressive episode followed by minor southward progradation; the top of the sequence is associated with a late Gelasian drowning event, related to the NE-ward migration of the Apennine foredeep.
- The Calabrian-upper Pleistocene Sequence, showing shallowing up deposits, is ascribed to the infilling of the accommodation space created by the late Gelasian drowning event. The upper part of sequence consists of the depositional units related to the paleo-Po deltaic system, infilling the remaining accommodation space and leading to the development of the actual shelf.

During the Upper Pleistocene (Tyrrhenian) three main transgressive events occurred in the Northern Adriatic sea. The first, 125 ky BP, brought the sea level at 7 m ± 1 m above the actual one, involving also the Gulf of Trieste (Antonioli & Silenzi, 2007c). The second and the third sea level rise are dated 100 ky and 80 ky BP, respectively, and reached 35 m below the present-day sea level, that probably was not sufficient for the flooding the easternmost part of the gulf (Silenzi, et al., 2004)(Romeo, 2009).
For the Northern Adriatic sea, (Trincardi, et al., 2011a) (Trincardi, et al., 2011b) conducted an analysis of sequence stratigraphy on the Late Quaternary deposits, and published the geological map regarding the distribution of the facies outcropping at the seabed (Fig. 25 and Fig. 26):

- HST (high stand system tract), last 5 ky, deposits of pro-delta facies (hs1), moving upwards to costal facies (hs2);
- TST (transgressive systems tract), 18-5 ky, deposits of paralic environment (tp), they are characterised by sandy and pelitic sediments with peat levels (tp1) with lenses of sand (tp2) distributed along elongated wedges parallel to the paleo-shorelines;
- FSST (falling stage system tract) and LST (low stand system tract) deposits of continental environment (ls).

The Authors described the fundamental aspects of evolution in the Late Quaternary sedimentation, by identifying three main steps:
1- the gradual landwards migration of the transgressive coastal deposits above the alluvial sediments of the previous glacial interval;
2- the condensed interval related to the minor sedimentary influx during the maximum marine transgression (corresponding to the maximum flooding surface, MFS);
3- the sediment distribution, along the coast, of the HST deposits, reflecting the position of the main fluvial systems and the re-distribution of the fine sediments by marine action, during the last 5 ky.
In Fig. 26, a zoom of the above mentioned geological map, represents the facies distribution in the Gulf of Trieste. The geological sections AA' and BB' show the exiguous thickness of the HST deposits, concentrated along the coastline. TST sediments are locally present and elongated in WSW- ENE direction, following the re-worked and eroded paleo-shores. The BB' section, furthermore, exhibits the downlap of the HST pro-delta sediments.
The last interglacial sea level rise in the Gulf of Trieste, was gradual and involved north-western Istria first (about 9 to 6 ky BP) (Covelli, et al., 2006). It developed towards north in the area of the present Marano Lagoon (4 to 2 ky BP) and definitely drowned also the Grado Lagoon (between 1000 and 500 years B.P.) at NE (Marocco, et al., 1984)(Marocco, 1989a) (Marocco, 1989b) (Marocco, 1991) (Triches, et al., 2011a). Before that inundation, the gulf was a wide alluvial plain dominated by the fluvial systems of Tagliamento, Isonzo, Timavo Rivers in the central-north (Marocco, 1991) and Rižana River in the southern area (Trobec, et al., 2017).
Despite this, several typologies of data (e.g. shoreline morphologies) show that the sea level rise does not fit exactly the reference curve (Fig. 24) proposed for the Northern Adriatic sea by (Lambeck, et al., 2011). These discrepancies are attributed to recent tectonic movements in the area of the gulf. In the eastern part of the Gulf of Trieste, archaeological, sedimentological and geomorphological markers (e.g. notches, beachrock, submerged platforms), bathymetric features, seismic evidences, broad-band long-base tiltmeters and tide gauge measures, were used to evaluate Pleistocene-Holocene sea level change, subsidence and tectonic movements at different time ranges (Braitenberg, et al., 2006) (Covelli, et al., 2006) (Antonioli, et al., 2009) (Romeo, 2009) (Furlani, et al., 2011a) (Furlani, et al., 2011b)(Zampa, 2014) (Biolchi, et al., 2015).

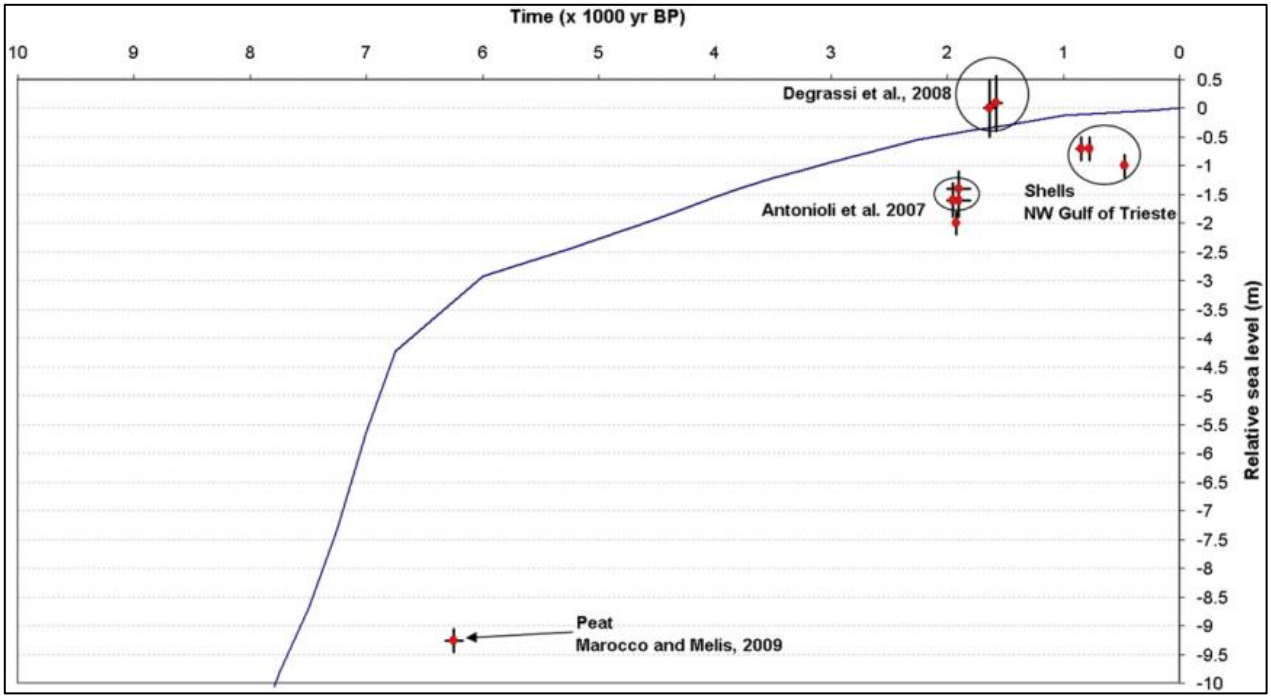

Fig. 24 - Model predictions of sea level change and observations ((Antonioli, et al., 2007b) (Degrassi, et al., 2008)(Marocco & Melis, 2009)) on coastal sea level markers in the Italian part of the Gulf of Trieste, based on (Lambeck, et al., 2011) model. (Furlani, et al., 2011a)

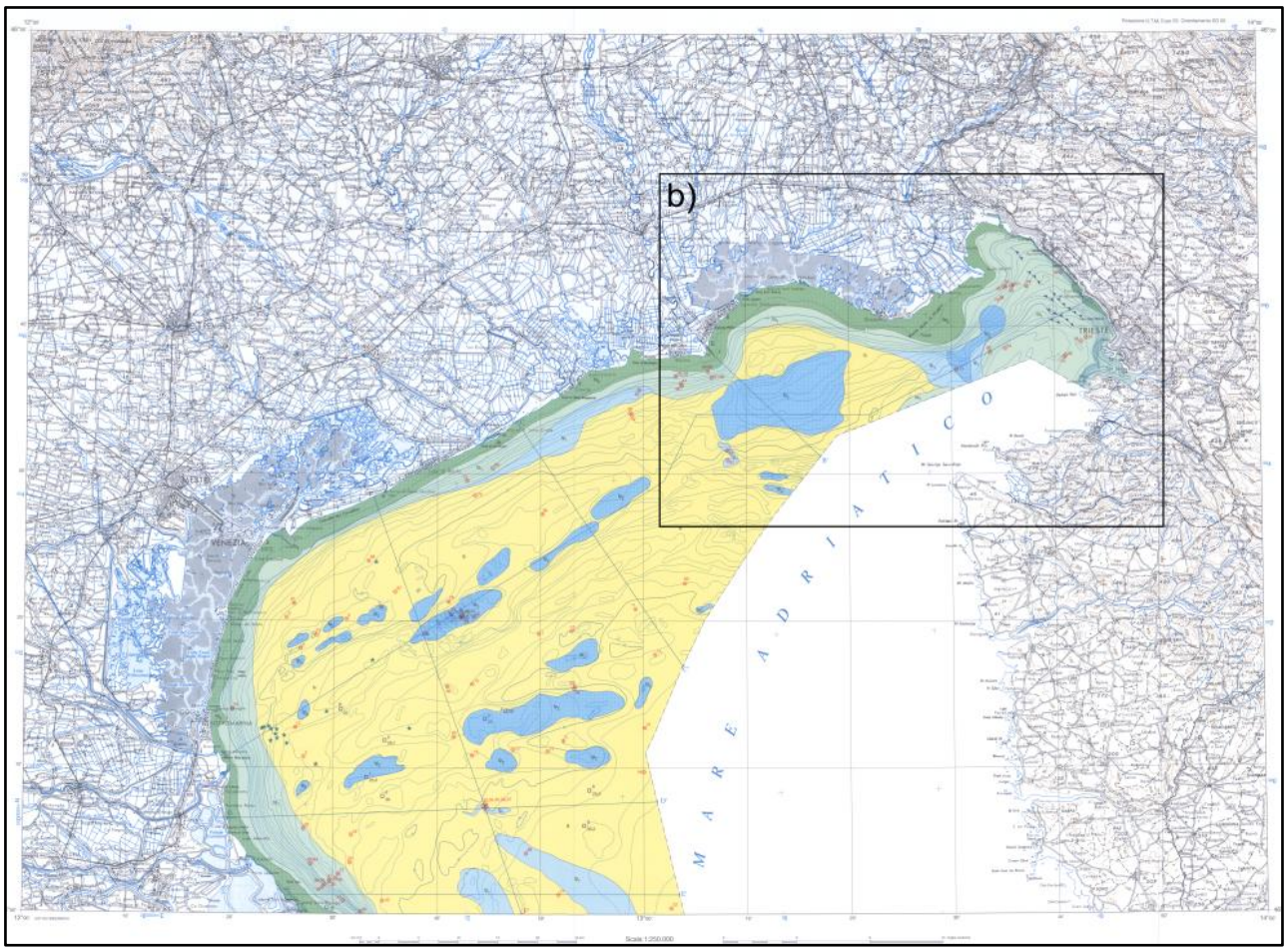

Fig. 25 - Geological map of the epicontinental platform of the Northern Adriatic. The outcropping facies are: high stand system tract (HST, green areas) of pro-delta (hs1) and costal facies (hs2) deposits; transgressive systems tract (TST, azure areas) of paralic deposits (tp) with peat levels (tp1) and sandy lenses (tp2); falling stage system (FSST) and low stand system (LST) tracts (yellow areas) with deposits of continental environment (ls). Simplified legend is reported in Fig. 26. Inset b): focus on the area of the Gulf of Trieste, with related geological sections, is shown in Fig. 26. Adapted from (Trincardi, et al., 2011a).

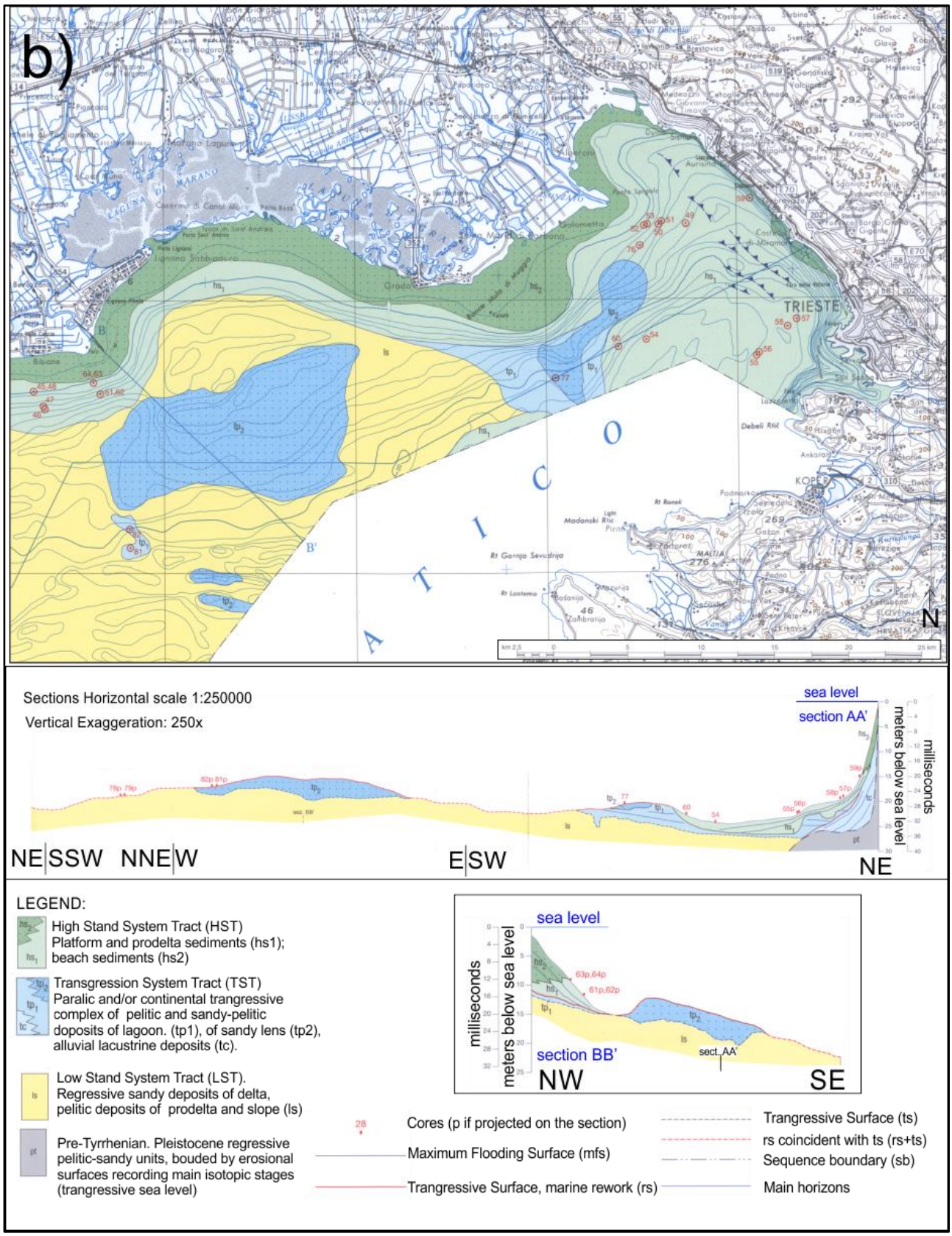

Fig. 26 – Zoom of the geological map of the outcropping facies in the area of the Gulf of Trieste, with related geological sections AA' (eastern part) and BB'. The geological profiles exhibit thin and down-lapping HST deposits, with TST sediments elongated in WSW - ENE direction. Location of this map portion is shown in Fig. 25b. Adapted from (Trincardi, et al., 2011a).

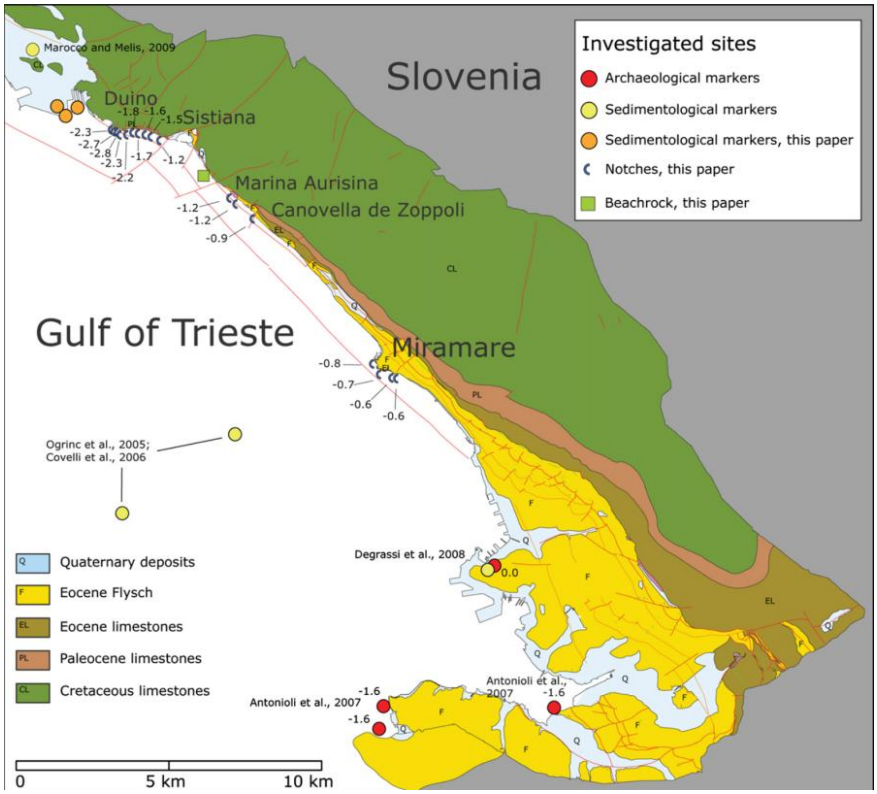

Fig. 27 – Map showing the location of the sites of archaeological (red circles), sedimentological (yellow and orange circles) and geomorphological (submerged notches and beachrocks in blue arc and green rectangle, respectively) surveyed in the eastern part of the Gulf of Trieste. The values represent the depth (m b.s.l.) of the notch and archeological markers. (Furlani, et al., 2011a).

2.2.5.1 Geomorphological Markers

Most of the geomorphological features characterising the coastlines and the bathymetry of the Gulf of Trieste are extensively described in the section “Geographical Setting”. In the sequel are summarised the characteristics of the main geomorphological markers and their significance in the reconstruction the sea level change in the Gulf of Trieste, that in turn can be also correlated to the neotectonics activity.

2.2.5.1.1 Notches

According to (Ambert, 1978) (Trenhaile, 1987) (Sunamura, 1992) (Antonioli, et al., 2004) (Furlani, et al., 2011a) (Fulani, et al., 2011c), notches are coastal morphologies consisting in indentations carved along rocky cliffs walls, mainly by marine action. They are considered very important morphological markers that can provide information on sea level change and, in turns, on tectonic vertical movements. In particular, these markers are very common along the Mediterranean costs. (Antonioli, et al., 2004) (Antonioli, et al., 2007b) (Furlani, et al., 2011a) (Furlani, et al., 2011b) identified 35 submerged notch depths along the north-eastern coast of the gulf of Trieste (Fig. 27). The deepest notches characterise the coast between Duino and Sistiana. At the first northern location, the depth is 2.8 m bsl (Cretaceous carbonates), becaming shallower towards Sistiana (Paleocene/Eocene carbonates) to 1.0 m. The carbonate (Eocene units) shoreline between Marina di Aurisina and Miramare hosts notches that depth gradually from 1.20 m to 0.9 m bsl at Canovella de’ Zoppoli and at 0.80-0.60 m bsl , further south on the Eocene carbonate olistoliths of Miramare. (Furlani, et al., 2011a) dated this displaced notch system along the shoreline, as post-roman (Fig. 31). Moreover, the depth distribution, , suggests significant vertical displacements have occurred in correspondence to some E-W oriented faults. The displacement probably occurred in response to creeping along discontinuities, within a regional NW tilting, during post-Roman time, and probably is still even active. Although, there is no trace in historical record related to a post-roman earthquake in the area, the notch depth distribution suggests a possible co-seismic event (Furlani 2011).

2.2.5.1.2Submerged and Buried Shore Platforms

Several submerged and buried shore platforms were identified in the proximity of the shoreline of the gulf (Morelli & Mosetti, 1968) (Furlani, 2003a)(Furlani, 2003b) (Furlani, et al., 2009a) (Romeo, 2009) (Zampa, 2014). Shore platforms developed due to the step back-wards of the rocky cliffs and subsequently submerged by sea level rise. (Furlani, et al., 2009a) recognized a submerged Flysch outcrop along the Sistiana-Duino coast, with a length of 170 m, a wideness of 45 m. The erosion affected the Flysch (Eocene) walls and stopped when it reached the more resistant carbonates. Considering its actual depth, ranging between 1.5 and 5 m bsl, and the 0.01-0.02 m/y erosional rate for the Flysch in marine environments (Sunamura, 1992) (Furlani, et al., 2009a) (Furlani, et al., 2011a), the Authors estimated that the relict platform formed in pre-roman age (Late Holocene), during the last sea level rise in the gulf. Moreover, slope-terrace systems characterise the buried Flysch in the offshore adjacent to the eastern side of the gulf (Morelli & Mosetti, 1968) (Romeo, 2009) (Zampa, 2014). They have been identified on high resolution geophysical profiles and at different depth intervals. These marine terraces in the Flysch extend for hundreds of meters,

similarly to the actual marine platforms described by (Furlani, 2003b) along the north-western Istria seaside. These features are partly related to tectonic activity, partly attributed to different sea level changes during Pleistocene and Holocene glacial/interglacial events. In particular, among the sequence stratigraphy analysis in the gulf by (Romeo, 2009) and (Zampa, 2014), two prominent patterns of depositional sequences (HST) and related surface terraces were identified in the offshore between Miramare and Muggia at depths of 36-37 m and 41-43 m bsl (Fig. 28 and Fig. 29). They were associated to the Tyrrhenian (125-75 ky BP) sea level rise consequent to a deglaciation phase, marked by several phases of sea level stand. The shallower terrace may be related to that identified by (Morelli & Mosetti, 1968) near the coast of Duino, at 90 m bsl. In onlap above these, a marine stratified unit represents a following transgressive event. This is buried below a transitional and continental units corresponding to a gradual regression and a further low stand sea level, probably related the LGM (about 20 ky BP). The top most well layered marine depositional unit, represents the last Holocene sea transgression, that, according to (Covelli, et al., 2006), started in the gulf 8270 ± 50 years BP. As concerns previous sea level fluctuations, at depths higher than 65 m bsl, (Romeo, 2009) identified Middle Pleistocene continental sediments deposited during the Riss glacial period. This was subsequent to a marine transgressive phase occurred about 190 ky BP, that led to 15 m lower sea level than today and to a progradational wedge now positioned at 80-90 m bsl (Fig. 29).

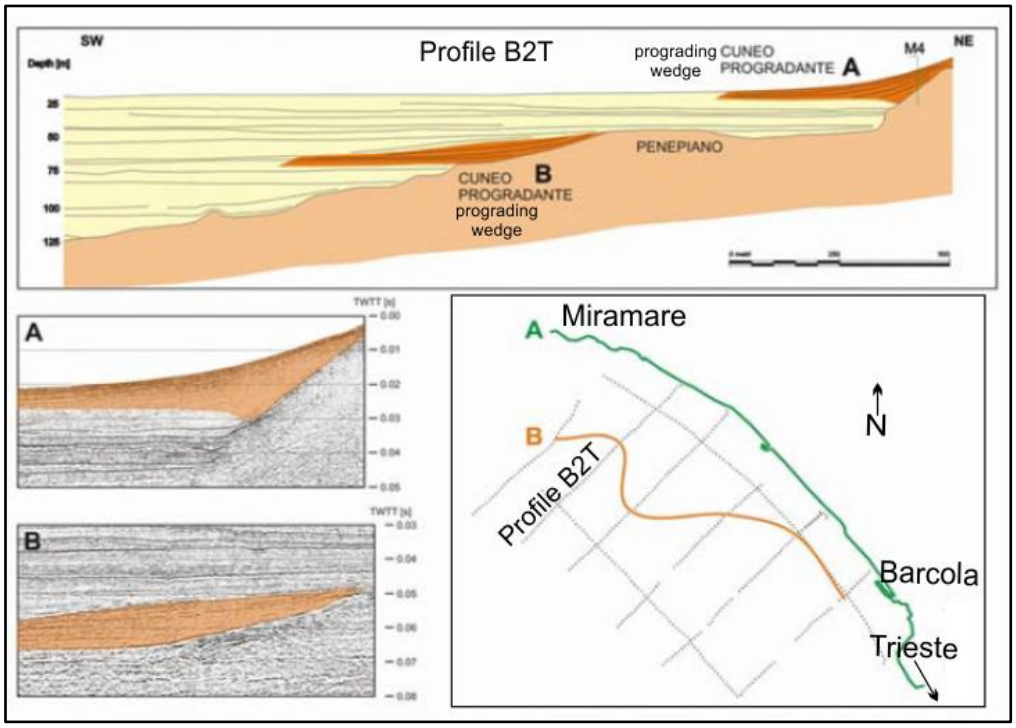

Fig. 28 – Prograding wedges (A and B) identified on high resolution Boomer profiles of the OGS 2003 Barcola survey located in the adjacent offshore of the Miramare-Barcola coastline (bottom right of the figure; or section 4.5 for details). The isoline of the actual coastline (green line A) is also shown, in comparison with the paleo-coastline B (orange line) that is reconstructed through the interpretation of the progradational wedge B on the geophysical data and it was referred to the marine transgression of the Upper Pleistocene (125 ky BP). Adapted from (Romeo, 2009).

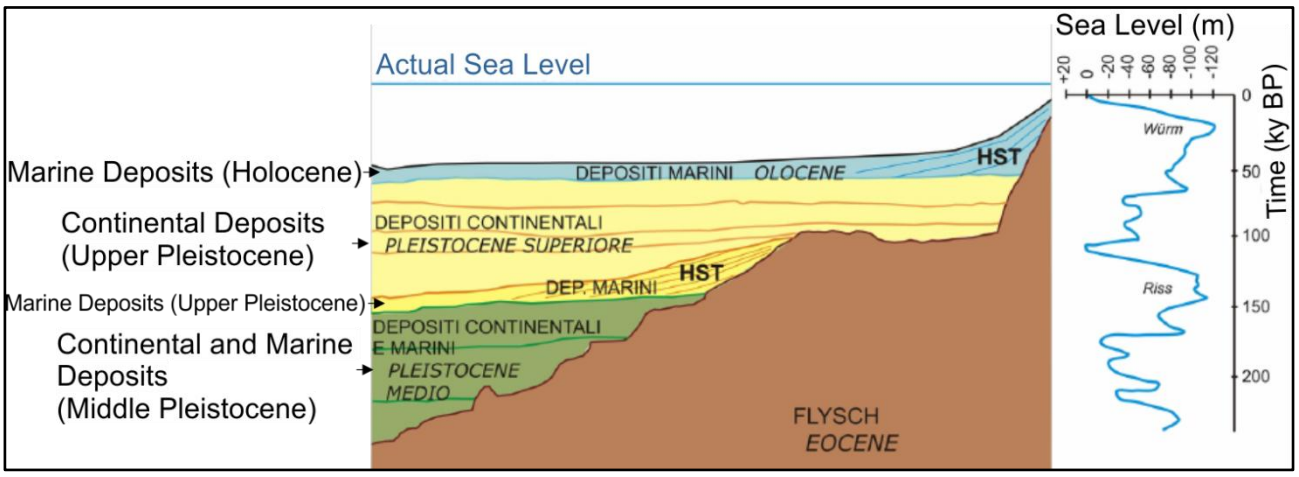

Fig. 29 – Scheme of the stratigraphic relationships among the recent marine and continental deposits (Middle Pleistocene to Holocene) identified on the high resolution Boomer seismic profiles of the OGS 2003 Barcola survey (section 4.5 for details) in the adjacent offshore of the Miramare-Barcola coastline. Note the Holocene and Upper Pleistocene system tracts (HST), corresponding to the prograding wedges A and B, respectively, of Fig. 28. These deposits are related to the sea level fluctuation that affected the gulf and that are reported in the graph on the right of the figure. Adapted from (Romeo, 2009).

2.2.5.1.3Submerged Beachrock

At a distance of 25 m from the shoreline of Costa dei Barbari, (Furlani, et al., 2011a) recognised a submerged beachrock located 3.5-5.1 m bsl, with wideness and length of 22 m and 120 m, respectively. It is made of silicate sand and gravel cemented by calcite and depicted by wave erosion (e.g. notch and channels, Fig. 24 and Fig. 27). The cementation was developed thanks to freshwater coming from the onshore area. Limestone and sandstone blocks hide the underlying Flysch between the coast and the beachrock. Rare foraminifera and mollusc fragments are present. Although this feature has not been dated yet (i.e. no archaeological elements were found), it can be use as additional marker to constrain the estimation of sea level fluctuation and neotectonic activity of the study area. The Authors suggest the development of the beachrock was already ended in Roman ages, after a sea level rise.

2.2.5.2 Archaeological Markers

Archaeological remains constitute another type of marker useful for the detection of sea level change (Fig. 24, Fig. 27). Within the Gulf of Trieste, have been discovered Roman age ruins, such as:

- a Roman bench near Muggia (Stramare) at 1.2 m bls. Since, at the construction time of the building the sea level was about 3 m lower than today, the rising rate of sea level can be estimated in 1.5 mm/y (Antonioli, et al., 2007a) (Furlani, et al., 2011a);
- a Roman harbour at Izola (S. Simonov), where a bronze ring used by ships to dock, is at 0.9 m, ((Antonioli, et al., 2007a) (Antonioli, et al., 2007b) (Antonioli, et al., 2009) and references therein).
- Roman structures at Punta Sottile, lying at 1.2 m bsl, storing also an amphora of the First Century AD, suggesting a sea level rise of 1.60 ± 0.30 m since Roman times (Antonioli, et al., 2007a);
- -in the Slovenian coast (S. Bartolomeo) an ancient walking surface present at 0.8 m bsl indicates a sea level rise of 1.40 ± 0.30 m since the time of its construction (Roman early imperial period) (Antonioli, et al., 2007a).

2.2.5.3 Sedimentological Markers

As concerns sedimentological markers (Fig. 24, Fig. 27), in Trieste two lagoon fossil samples from archaeological ruins, taken at 0.0 m asl and 0.1 ± 0.10 m asl, have been dated 1639±48 y BP 1576.5 ± 0.1 y BP, respectively (Degrassi, et al., 2008).
In the central part of the gulf, (Covelli, et al., 2006) analysed two peat samples, recovered by the R/V OGS Explora in 1996: at 25 m bsl with an age is 9140 ± 40 and at 26 m bsl with an age of 8810 ± 40 BP. According to the (Lambeck, et al., 2011) prediction curve (Fig. 24), the two samples should have been found at 35 m and 28 m bsl; therefore, (Furlani, et al., 2011a) estimated a tectonic uplift rate of +1.01 and 0.21 mm/y, respectively. At the harbour of Monfalcone, (Marocco & Melis, 2009) collected a lagoon peat from a depth of 9.26 m bsl dated 6245 ± 75 BP.
Near Duino (Villaggio del Pescatore), (Furlani, et al., 2011a) collected one sample of wood at 2.0 m bsl (1985 ± 25 BP) and three samples of lagoon shells, at 0.7 m, 1.0 m and 0.7 m bsl, respectively dated 1238 ± 35, 838 ± 35 and 1298 ± 51 BP. These values, compared with the (Lambeck, et al., 2011) estimation, indicate a tectonic subsidence rate ranging between 1.99 and 0.70 mm/y (Furlani, et al., 2011a).

2.2.5.4 Tidal Gauge Measurements

(Braitenberg, et al., 2006) compared tide gauge data of Trieste with respect to those at the stations of Venezia, Trieste and at the Istrian Koper, Rovinj and Bakar (Fig. 30b), belonging to the international PSMSL (Permanent Service for Mean Sea Level) network. Mean sea level (MSL) changes are compared along a lineal regression extending from 1955 to 2000, for all the stations except Koper, whose data are considered not enough reliable (the station moved to a near location in 1992). This time interval lies within the lower window for which it is still possible to determinate average sea level trends in long term (Douglas, 2001). This is due to the inherent variability of sea level changes. Differential rates of tide gauge measurements, in the NE Adriatic, show 0.54 mm/yr at Trieste, -0.15 mm/yr at Rovinj, 0.24 mm/yr at Bakar stations (Fig. 30a). The differential rate between Trieste and Rovinj is 0.7 mm/yr. This value is comparable with tidal notches depths distribution in the Gulf of Trieste. Furthermore, all the differential rates are related by the Authors to differential vertical coastal movements.
Moreover, at Venice station, providing recordings also between 1907 and 1970, the evidence of lower rate of sea level rise, during the second half of the past century, is broadly ascribed to reduction in the subsidence rate, since the water extraction in the industrial site of Marghera was stopped in late 1970s. Whereas, the motivation of the changing in slope of the two highlighted trends (1905-1970 and 1970-2000), at the Trieste measuring location, are still unknown.

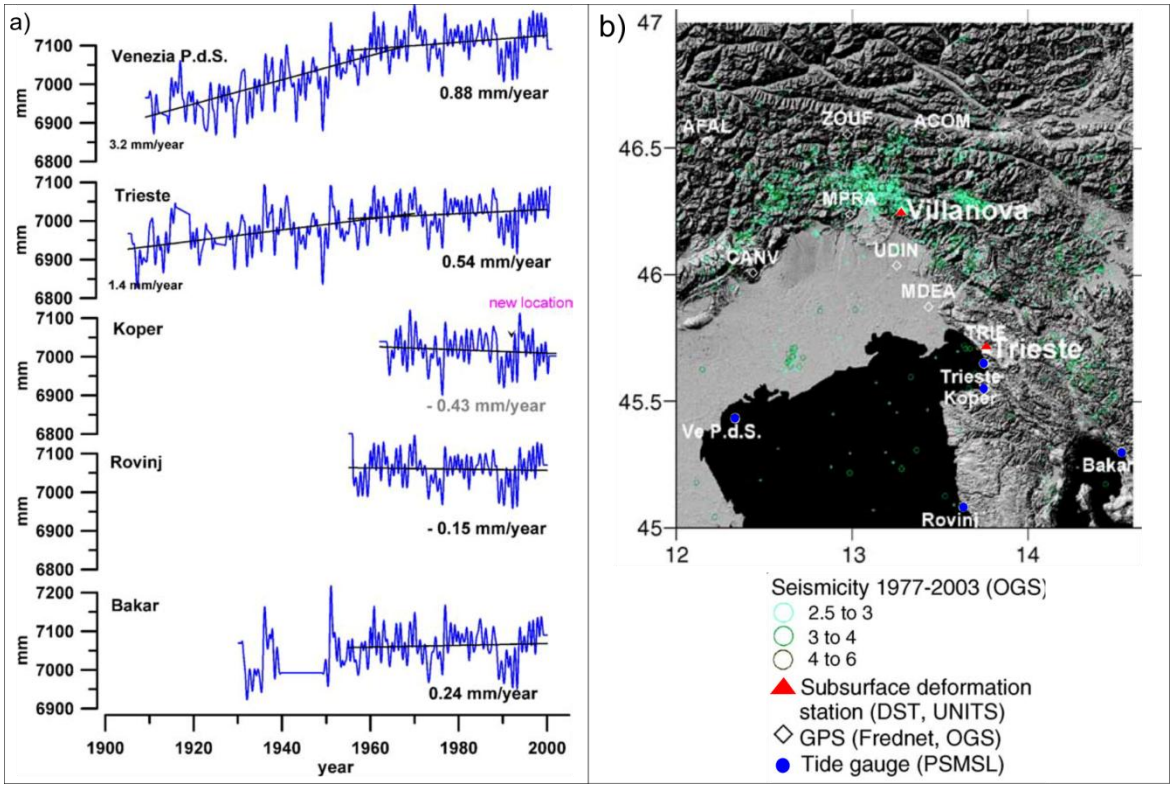

Fig. 30 – a) Monthly record of an international network of tide gauge measurement of sea level in the northern Adriatic, at the locations of Venezia Punta della Salute, Trieste, Koper, Rovinj and Bakar (blue points, positions in b). The regression lines are calculated on the common time interval of years 1955–2000. For Trieste and Venice, the mean sea level rise has also been calculated for the years 1905–1970 and 1907–1970, respectively. Adapted from (Braitenberg, et al., 2006).

2.2.5.5 Sea Level Change in the Gulf of Trieste, in a Nutshell

(Furlani, et al., 2011a) summarised the most recent sea level fluctuation in the Gulf of Trieste (Fig. 31), that results mainly from eustatic and tectonic factors. The reconstruction is based on the analysis of all the above listed typologies of markers (archaeological, sedimentological and geomorphological markers, bathymetric features, seismic evidences, tide gauge measures, broad-band long-base tiltmeters; see also section 3.7).
The Authors identified the following main stages:

- Pre-Roman age: the Holocene sea level rise led to the development of shore platforms on the Flysch. During this period, also the above described beachrock, found along the eastern coast of the gulf, formed.
- Roman age: the sea level rose, drowning the pre-existing geomorphological markers and new Roman structures (i.e. docks) were built along the coast.
- Post-Roman age: a tidal notch formed along the carbonate cliffs of the eastern seaside of the gulf.

More recently, the sector between Sistiana and Duino was intersected by vertical displacements, explained as creeping along pre-existent discontinuities (N-S and NE-SW oriented faults that affect the coastal sector), perhaps accelerated by seismic events that abruptly downdrop the notches northwards

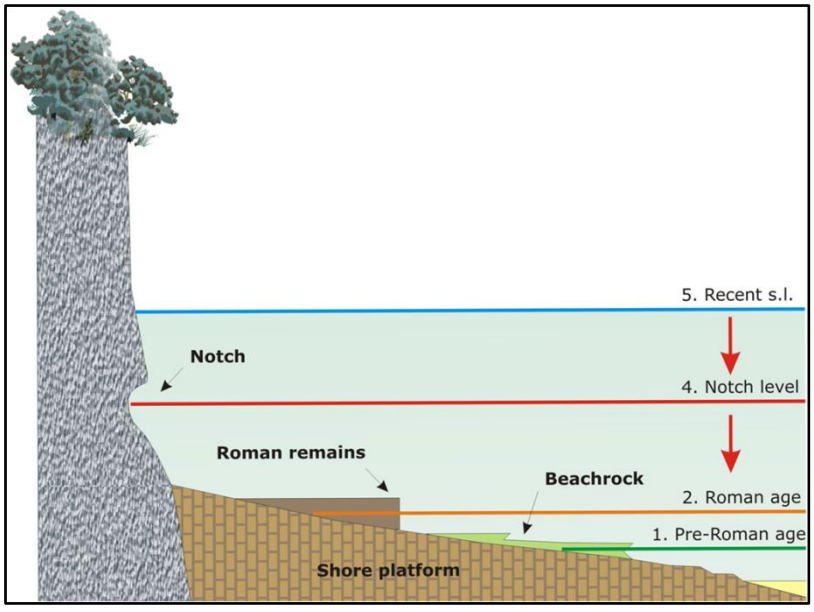

Fig. 31 – Scheme, along single 2D profile, of the coast of Trieste representing its current (blue line) and past sea levels (Notch-Post-Roman, Roman and Pre-Roman in red, orange and green, respectively). The main markers (archaeological remains, beachrock, notch), that help the reconstruction of the sea level fluctuation, are represented. (Furlani, et al., 2011a).

3 GEOLOGICAL AND TECTONIC SETTING

3.1 Foreword

The Gulf of Trieste (GT) is regionally settled in the easthern corner of the collisional domain between the Adriatic microplate and the Euroasian plate. The GT constitutes part of the double-polarity foredeep related to the Meso-Cenozoic chains of the NW-SE trending External Dinarides (SW-ward vergent) and the E-W oriented South-eastern Alps (S-ward vergent), that intersect together immediately to the N, Fig. 32, (Carulli, et al., 1980) (Casero, et al., 1990) (Fantoni, et al., 2003) (Galadini, et al., 2005) (Carulli, 2006b) (Castellarin, et al., 2006).

Fig. 32 – Scheme of the regional structural domains and setting of the Northern Adriatic Sea, to which the Gulf of Trieste belongs (dashed-blue rectangle) and neighbouring onshore. The study area of the present work is part of the foreland of both the Dinaric and Alpine thrust-belts (Dinaric domain in azure, Southern Alpine domain in green, Alpine domain in red), that intersect to the north around the national border between Italy and Slovenia. Geological information from (Galadini, et al., 2005)(Burrato, et al., 2008) (Cucchi, et al., 2008a) (Tunis, et al., 2008)(Zanferrari, et al., 2008) (Placer, et al., 2010) (Jurkovšek, et al., 2016). Map compiled by using ArcGis (ESRI, 2017) software; datum WGS84, projection UTM33.

Within the regional geodynamic evolution, the relative movement between Europe and Africa plates had a key role. At crustal scale, the motions led to a complex pattern of interference among continental lithosphere (Fig. 33 and Fig. 34), (Doglioni & Carminati, 2008):

- The S-ward subduction of the European plate beneath the Adria microplate (Alpine compression domain);
- The E-ward subduction of Adria microplate under European plate (Dinaric subduction). This is already depleted in the northern part while it is still ongoing in the southern one (e.g. Ellenides).
- The W-ward subduction presently active, of Adria beneath the Apennine margin (Apennine Subduction).
- The W-ward Carpatian subduction related to the extensional domain of the Pannonian basin E, where Astenosphere is rising.

Adria, in this area, is quite undeformed and has a crustal thickness of 30-35 km. The Moho depth increases up to 50 km towards the Alpine domain while between Trieste and Ljubljana it reaches 45 km and diminishes further E in the Pannonian Basin (Nicolich & Dal Piaz, 1990).

The external sector of the eastern Southern Alps is, at present, tectonically active with compressive kinematics, due to the ongoing movement of the Adria microplate towards north. This is testified by the Pleistocene deposits deformations of the Friuli Plain and by the seismicity on the frontal part of the Southern Alpine chain (Slejko, et al., 1989)(Galadini, et al., 2005) (Poli, et al., 2009)(Poli, et al., 2015))

Geological studies on the surrounding onshore have been conducted since the 19th Century (i.e. (Cornalia & Chiozza, 1851a) (Cornalia & Chiozza, 1851b)(Stache, 1889)), while subsurface studies of the offshore remained limited until recent time, when geophysical methods for the investigation of the crust structure and the sedimentary basins, started to be developed onshore (Amato, et al., 1977) (Finetti & Del Ben, 2005) (Nicolich, et al., 2004a) (Nicolich, et al., 2004b) and offshore (Morelli & Mosetti, 1955)(Morelli & Mosetti, 1968) (Finetti, 1965) (Finetti, 1967) (Scrocca, et al., 2003) (Ramella, et al., 2005) (Busetti, et al., 2008) (Busetti, et al., 2010b) (Cimolino, et al., 2010) (Zgur, et al., 2010)(Zgur, et al., 2013) (Busetti, et al., 2013)(Della Vedova, et al., 2014).

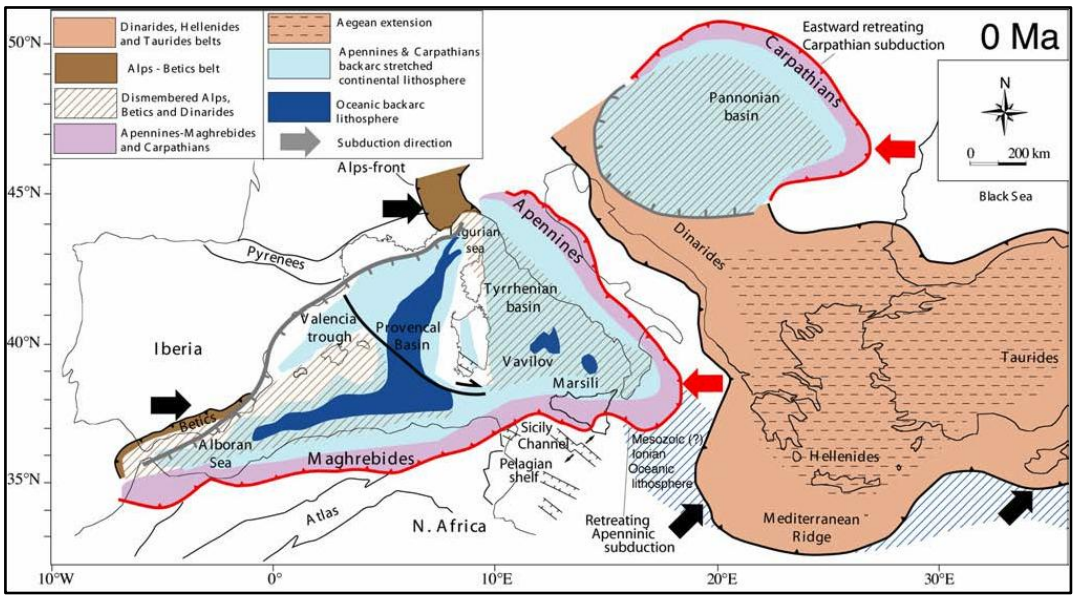

Fig. 33 - Present geodynamic framework of the Mediterranean. Focusing on the Adriatic region, three subduction zones are still active: the W-ward Apennines (-Maghrebides); the W-ward Carpathians; the NE-ward Dinarides-Hellenides (-Taurides). (Doglioni & Carminati, 2008).

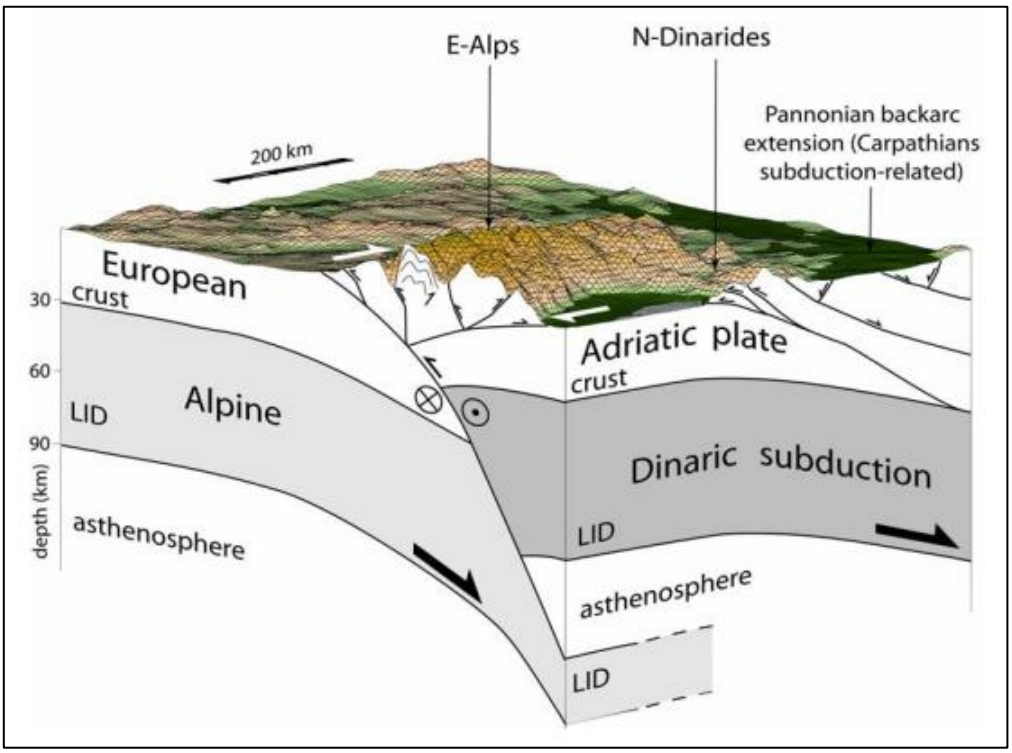

Fig. 34 - 3D sketch of the geodynamic setting at the crustal scale, in correspondence of North Adriatic Sea and neighbouring areas. The passive plate boundary is characterised by the collision between Adria microplate and the European plate. The Adria block subducted E-wards beneath Europe, giving rise to the Dinaric collisional phase. The European margin subducted S-wards under Adria, causing the Alpine compression phase. Moreover, extensional back-arc basins, characterising the Pannonian area and crosscutting the Eastern Alps and the Northern Dinarides, are related to the W - Pannonian-Carpatian subduction (Doglioni & Carminati, 2008).

3.2 Sedimentary Sequence

The onshore area located to the north of the Gulf of Trieste (between the Dinaric-Alpine foreland and the Eastern Alps; e.g. Fig. 32, Fig. 35, Fig. 36, Fig. 37) preserves, from a stratigraphic and tectonic point of view, entirely all the phases occurred since 460 My ago to the present. In the Ordovician (460 My ago) started a depositional phase that led to the sedimentation of about 4 km of mainly reef facies. This was stopped only in the Carboniferous, when the Variscan orogen (Carboniferous-Early Permian) developed, in the framework of the collisional event between Laurasia and Gondwana that generated the supercontinent of Pangaea (Vai, et al., 2002). At that time, the Carnic sector (Fig. 35, Fig. 36) was positioned at a latitude of 4°N (Venturini, 2006). The structures of this tectonic phase were then buried by arid climate deposits (e.g. sandstones of Val Gardena) and by the successive lagoon deposits of the Late Triassic–Cretaceous, for a total thickness of 10 km. From Late Cretaceous, new collisional phases took place: the Dinaric and Alpine compressions, associated with the terrigenous turbiditic deposition of the Eocene Flysch and Miocene Molasse (Carulli, 2006a) (Carulli, 2006b).

In the northern part of the region Friuli Venezia Giulia (corresponding to the Carnic Alps) and the north-western Slovenia (Fig. 32, Fig. 35, Fig. 36, Fig. 37), the lithologies belong almost exclusively to the depositional sequence of Paleozoic (Late Ordovician-Early Permian). This area extends E-W and and it is delimited to the north by the Periadriatic Line. It is tectonically bounded by the Val Bordaglia and the Mojstrana-Ljubljana Lines to the W and the E, respectively. The main direction of the tectonic strands belonging to the Variscan belt is NW-SE. Although the subsequent involvement in the Alpine deformation, the Paleozoic (up to the Carboniferous) sequence still preserves its original depositional characters and this represents a very important element for several typologies of geological reconstruction (as, for example, the paleo-environment) (e.g.(Vai, et al., 2002) (Venturini, 2006)).

The Southern Carnic Alps (Fig. 35, Fig. 36), delimited to the N by the Carnic Alps and to the S by the northern Tagliamento Valley, are constituted by the lithologies of the Mesozoic sequence. In particular, the middle Triassic deposits lie above the Permo-Triassic successions outcropping at the toe of the valleys (e.g. (Ponton, 2010)). To the east of the Italian area, the Julian Alps (Fig. 35, Fig. 36) have lithologies of Ladinian, Carnian and Norian age; they are bounded to the N by the Carnic Alps, to the S by the Resia Line and to the W by the Southern Carnic Alps (e.g (Fella River) (Ponton, 2010)). To the east, those lithologies are in continuity with the Permo-Triassic units outcropping in the Slovenian Júlijske Álpe area (GeoZS, 2017), Fig. 37.

The Carnic Pre-Alps (Fig. 35, Fig. 36) are characterised by Meso-Cenozoic lithologies; deposits of the Miocene Molasse are also present. These Alps are bounded to the N and E by the alpine path of Tagliamento River, while they close to the S in correspondence of the Western Friuli Plain (e.g. (Vai, et al., 2002)(Zanferrari, et al., 2008)).

Moving towards east, Meso-Cenozoic units (different from those of the neighbouring Carnic Pre-Alps) characterise the Julian Pre-Alps (S of the Julian Alps and N of the Eastern Friuli Plain; Fig. 35, Fig. 36) and the adjacent area between Tolmin and Nova Gorica (Fig. 37) are predominantly constituted by and by Eocene units (e.g. (Tunis, et al., 2008)).

The Moraine Arc (Fig. 35, Fig. 36) is located between the Carnic and Julian Pre-Alps, within the northern part of the Friuli Plain. It is constituted by three main arcs, left after the gradual N-wards retreat of the Würm glacier. The deposits are represented by association of both fine and coarse detritus (e.g. (Gortani, 1959) (Carulli, et al., 2000)).

The Friuli Plain (Fig. 35, Fig. 36) develops from the toe of the Alpine reliefs, to the S towards the Northern Adriatic coastline. It is subdivided by the E-W trending springs line, into High and Lower Plain. The boundary marks also the contact between permeable terrains (sands and gravels) to the N, and semi-permeable or even impermeable materials to the S (mud and clays) (e.g. (Carulli, 2006a) (Carulli, 2006b)).

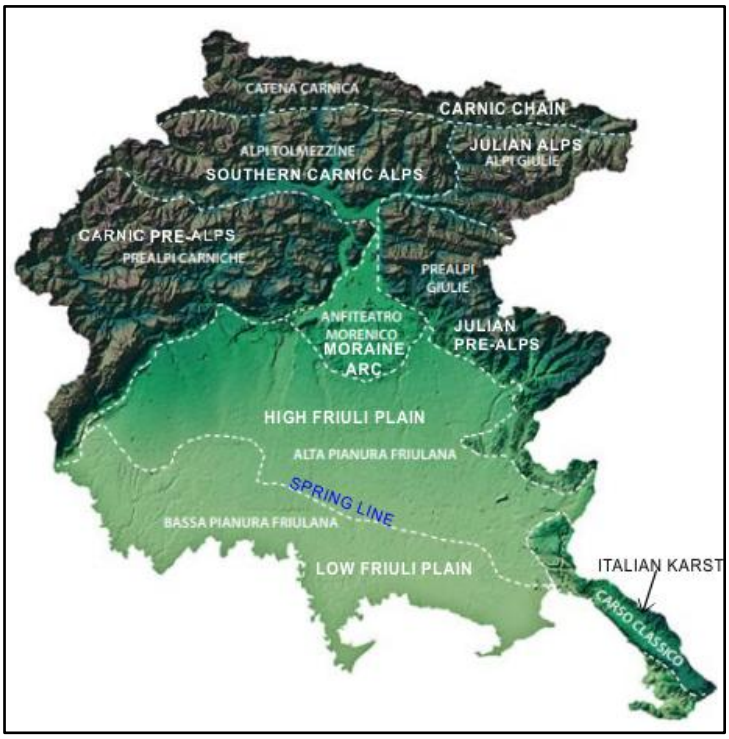

Fig. 35 - Topographic map of the Friuli Venezia Giulia showing the different orographic sectors, having also peculiar geological characteristics. From N to S. Carnic sector; Southern Carnic and Julian Alps; Carnic and Julian Pre-Alps; Moraine Arc; High and Low Friuli Plain; Karst on the south-eastern part. Adapted from (Cucchi, et al., 2009).

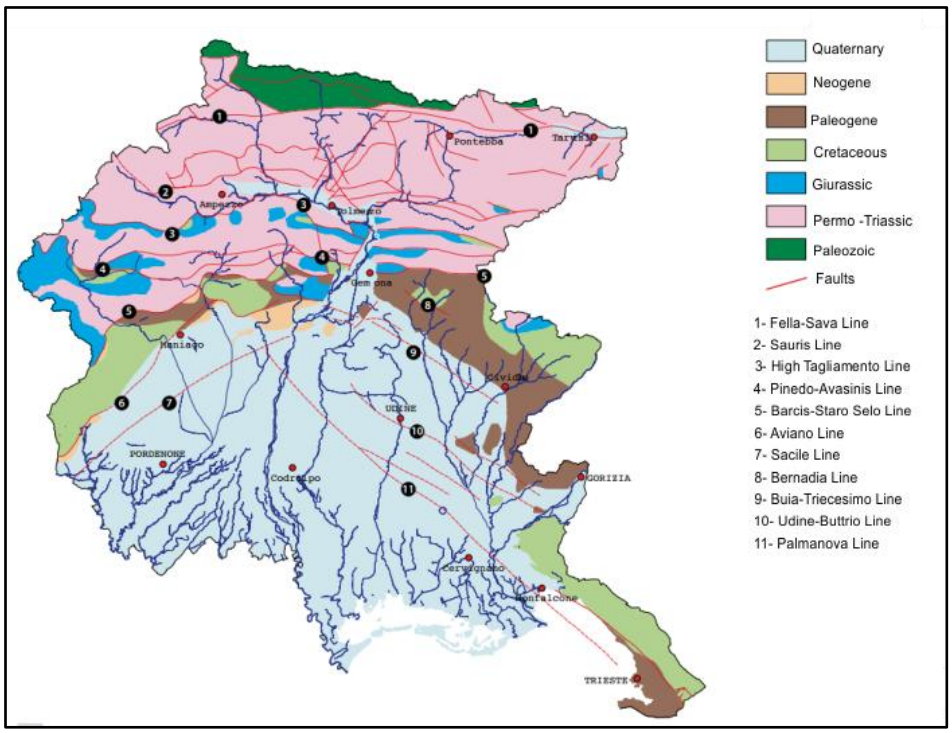

Fig. 36 – Simplified geological map of the Friuli Venezia Giulia Region (Carulli, 2006a) (Cucchi, et al., 2009). Note that the outcropping units are characterised by progressively younger lithologies moving southwards. The entire succession reflects an almost un-interrupted timing of deposition that spans from 460 My to Present.

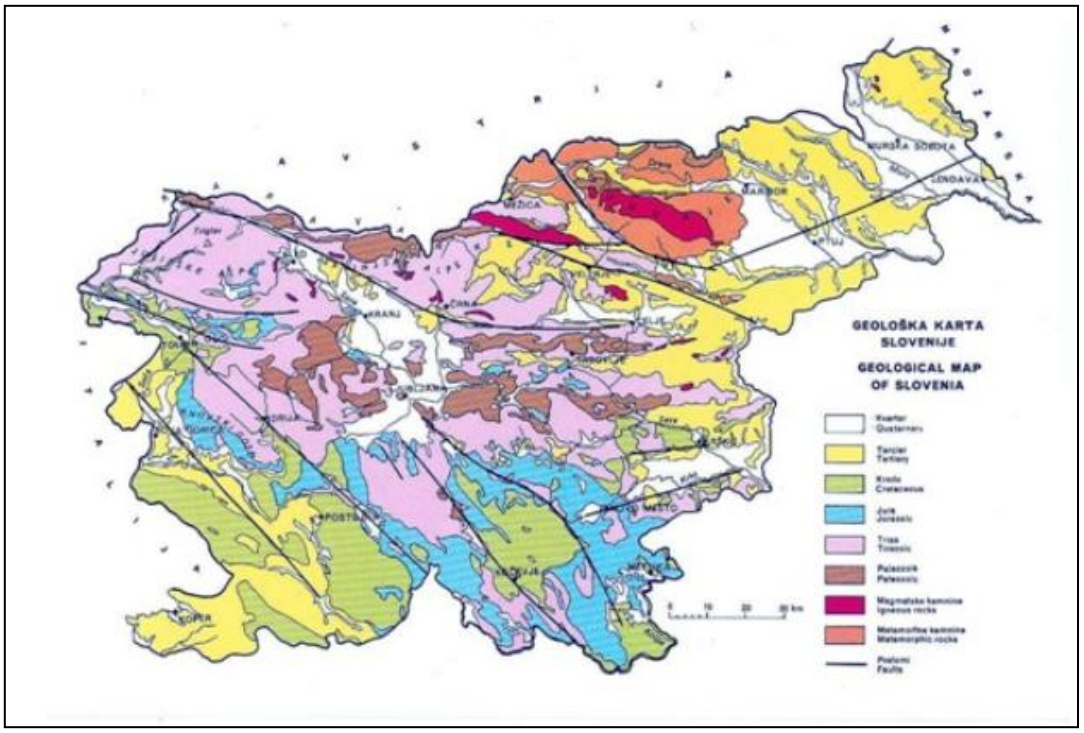

Fig. 37 – Simplified geological map of Slovenia. Note that, on the western part, the outcropping units are characterised by progressively younger lithologies . The entire succession reflects an almost un-interrupted timing of deposition that spans from the Paleozoic to Quaternary. (GeoZS, 2017)

The eastern onshore area adjacent to the gulf is characterised by the Classical Karst Plateau, (Fig. 35, Fig. 36, Fig. 37, Fig. 38, rising some hundred of meters above sea level (with a general deepening from S to N), where the thick sequence of the Mesozoic-Paleogene Friuli-Dinaric Carbonate Platform outcrops. Field studies identified its stratigraphic elements, reported inTab. 2 through both the Italian and Slovenian nomenclature. Moreover, in the SE part of the Karst, the Eocene terrigenous units of the Flysch outcrop (Tab. 2). This is made of alternation of silty marls and sandstones, with layers very variable in thicknesses. These deposits, as well as those characterising the Julian Pre-Alps and the Tolmin and Nova Gorica, are strongly disrupt by tectonics (e.g. (Tunis, et al., 2008) (GeoCGT-FVG, 2013) (Jurkovšek, et al., 2016)). In Fig. 39, it is reported a schematic representation of the lithostratigraphic units of the Meso-Cenozoic Friuli-Dinaric Carbonate Platform outcropping in the Italian Karst.
The carbonates are structured in the Karst anticline by the NE dipping Karst Thrust developed during the building of the External Dinarides (Fig. 38, Fig. 50, Fig. 51). The Karst Plateau extends in SW Slovenia and NE Italy, for 60 km and 15 km in NW-SE and SW-NE direction, respectively. It is bounded to the NW by the Isonzo River, to the NE by the Vipava valley (Flysch deposits), to the W and SW by the alluvial deposits of the Isonzo (Soča) River and the Gulf of Trieste, and to the E by the Reka River (Flysch of the Brkini area), to the S by the Čičarija region. It represents a world reference region for the study of karst morphologies (Cucchi, et al., 1989) (Jurkovšek, et al., 1996) (Jurkovšek, 2008) (Jurkovšek, 2010) (GeoCGT-FVG, 2013) (Jurkovšek, et al., 2016).

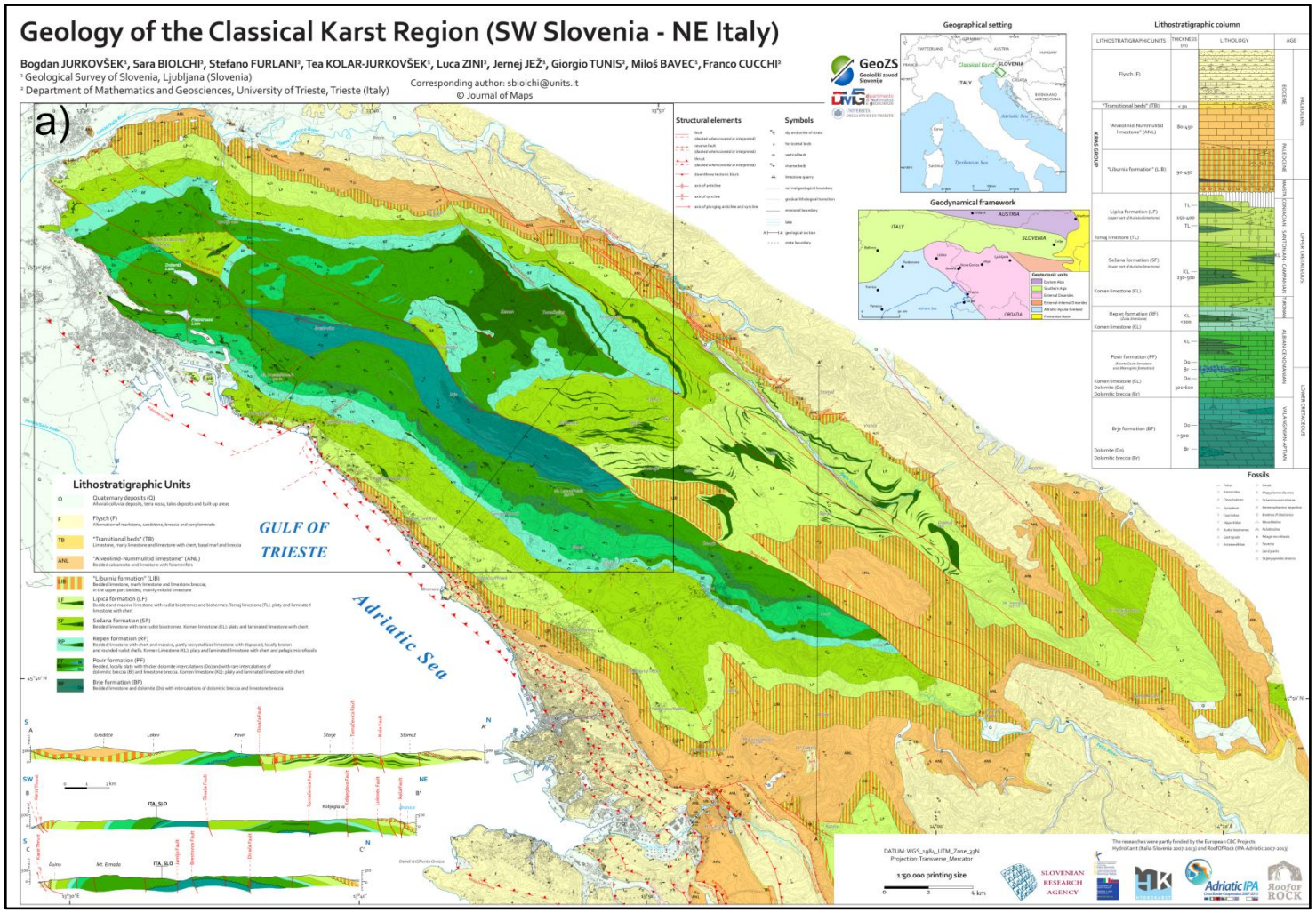

Fig. 38 - Geological map of the Karst, comprising SW Slovenia and NE Italy. A sequence of the Mesozoic-Paleogene Friuli-Dinaric Carbonate Platform outcrops. These carbonates are structured in the Karst anticline by the NE dipping Karst Thrust developed during the building of the External Dinarides. Moreover, Eocene Flysch units are present in the southern part. (Jurkovšek, et al., 2016). Zoom into area a) and geological profiles in Fig. 51.

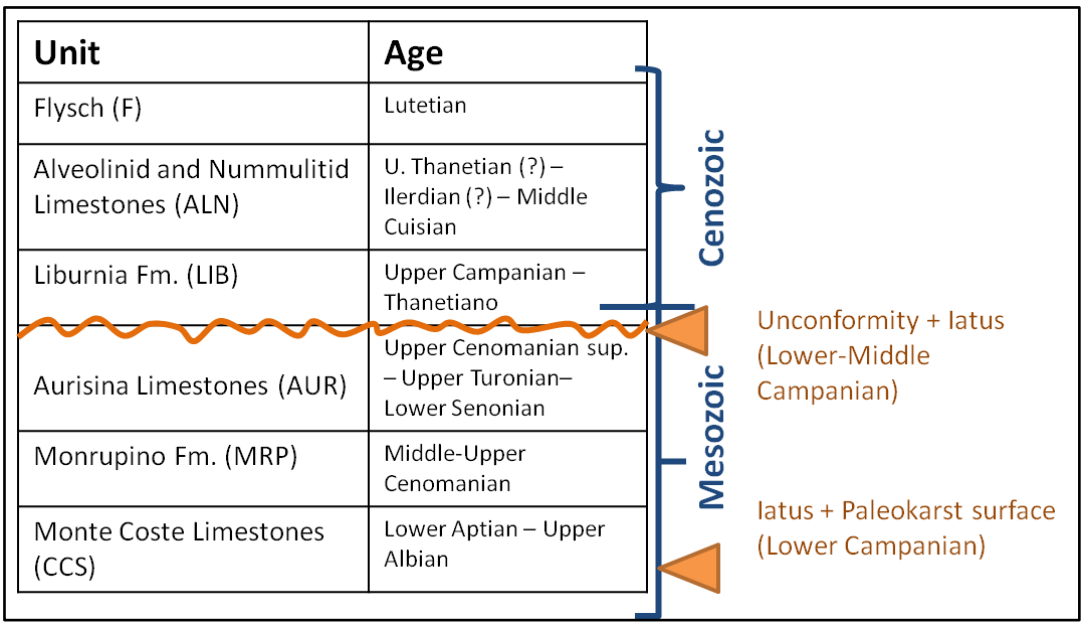

Fig. 39 – Schematic representation of the lithostratigraphic units of the Meso-Cenozoic Friuli-Dinaric Carbonate Platform outcropping in the Italian Karst, and Eocene turbiditic Flysch. Modified from (GeoCGT-FVG, 2013).

Eocene Terrigenous Unit - Karst		
Unit (Slovenian Literature)	**Unit (Italian Literature)**	**Description**
Flysch (F)	Flysch (F)	(Lutetian). It represent distal turbiditic sediments infilling the External-Dinaric foredeep. The marls intervals are millimetre to decimetre thick, while the arenaceous horizons span from centimetres to metre. Within the formation, arenaceous facies (FTa), marly sandtones (FT), pelitic facies (FTb) are defined. Internally to the FT, two sub-types are recognised: layers 1/2 m to 2 m thick (broadly present in the Muggia area); layers centimetre to decimetre thick. Rarely, FT shows complete Bouma sequences. Laminated intervals are quite frequent. The arenaceous content is composed by well classed grains (0.1-0.2 mm). Partly, arenaceous horizons are cemented by carbonate with rare feldspate, mica and heavy minerals. Their composition is 50% of silica (43-53% quartz, 6-11% flint), feldspate (18-26%) with dominant mica (4-6%), chlorite and muscovite, biotite and carbonate (16-20%); minor quantities (max 3%) of minerals such as Cr-spinel, glauconite, zircon). Carbonate clasts are present in the FT (re-worked Globigerina and mollusca). Marls are composed by micrite, clay, and a variable percentage of silt. Often rich in planctonic foraminifera (Globigerina). The lower limit of the Flysch corresponds to the beginning of the TB deposition. The upper limit is not identified in the Karst region. The Flysch outcropping in the Muggia Peninsula is characterised by uniform and horizontal stratification. In the rest of the area, the facies relationships are irregular, due to strong tectonic deformation.

Tab. 1 – Description of the Eocene terrigenous unit of the Flysch outcropping in the Karst. Compiled from (GeoCGT-FVG, 2013) (Jurkovšek, et al., 2016).

Meso-Cenozoic Friuli-Dinaric Carbonate Platform - Karst		
Unit (Slovenian Literature)	**Unit (Italian Literature)**	**Description**
Transitional Beds (TB)	Transitional Beds (TB)	(Lower Eocene). Hemipelagic marls, marly limestones and re-sedimented carbonates, characterized by glauconite and planktonic foraminifera. They represent the Eocene siliciclastic sediments deposited in the migrating foredeep of the Dinaric orogeny.
Alveolinid-Nummulitid Limestone (ANL):	Alveolinid-Nummulitid Limestone (ANL):	(Upper Paleocene-Lower Eocene). Middle slope Coral-algal limestone in the lower part. Bioclastic limestone with larger foraminifera occur in some layers (Thanetian), suggesting relatively deeper slope environment. Above these strata, typical ANL bio-facies association is present: benthic foraminifera such as alveolinids, nummulitids, orbitolitids and discocyclinids. The upper boundary is gradual or sharp, locally represented by hardgrounds. ANL thickness is variable, with a maximum of 350 m.
Liburnia formation (LIB)	Liburnia formation (LIB)	(Maastrichtian-Upper Paleocene). Limestones of shallow marine, brackish water environment. It was deposited on a paleo-karst relief during the Maastrichtian and Paleocene. Marine facies association: rudists and foraminifera (Rhapydionina Liburnica Stache). The K/T boundary is characterized by breccias with micritic matrix and Microcodium structures. The Paleocene parts of the formation are characterized by marly limestone with bivalves, tiny gastropods, ostracods, characeans and miliolids.

Meso-Cenozoic Friuli-Dinaric Carbonate Platform - Karst		
Unit (Slovenian Literature)	**Unit (Italian Literature)**	**Description**
Lipica Formation (LF): Sežana Formation (SF)	Aurisina Limestone (AUR)	(Upper Cenomanian – Upper Turonian– Lower Senonian) Lower part made of thick-bedded biomicrite deposited after a eustatic sea level drop in the Turonian, that established low energy environment. Fossils content: benthic foraminifera. It corresponds to Sežana Fm. The upper part is made of several types of bioclastic limestone. Bedded and massive biomicrites and biosparites with relatively large rudist fragments or entire shells. Keramosphaerina tergestina Stache also occur. Mostly deposited in the outer shelf. It corresponds to the Lipica Formation to 1000m of total thickness.
Repen Formation (RF) Povir Formation (PF)	Monrupino Fm. (MRP)	(Middle-Upper Cenomanian) It is made of inner platform limestones. The upper part has pelagic facies, the basal part has dolomitic tectogeno-diagenetic breccia bedded bituminous dolomite. Among the fossils, rudists, chondrodonts and foraminifera are present. Stratigraphic iatus at its base. It corresponds to the lower part of Repen Fm., except for its basal breccias that correspond to upper part of Povir Fm. The total thickness ranges between 200 and 500 m.
Povir Formation (PF)	Monte Coste Limestone (CCS)	(Lower Aptian-Upper Albian). It deposited after the reestablishment of shallow-marine conditions. It represents the oldest unit outcropping in the Italian Karst, along the State boundary. It is made of well stratified (metric) limestones with mudstone-wackestone alternation, reflecting low energy environment. It is affected by dolomitisation due to emersion phase related to tectonics (during Lower Cenomanian). Low content of fauna. The total thickness ranges between 350 and 400 m.
Brje Formation (BF)	Lower part of Monte Coste L. ?	(Valanghian-Aptian). It represents the basal unit of the Karst Plateau and outcrops only in the Slovenian part. It is made of bedded limestone with intercalation of dolostone breccias. It represents lagoon environment, with shallow water facies. Fossiliferous content is found in the upper part (e.g. Salpingoporella dinarica). The total estimated thickness is more than 500 m. Its top is depicted by erosion (iatus in the sequence) related to Aptian-Albian sea level drop

Tab. 2 - Description of the Meso-Cenozoic Dinaric Carbonate Platform units outcropping in the Karst. Compiled from (GeoCGT-FVG, 2013) (Jurkovšek, et al., 2016).

South of the Gulf of Trieste and the Karst Plateau, the Istria Peninsula extends through Slovenia and Croatia, from Čicarija to the Northern Adriatic Sea (Fig. 37, Fig. 40). From a geological point of view, it represents the north-western part of the Adriatic Platform (Frank, et al., 1983). It is mainly composed by outcropping carbonate rocks of shallow marine environment (Middle Jurassic-Eocene). The Mesozoic carbonates are subdivided in three mega-sequences (Fig. 40): Bathonian-Lower Kimmeridgian; Upper Tithonian-Upper Aptian; Upper Albian-Lower Campanian. Paleogene carbonates and turbiditic facies of the Flysch outcrop in the SW Slovenia and in the central part of

Croatia. They belong to the Paleocene-Eocene mega-sequence (Velić & Vlahović, 1994) (Velić, et al., 1995) (Vlahović, et al., 2005).
The Authors defined three regions on the basis of the outcropping lithologies.
The south and western Istria, with Jurassic-Cretaceous-Paleogene platform carbonates. In the area, the Buje Anticline, related to the Buje Fault, represents the front-most structure of the External Dinarides in Istria. The detachment level is settled in Permian-Triassic units (Placer, et al., 2010). Paleogene carbonates are here similar to those intercepted by the Grado-1 well (Cimolino, et al., 2010). The E and NE Istria (Plomin, Učka, Čičarija), characterised by Cretaceous-Paleogene carbonate-clastic sedimentation, affected by thrust faults. According to (Placer, et al., 2010), these belong to the Istria-Friuli Underthrust Zone, a NW-SE oriented Dinaric imbricated belt, characterised by the SW vergent thrusts as the Črni Kal, Petrinje, Hravstrovlje and Buzet thrusts). Moreover, at the Izola peninsula, along the Slovenian southern shoreline of the Gulf of Trieste, a Paleocene carbonate anticline outcrops, in correspondence of a tectonic window related to the Simon thrust, Fig. 52 (Placer, et al., 2010) (Poljak, et al., 2010).

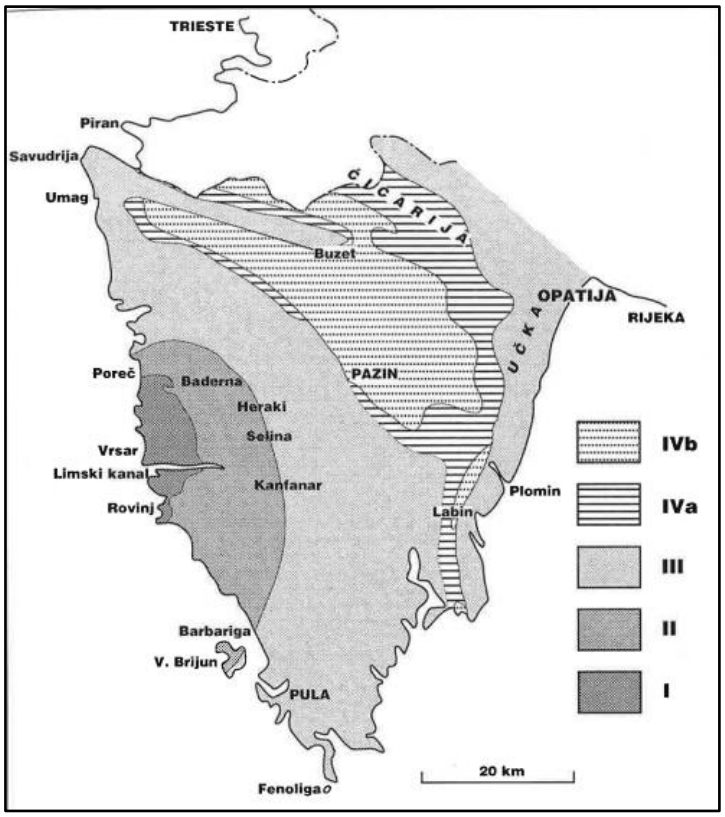

Fig. 40 – Map of Croatian Istria, showing areal distribution of the four outcropping mega-sequences: I- Bathonian-Lower Kimmerdigian carbonates; II- Upper Tithonian-Upper Aptian carbonates; III- Upper Albian-Lower Camapanian carbonates; IVa - Paleocene-Eocene carbonates; IVb- Paleocene-Eocene Flysch deposits (Velić, et al., 1995).

The buried sedimentary sequence characterising the Northern Adriatic sea and of the Friuli Plain has been investigated mainly by industrial and exploration wells, geothermal boreholes and offshore seismic data.
Twenty-five exploration wells were drilled by AGIP (Italian hydrocarbon Company, now ENI), (AGIP, 1972)(AGIP, 1977)(Cati, et al., 1987b) (AGIP, 1994), in the Veneto-Friuli plain and in the northern Adriatic Sea. Of these, three provide useful information to constrain the geological setting of the Gulf of Trieste since they are located some tens of kilometres from the study area.

The Cesarolo well, realised in 1960, and the Cavanella well, drilled in 1961, are located in the onshore adjacent to the north-western boundary of the gulf (Friuli Plain). The Amanda (Amanda 1 bis) is 20 km SW far from the Gulf of Trieste, in the centre of the Northern Adriatic sea, and it was executed in 1979. The three wells have a total depth (TD, depth where the drilling stopped) of: 4236 m, 1482 m, 7280 m, respectively (Fig. 41).
The detailed description, summarized by (Nicolich, et al., 2004a), of the drilled Permo-Meso-Cenozoic carbonate and Cenozoic terrigenous sequences is reported in Tab. 3 and Tab. 4. The carbonate units developed throughout the Paleozoic and the Mesozoic, their deposition, locally occurred also during the Paleogene. This resulted in a sequence with a total thickness higher than 3 km.
In particular, at the Grado Island facing the Gulf of Trieste there were drilled two exploration wells: Grado-1 e Grado-2. They were realised for the exploitation of the low-enthalpy geothermal energy (closed system) and they provide geological (cores and cuttings, with bio-stratigraphical analyses) and geophysical (log data) information (Fig. 41), that gave a further insights on the local stratigraphy and depth of the buried Meso-Cenozoic Friuli-Dinaric Carbonate Platform and of geothermal anomaly. In turn, these information allowed the characterisation of the geothermal reservoir, located in the structural highs of the carbonate platform, whose regional trend (Nicolich, et al., 2004a) (Ramella, et al., 2005)(Cimolino, et al., 2010) was previously defined by means of industrial wells and reflection seismic data available in the area (e.g. the OGS geophysical survey conducted in 2005).
The Grado-1 well was realised in 2008, on the beach in the western part of the town of Grado, about 100 m from the shoreline; it is 1110 m deep. The Grado-2 well was executed in 2015, on a structural high located in correspondence of the town centre; and it 1200 m deep. The two boreholes are about 1 km far from each other. In particular, the Grado-1 well was realised with the aim of a preliminary investigation of the potential of the geothermal resource, through the characterisation of the fluids and their circulation, along with the heat transfer and advection within the reservoir. The Grado-2 well was drilled to further define the geothermal production capacity and to complete the geothermal pilot plant conceived for the heating of public buildings. Thus, the geothermal district, actually, will provide geothermal water at 47-49° C transferring heat to the exchangers. The return water from the heat exchangers is collected and conveyed to the re-injection well into the same deep reservoir.
The stratigraphy along the wells was analysed and published by (Della Vedova, et al., 2008)(Cimolino, 2010)(Cimolino, et al., 2010) (Della Vedova, et al., 2014) (Piffer, et al., 2015), and is constituted by the following lithologies:

Recent fine sands (slightly cemented and locally with peat), characterised the most recent beaches.

Plio-Quaternary terrigenous sediments deposited in shallow marine, coastal and alluvial environment organized in several transgressive-regressive cycles and consisting of mainly sandy layers gravel and silt, with primary porosity extremely variable. Within the Holocene clay and silt sediments (with low permeability), gravel and sandy-silty beds, with fossil fragments, are present (with relatively higher permeability). These latter, in particular, lie at interval depths of 30-35 m (sands-gravels) and 75-80 m (silt-sands-peat), 110-115 (sands-silt-peat), 160-195 m (coarse sands), 222-260 (gravel-sands). Each of them represent aquifers. The base of the interval is characterised by clays and silt highly

cohesive. The thickness of the entire interval is 290 m and 255 m at the Grado-1 and Grado-2, respectively.

Neogene marl intervals and minor sandstones, with neritic and pelagic fossiliferous content, ascribed to Alpine Molassa of Oligo-Miocene age. These sediments deposited in shallow marine environment and are characterized by low matrix permeability, but locally affected by systems of fractures and faults. The sequence was intercepted at depths intervals of 290-530 m and 260-520 m at the Grado-1 and Grado-2, respectively.

Paleogene turbidites (Eocene Flysch) consisting of distal green marls with glauconite components, similar to the green marls recognised above the contact with the Paleogene carbonates outcropping in the Istria peninsula. The Flysch sediments are rich in deep sea pelagic fauna and are characterised by low to very low permeability. The unit lies between 530 and 616 m of depth, at the Grado-1 and between 520 m and 630 m of depth, at the Grado-2.

The top of the carbonate platform is at the depths of 616 m and 630 m in the Grado-1 and Grado-2, respectively. The upper part of the platform consists of a thick interval of Paleocene and Lower Eocene shelf carbonates, with typical Alveolinidae-Nummulitidae-Orbitolites association. This interval has a thickness of about 380-390 m.

At about 1007 to 1010 m of depth, high Uranium's peaks, also recognized offshore in the northern Adriatic oil wells, identified the carbonate Cenozoic-Mesozoic (K/T) transition in both the boreholes. Paleogene and Cretaceous carbonates, at their contact, show karst phenomena and erosion, that are evidences of subaerial exposure.

From the K/T transition down to the boreholes TDs, the Cretaceous Carbonates show dolomitisation of fossiliferous mudstone-packstone (peloids, bioclats, Miliolidae, calcareous algae). At the TD of the Grado-1 well, the fauna association indicates Maastrichtian age.

The significant thickness of the Cenozoic Carbonate layer suggests the presence of a tectonic duplex Paleocene-Lower Eocene interval, linked to a NW-SE oriented reverse fault and affected by open fractures, probably representing an active outer deformation front of the Dinaric thrust system. This feature involves also the Eocene and Miocene deposits of Flysch and Molasse and, with minor structures, the uppermost layers (Cimolino, 2010)(Cimolino, et al., 2010).

Within the Meso-Cenozoic Carbonates, the intervals with higher permeability, constituting the geothermal reservoir with confined aquifers, are located in Grado-1 at depths ranging between 725-750 m in correspondence of the fractured interval of the Paleogene Carbonates, and at 990-1025 m of depth at the Meso-Cenozoic Carbonate contact, both in Grado-1 and Grado-2 (Cimolino, et al., 2010) (Della Vedova, et al., 2014) (Piffer, et al., 2015).

The geochemical analyses indicate that the brackish waters of the aquifers, chemically sodium chlorinated, belong to an anoxic sea, more than 10 million years old. This suggests that the geothermal water circulates through a complex permeable network from the Cretaceous to the youngest Paleogene carbonate. Waters have a salinity higher than 30 ‰ and a temperature of 42 °C, increasing with depth, at the Grado-1 well and of 49.5 °C at the bottom of the Grado-2 well. The estimated volume of the reservoir is 75-100 km³ (Della Vedova, et al., 2014).

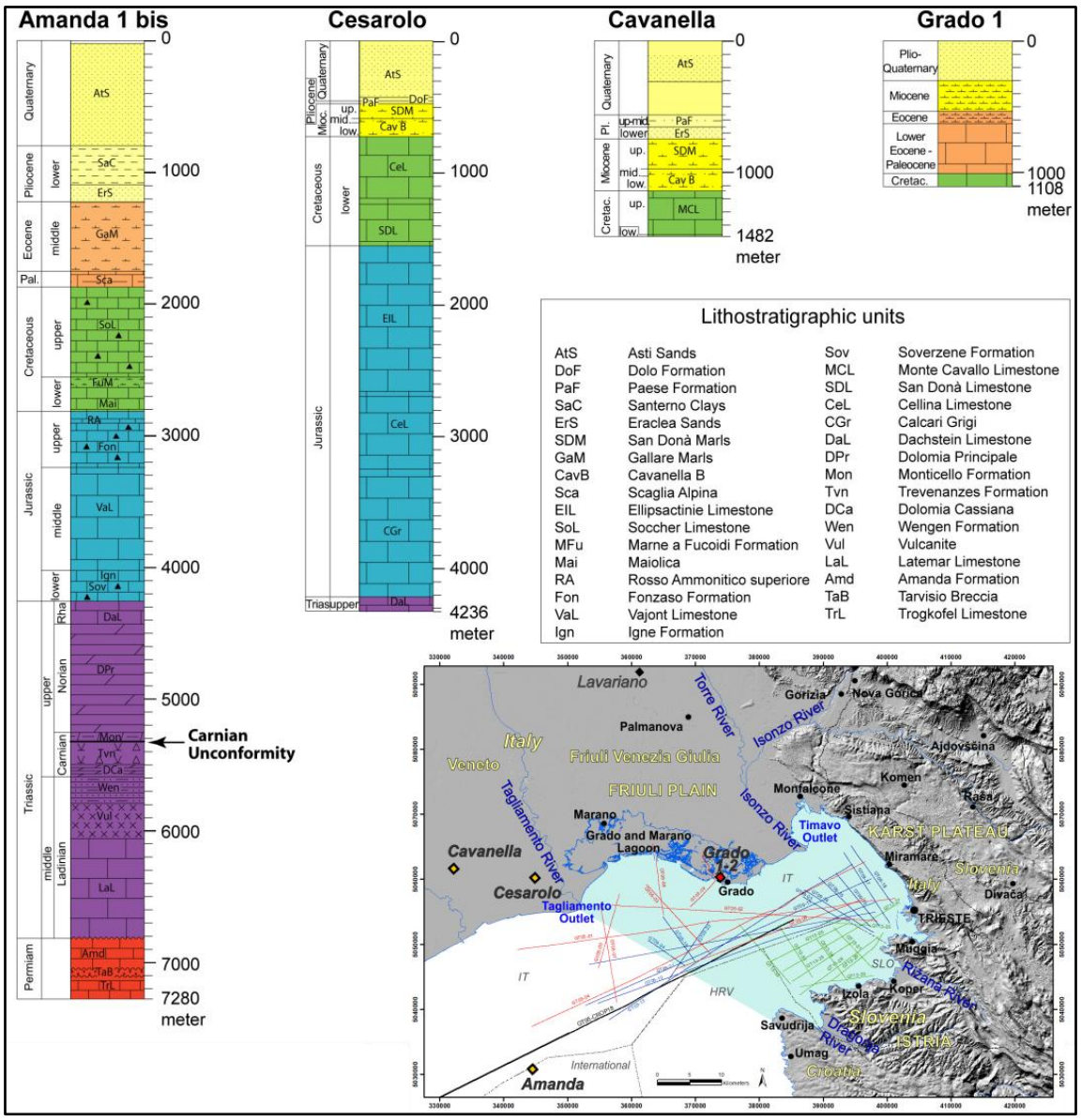

Fig. 41 – Stratigraphy of the three industrial and exploration wells executed by AGIP (Italian hydrocarbon Company, now ENI), located nearby the Gulf of Trieste. From left to right: Amanda 1 bis, drilled in 1979 in the Northern Adriatic offshore; Cesarolo and Cavanella realised in the Friuli Plain in 1960 and 1961, respectively. In the figure, to the top-left it is also represented the stratigraphy of the geothermal well Grado 1, drilled in 2008. Location of the wells in the map, with squares: Amanda, Cesarolo and Cavanella, in yellow; Grado1 (and 2) in red. (Busetti, et al., 2010b), modified from (AGIP, 1972)(AGIP, 1977) (AGIP, 1994) (Cimolino, 2010).

Permo-Meso-Cenozoic Carbonate Sequence	
Lithological Unit	**Description**
Trogkofel limestone (TrL)	(Upper Permian). Formation of limestones, marls and dolomitic limestones, with abundant fossiliferous content like algae and briozoas. Intercepted by the Amanda 1 bis well between 7280 m (TD) and 7130 m. Its top surface is erosional.
Tarvisio Breccia (TaB)	(Upper Permian). Unit composed of carbonatic clasts of the eroded TrL, lying underneath with angular unconformity. Intercepted by the Amanda 1 bis well between 7130 and 7070 m. Its top surface is erosional.
Amanda Formation (Amd)	(Upper Permian). Composed by platform carbonatic facies, indicating the onset of marine environment. Intercepted by the Amanda 1 bis well between 7070 and 6840 m. Its top surface is erosional.
Latemar Limestone (LaL)	(Middle Triassic, Upper Ladinian). Reef limestones and dolostones. Intercepted by the Amanda 1 bis well between 6840 and 6085 m.
Vulcanite (Vul)	(Middle Triassic, Upper Ladinian). Submarine basic lavas, showing pillow-shapes and dykes. Intercepted by the Amanda 1 bis wells between 6085 and 5800 m and by two others industrial boreholes in the Veneto-Friuli Plain (Cargnacco 1, Ballan 1).
Wengen Formation (Wen)	(Middle Triassic, Upper Ladinian). Hyaloclastite (hydrated tuff-like breccia rich in volcanic glass, formed during volcanic eruptions under water) at its lower part; followed by sandstones, marls and clays mainly of volcanic origin. These represent erosional deposits from the sub-aerial exposure of the volcanic areas. Intercepted by the Amanda 1 bis well between 5800 and 5621 m.
Dolomia Cassiana (DCa)	(Upper Triassic, Carnian). Reef carbonates developed above the terrigenous deposits of Wen. Intercepted by the Amanda 1 bis well between 5621 and 5530 m.
Raibl Group (GRb)	(Upper Triassic, Carnian). Heterogeneous conglomerates, dolostones and evaporite rocks. Its topmost boundary represents the Carnian Unconformity. The Travenanzes Formation (Tvn), made of sands, marls and clays with various colors, was intercepted by the Amanda 1 bis well, between 5530 and 5320 m. Tvn was drilled also by the Cargnacco 1 and Assunta 1 wells.
Monticello Formation (Mon)	(Upper Triassic, Upper Carnian-Lower Norian). It is characterised by cyclic sequences of grey dolostones, intercalated by pelitic layers locally rich in organic matter. Subtidal-lagoon environment. It is always present at the base of the DPr. Intercepted by the Amanda 1 bis well between 5320 and 5260 m. Drilled also by the Cargnacco 1 and Ballan 1 wells.
Dolomia Principale (DPr)	(Upper Triassic, Norian). Organised in peritidal cycles of homogenous white dolostones blocks (with Megalodon and gastropods), alternated with dolostones stratified layers with traces of pedogenetic structures. Tidal flat and lagoon depositional environment. The peculiar facies succession indicate precipitation at gradually shallower depths with temporary sub-aerial exposure. Intercepted by the Amanda 1 bis well between 5260 and 4420 m. Drilled also by the Cargnacco 1 and Ballan 1 wells.

Permo-Meso-Cenozoic Carbonate Sequence	
Lithological Unit	**Description**
Dachstein Limestone (DaL)	(Upper Triassic, Norian-Rhaetian). It is made of grey-brownish micritic limestones deposited at shallow depths. Thick stratifications with big Bivalvia. Intercepted by the Amanda 1 bis and Cesarolo wells at depths ranges of 4420-4250 m and 4236 (TD)-4200 m, respectively. Drilled also by the Ada 1 bis and Assunta 1 wells. They show peritidal sequences, similar to those of the DPr, with intraclast intervals containing Megalodon, stromatolites and dissolution structures. These deposits overlain the DPr, although the two units are heteropic in some areas.
Triasina Unit (Tr.na)	(Upper Triassic, Rhaetian). Dolostone (found at the Cargnacco 1 well) correlated to similar facies in the Amanda 1 bis well. Containing mainly foraminifer Triasina Hantkeni.
Calcari Grigi (CGr)	(Lower-Middle Jurassic). Mainly characterised by grey-brownish fine grained limestones in banks or strata of lagoon environment. Intercalations of bioclastic and oolite limestones. They indicate shallow water deposition in carbonatic platform adjacent to oolite reefs. Intercepted by the Cesarolo at depths 4200-3250 m. Drilled also by the Cargnacco 1 and Ballan 1 wells. They are heteropic with the Soverzene Formation.
Soverzene Formation (Sov)	(Lower-Middle Jurassic). It is composed of grey-brown flint limestones, often dolomitized. Frequent turbiditic intercalations, related to a syn-sedimentary rifting stage. Intercepted by the Amanda 1bis at depth interval 4250-4100 m (Lower Jurassic). Drilled also by the Ada 1 bis and Assunta 1 wells. This deposit is typical of transitional and basinal environment. It lies above the DPr, but in the distal basinal sectors it buries the CGr.
Igne Formation (Ign)	(Lower Jurassic, Toarcian). Flint limestone-marlstone with various colours, well stratified containing ammonoidea. Intercepted by the Amanda 1 bis well at depths 4100-4050 m. Drilled also by the Ada 1 bis. This formation lies directly on the Sov Formation and represents the prosecution of the basinal sedimentation of the prior cycle.
Vajont Limestone (VaL)	(Middle Jurassic). They are mainly made of oolite limestone with thin intercalations of micritic limestones with radiolaria. Intercepted by the Amanda 1bis at depth interval of 4050-3200 m. Drilled also by the Sedico 1 and Ada 1 bis wells. The unit is the result of sedimentation of neritic deposits from the margin of the Friuli Platform; while the fine layers represent basinal deposition.
Cellina Limestone (CeL)	(Middle and Upper Jurassic-Lower Cretaceous). It is made of well stratified limestones of lagoon and tidal flat. The colour varies from white to grey to brownish; it contains scarce macrofossils and shows frequent structures indicating phases of emersion, with breccias and stromatolites. Intercepted by the Cesarolo well at depth intervals of 3250-2700 m (Jurassic) and 1250-700 m (Lower Cretaceous). Drilled also by the Arcade 1, Nervesa 1, Cargnacco 1 and S. Donà di Piave 1 wells. They are heteropic with the EIL and in the upper part they turn into the Monte Cavallo or Monrupino limestones.

Permo-Meso-Cenozoic Carbonate Sequence	
Lithological Unit	**Description**
Fonzaso Formation (Fon)	(Upper Jurassic, Oxfordian-Kimmeridgian). Mainly made of fine grained and well stratified micritic limestones, rich in flint nodules with abundant radiolaria. Intercepted by the Amanda 1 bis at depth interval of 3200-2900 m. Drilled also by the Sedico 1 and Ada 1 bis wells. The thickness of Fon becomes greater towards the eastern margin of the basin, where calcarenite and calcirudite layers, related to turbidites come from the margin of the Friuli Platform.
Ellipsactinie Limestone (EIL)	(Upper Jurassic, Oxfordian-Kimmeridgian). Breccia and bioclastic limestones, that from the internal platform turn into the CeL; they represent reef facies. Intercepted by the Cesarolo at depth interval of 2700-1550 m. Drilled also by the Span 1 and S. Donà di Piave 1 wells. This unit is found at the Bernadia 1 well (north of Udine, in the Julian Pre-Alps), where it overthrusts the Grivò Flysch, due the Dinaric deformation.
San Donà Limestone (SDL)	(Upper Jurassic-Lower Cretaceous). Bioclastic limestones with corals and mollusca. These are typical deposits of platform margin. Intercepted by the Cesarolo at depth interval of 1550-1250 m (Lower Cretaceous). Drilled also by Merlengo 1 and S. Donà di Piave 1 wells.
Rosso Ammonitico superiore (RA)	(Upper Jurassic, Upper Kimmeridgian-Lower Titonian). Flint limestones showing nodular aspect and grey-red colour. Intersected by the Amanda 1 bis at depth interval of 2900-2800 m. Drilled also by the Sedico 1 and Ada 1 bis wells. It is a condensed interval related to a phase of minor sedimentary supply.
Maiolica (Mai)	(Upper Jurassic-Lower Cretaceous, Upper Titonian-Barremian). Limestone well stratified, fine grained, brown-gray colour, with flint nodules. Intercepted by the Amanda 1 bis at depth interval of 2800-2650 m. Drilled also by the Sedico 1, Ballan 1, Ada 1 bis, Assunta 1 and Amira 1 wells. Mai is the product of the deposition of mud and microcrystalline carbonate in the pelagic basins.
Soccher Limestone (SoL)	(Upper Jurassic-Cretaceous). Mudstones rich in dark-red flint, interbedded by marls, calcarenites, calcirudites ad and of sediments brought from the Friuli platform. Intersected by the Amanda 1 bis at depth interval of 2500-1900 m (Upper Cretaceous). They represent typical deposits of the marginal areas of the pelagic basin; they are heteropic with Mai.
Marne a Fucoidi Fromation (FuM)	(Lower cretaceous, Aptian-Albian). Marls with very this stratifications, with variable color. Intersected by the Amanda 1 bis at depth interval of 2650-2500 m. Drilled also by Sedico 1, Ballan 1, Ada 1 bis, Assunta 1 and Amira 1 wells.
Bonarelli Level (LB)	(Turonian). Guide-level indicating anoxic conditions. Found at the Sedico 1 well (Belluno).

Permo-Meso-Cenozoic Carbonate Sequence	
Lithological Unit	**Description**
Scaglia Alpina (Sca)	(Aptian-Lower Eocene). Calcareous mudstones, green marls, calcirudites and breccias. It is composed by alternation of in-situ and resedimented neritic deposits. Starting from the Upper Cretaceous, siliciclastic materials of the Flysch arrived from the neighbouring areas. Intersected by the Amanda 1 bis at depth interval of 1900-1750 m. Drilled also by the Volpago 1, Sedico 1, Ballan 1, Ada 1 bis, Assunta 1, Amira 1, and Eraclea 1.
Monte Cavallo Limestone (MCL)	(Upper Cretaceous, Cenomanian–Campanian). This formation is made of white biocastic limestones, well stratified. They contain fauna assocation of rudists, representing platform margin facies. They are heteropic with Monrupino and Aurisina Limestones. Intercepted by the Cavanella well at depth interval of 1482(TD)-1150 m. Drilled also by the S. Stino 1, where they lie above the Cellina Limestone.
Scaglia Cinerea (ScaC)	(Paleocene-Eocene). It is made of grey marly limestones and grey marls with clay content. It is heteropic with the upper part of the Scaglia Alpina. As concerns its terrigenous-pelitic fraction, it is considered as a pre-Flysch deposit with respect to the overlain Flysch. Drilled by the Ballan 1, Sedico 1, Paese 1, Eraclea 1, Jesolo 1 and S. Stino 1 wells.

Tab. 3 – Description of the sedimentary units characterising the Permo-Mesozoic Carbonate Sequence drilled by the industrial exploration and geothermal wells, in the Northern Adriatic and Friuli Plain. The entire stratigraphy identified at the Amanda 1, Cesarolo, Cavanella and Grado-1 boreholes is represented in Fig. 41. (Nicolich, et al., 2004a).

Cenozoic Terrigenous Sequence	
Lithological Unit	**Description**
Masarolis Flysch (MaF)	(Middle-Upper Paleocene). It is mainly arenaceous and characterised by carbonate clasts. Drilled by the Span 1 well.
Grivò Flysch (GrF)	(Upper Paleocene-Lower Eocene). Composed of siliciclastic and carbonate turbidites with carbonate strata. Drilled by the Span 1 and Bernadia 1 wells. It originated from huge carbonate submarine landslides. In some locations (e.g. at the Bernadia 1 well) it is in angular unconformity with the Meso-Cenozoic Carbonate Platform.
Cormons Flysch (CoF)	(Lower-Middle Eocene). It is made of pelitic-arenaceous alternations, with rare carbonate layers. It contains flint and quartz clasts, that turn into deltaic deposits towards the top. Drilled by the Cargnacco 1 well.
Clauzetto Flysch (ClF)	(Lower Eocene). Grey marls alternated by clay marls, rich in planctonic foraminifera content. In the upper part, arenaceous and carbonatic layers are present. Drilled by the Gemona 1 well. It represents a unit that deposited during the long-lasting Eocene turbiditic phases.
Jesolo Flysch (JeF)	(Upper Eocene). Deposited, by weak siliciclastic-turbiditic cycles, S of the southern margin of the Friuli Platform. Drilled by Eraclea 1 and Jesolo 1 wells.
Belluno Flysch (BeF)	(Eocene). Typical turbiditic deposit made of alternated arenaceous and marly strata. This latter contains also bio-calcarenites and calcirudites. Drilled by the Volpago 1 and Sedico 1 wells. The unit is younger towards W, due to the migration of the depocenter of accomodation basin related to the migration of the Dinaric thrusts front.
Possagno Marls (PoM)	(Middle-Upper Eocene). Marls without any content of coarse clasts. Volpago 1, Eraclea 1 and Jesolo 1 wells.
Gallare Marls (GaM)	(Middle Eocene-Miocene). Layers of marls or clays, with thinner arenaceous beds, related to turbiditic deposits. They sedimented between neritic and batial environment. Intercepted by the Amanda 1 bis well, at depth interval of 1750-1200 m (Middle Eocene). Drilled by the Paese 1, Merlengo 1, Arcade 1, Volpago 1, Assunta 1 and Amira 1 wells.
Cavanella Group (Cav)	(Oligo-Miocene, Chattian-Langhian). Terrigenous-carboante platform deposits (outcroppin in the Pre-Alps), rich in glauconite. The group is subdivided into the Cavanella A (CavA) of the Chattian-Aquitanian and the Cavanella B (CavB) of the Burdigalian-Langhian. This latter is intercepted by the Cavanella and Cesarolo wells at depth intervals of 700-600 m and 1150-1000 m, respectively. Cav is drilled also by the Paese 1, Merlengo 1, Arcade 1, Nervesa 1, Volpago 1, Gemona 1, Lavariano 1, Ballan 1, Ada 1 bis, Eraclea 1, Jesolo 1, S. Donà di Piave 1 and S. Stino 1.

Cenozoic Terrigenous Sequence	
Lithological Unit	**Description**
San Donà Marls (SDM)	(Upper Miocene, Tortonian). Cemented marls and sands, with minor clay content. This indicates the clastic progradation. Intersected by the Cavanella and Cesarolo wells at depth intervals of 1000-750 m and 600-450 m, respectively. Drilled by the Paese 1, Merlengo 1, Arcade 1, Nervesa 1, Volpago 1, Gemona 1, Lavariano 1, Ballan 1, S. Donà di Piave 1 and S. Stino 1 wells.
Montello Conglomerates (MoC)	(Miocene, Tortonian - Messinian). They are made of limestones and dolostones, intercalated by sands and silt with organic matter. Drilled by the Paese 1 dir, Merlengo 1, Arcade 1, Nervesa 1, Volpago 1 and Gemona 1 wells. This formation is related to trasgressive-regressive (T-R) cycles.
Eraclea Sands (ErS)	(Lower Pliocene). Mainly made of sandy deposits, with intercalations of clays. Intercepted by the Amanda 1 bis and Cavanella wells at depth intervals of 1200-1100 m (where they lie above the GaM) and 750-650 m (where they lie above the SDM), respectively. Drilled by the Ballan 1, Lido 1, Assunta 1, Rachele 1, Eraclea 1, Jesolo 1, S. Donà di Piave 1 and S. Stino 1 wells.
Gisella Sands (GiS)	(Lower Pliocene). They are mainly made of sandy and silty sediments. Drilled by Assunta 1 and Amira 1 wells.
Santerno Clays (SaC)	(Lower Pliocene-Pleistocene). It is made of fine and dark (gray-green) clays, locally intercalated by sandstone and sandy layers. Intersected by the Amanda 1 bis well at depth interval of 1100-800 m, directly above the Eraclea Sand. Drilled by the Ada 1 bis, Assunta 1, Rachele 1 and Amira 1 wells.
Lido Formation (LiF)	(Lower Pliocene-Pleistocene). Limesones testifying the presence of small carbonate platforms. Drilled by the Lido 1 and Assunta 1 wells, in correspondence of the peripheral high of the Venetian coast.
Paese Formation (PaF)	(Quaternary). Formation with prevailing clay matrix, interbedded by sands. Drilled by the Paese, Merlengo 1, Ballan 1, Lido 1, Eraclea 1, Jesolo 1, S. Donà di Piave 1 and S. Stino 1. Intercepted by the Cavanella 1 and Cesarolo wells at depth intervals of 650-550 m (above the Eraclea Sands) and 450-425 m (above the San Donà Marls), respectively.
Dolo Formation (DoF)	(Quaternary). It is composed mainly by a sandy matrix, intercalated by gravel beds. Drilled by the Paese 1, Merlengo 1, Arcade 1, Nervesa 1,Volpago 1, Lido 1, Eraclea 1, Jesolo 1, S. Donà di Piave 1 and S. Stino 1 wells. Intercepted by the Cesarolo well at depth interval of 425-400 m (above the Paese Formation).

Cenozoic Terrigenous Sequence	
Lithological Unit	**Description**
Asti Sands (AtS)	(Pleistocene). Clayely sand, sandy clays and silt. Gradually passing from one litotype to the other. These deposits show shallow marine deposition during the filling of the accomodation spaces in the basins. Intersected by the Amanda 1 bis, Cesarolo and Cavanella 1 at depth intervals of 800-0 m, 425-0 m, 550-0 m, respectively. Drilled by the Paese 1, Lavariano 1, Ballan 1, Eraclea 1, Jesolo 1, S. Donà di Piave 1 and S. Stino 1.
Carola Formation (CaF)	(Pleistocene). It is present within the Asti Sand. It is made of clays and sands. Drilled by the Ada 1 bis, Lido 1, Assunta 1, Rachele 1 and Amira 1 wells.
Ravenna Formation (RaF)	(Pleistocene). This formation is part of the Asti Sand and it is mainly made of sands. Drilled by the Merlengo 1, Ada 1 bis, Lido 1, Assunta 1, Rachele 1 and Amira 1 wells.

Tab. 4 - Description of the sedimentary units characterising the Cenozoic terrigenous sequence drilled by the industrial exploration and geothermal wells, in the Northern Adriatic and Friuli Plain. The entire stratigraphy identified at the Amanda 1, Cesarolo, Cavanella and Grado-1 boreholes is represented in Fig. 41. (Nicolich, et al., 2004a).

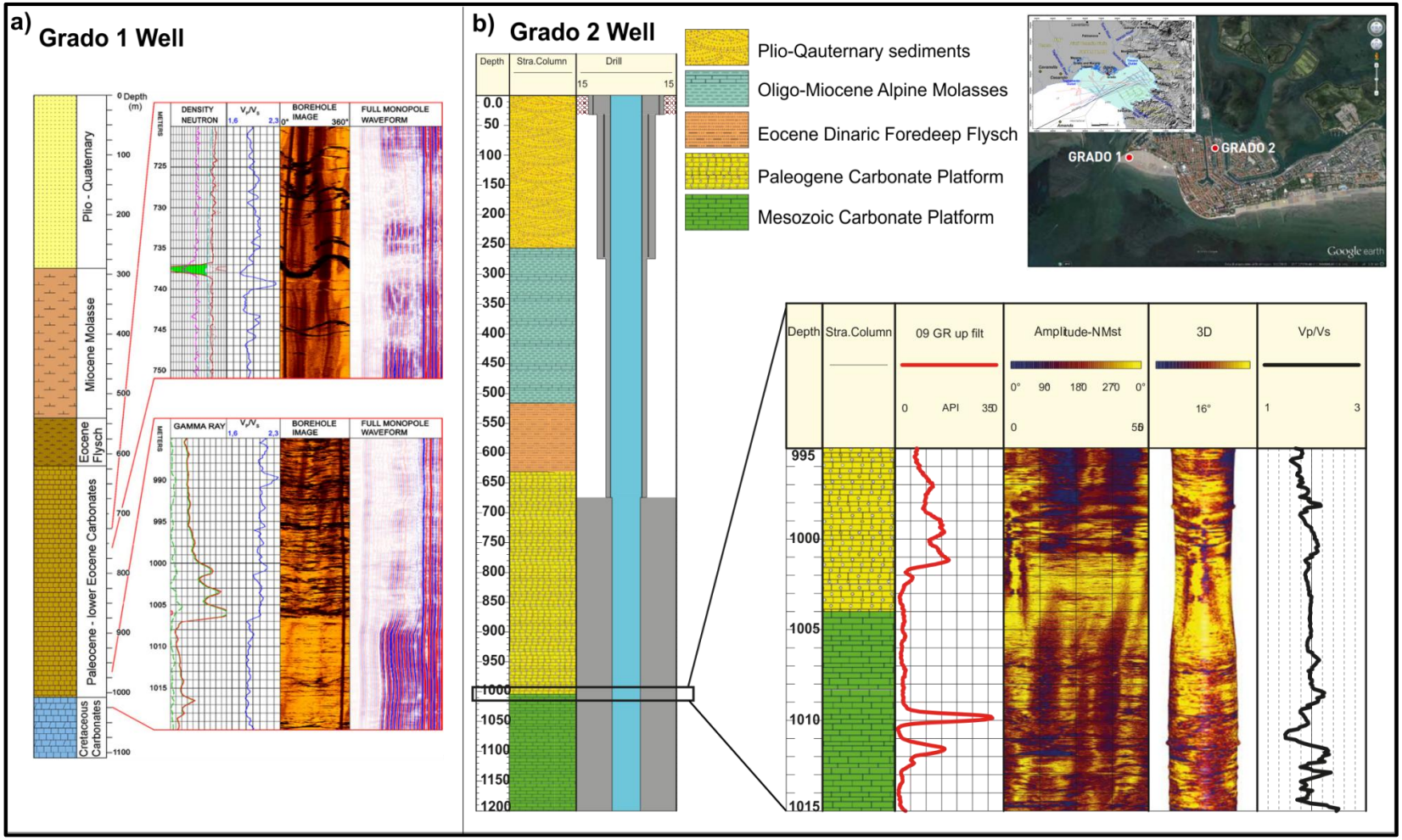

Fig. 42 – Stratigraphy and details of borehole logs of the a) Grado-1 well and b) Grado-2 well. As concerns the Grado-1, the main fracture zone in the Palaeogene carbonates is located at -736 m, depicted by a negative pick in the neutron density log, by a positive pick of Vp/Vs ratio from sonic log, by the acoustic image and by the full waveforms attenuation (P, S and Stoneley waves) obtained by a monopole source. The Paleocene-Mesozoic contact, at depth of 1007 m and 1010 (Grado1 and 2, respectively) is evidenced by the uranium peaks in the gamma ray log near the base of Paleocene (K/T transition). Location of the Grado-1 and Grado-2 boreholes at the top-rigth of the figure. Adapted from(Cimolino, et al., 2010) (Piffer, et al., 2015).

The offshore sedimentary sequence of the Northern Adriatic has been reconstructed also by means of on multichannel seismic reflection profiles.
The deep penetration MCS reflection profile CROP-M18 (recorded by the R/V OGS Explora in 1995), provides deep crustal tectono-stratigraphic information in the Northern Adriatic Sea (Finetti & Del Ben, 2005). The line strikes NE-SW for 97 km (20 km are located in the GT), and is calibrated by the Amanda 1 bis industrial well, about 2 km south of the central part of the line (Fig. 43). The Authors interpreted several seismic horizons, along with tectonic structures: Quaternary base (A_0), Plio-Quaternary base (A), Miocene base (C), top Eocene (E), top Carbonate (K), top Maiolica (M), top Jurassic (J), top Dolomia Principale (T_1), Middle Triassic Unconformity (T_x), Basement (Z), Top Lower Crust (TL), Moho (MO).
A_0, C, E are horizons with more local significance than the others, that can be interpreted also along other CROP profiles of the Adriatic.
The thickness of the sedimentary sequence ranges from 3 to 5 s (twt) in the east (the GT) and the West, respectively. Whereas, the upper crust (UC) and lower crust (LC) are relatively thicker in the GT area (6.8 s twt, about 20 km), while they thin towards West. Permo-Triassic and Lower Jurassic rifting faults were also interpreted as related to left transcurrent kinematics (in the western area). In the GT (E of the margin platform), the Carnian Unconformity (T_x) is identified at about 2 s twt, the top of the Meso-Cenozoic carbonates (K) at 0.6-0.7 s twt. Both the surfaces deepen towards the W, after the margin of the platform.

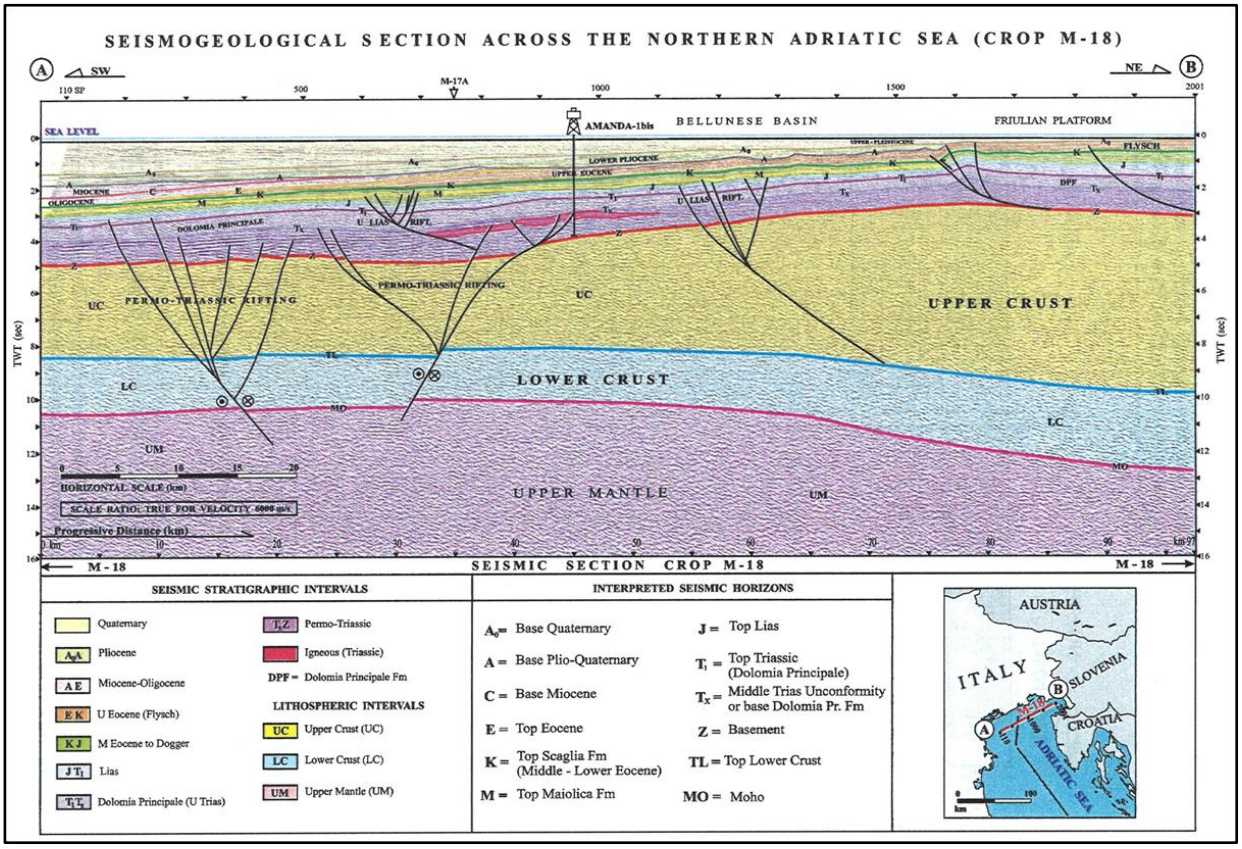

Fig. 43 – Interpreted deep crustal profile (CROsta Profonda) CROP-18, along the Northern Adriatic Sea. The NE part (20 km) is located in the GT. It provides information about the sedimentary sequence, the deep crustal intervals and the tectonic structures (Finetti & Del Ben, 2005).

More into detail, within the North-Eastern Adriatic Sea, higher resolution multichannel seismic profiles allowed the identification of the following seismic units and surfaces, Fig. 44, according to (Busetti, et al., 2008) (Busetti, et al., 2010a) (Busetti, et al., 2010b) (Busetti, et al., 2013):

Carnian Unconformity: (Upper Triassic). It marks the base of the Dolomia Principale. Encountered by the Amanda1 bis well, at a depth of 5340 m. According to (Poli & Zanferrari, 2008), it constitutes one of the detachment surface of the thrust systems.

the Mesozoic-Paleogene Friuli-Dinaric Carbonate Platform: defined by strong amplitude and low frequency seismic horizons on the top in the eastern part of the gulf. It shows higher frequencies in the structural high of the margin (made of CeL, Upper Cretaceous, if calibrated with near onshore wells). In the western side of the margin it is discontinuous and it has lower amplitudes. The carbonates are mainly Mesozoic, but Paleogene units also occur. These represent intra-platform basin deposition and they were intercepted by the Grado-1 and 2 wells. At the borehole sites, they have a thickness of about 380-390 m. They are seismically recognised as well organised layers infilling the intra-platform basin extending for several kilometres and bounded by faults.

Eocene Flysch: distal turbiditic deposits from the erosion of the developing Outer Dinaric chain, infilling the related foredeep. They lie at the top of the carbonates, in the eastern side of the margin.

Scaglia Alpina: (Aptian-Lower Eocene). It deposited in the basinal area in western part of the gulf, and consists of reworked marly and limestone sediments. It is seismically characterised by low frequencies.

Gallare Marls (Middle Eocene-Miocene). It deposited in the basinal area in western part of the gulf, and are constituted by layers of marls or clays, with thinner sandstone beds. They are typical of neritic-batial environment. Top depicted by valleys.

Messinian Unconformity: it extends in all the north-Adriatic area, and it is depicted by sub-aerial erosion, due to the marine regression of the Messinian Salinity Crisis (Fantoni, et al., 2002), and, it is characterised by valleys and ridges.

Pliocene Unconformity: characterised by erosion of the underlying sediments. The overlying deposits are in onlap on it.

Middle Pliocene - Quaternary sediments: continental-marine sediments related to sea level transgressive and regressive cycles.

The platform margin, representing the peripheral bulge of the External Dinaric foredeep-thrust belt system, subdivides two zones with different Paleocene-Miocene evolution. In the eastern part, the carbonate shelf is flexured in the foredeep, deepening towards East. More than 1000 m of Eocene turbiditic Flysch overlaying the carbonates, filled the foredeep in early phases of the orogenesi, and thins towards W, pinching out on the margin. A steep slope connects the margin to the deep basin towards W. The Scaglia Alpina deposited in onlap on the talus zone of the slope. It is overlain by the Gallare Marls deposited, as basin facies, during the Neo-Alpine orogeny.

During Messinian, the gulf underwent erosion due to the sea level drop; in the eastern part sub-areal conditions lasted until Early Pliocene. The Pliocene marine transgression involved the western part and led to the deposition of marine-continental sediments, draping the previous Messinian valleys. An erosion phase, in Early Pliocene (Fantoni, et al., 2002), is related to a regression that involved the Adriatic. Quaternary marine and continental sediments cover the

Pliocene unconformity. They are 600 ms twt thick in the western part of the study area and become thinner (up to 100-200 ms twt of thickness) towards east.

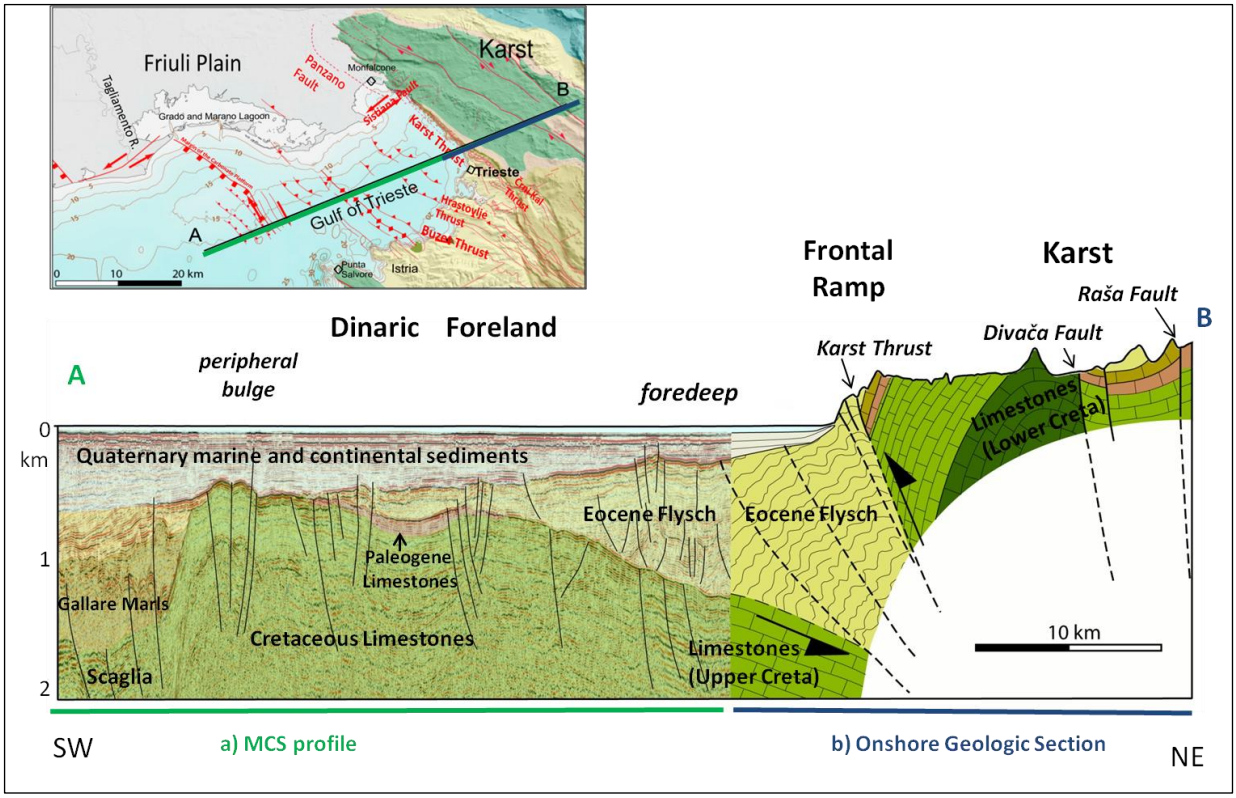

Fig. 44 – Stratigraphy and tectonic setting of the Gulf of Trieste and onshore Karst, (modified after (Busetti, et al., 2012)) by means of a) Seismic profile (OGS 2005 survey) crossing longitudinally (NE-SW) the GT (Busetti, et al., 2012). b) geological section (NE-SW) of the adjacent outcropping Karst from (GeoCGT-FVG, 2013) 200x. Geological tectonic map at the top left, shows the position of a) and b); onshore stratigraphy from (Jurkovšek, et al., 1996) (Placer, et al., 2010) (Cucchi, et al., 2008a) (Cucchi, et al., 2008b).

3.3 Sedimentary Evolution

The origin of the above listed stratigraphic units is closely related to the coeval main tectonic phases that occurred in the area: Mesozoic rifting and Cenozoic compressions.
In other words, the structural and geological setting of the study area is the result of different tectonic phases.

3.3.1.1 Mesozoic-Paleogene Sedimentary Evolution - Mesozoic Rifting Phase

On the basis of information derived from industrial seismic data, (Cati, et al., 1987a) (Cati, et al., 1987b) (Casero, et al., 1990) proposed a paleo-geographic reconstruction of the Periadriatic area for the period Upper Triassic to Lower Eocene (Fig. 45, Fig. 46).
In the Triassic, a wide carbonate platform (e.g. Dolomia Principale) was extending NW-SE from the present day Southern Alps trough the Veneto-Friuli Plain, the Adriatic Sea and the eastern part of the Balcanic area. It was bounded to the west by an evaporite platform and to the east by the Bosnian basin. During the Middle Jurassic and the Early Cretaceous, an extensional phase affected the Triassic platform of the Dolomia Principale. It generated NE-SW trending normal faults, starting from the northern part of the Apula microplate (Upper Triassic – Lower Jurassic), related to the Neotethys opening. This led to an horst and graben configuration, characterised by different paleo-geographic units (Cati, et al., 1987b) (Tišljar, et al., 2002). Among them, basin and shelf areas can be distinguished.
In correspondence of the horsts, shallow shelf carbonate environments developed. In this contest, the Apula, Adriatic, Trento and Friuli platforms originated. In particular during Middle Jurassic and Cretaceous, the Friuli Platform was characterised by a very high aggradation rate.
Among the grabens, the Tolmin (or Slovenian) Through, to the north-east, and the Belluno basin, on the west, developed while bordering the structural high on which a slow subsidence stage allowed the aggradation of the Late Triassic, Jurassic and Cretaceous Friuli Carbonate Platform (present Pre-Carnic Alps and Karst). This brought the shelf surface higher of 1.2-1.5 kilometres respect to that of the adjacent basins (Fantoni, et al., 2002).
The southern side of the Southwestern Friuli Platform is depicted by the margin, identified by the Cesarolo, Cavanella and San Donà wells. In particular, the Cesarolo well (in the present lower Friuli Plain) intercepted the complete margin succession (Jurassic to Cretaceous units) of the Friuli Platform. The Lower Cretaceous sequence testifies the progradation of the margin towards the basin.
Shelf carbonate facies, now outcrop in the Karst area (as the Monrupino Formation and the Aurisina Limestone), Istria and in the southern External Dinaric sector.
Moreover, in the in the Carnic Pre-Alpine sector, reef facies are represented by the Cellina Limestone, that is in contact, laterally and vertically with the Ellipsactinie Limestone. A successive subsidence of the margin, led to the development outer platform bioclastic facies of the Monte Cavallo Limestone (Casero, et al., 1990) (Vai, et al., 2002).
At the Cenomanian - Turonian limit, a sea level rise affected the southern Istria, bringing to the drowning of the platform and the deposition of pelagic facies. At the same time, a tectonic uplift in the northern Istria that led to an emersion and the successive deposition of bauxite beds. The sin-sedimentary tectonics played therefore a dominant role against the global eustatic sea level change (e.g. (Vlahović, et al., 2005) (GeoCGT-FVG, 2013) (Jurkovšek, et al., 2016) (Placer, 2015)).

The shelf edge deepens with high angle towards SW where the deep basin (drilled by the Amanda 1 bis borehore) represents the continuation of the Belluno basin, drowned from the Jurassic. Amanda 1 bis penetrated the thick basinal carbonate units that, from Lower Jurassic to Lower Eocene, are recognisable also in the Belluno basin. Whereas, the Middle Triassic facies represent shallow platform environment. At its top, the 450 m thick Ladinian volcanites are related to the extensional tectonic activity. The central part, between the basin and the platform, show indicators of drowning stage during Early-Middle Jurassic.
In the Belluno basin deposited pelagic facies and turbiditic sediments from the eroded outer shelf (e.g. Soverzene Formation, Vajont Limestone, Fonzaso Formation, Maiolica, Scaglia Alpina), now outcropping in the Carnic Pre-Alpine sector. Other outer units, such as the Rosso Ammonitico Superiore in the Tolmin Through.
At the end of the Cretaceous, it started a series of strong paleo-environmental changes that brought to the drowning of the Friuli platform and to the progressive migration of the basin towards SW (Casero, et al., 1990) (Vai, et al., 2002).

As concerns the presence Friuli Basin and the paleo-geographic definition of the Southwestern and Northeastern sectors of the Friuli Platform, there is presently a large debate. According to (Cati, et al., 1987b), the origin of the Friuli Basin (known also as Epiadriatic), characterised by a Dinaric trend, should have been controlled by the Dinaric deformation, in Jurassic-Cretaceous time. Therefore, it should be connected with the Outer Dinaric Budva Basin, extending south towards the Hellenids. Moreover, this basin divides two sectors of the Friuli Platform: the external Southwestern one, linked to the wider Adriatic Platform (Dalmatian zone) and the Northeastern one, linked to the Dinaric Platform (or High Karst zone); Fig. 46. It should be buried under the Karst Dinaric thrusts ((Cati, et al., 1987b) (Vlahović, et al., 2002)). Recent evidences of margin facies from boreholes and outcrops in the Outer Dinarides, do not support this hypothesis (Buser, 1989) (Gušić & Jelaska, 1993) (Pamič, et al., 1998) (Tari, 2002).
The Adriatic Carbonate Platform extends along a NW-SE trend for almost 700 km, whose north-western part represents the Friuli Platform (Tišljar, et al., 1998). In Literature other names refer to it: Dinaric Carbonate Platform (e.g. (Buser, 1989)); Outer Dinaric Carbonate Platform (e.g. (Tišljar, et al., 2002)); Adriatic Dinaric Carbonate Platform (e.g. (Gušić & Jelaska, 1993)). Moreover, for the Croatia Sector it is known as Istrian Platform (Frank, et al., 1983). In this work, it is used the term Mesozoic-Paleogene Friuli-Dinaric Carbonate Platform, to refer to the Northern Adriatic, Karst and Friuli Plain portion.

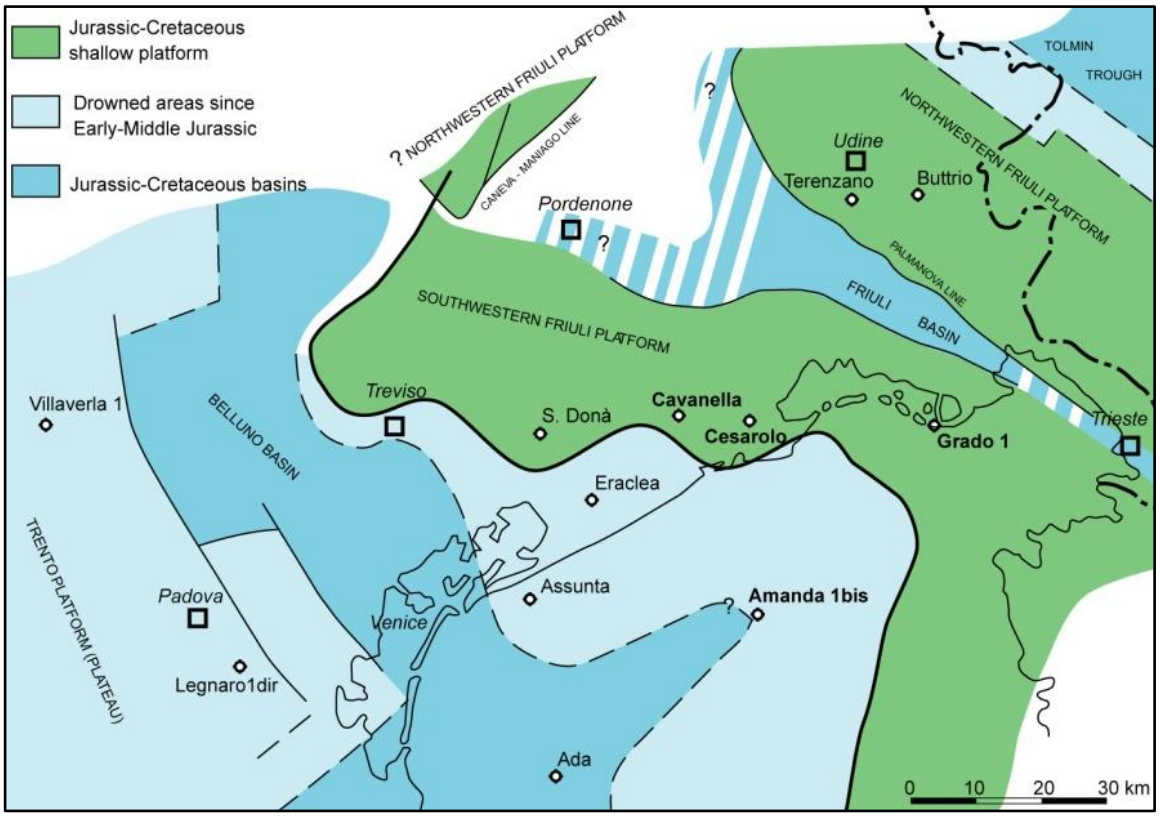

Fig. 45 – Paleo-geographic reconstruction of the Mesozoic Carbonate Platform in the Northern Adriatic area. modified after (Cati, et al., 1987b).

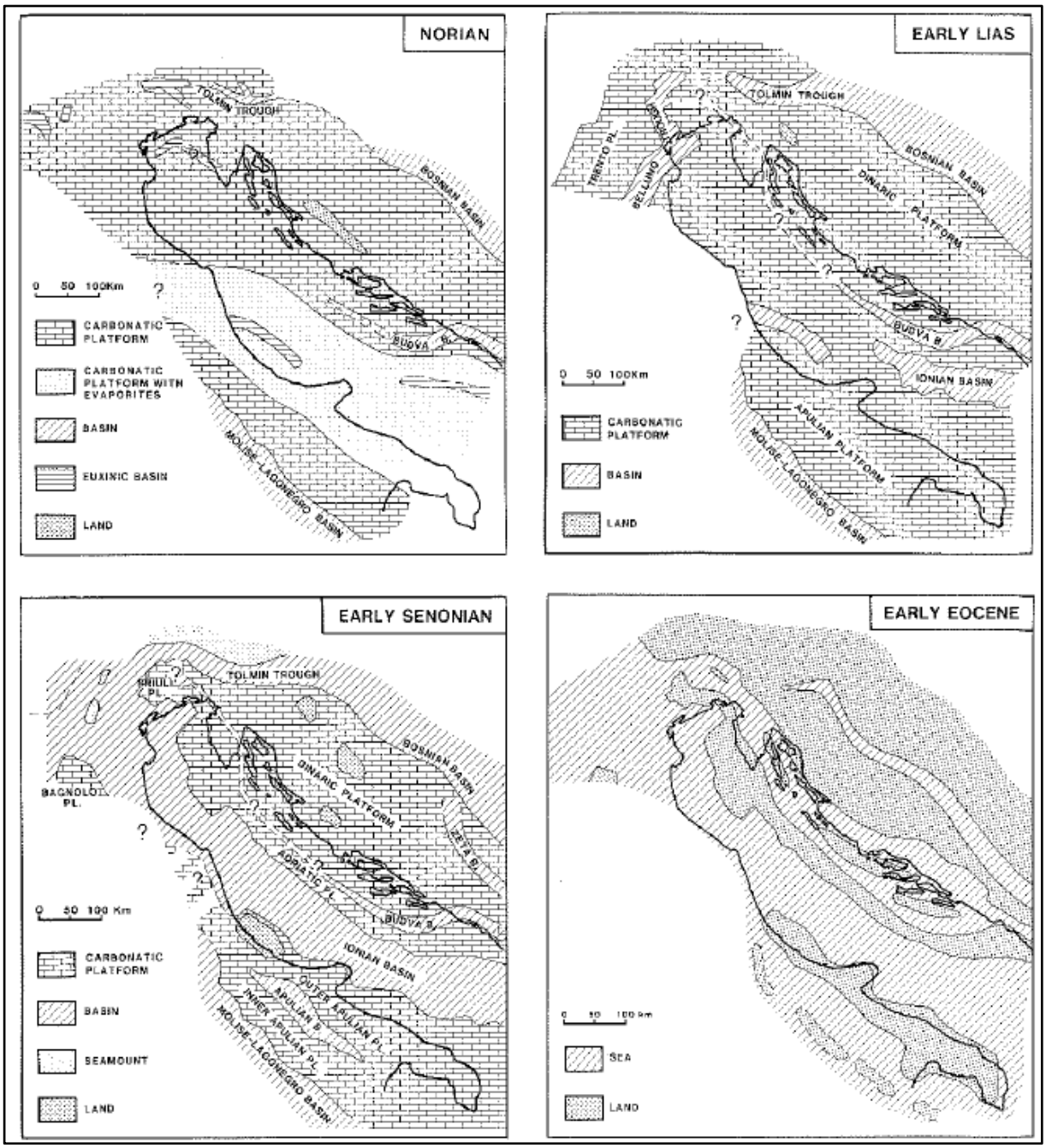

Fig. 46 – Paleo-geographic evolution of the Periadriatic area, from Upper Triassic to Late Eocene.(Cati, et al., 1987b).

3.3.1.2 Sedimentary Evolution During the Cenozoic Compression Phase

Between Late Cretaceous and Paleogene, the Dinaric collision, led to the deposition of terrigenous sediment within the accomodation space made available by the contemporaneous development of the foreland basin. The terrigenous sedimentation spans from deep water turbidites, named Flysch, to shallow water marls and sandstone mainly related to delta environment. Later, in the Oligo-Miocene, the Neoalpine orogenic phase caused the sedimentation of the foredeep terrigenous Molasse units. These are followed by the Plio-Quaternary deposits mainly related to alluvial, continental and marine systems (i.e. transgressive and regressive cycles).
The Friuli Plain, northern onshore area adjacent to the gulf, is covered by continental and marine Plio-Quaternary deposits that are the overburden of the Eocene turbiditic deposits of Flysch and of the Miocene Molassa. These sequences lie on the flexured Mesozoic-Paleogene Friuli-Dinaric Carbonate Platform (Amato, et al., 1977)(Nicolich, et al., 2004a)(Cimolino, et al., 2010) (Della Vedova, et al., 2014).
The Outer Dinaric system, that formed during the Maastrichtian-Late Eocene compression (known also as Meso-Alpine phase), is characterised by folds and thrusts NW-SE oriented and with SW vergence (e.g. (Jurkovšek, et al., 1996) (Vai, et al., 2002) (Poljak, et al., 2010) (Ponton, 2010) (Zanferrari, et al., 2013)). During relaxation phases, part of these structures acted as normal faults (Jurkovšek, et al., 1996) (Poljak, et al., 2010). Moreover, (Jurkovšek, et al., 1996) infers that normal faults in opposite direction, NE-SW formed as secondary strands with transcurrent motion. Meanwhile, the related foreland migrated progressively SW-wards, from the Slovenian Basin to the Friuli Basin. This produced, therefore, the E-ward flexure of the Meso-Cenozoic Friuli Dinaric Platform, as shown in the map of Fig. 49. Eroded terrigenous materials, from the developing Dinarides, deposited in downlap/onlap with the younger carbonates. The boundary between carbonate platform facies and siliciclastic sediments is marked by clay-silt limestones of the transitional beds (TB) (Tunis & Venturini, 1985). The drowning of the Friuli Platform is registered in different areas, at different times; it is generally progressively younger towards SW. Along part of the Italy-Slovenia border, the transitional beds deposited in Campanian-Maastrichtian. In the southern Julian Pre-Alps, the contact occurs with the Paleocene-Eocene Grivò and Cormons Flysch (Tunis & Venturini, 1992). In the Karst and Istria, the onset of Flysch deposition is settled by Lutetian (Cucchi, et al., 1989) (Jurkovšek, et al., 1996) (Placer, et al., 2004). The final stage of this compression generated the outermost thrust structures in the Gulf of Trieste and Istria (Busetti, et al., 2010a) (Busetti, et al., 2010b) (Cimolino, et al., 2010) (Placer, et al., 2010) (Busetti, et al., 2013).
The following N-S oriented Oligocene-Late Cenozoic Alpine compression (known also as Neo-Alpine phase) led to the formation (or reactivation) of reverse and thrust faults, with approximate E-W orientation and N dipping, in the South-Eastern Alpine domain and in the foreland of the Friuli Plain (e.g. (Zanferrari, et al., 1982) (Fantoni, et al., 2002) (Vai, et al., 2002) (Ponton, 2010) (Zanferrari, et al., 2013)). During the rising of the Southern Alpine chain, deposition of terrigenous sediments occurred in the foreland basin. The infilling was completed by the Chattian-Aquitanian. During the Burdigalian-Langhian, a terrigenous-carbonate sedimentation occurred (Fantoni, et al., 2002). The geometries of these deposits suggest that the foreland (expecially the foredeep) started to slightly dip towards N. During Serravallian-Messinian, the northern part of the area was affected by further strong subsidence that led to the deposition of a thick, up to 3 km, sedimentary sequence (Miocene Molassa). The Molassa gradually thins S-wards in the Friuli Plain and in the Northern Adriatic. Further intense Alpine tectonic phases occurred between the Late Messinian and Early Pleistocene, but there is no evidence that this influenced the N-ward flexure

of the southern part of the foreland (Fantoni, et al., 2002) (Vai, et al., 2002). The N-ward tilting the of the Southern Alpine foreland, developed during the Neo-Alpine phase, is also testified by the top Meso-Cenozoic Friuli Dinaric Platform trend, Fig. 49, and by the regional Bouguer gravity anomalies (e.g. Fig. 49).
This Neo-Alpine tectonic phase influenced also the northern part of the Outer Dinarides. Here it reactivated inherited Eocene structures, with a transpressive motion. Paleomagnetic data, suggest that the Trieste-Komen Plateau rotated of about 30° anti-clockwise during the post Eocene time (Márton, et al., 2008). Among the others, reactivation involved Raša and Divača faults of the plateau and the Idrija lineament further east. Horizontal movements along the Dinaric structures, may be ascribed to Pliocene age (Buser, 1989) or Neogene-Quaternary (Poljak, et al., 2010).

3.4 Surficial Heat Flow Map

The heat flow (HF), or thermal flux, is a flow of energy per unit of area per unit of time. In SI its units are watts per square metre (W·m−2). It is a vector quantity, having a direction and a magnitude. The mean HF within the continental crust is about 65 mW·m−2, while it has an average value of 100 mW·m−2 in the oceanic crust. It varies through time and space and the factors affecting it are mainly related to geodynamic processes (e.g. extension, subduction, volcanism, sediments). Nevertheless, it is influenced also by radiogenic heat generated within the lithosphere. Thus, the HF measured at the Earth's surface reflects the thermal processes occurring at high depths. It is quite difficult to determine HF, because the deep signals are often masked by the factors occurring within the shallower crust, such as fluid circulation (Della Vedova, et al., 2001). Two types of heat transfer can occur: convection (in active areas) and conduction (in stable areas). The HF map, shown in Fig. 47, was redacted by using information from industrial wells and from boreholes for the investigation of the water resource in the Friuli Venezia Giulia Region(Calore, et al., 1995) (Della Vedova, et al., 2001) (Nicolich, et al., 2004a) and in the Northern Adriatic and in Slovenia (Ravnik, 1991). It evidences the areas where the HF distribution, within the first kilometres of depth, are strongly affected by shallow processes (e.g. hydrogeology circulation and presence of sediments). These areas are:

- Those characterised by highly permeable layers, where rainwater reduce the HF (with values lower than 40 mW·m−2.
- Those characterised by the presence of thermal waters springs at the carbonate-terrigenous deposits contact, causing rise in HF values.
- Those with Neogene-Quaternary sediments, affected by negative anomalies (lower than 50 mW·m−2).
- Those interested by convective fluid flow, within shallow reservoirs confined by low permeability terrains. These determine a rise in the HF values (higher than 60-70 mW·m−2).

Positive HF anomalies are located at Belluno, Cargnacco and at the structural high of Cesarolo-Grado, allowing the identification of the carbonates where hydrothermal circulation occurs. In fact, they represent potential reservoirs for the exploitation of the low enthalpy (water temperatures of 40-60°C, maximum 1 km deep) geothermal resource, as that of Grado. Moreover, along the Veneto and Friuli shoreline and lagoons, a wide (about 700 km^2) positive anomaly is present. This is due the hot-salty-water convection within the carbonate platform (60°C of temperature); the impermeable rocks isolating the hot circulation of the deep aquifers; shallow aquifers heated by the deeper ones, by means of conduction. The 38°C of waters, at the

Monfalcone roman baths, are related to a local anomaly rising from the carbonates (Della Vedova, et al., 2001) (Carulli, 2006b).

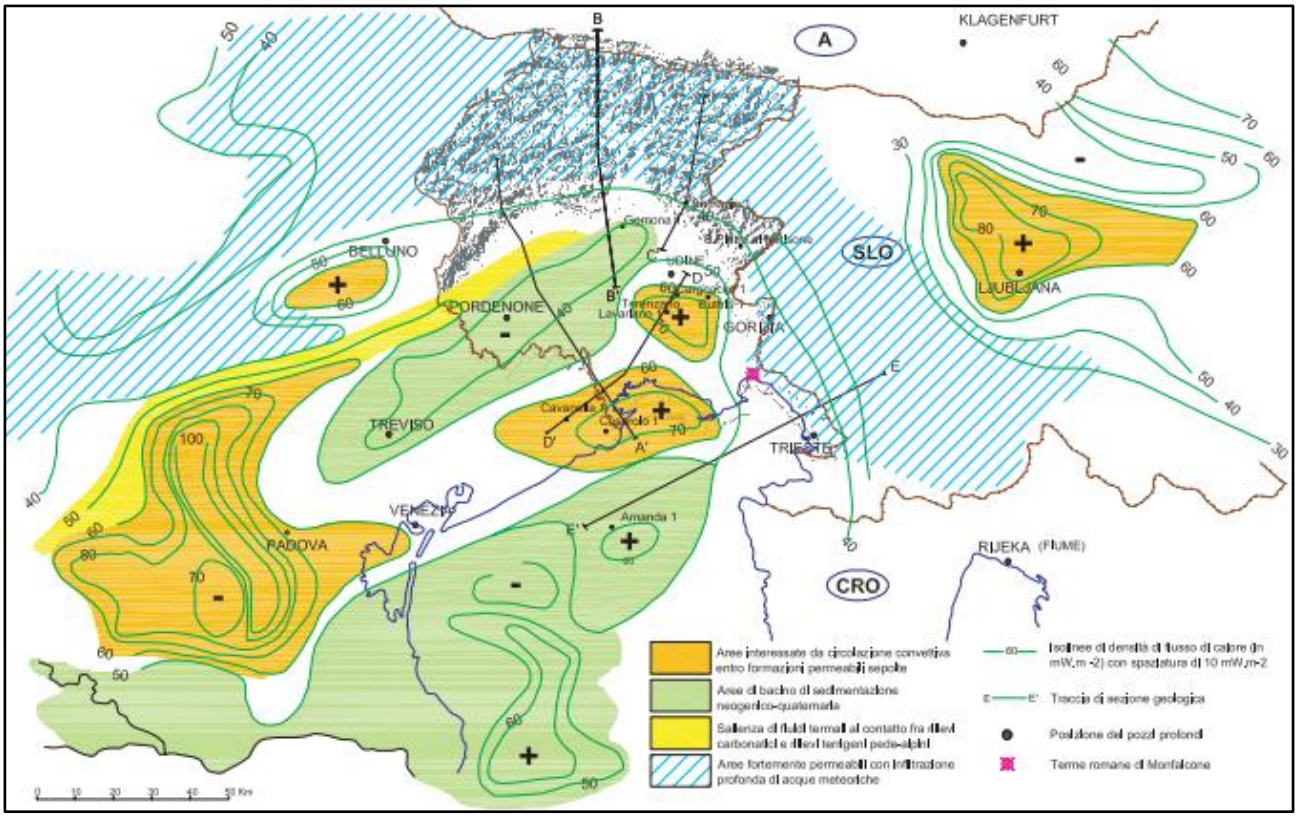

Fig. 47 – Surficial Heat Flow (HF) map of the northern Adriatic and onshore areas derived from borehole data ((Ravnik, 1991) (Calore, et al., 1995) (Della Vedova, et al., 2001) (Nicolich, et al., 2004). Green lines with number indicate isoline of HF values (every 10 W·m−2). Anomalies are present in areas of convection circulation within buried reservoirs (orange areas), sector of Neogene-Quaternary sediments (green areas), thermal water springs at the carbonate-terrigenous deposits contact. Dashed areas represent zones of rainwater infiltration. Black circles represent the deep wells and the pink square the Monfalcone roman baths (Della Vedova in (Carulli, 2006b).

3.5 Gravity Anomalies

Bouguer anomalies (Milligal, mGal) represent the deep density variation in response to different mass distribution and composition. The Friuli Venezia Giulia field id dominated by a negative trend from S to N: -20 mGal near the shoreline, -100 mGal northward in the mountain area near the State boundary. The increasing of the negative anomaly is associated to the thickness of the crust ain the Alpine – Southern Alpine zone. In front at this latter, a limited negative anomaly is present in correspondence of a small flexured sedimentary basin (Cati, et al., 1987a) (Carulli, 2006b).
In the Gulf of Trieste, the Bouguer gravity anomaly map was calculated with Data have been collected during the 2005 OGS survey. The map of Fig.48 shows a negative trend towards N and E: these are related to the general dipping trend of the flexured carbonates toward the base of the southern-Alpine and External Dinaric reliefs. In the offshore, a positive gravimetric anomaly NW-SE oriented, is related to the extension and depth of the carbonate platform that rises towards the Istrian coast. In fact, from depths of 800 m below the northern coastal area, it rises up and outcrops at Savudrija Ritč (Fig. 49) (Busetti, et al., 2010b).

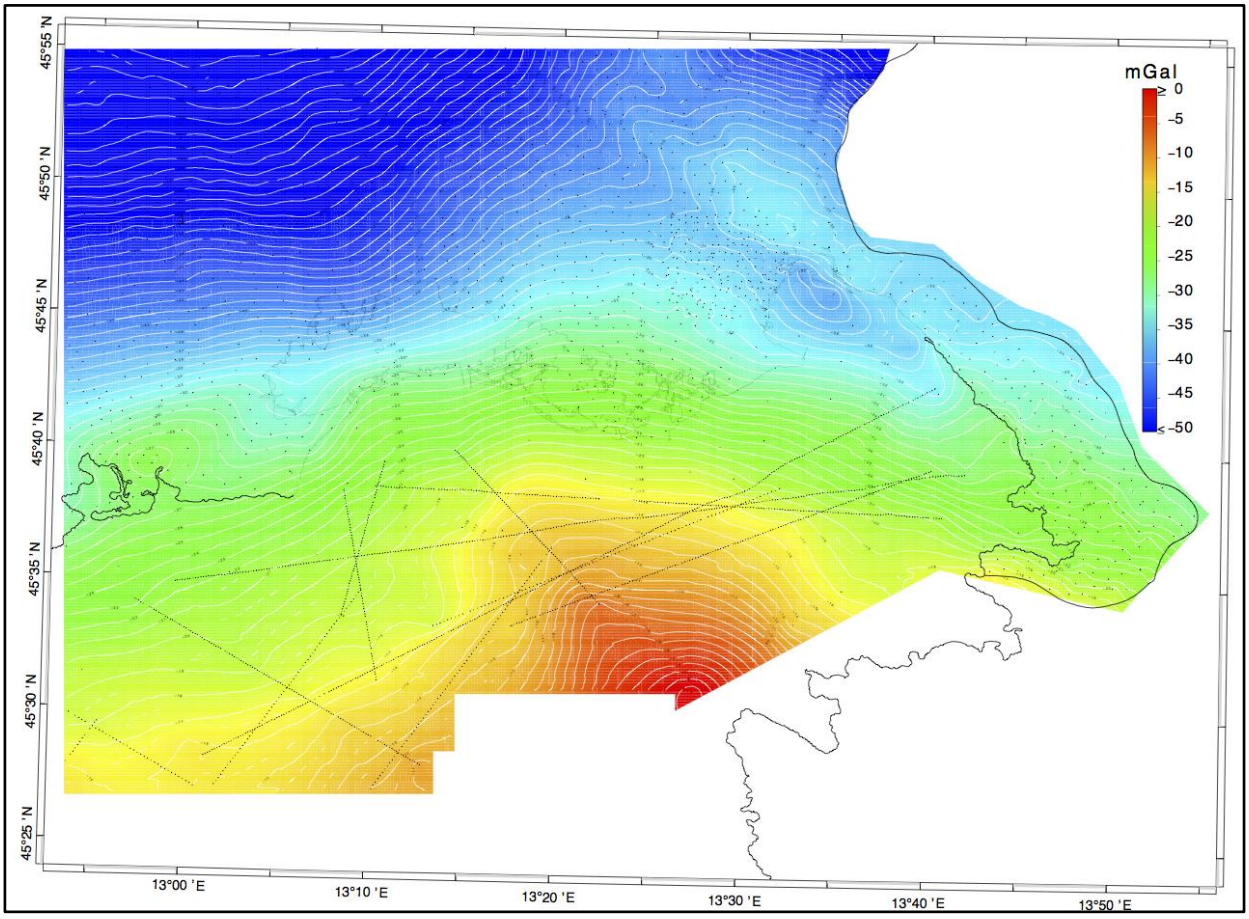

Fig. 48 – Map of the Bouguer gravimetric anomalies (mGal) for Gulf Trieste (OGS 2005 survey) and near onshore (AGIP measurements stations, black dots). The map highlights the deepening trend of the carbonates N and E wards, related to the influence of the Alpine and Dinaric chains. Moreover a rising trend NW-SE oriented is present towards the Istria coast, parallel to the shelf margin of the carbonate platform. (Busetti, et al., 2010b).

3.6 Top Mesozoic-Paleogene Friuli-Dinaric Carbonate Platform Map

The map of the Top of the Mesozoic-Paleogene Friuli-Dinaric Carbonate Platform (Fig. 49), was compiled in the framework of the redaction of the geological-technical chart of the geothermal resource and the definition of the guide-lines for its exploitation ("Risorsa Geotermica RA-FVG" project; agreement "Rep. 8493, dd. 24/11/2004"), in the lower part of the Friuli plain

The shelf margin represents a structural high that lies about 700-800 m depth (Cesarolo High) and corresponds to a positive geothermal anomaly (60-70 mW m^{-2}) (Calore, et al., 1995) (Della Vedova, et al., 2001) (Nicolich, et al., 2004). Onshore, it is alternatively oriented NW and NE with high bending angles (Nicolich, et al., 2004). Offshore, it is NW-SE oriented and parallel to the rising up trend of the surface towards the Istrian coast. This trend is also highlighted by the gravity map shown in Fig. 49. In the northern part of the gulf, south of the Cesarolo High, the top carbonate surface has a depth of 500 m; whereas, in the central part of the gulf, to the SE, it is shallower (350 m deep). It connects further south to the carbonates outcrops at Savudrija Ritč in Croatia (Busetti, et al., 2010b). East of the margin, the carbonates gradually deepen towards the north-eastern coast of the gulf. Similar trend can be also detected along northwards direction, in correspondence of the onshore. These are due to the foredeep flexuring of the Dinaric and Alpine chains, NW-SE and E-W trending respectively, (Nicolich, et al., 2004) (Busetti, et al., 2010b).

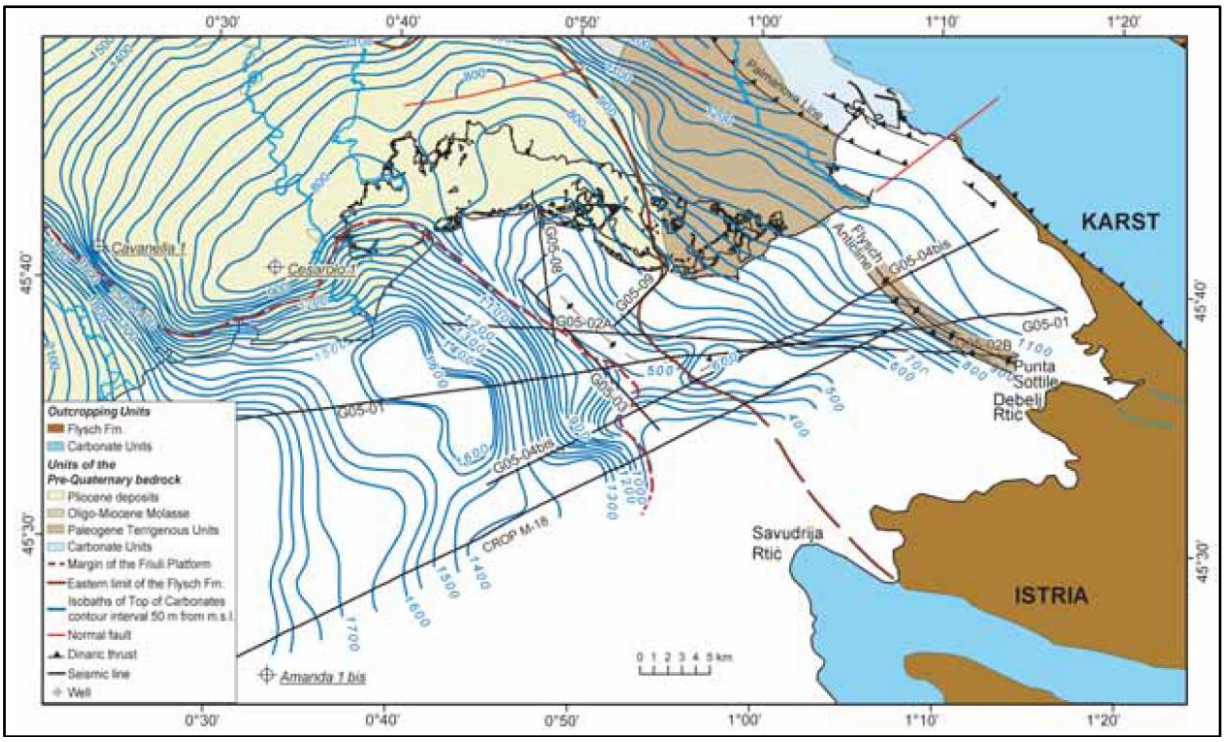

Fig. 49 – Isobath map of the top of the Mesozoic-Paleogene Carbonate Platform, reconstructed by seismic data (2005 OGS survey) and borehole (blue circles) in the Gulf of Trieste and in the northern onshore. The shelf margin of the carbonate platform (red dashed line) is NW-SE oriented in the gulf offshore, while it bends in correspondence of the Grado and Marano Lagoon, assuming an alternating NE-SW and NW-SE trend with high bending angles. Higher features, along the shelf margin, are located at the 800 m deep Cesarolo High; 500 m and 350 m deep areas south of Grado and Marano Lagoon and in the central part, respectively. The isobaths show deepening trend N and E wards, related to the foreland flexure of the Alpine and Dinaric chains. The western limit of the Flysch formation is also shown (brown dashed line), pinching out on the rising up carbonate surface. Moreover, onshore outcropping units are the Meso-Cenozoic Friuli Carbonate Platform (azure), the Flysch (brown) and the Plio-Quaternary units (light brown, yellow and grey). Contours every 50 m. (Busetti, et al., 2010b).

3.7 Present Tectonic Setting

The present structural setting of the study area is the result of the three main tectonic phases above described. Among the folds and thrust faults having a Dinaric fingerprint (NW-SE), the most significant are hereafter listed. Main anti-Dinaric lineaments are also reported.
The Karst Plateau (Fig. 44, Fig. 38) is settled on a wide asymmetric anticline, with NW-SE axis, that brings the Meso-Cenozoinc Friuli-Dinaric Carbonate Platform above the younger Eocene Flysch (Carulli & Cucchi, 1991) (Jurkovšek, et al., 1996) (Carulli, 2006a) (Jurkovšek, 2008) (Jurkovšek, 2010) (GeoCGT-FVG, 2013). It represents the hangingwall of the Karst Thrust system, the Dinaric thrust system NW-SE oriented and SW vergent (Fig. 44, Fig. 38, Fig. 50, Fig. 51). On the basis of interpretation of the geophysical data acquired since 2003, it was inferred that it runs along the north-eastern rocky coast of the GT and extends with an accomodation belt located up to 2-3 km offshore (Busetti, et al., 2010a) (Busetti, et al., 2010b). It gives a vertical displacement of more than 1400 m between the carbonates outcropping in the Karst and those lying in the easternmost area of the gulf (Busetti, et al., 2010a) (Busetti, et al., 2010b). The overlying Flysch is here about 1000 m thick, it was involved in the deformation of the thrust after its deposition (Busetti, et al., 2008) (Busetti, et al., 2010a) (Busetti, et al., 2010b). The Trieste Karst (Fig. 52), inferred by (Del Ben, et al., 1991), and corresponding to this system, is interpreted by the Author as a transpressive fault related to the Meso-Alpine phase (Paleogene) and reactivated during the Neo-Alpine phase, with a consistent dextral strike-slip component. (Placer, 2008) (Busetti, et al., 2010a) (Placer, et al., 2010) suggested the continuation of this structure towards south-east in Istria, as the Črni Kal Thrust. Moreover, (Busetti, et al., 2010a) suggest the relation of this feature with the Panzano Fault, located to the north and displaced to the NW of 1-2 km. This offset is given by the Sistiana Fault, a NE-SW trending normal fault with a left transcurrent component (Fantoni, et al., 2003) (Nicolich, et al., 2004a) (Nicolich, et al., 2004b).
Compressional tectonic features (Fig. 50) were detected in same seismic data by (Busetti, et al., 2008)(Busetti, et al., 2010a) (Busetti, et al., 2010b). They consist of thrusts and fold with Dinaric orientation and SW vergence. They are up to 1 km wide and some hundred of meters high. Horizons in the Flysch lie in discordance with the underlying carbonate, quite undisturbed. Therefore, it is supposed that the deformations originated along this detachment level. In the north-western part of this structure, the deformation is more intense and younger, affecting also the Messinian-Early Pliocene unconformity and generating 30 m high escarpments. This area is also characterised by the presence of back-thrusts, SW dipping, on the east of the fold. Furthermore, this area in about 1 km shifted apart on the W, respect to the southern one. A NE-SW fault system, with sinistral shear component, is hypothesized, in correspondence of a valley in the top of the Flysch, shown by the morphological map of (Morelli & Mosetti, 1968). The tectonic lineaments with Dinaric orientation are interpreted by the Authors as connected, on the Istrian onshore, to the Istrian Hrastovlje Thrust. At the Debelj Rtič and Punta Sottile coast, the structure may be dissected by the NE-SW offshore continuation of the Monte Spaccato trancurrent Fault. As in the onshore Karst, the normal component of this fault is testified by the different elevation of the folds: in the gulf they are present at a depth of about 120 m bsl; while onland they are at about 200 m asl.
In the onshore area N of the Grado-Marano Lagoon, multichannel seismic data show a thrust fault within the Flysch and the Molassa and a thrust fault gently folding the Miocene Molassa and

disrupting the Plio-Quaternary sediments (Busetti, et al., 2010a). The about 400 m thick Palaeogene carbonate interval drilled by the Grado-1 well was also interpreted, as a reverse fault that doubled the Paleogene sequence, affected by fractures (Cimolino, et al., 2010). The features, NW-SE oriented, are considered the western-most deformation front of the Dinaric thrusts system, probably still active, buried below the southern Friuli Plain, Fig. 50, (Busetti, et al., 2010a) (Cimolino, et al., 2010).

The Panzano Thrust (Fig. 38, Fig. 50, Fig. 51), NW-SE oriented for about 15 km between the Sistiana Line (in the Panzano Bay) and the lower Friuli Plain; it acquires a N-S direction in its northernmost part (3 km long). It passes just E of the city of Monfalcone and it is dissected about 1-2 km to the W from the Karst Thrust system by the Sistiana Line (Fantoni, et al., 2003) (Nicolich, et al., 2004) (Carulli, 2006a) (GeoCGT-FVG, 2013). This structure, was previously considered in Literature as Palmanova Fault, linking towards NW the line was thought to continue straight, with NW-SE direction, into the gulf offshore, about 4 km from the coast. This was supposed by means of onshore geological information and scarce geophysical data (Cavallin, et al., 1979) (Carulli, et al., 1980) (Zanferrari, et al., 1982) (Carulli, 2006a), but the recent MCS data available in the GT, do not show any evidence of the Palmanova thrust faults involving the carbonates in this zone (Busetti, et al., 2008) (Busetti, et al., 2010a) (Busetti, et al., 2010b).

Sistiana Fault (Fig. 38, Fig. 50, Fig. 51) is an anti-Dinaric NE-SW fault crossing the north- western coastal Karst and prosecuting into the gulf for few kilometres. It is interpreted as a vertical plane along which left strike slip displacement has occurred (Carulli & Cucchi, 1991) (GeoCGT-FVG, 2013) (Nicolich, et al., 2004a). From analysis of morphological features along the coast (e.g. notch, it is affected by very recent (post-roman age) vertical displacements (Furlani, et al., 2011a). Moreover, it separates the Karst Thrust from its NW continuation in the Panzano Thrust, with a W-wards slip of about 1-2 km (Busetti, et al., 2010a).

Monte Spaccato Fault (Fig. 50) is an anti-Dinaric NE-SW fault. It shows morphological evidences in the outcropping carbonates in the south-eastern Karst (Carulli & Cucchi, 1991) (GeoCGT-FVG, 2013).

The Izola Anticline (Fig. 52a), Paleogene carbonate fold outcropping at the Izola peninsula coastline. Onshore, it has a Dinaric NW-SE axis trend and it is bounded by the Simon Thrusts having same orientation (Placer, et al., 2010). It prosecutes northwest-wards into the gulf, and by the MCS profiles acquired in 2013 (Busetti, et al., 2013).

The faults of the Istria-Friuli Underthrust Zone (Placer, et al., 2010) characterise the eastern coast of Istria (Fig. 50, Fig. 52), down to the Kvarner Bay. Their origin is related to the NE-wards subduction of Adria and begun in post-Miocene. According to the Authors, the Črni Kal Thrust (southern continuation of the Karst Thrust) is the prominent lineament with Dinaric orientation NW-SE, with NE/25°-30° dip. It produces vertical displacement higher than 10 km. Within its footwall and hangingwall, it is affected by several thrust faults. Among these, the Petrinje Thrust gives the shortest displacement (400-500 m) in the hangingwall. Towards SW, the Hravstrovlje, Buzet and Simon thrusts show decreasing dipping angles up to 0°. The Simon Thrust, in fact, forms the Izola tectonic window (outcropping carbonate anticline), facing the GT. The deepest Buje Fault bounds, to the SSW, the Buje Anticline and it represents the Istrian thrust front of the External Dinarides. The detachment level is settled along Permian-Triassic carbonates units, similarly to the Dinaric thrusts of the lower Friuli Plain (e.g. Palmanova, Panzano thrusts). This imbricated belt shows transpressive displacements, due to its reactivation in the Neo-Alpine phase. Moreover, the Črni Kal Thrust is thought to have been active at least until Plio-Pleistocene.

The strike-slip faults of the External Dinarides are NW-SE oriented (Fig. 38, Fig. 53, Fig. 51). Of these, the Divača, Raša and Colle Nero faults are located in the Cretaceous carbonate terms of the Karst Plateau. The area is overall affected by dissecting vertical faults with anti-Dinaric orientation (e.g. (GeoCGT-FVG, 2013) (Jurkovšek, et al., 2016).

- The Divača fault runs for about 30 km from Gorjansko to Divača (Slovenia); it shows horizontal movement and downthrown blocks on its eastern side (Jurkovšek, et al., 1996) (Jurkovšek, 2008) (Jurkovšek, 2010).
- The Raša fault (Fig. 38, Fig. 53, Fig. 51), more to the E, is about 50 km long. Originally inverse (Jurkovšek, et al., 1996), it was reactivated by the Neo-Alpine phase with a transpressive kinematics detected by recent low magnitude seismicity (Del Ben, et al., 1991) (Michelini, et al., 1998). At present, it is also characterised by left-lateral and reverse displacement rates of up to 0.5 mm/year (Gosar, 2007).
- The Colle Nero Fault (Fig. 38, Fig. 51) is NW-SE oriented and it is located in the northern part of the Italian Karst. It has a right-lateral transpressional component. (Tentor, et al., 1994) (GeoCGT-FVG, 2013).

Moreover, outside the Karst Plateau, the Idrija and Rijeka lines (Fig. 53) also belong to the External Dinarides system (Poljak, et al., 2010). Together, they are considered as the boundary faults accommodating the NNW motion of Adria plate (Del Ben, et al., 1991):

- the Idrija line (Fig. 53) is morphologically well detected in W Slovenia. It runs from the Italian border near Bovec (South-Eastern Alps) to Croatia in Gorski Kotar (N of Rijeka), for a length more than 120 km (Gosar, 2007). It is one of the most active faults in the northern Dinarides and shows vertical plane with dextral prominent strike-slip kinematics (Del Ben, et al., 1991) (Poljak, et al., 2000). In the Southern Alpine sector, it is characterised by a compressive style (Del Ben, et al., 1991). The 1511 earthquake with M=6.8 (strongest ever recorded at the South Alpine-External Dinarides Junction) is attributed to this line (Fitzko, et al., 2005). Local left-lateral displacement (0.38 mm/year) is also detected (Gosar, 2007).
- The Rijeka line (Fig. 53) runs from the Rijeka coast (Croatia) to the Vipava Valley (Slovenia). It is a dextral strike-slip fault (with slight transpressive component) that terminates along on the Idrija line, in the vicinity of the Idrija village (Del Ben, et al., 1991).

Tectonic lineaments showing both Dinaric and Alpine orientation are located in the south-eastern Friuli Plain:

- The Palmanova Thrust, in the eastern Friuli Plain, was generated in the Paleogene with a Dinaric NW-SE orientation. It turns into a WSW- ENE trend in the eastern part and it represents the front of the Alpine compression (Merlini, et al., 2002) (Zanferrari, et al., 2013). Recognised on seismic and well data, it detaches along Carnian units (Merlini, et al., 2002), displacing the Mesozoic carbonate sequence with 1500 m of vertical throw (Zanferrari, et al., 2008). The related fold is filled by coeval Grivò Flysch (Upper Paleocene-Lower Eocene). The onlapping Cormons Flysch (Lower-Middle Eocene) testifies the deactivation of the Dinaric phase. In Middle-Late Eocene it reactivated under Neo-Alpine compression, generating 700 m of vertical throw within the Cavanella Group (Oligo-Miocene, Chattian-Langhian). Moreover, it has been active in recent time, since it provides a differential depth in the Quaternary base of about 300 m (Merlini, et al., 2002).
- The Medea Thrust has a Dinaric NW-SE trend that bends to an Alpine ENE-WNW direction into the eastern part. It lies north of the Palmanova Thrust and it is related to the uplift of the Medea Hill. There is structural evidence of Pliocene to Holocene activity (Poli, 1996). It detaches at approximately 7 km within the Carnian units (Burrato, et al., 2008). The Medea Thrust is related to

potential source of Mw=6.4 earthquakes, both as an individual source and as a seismogenic area (Galadini, et al., 2005) (Burrato, et al., 2008).

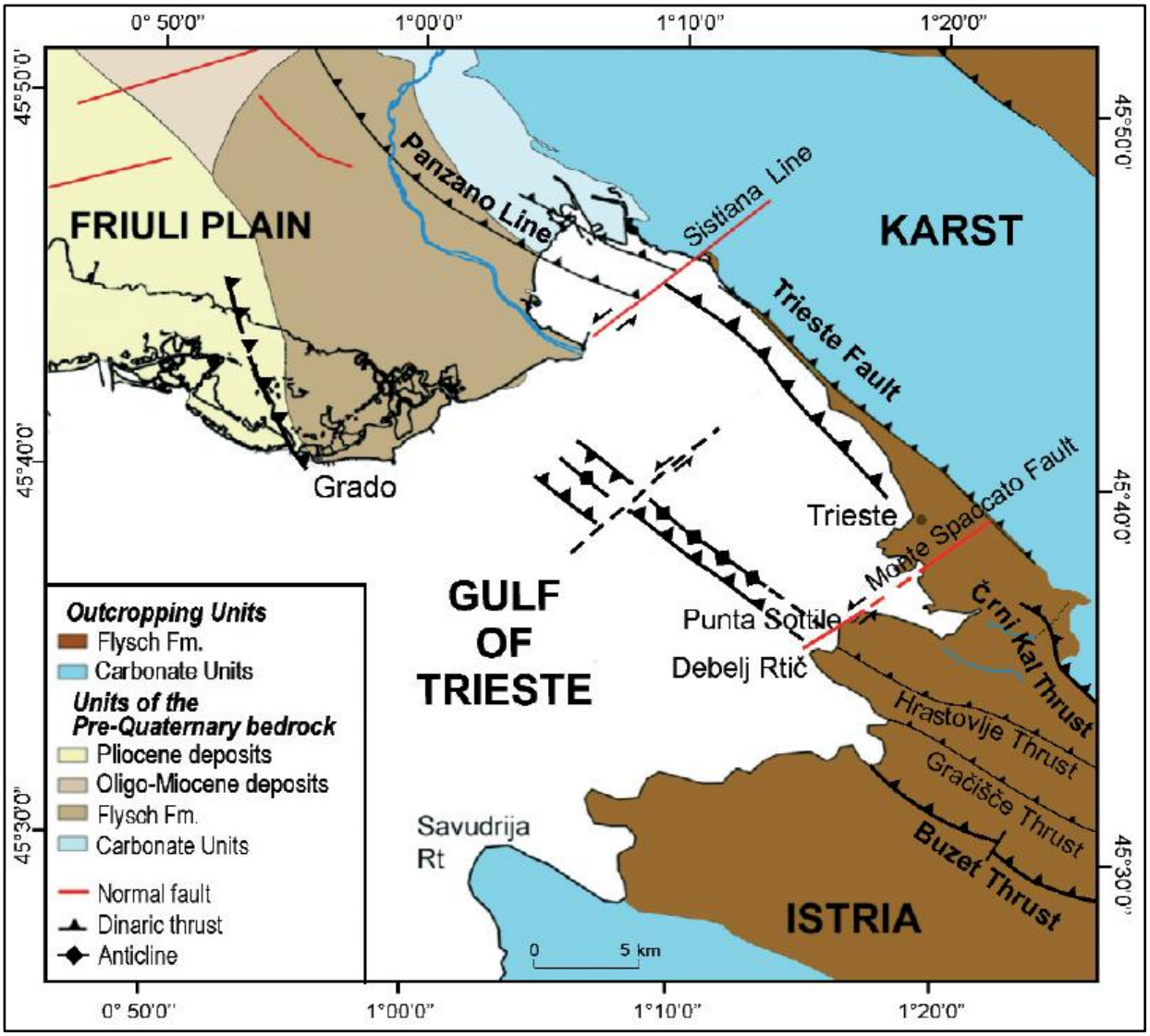

Fig. 50 – Map showing the structural setting of the Gulf of Trieste and adjacent onshore area. The Karst Dinaric thrust system (with the prominent Trieste Fault/Karst Thrust) runs along the north-eastern coast and affects the 2-3 km wide frontal area. It extends, to the NW and SE, with the Panzano Fault and the Črni Kal Thrust, respectively. The Sistiana Fault, dissects the lineament on the north with a left component. NW-SE oriented compressional tectonic features affect the Flysch deposited in the eastern gulf. A NE-SW left strike-slip fault system offset these structures. Moreover, these features are thought to be related to the Istrian Hrastovlje Thrust; they dissected by the Monte Spaccato left-transcurrent Fault. In correspondence of the Grado Lagoon, a thrust fault represents the western-most front of the External Dinarides. (Busetti, et al., 2010a).

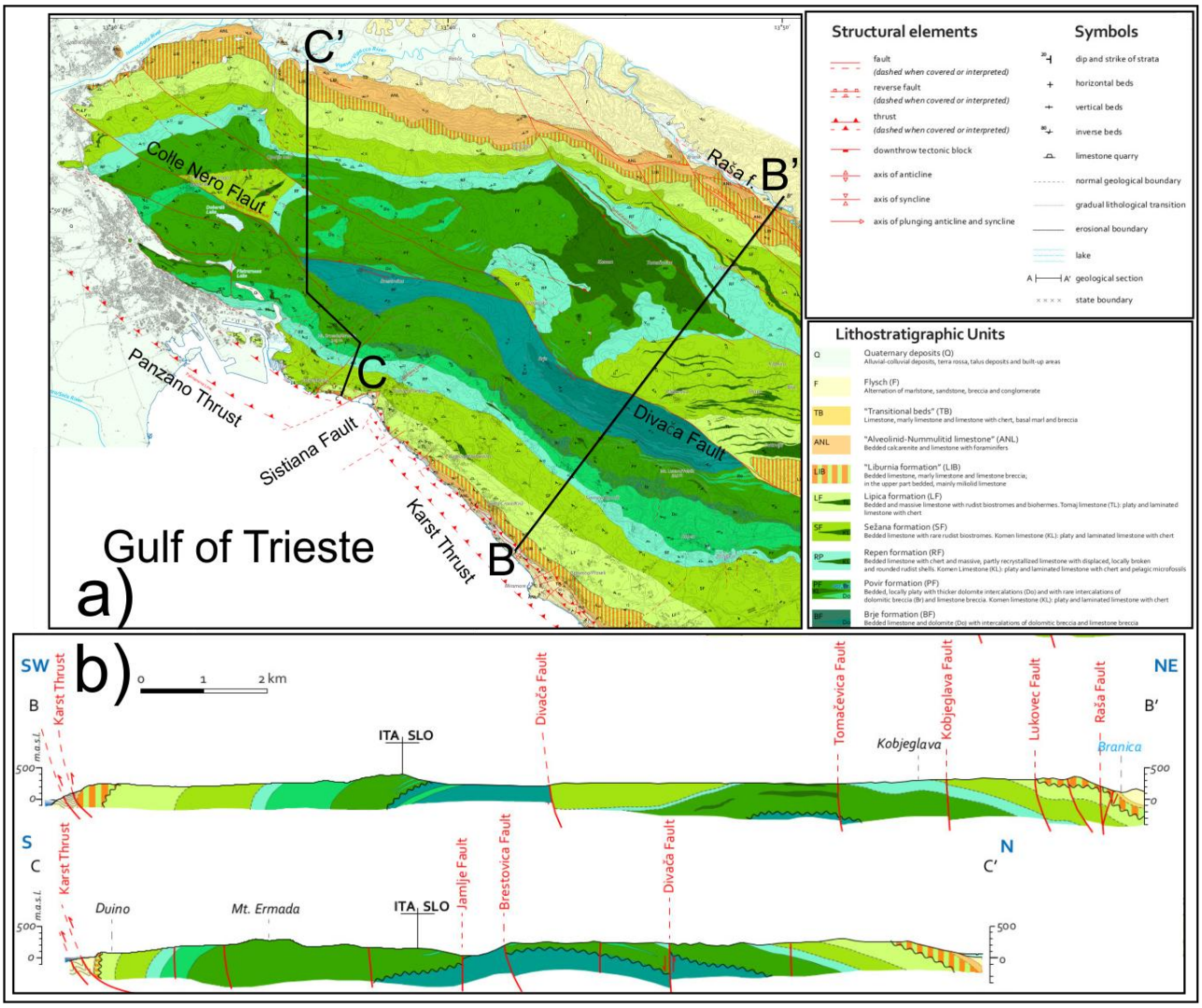

Fig. 51 – Geological map of the Karst Plateau. Location of inset a) in Fig. 38. Geological profiles shown in b). B-B' and C-C' are oriented SW-NE and SW-NE (with short part SSE-NNW), respectively. The Dinaric fingerprint of the Karst anticline, with NW-SE axis, brings the Meso-Cenozoinc Friuli-Dinaric Carbonate Platform above the younger Eocene Flysch. It represents the hangingwall of the Karst Thrust system (NE dipping). Among the other lineaments described in the text, the Divača (with vertical displacement, in B-B'), and the Raša strike-slip faults are represented crosscut in the profiles . Modified after (Jurkovšek, et al., 2016).

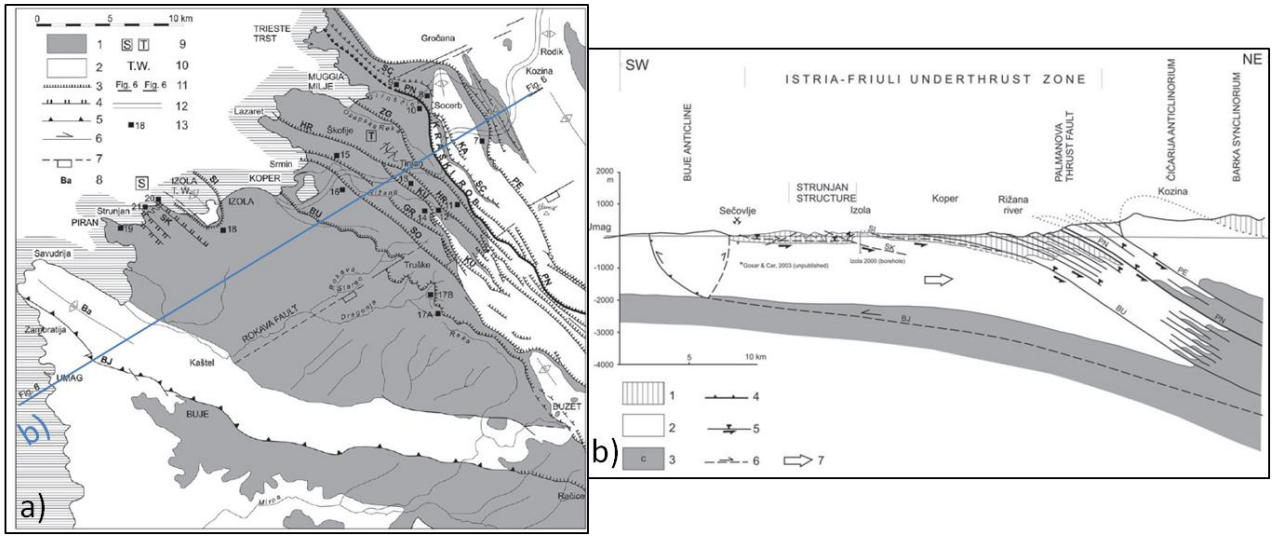

Fig. 52 – Istria-Friuli Underthrust Zone: a) map with location (azure line) of the SW-NE section in b), located across the inland of the eastern Istrian coast. Among the structures of the NW-SE oriented Dinaric imbricated belt, described in the text: the NE/25-30° dipping Črni Kal Thrust (PN) and the gradually lower dipping thrusts SW-wards (Petrinje Thrust - PE, Hravstrovlje - HR, Buzet – BU and Simon - SI thrusts). Note the SI bounds the Paleogene Carbonates (2) of the Izola Anticline. The deepest Buje Fault (BJ), with the Buje Anticline, represents front-most structure of the External Dinarides in Istria. The detachment level is settled in Permian-Triassic units (3c in b)); the outcropping Flysch (1) and the Meso-Cenozoic carbonates (2) were involved in the thrust deformations. (Placer, et al., 2010).

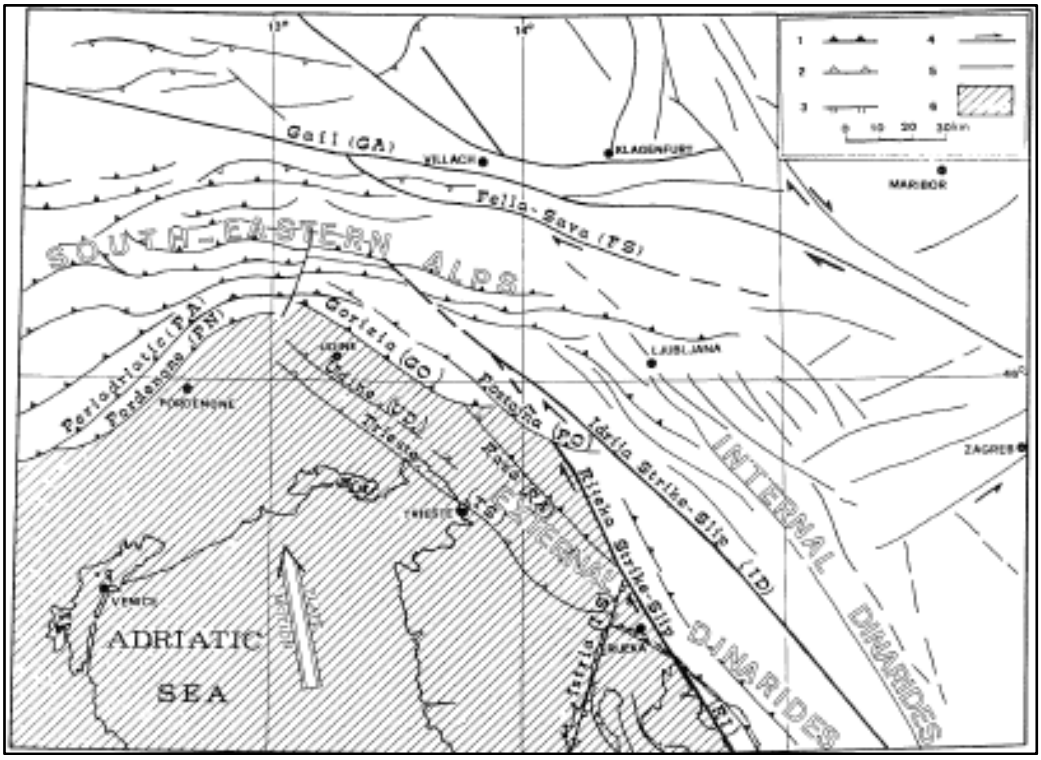

Fig. 53 – Regional tectonic sketch of the Southern Alpine and Exernal Dinarides domains. It is reconstructed by 3D seismicity distribution. Among the structures described in the main text: the NW-SE trending Idrija and Rijeka lines accommodate the NNW motion of Adria plate, with a dextral strike-slip kinematics. Moreover, the strike-slip Raša Fault is one of those located on the Karst Plateau. Bounding the eastern side of the Karst, the Trieste Line (Karst Thrust) continues N and S-wards on the onshore Friuli Plain and Istria, respectively. (Del Ben, et al., 1991).

3.7.1 Neotectonics

Several definition of the concept related to the word “neotectonics” have been proposed through time. Here some major examples:
- (Pavlides, 1989) considers neotectonics as the study of young tectonic events (deformation of upper crust), which have occurred or are still occurring in a given region after its final orogeny (at least for recent orogenies) or more precisely after its last significant reorganization.
- According to (AGI, 2009), neotectonics is the study of the post-Miocene structures and structural history of the Earth’s crust.
- (Christophersen, et al., 2015), describes neotectonics as related to faults and folds that have been active in the current tectonic regime of a region. The time period will vary from region to region with longer time intervals required to characterise fault activity in low strain regions.
According to the Authors above cited, investigation on neotectonics should be tied to the geological and morphological conditions of each specific area.
In particular, in the offshore, the tectonic structures can be investigated mainly with geophysical methods. Multichannel seismic data are a valuable example: through imaging they allow depth reconstruction of the main geological features (e.g. for the GT (Nicolich, et al., 2004a)(Carulli, 2006b) (Busetti, et al., 2010a) (Busetti, et al., 2010b) (Busetti, et al., 2013)). The detection of shallow deformations (e.g. that related to neotectonic activity) is possible but only when their dimensions are comparable or higher than the resolution of the data. Higher resolution acoustic data (e.g. sub-bottom profiles), permit a more detailed identification of shallower elements (e.g. (Busetti, et al., 2010a) (Trobec, et al., 2017)). On shore, the link, between even smaller neotectonic markers and deep structures, can be carried out with other very high resolution methodologies, such as field geological surveys and paleoseismological trenches (e.g. (Poli, et al., 2009) (Poli, et al., 2015)). Moreover, regional and local deformation can be observed through geodesy data (e.g. (Poljak, et al., 2010) (Weber, et al., 2010)). These methods provide information about actual deformations, tied on variable time intervals (decades to days). Similarly, the detection of the seismicity helps in the identification of active structures at present time (e.g. (Burrato, et al., 2008) (Rebez, et al., 1987) (Del Ben, et al., 1991)).
Hereafter are briefly described the hints of neotectonic activity recorded in the Gulf of Trieste and neighbouring areas, detected by methods providing different resolutions in time and in space.

3.7.1.1 Evidences from Geomorphology and Archeology

As explained in the chapter Sea Level Change, archeological and geomorphological markers (e.g. Roman remains and notches) were used to evaluate Late Pleistocene-Holocene subsidence and tectonic movements in the eastern part of the GT (Antonioli, et al., 2009) (Furlani, et al., 2011a) (Furlani, et al., 2011b).

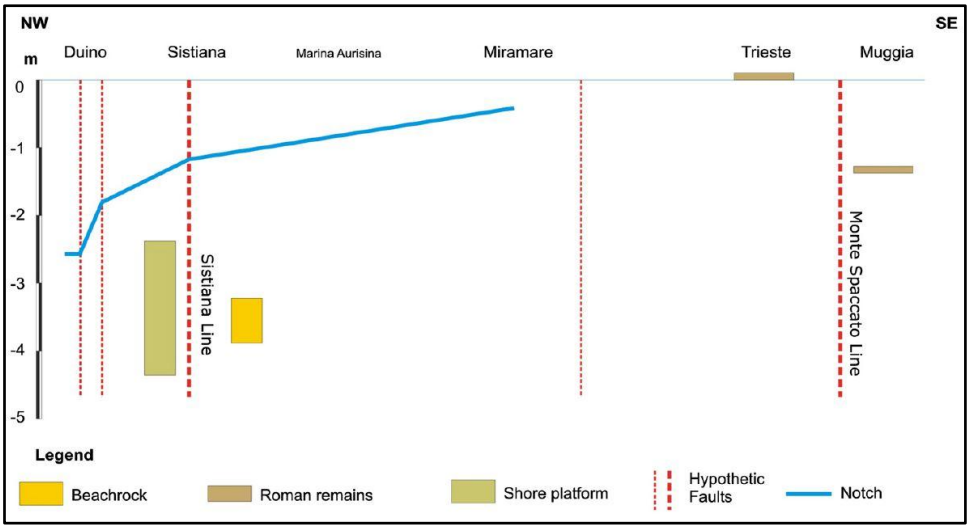

Fig. 54 – NW-SE evolutional trend of the north-eastern coast of the Gulf of Trieste. The diagram reports the relative position among different age and type of geomorphological and archeological markers and their spatial relation with the anti-Dinaric Monte Spaccato and Sistiana faults (Furlani, et al., 2011a).

From the analysis of these data, (Furlani, et al., 2011a) summarised the time (see also section 2.2.5) and space (Fig. 54) variations on sea level change and related recent tectonic movements along the eastern coast of the Gulf of Trieste. Differences have been highlighted, in the evolution since Roman times, between the northern and the southern part. In particular in the southern area, between Trieste and Muggia, Roman age remains, located at different depths respect to the present sea level, suggest the recent activity of the offshore sector of the Monte Spaccato Fault. Moreover, Post-Roman age notch deepens NW-wards; between Sistiana and Duino it displays a steep downdrop. This is attributed to vertical displacements, related to N-S and NE-SW oriented faults that affected the coastal sector with recent tectonic activity (e.g. Sistiana Fault).

3.7.1.2 Evidences from Very-Broad-Band Tiltmeter

The couple of horizontal pendulums, 95 m long, installed in 1966 within the 107 m high Grotta Gigante of the Karst, is enabled to record crustal deformations on broad-band frequencies ranging between secular tilt signals, through tides, to seismic waves. It provides 40 years of continuous registrations (secular-term) revealing a NW tilting of 23.4 nrad/year (Fig. 55) (Braitenberg, et al., 2005).
According to the Authors, the NW tilting on long term rates of the data collected inside the cave, can be extrapolated to the surrounding Karst Plateau, with a certain confidence. The genesis of this movement is attributed to tectonic activity, since long term tilting and its rates of variation are not due to atmospheric, hydrological is sea loading effects.
The evaluated crustal movement results in NW tilting by the amount of 15 nrad/year (55 m depth difference over a distance of 30 km in 125 ky) and with minimal tilting rates in the instrumental period 1979-1981 and 1995-1997 (Braitenberg, et al., 2005).
The NW secular term tilting, observed by the pendulum and the differential sea level change detected from the North Adriatic tide gauges, can be related to the geomorphological evidences of a Plio-Quaternary tilting of the eastern sector of the GT: regional tilting is not regular. In fact, this regional behaviour is modulated by discrete tilting as the result of differential movement between distinct blocks separated by anti-Dinaric NE-SW faults (Braitenberg, et al., 2005) (Romeo, 2009) (Furlani, et al., 2011a) (Zampa, 2014)).

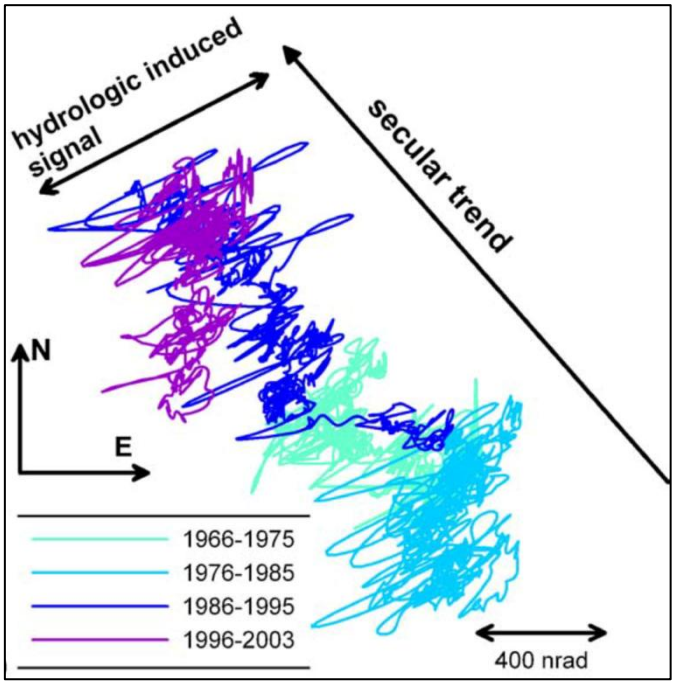

Fig. 55 - Tilt-hodograph, showing the secular variation of the tilt-vector (daily sampling filtered from the yearly variation). The colour coding refers to different time windows (light azure: 1966-1975; azure: 1976-1985; blue: 1986-1995; purple: 1966-2003. It is highlighted the NW tilting of the Grotta Gigante cave and, by extrapolation, of the surrounding Karst Plateau. (Braitenberg, et al., 2005)

3.7.1.3 Evidences from Fluid Occurrence at Sea Bed and within Quaternary Sediments

Fluid occurrence and migration in the Quaternary sediments are indentified on the MCS and sub-bottom profiles available in the GT (Busetti, et al., 2013). These are generally detected by very low amplitude of the acoustic signal (e.g. Fig. 56). The seismic data provide evidence of neotectonic deformation that affected both the Mesozoic extensional faults (at the paleo-shelf and at the basin of the carbonate platform) and the Dinaric thrusts and folds in the eastern side of the margin (Fig. 44, Fig. 56). These tectonic elements show transpressional activity related to the Neo-Alpine phase. Therefore, they are responsible for the vertical offsets within the Messinian-Pliocene unconformity. Moreover, they induced weak deformation also in the overlying marine and continental Quaternary sediments where fluid accumulation occurs. The Authors suggest that fluids migrate from deep layers towards the surface, along the main tectonic strands of the gulf. Fluids, within the buried carbonates, are those hosted in the fractured carbonate reservoir exploited by the Grado1-2 geothermal wells (Della Vedova, et al., 2008)(Cimolino, 2010).
Also high resolution acoustic data (Chirp) show accumulation of fluid in Late-Pleistocene sediments and just below the sea bed. Chirp data detect also fluids escape into the water columns as plumes. In correspondence of plumes, metric mud volcanoes and pockmarks also are present (Busetti et al., 2013).
In correspondence of fluid leakages in the northern-central gulf, (Gordini, et al., 2004) identified rocky outcrops (grebani or trezze). Outcrops are densely distributed and consist of hard grounds, built by chemosynthetic bacteria, where biota colonisation developed. Analysis of the chemical composition on seepages revealed their composition: 81-84% biogenic methane; 15-18% nitrogen and 0.7-1.3% oxygen (Gordini, et al., 2010).
Low enthalpy natural springs (38°) are present onshore the north-eastern coast, at the Roman Baths of Monfalcone and they are linked to karst conduits and heat a local geothermal anomaly rising from the carbonates (Della Vedova, et al., 2001) (Carulli, 2006b). Furthermore, (Žumer, 2004) reported eight submarine thermal springs (22-30°) on the south-eastern gulf, close to Izola.
On the basis of these evidences, (Busetti, et al., 2013) suggest that fluid occurrence is due to permeable fracture systems related to the neotectonic activity in the area.

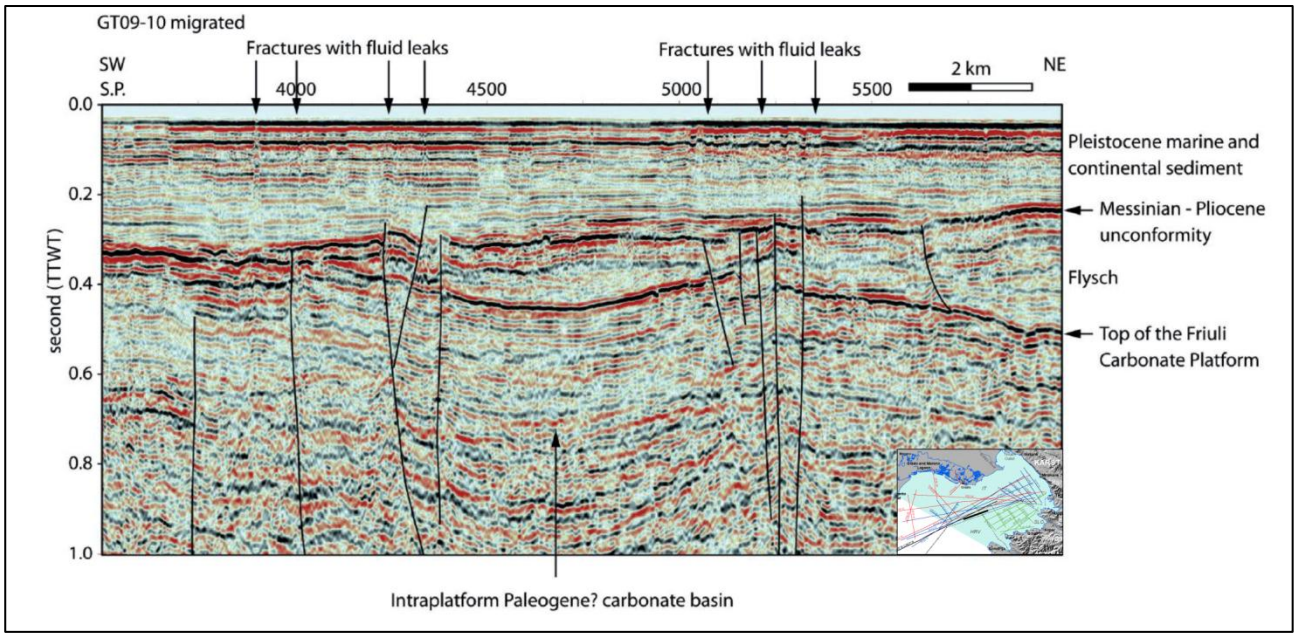

Fig. 56 – Part of the GT09-10 MCS profile acquired by the R/V OGS Explora in the GT. It shows the intraplatform basin, just east of the platform margin, infilled by Paleogene carbonates. Fault strands tectonically control the margin and disrupt the Messinian-Pliocene unconformity. They show a transpressional style reactivated in post-Miocene time. Above this fault zone, pervasive fractures occur in the Quaternary marine and continental sediments, characterised by presence of fluid in correspondence of low amplitude signals. (Busetti, et al., 2013).

3.7.1.4 GPS Measurements and Seismicity

The current N-wards motion of the Adria plate in detected by GPS measurements.
Measurements, from the Friuli Regional Deformation Network (FReDNet), define an area that is characterized by 1.6 to 2.2 mm/y of Friuli deformation (relative to stable Eurasia) in a NNW direction (Bechtold, et al., 2009). N-S oriented displacements, with velocities of 0.5 to 2 mm/y (Vrabec & Fodor, 2006) and average of 3 mm/y (Poljak, et al., 2010) are detected by GPS measurements at the Dinaric-Alpine junction in Slovenia. This movements are responsible for the overthrusting effects on the Southern Alpine sector (Burrato, et al., 2008) (Peruzza, et al., 2002a) (Peruzza, et al., 2002b) (Weber, et al., 2010). Seismicity is concentrated, in fact, in this area and along the NW-SE oriented dextral transpressive fault systems of the External Dinarides (e.g. Idrija) (Vrabec & Fodor, 2006) (Gosar, 2007) (Poljak, et al., 2010) (Weber, et al., 2010). Seismicity detected by the OGS seismic network between 1977 and 2015 (OGS, 2017) identifies main activity located along these sectors (Fig. 57). Two important events were recorded: the 1998 Bovec (Mw= 5.66) and the 2004 Kobarid (Mw=5.19) earthquakes. Both showed strike-slip mechanism and were attributed to the reactivation of some sectors of the Idrija fault system (Bernardis, et al., 2000) (Kastelic, et al., 2008). In correspondence of Istria, the Gulf of Trieste and the lower Friuli Plain, minor (MD<4) and fewer events were recorded by the OGS seismological network. However, this may be influenced by low deformation rate and or long recurrence time of earthquakes (Busetti, et al., 2013). In 1976, Mw=6.4 and Mw= 5.9 earthquakes occurred in the central Friuli, along E-W oriented compressional fault systems of the Southern Alpine domain (Zanferrari, 1978) (Peruzza, et al., 2002a) (Burrato, et al., 2008) (Rovida, et al., 2016). Focal depth of the recent events, in the area, are located in the upper crust and rarely exceed 15 km (e.g. (Rebez, et al., 1987) (Poljak, et al., 2010) (Peruzza, et al., 2002b) (Rovida, et al., 2016).
As concerns the historical seismicity, the 26th March 1511 earthquake, Mw=6.3 (Rovida, et al., 2016) Mw=7.2 (Ribarič, 1982), is considered the strongest one. It caused extensive damages between Ljubljana and Bovec and its exact location and nature are still uncertain; it is probably related to reactivation of the central sector of the Idrjia fault (Fitzko, et al., 2005) (Poljak, et al., 2010).
Analysis on seismological data related to Friuli and Slovenia, suggest different seismicity behaviour between the two areas. The boundary is located along the zone of the superficial contact between the South-eastern Alps and the Dinarides. The first area shows periodic strong seismic sequences related to compressive tectonics; while the latter is characterised by more diffuse activity in time, related to transcurrent movements. Despite this, the total amount of energy released is similar for the two areas (Rebez, et al., 1987) (Del Ben, et al., 1991).
(Kastelic, et al., 2012) assume Mw=6.5 possible earthquakes (at depths of 1-15 km) in the north-eastern Adriatic domain, related to two composite seismogenic sources (CCS). These are named Northern Trieste Gulf (ITCS100) and the Southern Trieste Gulf (ITCS101). According to the Authors, the ITCS100 comprises the NW-SE oriented Črni Kal thrust fault in Istria and the Karst Trust system on the eastern side of the Gulf of Trieste. The estimated magnitude is based on structural configuration defined from onland field analyses and offshore seismic data. Anyhow, this estimation should be constrain by further detailed information on the geometry, depth and areal extension of the fault surfaces, that at present are still not precisely known.

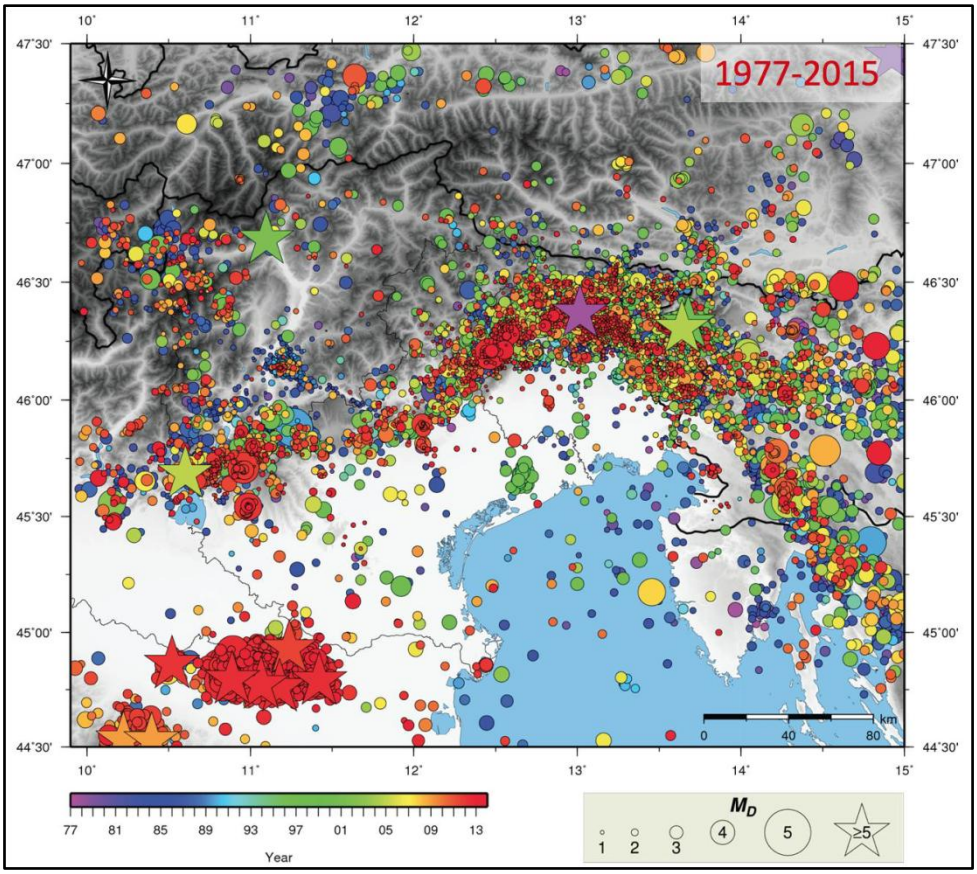

Fig. 57 – Map showing the seismicity recorded by the OGS seismological network, from 1977 to 2015. The colours indicate the year of the events, while the circles dimensions are proportional to the magnitude MD. Stars evidence the events with MD higher than 5 (Bovec 1998 and Kobaric 2004 in green; Friuli 1976 in purple). In the Southern Alpine – External Dinaric sectors, seismicity is concentrated along main NW-SE Dinaric fault systems and E-W Alpine lineaments. In the Gulf of Trieste few and low magnitude (MD<4) events are recorded by instruments. (OGS, 2017).

4 METHODS

4.1 Foreword

Geophysics refers to those quantitative and indirect methods used for the study of the physical properties and processes of the Earth (Sheriff, 2002). From a general point of view, these are related to subsurface geological applications, but include also the methodologies giving insights on the processes characterizing the atmosphere (e.g. electricity and magnetism of the ionosphere) and the hydrosphere (e.g. dynamics of ocean and ice systems).
As concerns application to the solid Earth, geophysics encompasses indirect methods aiming at the analysis of its gravitational and magnetic fields, shape and internal structure, dynamics and composition. The techniques investigating these features provide information at different time and space scales. These can vary from short (e.g. minutes, days, years) to long periods (e.g. geological times) and from local areas (e.g. meters to tens of kilometers) to wide regions (hundreds of kilometers or more). Moreover, they supply also a wide range of depth resolution, with orders of magnitudes spanning between centimeters to hundred of kilometers. Usually, data obtained from different geophysical disciplines, such as geodesy, seismology and active seismic, are combined to gather more accurate and reliable results (e.g. Nicolich et al. (2004a,b); Braitenberg et al. (2006); Carulli (2006a,b); Romeo (2009); Busetti et al. (2010a,b); Poljak et al. (2010); Weber et al. (2010); Busetti et al. (2013)).
Among these techniques, the active seismic method is one of the most important for indirect subsurface investigation, at shallow (some meters) and deep (several kilometres) depths. The seismic acquisition is performed both on-shore and in the marine offshore. Its principal goal is to provide a 2 or 3 dimensional acoustic image of the subsurface that should give information about structure and properties of the investigated *medium*, with the maximum possible accuracy. The application of this methodology started in the 1920's, with the purpose of investigating sedimentary basins for oil and gas prospecting. Since the 1970's this technique further developed becoming very important for the understanding of the mid-lower crust structure (e.g. Sheriff & Geldart (1995); Telford et al. (1990); Yilmaz (2001)).
In the framework of the present study, a network of multichannel seismic (MCS) data, acquired in 2009 and 2013 by the R/V OGS Explora, is accessible as SEGD and SEGY file. It is available in time domain, in the form of pre and post processing (this latter managed in the Kingdom (IHS, 2014) software database). Moreover, the profiles allow the investigation of the subsurface up to five kilometres. Their maximum resolution permit to get insights on the depth relationship among the main Meso-Cenozoic geological units characterising the Gulf of Trieste.

4.2 The Active Seismic Geophysical Method

The aforementioned seismic method is an active technique consisting in the generation of elastic waves at a source and the recording of the seismic energy returned to the surface, after having travelled through the subsurface. The reflection occurs when a seismic wave encounters a boundary between two materials with different acoustic impedances, part of the energy is reflected at the boundary, while part of the energy propagates through the underlying material. Each reflected event is registered through time by the surface sensor and the so-obtained series of events constitutes the seismic trace.
In particular, the MCS reflection technique concerns the recording of a reflected event across a number of different seismic receivers (arranged along a streamer in the offshore or an array in the onshore) to get an ensembles of traces bringing information from the same vertical position of the medium. The availability of multitrace data ensembles permits an enhanced signal data processing that is crucial to obtain good images of the investigated subsurface, both in time and depth domain. Data processing encompasses the execution of a wide array of operations, such as amplitude correction, velocity analysis, static and dynamic correction, deconvolution, stack, migration.

4.2.1 Foreword on Wave Basics

A wave is a disturbance propagated through a body or on a surface of a medium without involving net movement of material (Sheriff, 2002).
Seismic waves include body and surface (e.g. Rayleigh and Love waves) waves that travel in three dimensions through a medium and along its free surface, respectively.
Two types of body waves are distinguished, on the basis of the different motion of the wave respect to that of the particles in the medium through which they propagate:

- compressional or longitudinal waves (P-waves): they propagate along a direction that is parallel to that of the particles motion. The medium undergo dilatation and compression alternatively. The P-wave velocity (Vp) propagation depends on the elastic properties (k=bulk modulus; μ=shear modulus) and on the density (ρ) of the medium. These quantities are related as follows:

$$Vp = \sqrt{\frac{k + \frac{4}{3\mu}}{\rho}}$$

- shear or transverse waves (S-waves): the displacement of the particles is perpendicular to the direction of wave propagation and these waves cannot propagate in fluids. Particles can move along the horizontal (S_H) and the vertical (S_V) plane and the medium is not affected by changes in volume. The S-wave velocity (Vs) propagation depends on the elastic shear modulus (μ) and on the density (ρ) of the medium. These quantities are related as follows:

$$Vs = \sqrt{\frac{\mu}{\rho}}$$

Within an homogeneous medium compressional and longitudinal waves propagate independently; moreover, P-waves arrive first than S-waves, since they have higher velocity. In the active seismic reflection method, the use of body waves.

4.2.2 The Seismic Velocity Field Detection

The construction of a detailed and reliable seismic velocity field is crucial for an accurate estimation of the depths of geological elements and can also provide information on underground rocks and fluid properties. There are several methods that permit to estimate this seismic attribute (e.g. Bishop et al. (1985); Dobrin & Savit (1988); Sheriff & Geldart (1995) Yilmaz (2001)).
The conventional velocity analysis is based on the evaluation of the stacking velocity by means of the hyperbolic approximation. The common depth point (CDP) gather, composed of traces bringing information from the same position of the subsurface, is represented in a section whose horizontal axis is represented by a distance (offset), while the vertical axis is represented by time (seconds). With offset value increasing, the path followed by the seismic wave (toward and from the same reflector, supposed parallel with the acquisition plane) increases, together with the arrival time (relatively to the same geological reflector). The law of motion which describes arrivals of reflected events, with the change of the source-receiver distance, is hyperbolic.
The Normal Move Out (NMO) operation makes hyperbola reflections, within a CDP gather, horizontal. The operation eliminates the delay time of events registered by those receivers that are placed at a offset values different from zero. The correction uses the two way travel time versus stacking velocity values picked during the velocity analysis. If the selected velocity is too high than the right one, the hyperbola will be positioned below the horizontal position (undercorrected). If the selected velocity is too low, the hyperbola will be positioned above the horizontal position (overcorrected), Fig. 58. The dynamic correction encompasses also an algorithm automatically explores the solution space (coherency functional) delivering panels of root mean square velocities as function of arrival time of each reflected event to which is associated the supposed best fitting velocity to be used in the calculation of NMO. The application of these methods is subjected to several assumptions such as the small spread approximation (offset minor than reflectors depth and plane-parallel and sub-horizontal strata (the maximum dip acceptance is about 15°). As the arrival time (t_0) of the reflected event increases, the NMO correction becomes less sensitive to the changes of the velocity values. This results in a less defined amplitude contour which covers a wide range of possible velocity picking. Furthermore, the velocity spectra and hyperbolic analysis are subject to individual user interpretation.

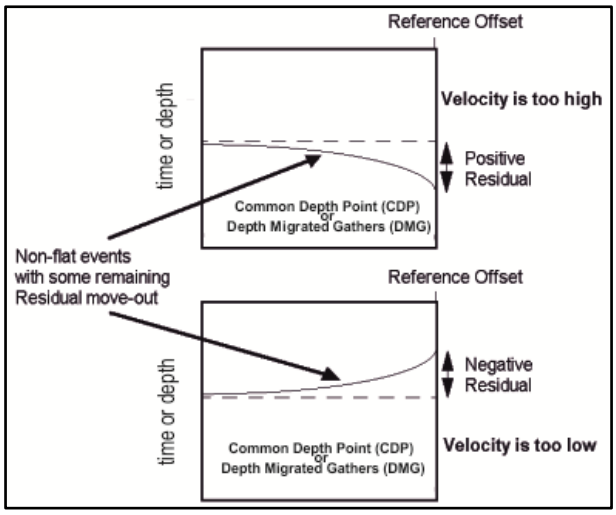

Fig. 58 - Representation of under/overcorrected residual move-out on a common depth point (CDP)/depth migrated gather (DMG). The aim of the move-out correction is that of the visual detection of the velocity value (maximum amplitude coherence on semblance panels) that permits to flatten the reflected event observed on a CDP/DMG. If the selected velocity is too high, the event will be undercorrected (positive residual, respect to a reference offset), while when the velocity is too low the event will show a negative residual related to an overcorrection.

Seismic tomography provides a versatile tool for the velocity estimation from either borehole or surface reflection data. Respect to the conventional velocity analysis, it allows resolution of vertical as well as lateral velocity gradients, that are considerably important for the better definition of the correct geometries. It relies on ray tracing and iterative procedures that are based on the Snell's law and that minimize the difference between the modeled and measured traveltimes. Therefore, it can deal with the problem of complex geological structures, recontructing them with higher accuracy (e.g. Böhm et al., 1999; 2000; Vesnaver and Böhm, 2000; Rossi et al., 2001; 2011). The word tomography is derived from the Greek "tomos" meaning cut or slice. The term literally means "graphing slices of an object". The goal of tomography is the imaging of material properties by using observations of wave fields which have passed through the body. The tomographic method has been used in many fields including medical imaging, materials testing, civil engineering, and geophysical exploration.
Hereafter it will be treated mainly for the estimation of seismic velocities by using travel-time information. Traveltime tomography provides a 3D velocity volume which can be used to recover the depth of the geological sedimentary units and the geometry the related surfaces.

4.3 The Seismic Tomography Technique

Seismic tomography is a valuable instrument for the velocity analysis, it started to be used in the 1960s (Backus & Gilbert, 1967). Clayton (1984) defined "seismic tomography" as the reconstruction of a field from the knowledge of linear path integrals through the fields. If the response of the system to a perturbation is known, it is possible to try to deduce its physical properties. The tomographic method uses the theory of the inversion to infer these parameters, starting form a dataset of measures. The limit of the inverse problem is the non-uniqueness solution, that can also be related to the typology and quality level of the dataset used for the inversion. The problem of non-uniqueness of the inverse modelling can be reduced by performing an iterative algorithm constrained by known geological information that makes it as much as possible similar to the real model.
There are several current applications of travel-time tomography to seismic exploration and the method represents a viable approach to these problems, since tomography is based on a very general description of the Earth's subsurface. Due to its generality and wide range of applications, tomography has been used for many exploration problems involving both borehole and reflection/refraction data.
The travel-time tomography method consists of the following steps (Yilmaz, 2001):
- The data gathering step, consisting in the identification of seismic traveltimes for various source-receiver positions.
- The modeling step, consisting on the ray tracing to formulate traveltime equations.
- The inversion step, computing the solution of traveltime equations and the estimation of the updated velocity models.
The first step is generally the most time-consuming, in terms of a geophysicists effort, since the picking of traveltimes essentially involves the interpretation of pre-stack seismic data. The user-interpretation session involves the identification of tens of thousands of arrival times, typically requiring long time. For good data, automatic picking can substantially decrease the amount of time taken by the interpreter for this step. However, even with good data, travel-times from automatic picking procedures should be inspected for possible errors. Since the travel-times represent the data to be inverted in tomography, the interpretation step is very important. Although it is time-consuming, the traveltime picking phase allows to avoid noise data and visually filter them directly during the interpretation. Step 2 involves the modeling of the traveltimes for some velocity model. Generally, ray tracing is used to compute the traveltimes for some velocity configuration. The ray tracing method, applied in this work, is based on the principle of minimum time and honors Snell's law by curving rays in the presence of velocity gradients at the interfaces. The third step in the procedure involves combining the results of Steps 1 and 2 and finding a solution of the traveltime equations.
The traveltime equations can be expressed as $t = Du$ where t is a vector containing the traveltimes of a raypath, u is a vector containing slowness values for each cell, and D is a matrix of values, D_{ij}, which represents the distance travelled by the *ith* ray in the *jth* cell. This system appears to describe a linear relationship between traveltime and slowness. However, raypaths bend according to Snell's law and, therefore, this system is generally nonlinear since the distance values are themselves functions of slowness. Thus, as with most nonlinear systems, we iteratively solve a series of linearized problems in order to obtain a solution.

4.3.1 Traveltime Tomography

The method applied in this work consists of the picking of the traveltimes of the main reflections at different offsets and the subsequent tomographic inversion.
The seismic tomographic analysis is performed on observed P-waves traveltimes of two main reflectors (the seabed and the top surfaces of flysch and carbonates) on part of the multichannel seismic reflection profiles acquired by OGS in 2009 and 2013 (see section Geophysical and Geological Dataset and chapter Results).
The input consists in the reflected and refracted P-wave traveltimes picked on pre-stack MCS seismic data sorted by common shot gathers (traces having the same source location and recorded along the receivers array). The common offset gather type of trace sorting (traces recorded by channels that have in common the same distance from source and related to different source positions) was also used to help the picking, since it shows a section whose horizontal axis is represented by a distance and vertical axis is represented by two-way-traveltimes. In particular, the near offset section (minimum common offset gather) can show a first indicative image of the explored *medium*. Nevertheless, the pre-stack section is affected by numerous diffractions and multiples, by weak amplitude of the deepest reflections and by a low signal/noise ratio. For this reason, the observation of the main events was aided also by the seismic interpretation of stacked and migrated data in time domain.
The tomographic algorithm used herein (Böhm et al., 1999; 2000; Vesnaver and Böhm, 2000; Rossi et al., 2001; 2011) estimates the velocity field and reflector structure in sequence, from the shallower to the deeper horizon (layer stripping method). Reflected, refracted, direct waves and both P and S waves may be analysed by the package.
The adopted tomographic iterative inversion procedure is represented in Fig. 59.
It starts with an initial model for the velocity field and interface structure, generally it consists of homogeneous layers and flat-parallel surfaces. The inversion procedure, performed by the CAT3D software (OGS, 2014), uses the observed travel times to calculate the minimum-time ray tracing. The path between source and receiver is defined through an iterative process following the Fermat's principle (Böhm et al., 1999). The procedure continues for traveltime inversion, by applying the Simultaneous Iterative Reconstruction Technique (SIRT) and detects the seismic velocity through an iterative process that minimizes the traveltime residuals (Van der Sluis and Van der Vorst, 1987; Stewart, 1991).
Then, following the principle of minimum dispersion of the reflected/refracted points (Carrion et al., 1993), the depth and geometry of the new interfaces are estimated. The travel time residual associated to each reflected/refracted event is converted into depth by using the velocity field updated in the first step of any iteration.
The loop ends when the variations, of the resulting model with respect to that of the previous step, are sufficiently small. This occurs when the dispersion of the estimated reflection points reaches a minimum, so that the reconstructed interface geometry does not vary considerably anymore.
The reliability of the tomographic result can be evaluated by computing the time residuals, that represent the differences between the picked and the computed travel times (Zelt and Smith 1992). Furthermore, another measure for the reliability of the tomographic inversion is the null space energy, based on the singular value decomposition of the tomographic matrix (e.g. Vesnaver 1994). This is a measure not only of the ray number in each pixel, but also of the independence of

the tomographic matrix equations, and therefore of the matrix rank (see section Error Estimation and Reliability of the Tomographic Inversion).

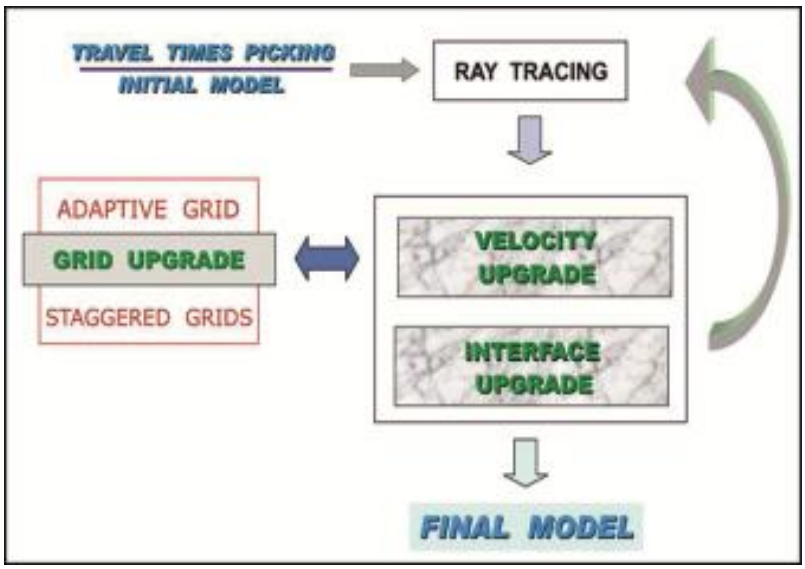

Fig. 59 – Scheme representing the iterative procedure for the traveltime tomographic inversion adopted by the CAT3D software (OGS, 2014): starting from the observed traveltimes and an initial 3D guess model, the code calculates the minimum-time ray tracing, detects the velocity field and the estimates the surface depth and geometry. During each inversion step, staggered or irregular adaptive gridding procedures can be applied to better upgrade the velocity grid. (OGS, 2014).

4.3.1.1 The Initial Model and the Updated Grid

Generally, the 3D model, handled by the adopted CAT3D (OGS, 2014) software, consists of N layers, representing velocity domains and N+1 interfaces. Layers and interfaces constitute two macro-elements, that are together represented by a grid.
The grid can be regular or irregular, depending on the pattern chosen for the discretization of the macro-elements. Usually, the grid sampling choice, should be done considering the available ray density characterizing the model, to preserve the related resolution and stability of the result. The complexity of the geological structure, that has to be reconstructed, influences as well. Moreover, time and computational cost change in different cases (Böhm & Vesnaver, 1999; Böhm et al., 1999;2000).
Every layer is bounded by two interfaces, one at its top and one at its base. It is made up by a set of polyhedral elements, or voxels, with lateral vertical boundaries and bases (pixels) given by regular (e.g. quadrangular) or irregular (e.g. hexagonal, rhombic, triangular) polygons, with convex forms. The velocity is assumed to be vertically constant within each voxel, bounded by two interfaces along the Z axis. Whereas, the field values can vary laterally, passing through the layer's voxels along the X and Y axes. As concerns the characteristics of the pixels, that will in turn concur to define the grid type, a regular quadrangular pattern allows, for example, a simple and efficient ray-tracing; while the complexity of the hexagonal one requires higher calculation cost, but provides an optimum discretization for the detection of the velocity field.
The interfaces of the grid represent vertical discontinuities within the model and they are related to reflected or refracted events. They can be characterized by horizontal or dipping planes, discretized by nodes interpolated by triangular network of facets. The model can be modified at each step on the inversion by varying the number of layers, by re-sampling the both the macro-elements independently, changing the depth of the interfaces and the velocity values within the voxels.
Generally, the starting model consists of layers, each of these having constant velocity values (e.g., single voxel), and interfaces initially set as horizontal and flat. It is improved at each iteration step of the tomographic inversion (Bishop et al., 1985). Moreover, constantly adapting the pixel shape and distribution, through a trial and error approach, can considerably improve the resulting quality of the inversion (Böhm & Vesnaver, 1999; Böhm et al., 1999).
Within each step of the tomographic inversion, staggered and irregular adaptive gridding procedures can be applied to optimize the velocity grid. Both gridding methods improve the resolution of the velocity model while preserving the stability of the inversion (Böhm et al., 2000; Vesnaver and Böhm, 2000). In fact, in the case of limited and non-uniform coverage, the solution of the tomographic inversion is not unique.
The staggered grid process (Fig. 61) applies small shifts to a coarse and well-conditioned base grid along two mutually orthogonal directions. The results of the tomographic inversion carried out for each shifted grid are averaged, resulting in a smoothed image, but with a higher resolution compared to the base grid (higher number of resulting voxels), without losing reliability (Vesnaver and Böhm, 2000). The initial grid may be regular or irregular, the former is the most colud represent an optimum choise when the raypth distribution is homogeneous.

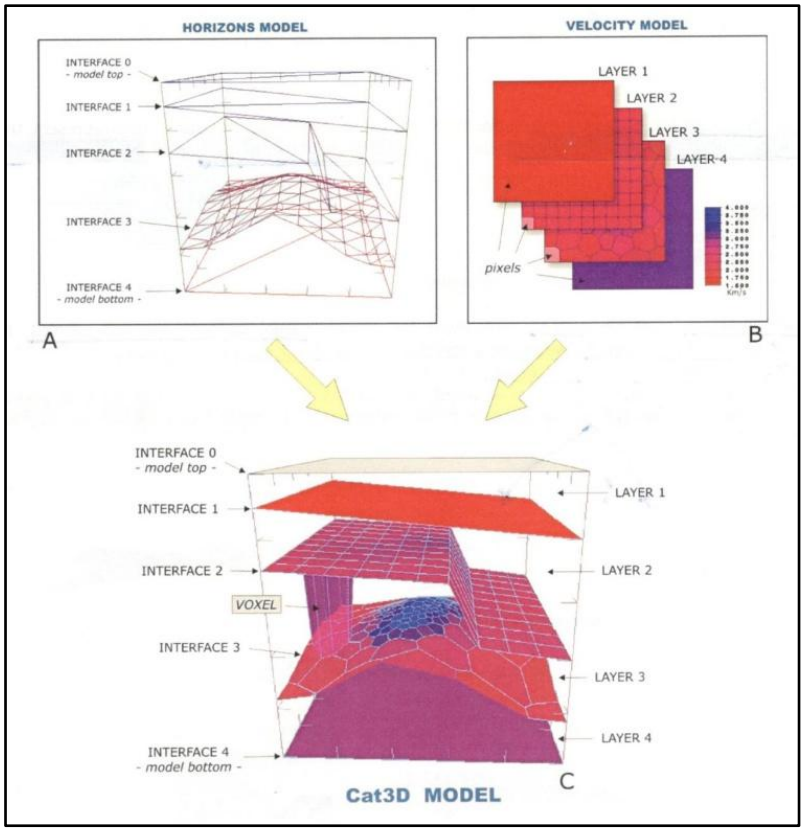

Fig. 60 – Representation of the macro-elements, that consist in discretized N+1 surfaces (a) and N layers (b). Together, they are used to build the 3D model (c) adopted by the CAT3D software (OGS, 2014), to perform the traveltime tomographic inversion. The interfaces represent vertical discontinuities and can be defined as horizontal or dipping planes, sampled by triangular facets. Between two interfaces, a layer is present. It is characterized by voxels, whose convex bases (pixels) can be regular or irregular. (OGS, 2014).

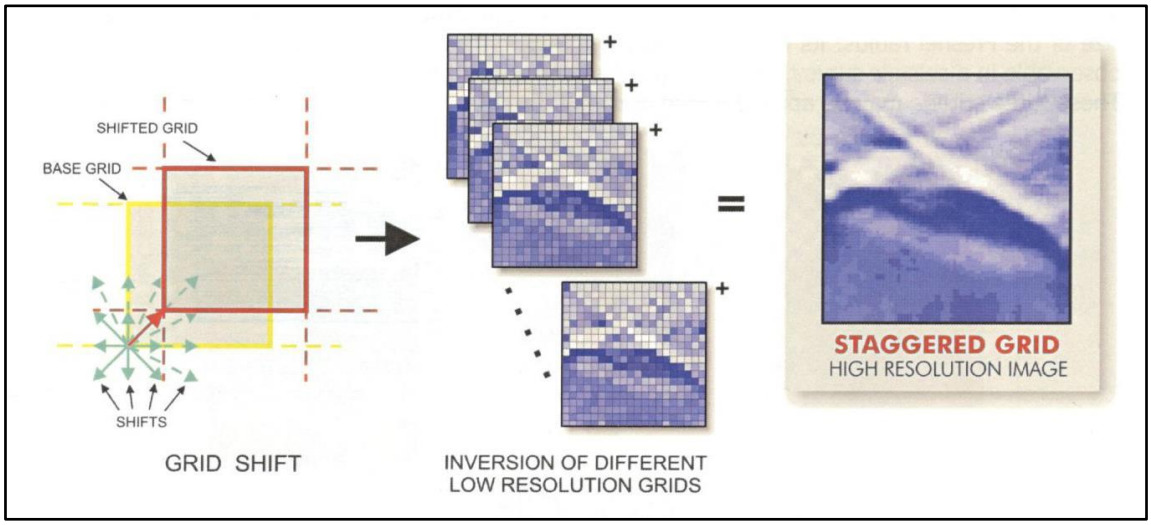

Fig. 61 – Representation of the staggered grid procedure, that consists of the superimposition, on a base grid, of others, obtained by shifting the initial one. The resulting staggered grid, after a tomographic inversion carried out for each shifted grid, is an higher resolution image (made of larger number of voxels), that still preserves the initial reliability.

4.3.1.2 The Ray Tracing

The minimum-time ray tracing approach represents the first step of the adopted traveltime tomographic procedure. It is based on the calculation of the path between source and receiver through an iterative process, based on the on Fermat's principle (e.g. Böhm et al., 1999). The principle is based on the reconstruction of the ray path, connecting two points, which minimises the traveltime.
An iterative algorithm minimizes the difference between the modeled and measured traveltimes through the relation:

$$\Delta t = t^{OBS} - t^{CALC} = \sum_{j} \Delta s_j \Delta u_j$$

where t^{OBS} is the observed traveltime on the data, t^{CALC} is the the traveltime generated by a ray tracing through a discretized tomographic model, Δs_j is the ray segment within the j^{th} pixel, and Δu_j is the slowness (inverse of the velocity) variation in the jth pixel.
The CAT3D (OGS, 2014) software, recontructs the ray tracing through a group of three consecutive points that are found by the intersection of the ray with the voxels of the 3D grid. The procedure can be performed in the case of direct, reflected, refracted (and head), diving waves, with different precautions in the different cases.
In general, for the reflected waves, the method starts considering a straight path along the first three points, these are in turn repositioned along the borders of the pixels. Base on the Fermat's law, the trajectory of the rays is reconstructed by tacking into account the varying velocity through the adjacent pixels and therefore creating bent rays (Fig. 62). The procedure continues by involving the subsequent triplets along the intial guess segment, ant it stops when the end parth is reached. At this point the ray tracing is preformed on the way back to the first point. This iteration is repeated antil the recontructed ray path has reaches a minimum acceptable difference respect to the previous iteration. The number of iterations that can be applied, thus, depends on the precision level that the user intends to achieve and, of course, on the complexity and desity discretisazion of the grid.
The algorithm adoped by the CAT3D software for the ray tracing applies the first derivative of the raypath traveltime. Successively, it finds the solution related to the minimum time by equalising the derivative to zero.

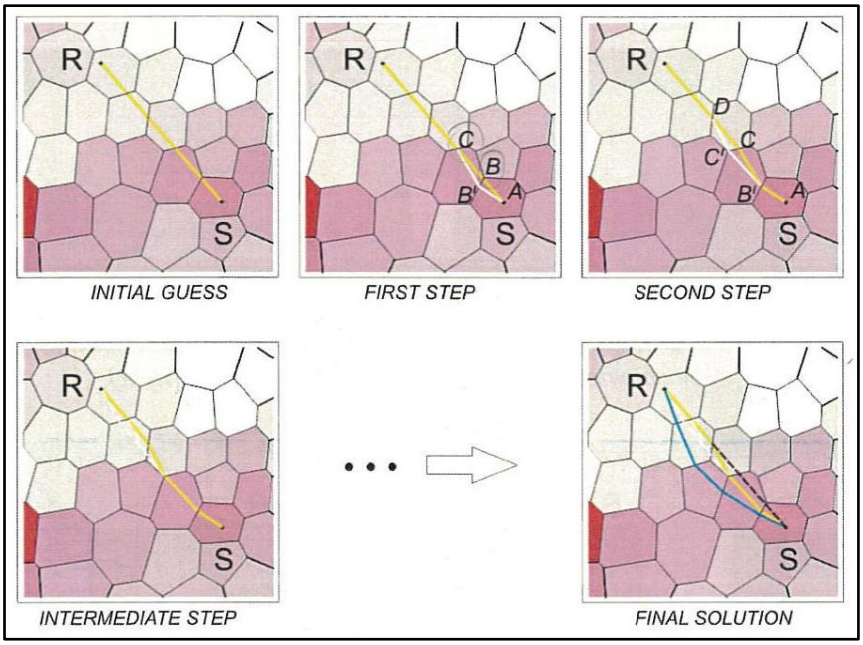

Fig. 62 – Representation of the procedure that the CAT3D software (OGS, 2014) encompasses for the reconstruction of the ray path, connecting two points (R and S). The iterative algorithm, on the basis of the Fermat's principle, equalises the first derivative of the ray path traveltimes. The method considers triplets of point (intersection between the ray path and the borders of the grid pixels) and constructs bent rays, moving from S to R and backwards, until the difference between the modeled and measured traveltimes is minimized. (OGS, 2014).

4.3.1.3 The Layer Stripping Method and Other Possible Constrains

The adopted CAT3D (OGS, 2014) software allows the application of the “layer stripping” method (Fig. 63). It consists of the inversion of each layer of the model, one by one, from the shallower to the deepest. During the inversion of a layer, the velocity and geometry estimated in the previous steps can be constrained. Therefore, it is possible to avoid a velocity averaging through the entire model. A delicate aspect of the layer stripping method has to be taken into account. It is possible that the eventual errors, that has been previously produced, propagate while proceeding into depth. Thus, the reliability and the precision of the results decreases at increasing depths. Thus, The joint inversion, inverting together traveltimes related to different interfaces, can be valuable, at the end of the layer stripping procedure (Vesnaver et al., 2000; Accaino et al.; 2005 Rossi et al., 2007).
The CAT3D (OGS, 2014) software permits also to constrain the detected velocity result. It can be done by defining a range limit for the local velocity in each voxel (local constrain), of by forcing the limits to all the layers of the model (global constrain). It is also possible to set a constant velocity, that is useful especially in the layer-stripping procedure. Thus, the velocity estimation is focussed only on the layer that has to be newly processed, allowing a more detailed result for it.
Moreover, these constraints to be applied in two ways(Fig. 64). One (normal) lets the estimated velocities vary, during each iteration, only inside the limits range. The other (datum) lets the inversion algorithms to take into account only the part of the ray passing through the current inverted layer, as if the sources and receivers were repositioned just above the processed layer. This latter is useful, for example, to better resolve a deeper and thinner layer, covered by thicker unit (e.g. thick water column in offshore seismic data), otherwise the traveltime variation of the former results too small respect to that of entire ray path.

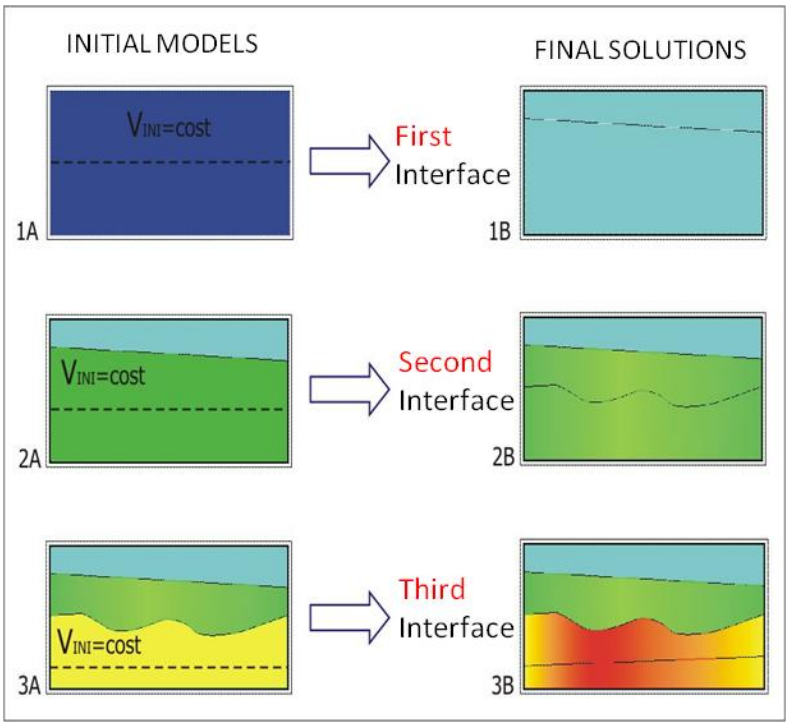

Fig. 63 – Flow chart of the layer stripping method, applied by the CAT3D(OGS, 2014) software. Starting from an initial model (1A), the tomographic inversion is performed for of each layer and related interface of the model, subsequently from the shallower (1) to the deepest (3). During each inversion, the velocities and geometries estimated in the previous steps are constrained.(OGS, 2014).

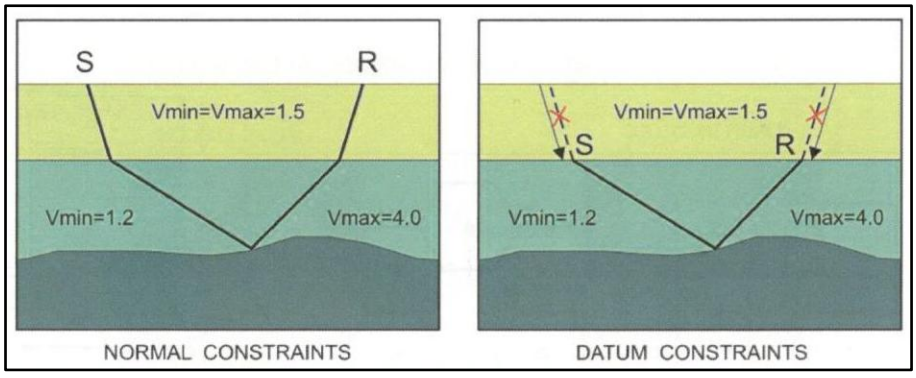

Fig. 64 – Sketch representing the characteristics of the normal (left) and datum (right) constraint applications in the CAT3D software. In the first case, the inversion procedure considers fixed (inside the defined limit ranges) only the velocity field of the layer overlying that is being processed. The ray path is entirely taken into account by the tomographic algorithms. The second case differ from the former for the fact that the ray-segments crossing the overlaying layers are not taken into account. This results in a source-receiver configuration that is re-datum at the top of the inverted layer. (OGS, 2014).

4.3.1.4 Velocity Field Detection

The CAT3D (OGS, 2014) software adopts the different algorithms (e.g. ART, Algebraic Reconstruction Technique; SIRT, SImultaneous Iterative Reconstruction Technique) for the detection the seismic velocity field.

Both ART and SIRT are series of expansion methods. They differ in their convergence velocity. ART is faster and detects sharp velocity variations, while the SIRT method (Van der Sluis and Van der Vorst 1987) is slowly converging. Nevertheless, it is more robust also in the presence of noise. Moreover, it gives a generally smooth velocity field as solution (e.g. Dobroka et al. 1992). This difference is due to the fact that ART updates the tomographic model at each ray path inversion. Whereas, SIRT accumulates and averages the correction obtained from each ray inversion. Only at the end of the entire set of ray tracing reconstruction, it applies this correction. Therefore, the result obtained from ART depends on the order of the inverted ray path. This does not occur for the SIRT. The combined application of ART+SIRT is sometimes useful to perform a faster inversion, reducing anyhow the ART limit of a sharper result.

A useful property of SIRT is the possibility of applying some constraints on the solution, obtained from other kinds of information, such as logs or geological models, although a limitation of SIRT is that it allows larger amplitudes for the solution in pixels that are poorly crossed by rays. It is therefore necessary to minimize the ray-count differences in the pixels, or to evaluate the reliability of the solution for each one of them.
The SIRT algorithm is used in the present study to estimate the seismic velocity field.
Let's start considering a 3D model composed of voxels characterised each one by a constant velocity. The ray path between the starting point S and the endind point R, is constituded by a numebr of straight segments. The ray (i^{th}) segment has the length (d_j) inside the voxel (j^{th}), the slowness (s_j inverse of velocity) characterizes every voxel of the model, where (m) is the total number of the involved voxels. These are related by the following relation for the traveltime (t):

$$t^i = d_1^i s_1 + d_2^i s_2 + d_3^i s_3 + \dots + d_m^i s_m = \sum_{j=1}^{m} d_j^i s_j$$

The ART and SIRT algorithms perform the computation through an iterative process that minimizes the traveltime residuals. This produces the following optimal solutions, where Δt^i represents the residual traveltime in the i^{th} ray

For ART: $\Delta s_j^i = \frac{\Delta t^i d_j^i}{\sum_{j=1}^{m} \left(d_j^i\right)^2}$

For SIRT: $\Delta s_j = \left(\frac{1}{N}\right) \sum_{i=1}^{N} \left(\frac{\Delta t^i d_j^i}{\sum_{j=1}^{m} \left(d_j^i\right)^2} \right)$

The procedure applied by the ART and SIRT methods can be graphically represented in the case the intention is that of searching the intersection (I) between two straight lines in the X-Y plane (Fig. 65). The lines represents two observed physical parameters. Starting from the initial guess, the nearest line is identified by tracing a normal path respect to it. The point 1 results from the

intersection of the ray path with the straight line and with the half distance between the two straight lines for the ART and SIRT, respectively. Point 2 represents a updated and better estimation of the intersection point (I). Restarting the procedure from the point 1, the orthogonal segment respect to the other line is detected. The new point 2, further nearer to the point I is then identified. The loop continues until the best solution possible for the point I is reached. The Fig. 65 highlights that the convergence criterion, for the two algorithms, is different: while ART oscillates around the solution, SIRT has an asymptotic convergence. Therefore, this demonstrates that the SIRT method is more stable that the ART one. As said, SIRT updates the inverted model after having inverted all the system equation. The correction will be applied at the end of the procedure and consists of an averaged value related to all the traced rays.

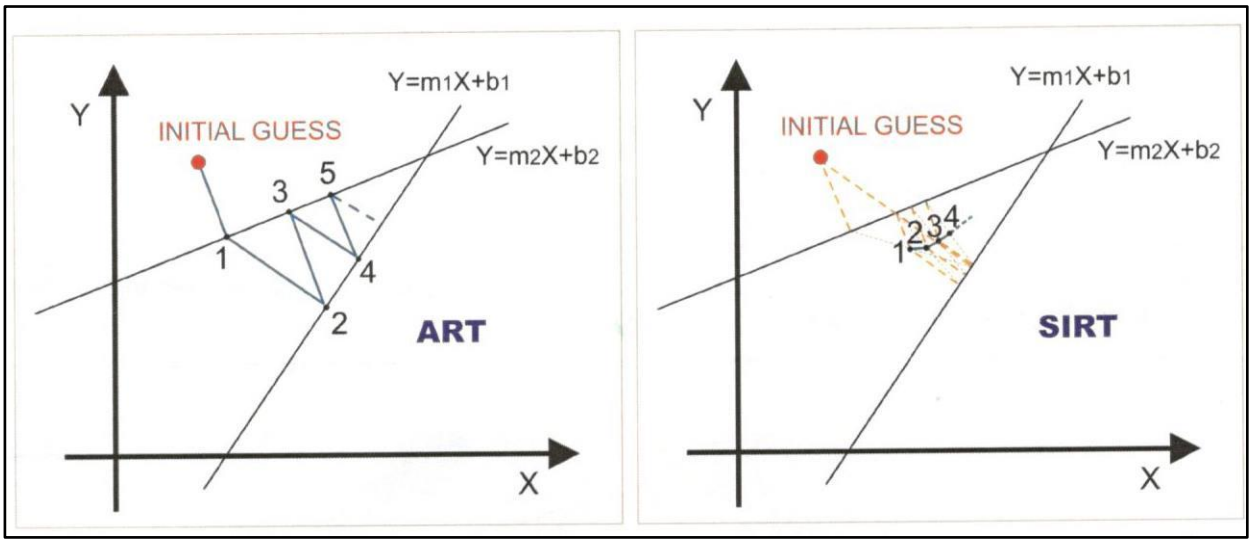

Fig. 65 – Graphical representation of the iterative procedure applied by ART (left) and SIRT (right) methods . The loop searches the intersection between two straight lines in the X-Y plane. ART, although it is faster, oscillates around the solution; while SIRT is slower, but provides a smoother convergence. (Stewart, 1991).

4.3.1.5 Interface Estimation

An algorithm, based on the principle of the minimum dispersion of the estimated reflection/refraction points (Carrion et al., 1993), estimates the depth and geometry of the interfaces. The procedure is stopped when the dispersion of the estimated reflection points reached a minimum, meaning that the shape of the surface does not show sensible changes.
At this point of the iterative procedure performed by the CAT3D (OGS, 2014) software (Fig. 59), the velocity field is obtained through the ART of SIRT methods (described in the previous section 4.3.1.4).
The software can now use the local velocity, at the reflection/refraction points, to convert the residual traveltimes into depth (dz, depth residual). This is done for the reflected/refracted events at the discontinuities within the model. The depth of the interface is therefore updated by adding the newly estimated dz (Fig. 66). The surface can be represented by a spline function that interpolates, with the best approximation possible, all the updated depth points. These may be dispersed by different error values (e.g. Fig. 70), also related to the number of inversion the procedure underwent. At the beginning, for example, higher dispersion characterizes large offsets arrivals.
At this point, the a completely inverted tomographic model is obtained. A new loop of traveltime tomography can be performed, restarting from the first step related to the ray tracing. Anyhow, if the last resulting model do not display sensible variations with respect to the previous one, the last model can be considered as final and the tomographic inversion is can be stopped.

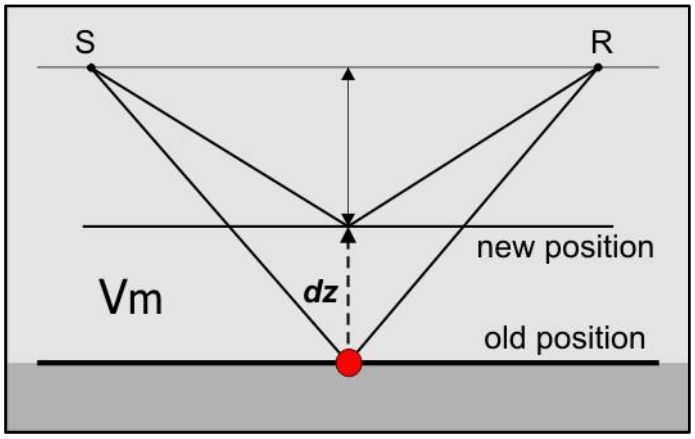

Fig. 66 - Scheme representing a section where a cell of the tomographic model is bounded at the top and bottom by two surfaces. The depth vertical correction (dz) can be estimated (by using the previously detected ray path, Vm velocity and depth and geometry of the voxel) to update the position of the reflected point (red point), back-scattered by the interface. (OGS, 2014).

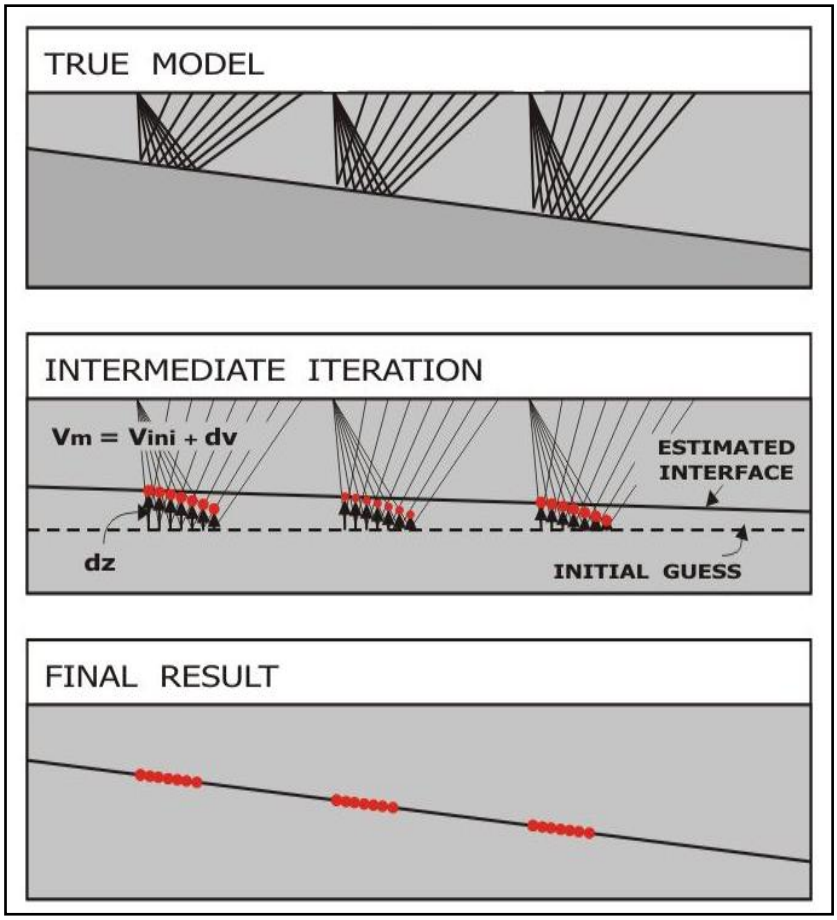

Fig. 67 – Scheme representing the steps through which the depth and geometry of an interface are reconstructed, to obtain a final result that represent, with maximum accuracy possible, the real geological structure (true model). Once the velocity field of a voxel is detected, the residual traveltimes are converted into depth, giving the depth residual (dz). The depth vertical correction is then applied to the reflected points, whose new position will define, in turn, the depth and geometry of the updated surface. The procedure is based on the algorithm of the minimum dispersion of reflection points. (OGS, 2014).

4.3.1.6 Error Estimation and Reliability of the Tomographic Inversion

The evaluation of the total error, of the tomographic inversion result, is hard. There are several factors that concur, such for example the traveltime picking, the noise in the data, the source-receiver coordinates, the smoothness in the ray tracing. It is generally difficult to keep track of their quantitative contribution in the total error. Nevertheless, some type of analysis can be applied to try to assess the reliability of the tomographic inversion.
Here, two of these methods are described. The first one refers to the error evaluation performed directly of the analysed data. The second one concerns the system of linear equations referring to the tomographic system.
The reliability of the tomographic result can be determined by computing the time residuals, that represent the differences between the picked and the computed travel times (Zelt and Smith 1992). These residuals, can be calculated by statistical means, such as root mean square, mean, average deviation, standard deviation, variance.
The evaluation of the error can be computed at the end of the tomographic inversion, but also during the intermediate steps of the iterative procedure. This latter is functional for the identification of those traveltimes that exceed a chosen threshold, these and therefore can be excluded from the set of traveltimes give in input for the subsequent inversion step. Alternatively, these can also represent a clue regarding errors in the traveltime picking, that can be therefore adjusted.
Considering the t^{OBS} (observed traveltime on the data), t^{CALC} (calculated traveltime) and t^{RES} (traveltime residuals), their relation Is described as follows: $t^{RES} = t^{CALC} - t^{OBS}$
t^{RES} can be expressed as absolute values or, for example, as percentage of the t^{OBS}: $t^{RES}\% = (t^{CALC} - t^{OBS})/t^{OBS}$. These can be then plotted in histograms, such as the Gauss distribution of Fig. 68.
Furthermore, considering a set of n values of t^{RES} (R), statistical indicators can be quantified, such as the following (OGS, 2014).

Root mean square: $rms = 1/n\sqrt{\sum_{i=1}^{n} R_i^2}$

Mean: $\bar{M} = \frac{1}{n}\sum_{i=1}^{n} R_i^2$

Average deviation $= \frac{1}{n}\sum_{i=1}^{n}|R_i - \bar{M}|$

Standard deviation: $\sigma = \sqrt{\frac{1}{n}\sum_{i=1}^{n}(R_i - \bar{M})^2}$

Variance = σ^2

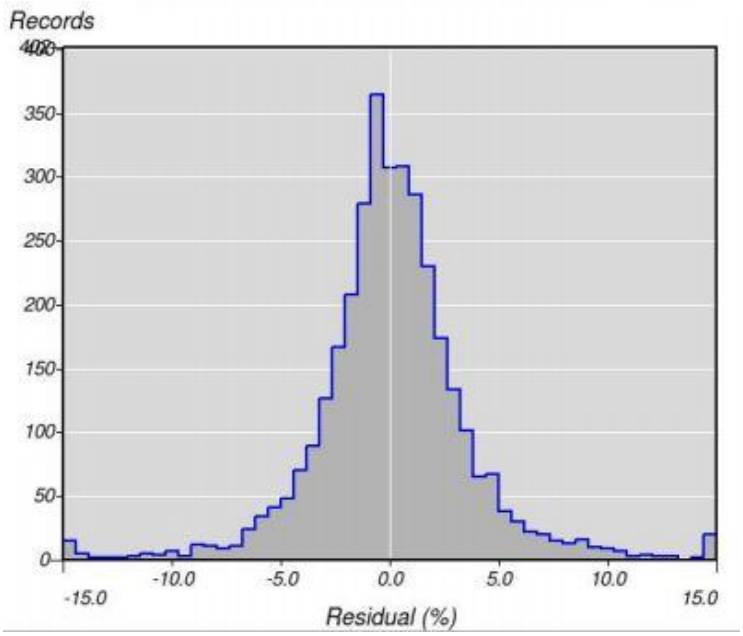

Fig. 68 – Example of Gauss distribution of the traveltime residuals of an experiment inversion, expressed in percentage. (OGS, 2014).

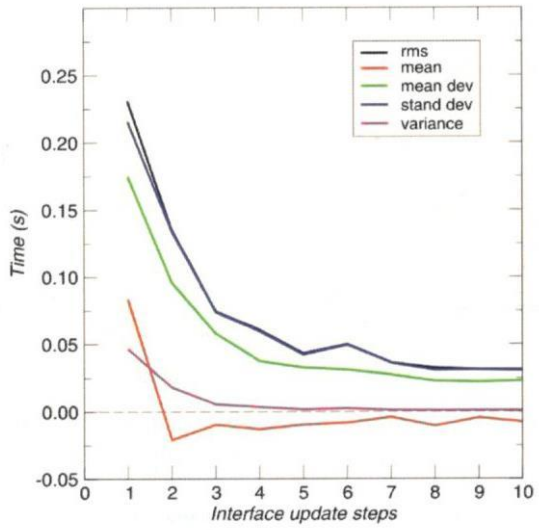

Fig. 69 – Plot providing an example of statistical indicators (root mean square, rms, black line; mean, orange line; mean deviation, green line; standard deviation, blue line; variance, purple line) of traveltime residuals, computed for the first 10 iteration steps of an experiment of interface update. (OGS, 2014).

Moreover, the measure of the dispersion of the reflection/refraction points can be sometimes performed, to detected the error in the interface estimation. In this case, the convergence can be considered or not acceptable, by analyzing the best fitting degree between the estimated reflection points from both large and small offsets arrivals (Fig. 70). The optimum situation occurs when the depth difference between the estimated points and the reconstructed interface is null (OGS, 2014).

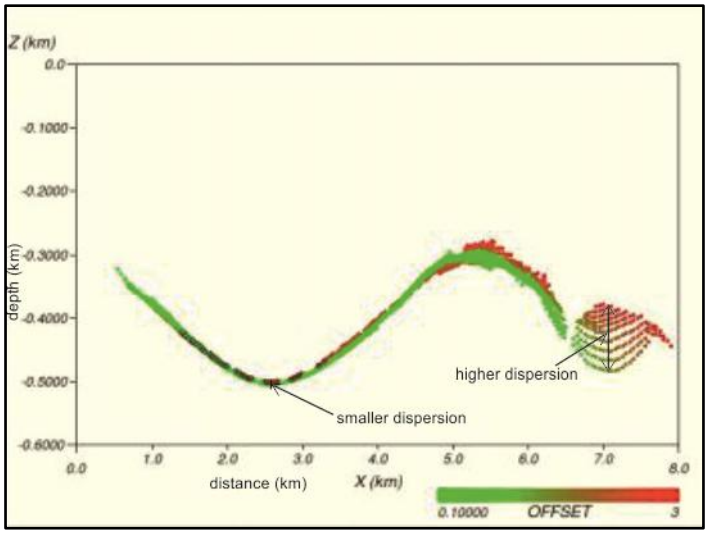

Fig. 70 – Dispersion of the estimated reflection points along for an inverted horizon. The points (small offset, green and large offset, red) are here plotted in a graph distance versus depth. It can been seen as in the left side the convergence (smaller dispersion of point from both and large offsets) results to be more satisfactory respect to that in the right part (characterised by higher dispersion). Adapted from (OGS, 2014).

The reliability of the tomographic result can also be assessed in first approximation, by the ray density that represents the number of rays that cross a voxel of the 3D tomographic grid.

The traveltime tomographic inversion consists in the solution of a system of linear equations:

$$\begin{aligned} t_1 &= a_{11}s_1 + a_{12}s_2 + a_{13}s_3 + \ldots + a_{1n}s_n \\ t_2 &= a_{21}s_1 + a_{22}s_2 + a_{23}s_3 + \ldots + a_{2n}s_n \\ t_3 &= a_{31}s_1 + a_{32}s_2 + a_{33}s_3 + \ldots + a_{3n}s_n \\ &\ldots \\ t_i &= a_{i1}s_1 + a_{i2}s_2 + a_{i3}s_3 + \ldots + a_{in}s_n \end{aligned}$$

Where the t_i represents the traveltime of the i^{th} ray, a_{ij} represents the ray segment length inside the j^{th} voxel, s_j is the slowness (inverse of velocity) characterizing every voxel of the model.

The system of equations can be written also in matrix form, where $\boldsymbol{t}$ is traveltimes vector, $\boldsymbol{A}$ is the matrix depending on ray paths, $\boldsymbol{s}$ represents the slowness vector (unknown parameters):

$$\boldsymbol{t = As}$$

The rows of the matrix A represent the ray segments that intersect the voxels of the model. The operation solves a system of linear equations NxM.
- N is the number of the unknown parameters (columns of the matrix A), e.g. the slowness characterizing the voxels that discretize the model.
- M is the number of equations (rows of the matrix A), e.g., the traveltimes.
The nulls space represents the ensemble of the solutions that produce indetermination.
Its dimension is given by:

$$\mathrm{dimD(A) = N - K(A)}$$

where K(A)<=M is the number of the linearly independent equations of the system.
The ideal situation occurs when K(A)>=N and thus D(A)<=0, meaning that the number of rays is bigger that the number of unknowns. Therefore the system results to be over-determined.
On the contrary, if the model, for example, is too much discretized, N could become bigger respect to the number of independent rays and the value of D(A) increases. In this case, the system results to be under-determined.
The null space energy is based on the singular value decomposition of the tomographic matrix (e.g. Vesnaver, 1994). This is a measure independence of the tomographic matrix equations, and therefore of the matrix rank. Null space energy values vary from 0 to 1, where 1 is related to underdetermined matrices, and to an infinite number of solutions that satisfy the system. Thus, the regions of the model, where the null space is low and therefore the reliability is high, are acceptable; while the regions, where the reliability is poor, should not be considered.

4.4 Imaging in Depth

In order to further refine the obtained velocity model, it was employed an iterative imaging technique involving pre-stack depth migration, residual move-out analysis and horizon based tomography (Fig. 71), by using the Geodepth (Paradigm, 2016) commercial software.
The method of performing residual move-out analysis utilises semblance sections, obtained by scanning various residuals, and it is similar to that of standard stacking velocity analysis (Fig. 58). The process goes on until the residual move-out become sufficiently small, which means a model with a flat sequence of events. In this case, the velocity field is estimated with sufficient accuracy, allowing to obtain an optimally focused depth image.
The initial model is that obtained from the tomographic inversion computed by CAT3D software (OGS, 2014).
At every iteration both velocity and reflector geometries are updated, until the two set of parameters reach a good degree of stability and consistency. Subsurface imaging is finally obtained by pre-stack depth migration, which uses the velocity field to convert the seismic data in an image of the subsurface. The more reliable is the velocity field, the more realistic will be the migrated image. Residual move-out analysis can be further performed on Depth Migrated Gathers (DMG), in order to assess the remaining error in the velocity field (Fig. 58, Fig. 72). In other words, the degree of non-flatness of the reflection events on the DMGs is a measurement of the error in the model (Yilmaz, 2001).
The seismic data were analyzed by adopting an iterative modeling and imaging procedure, with the main purpose to build a final 3D image in depth. The technique described in this work consists in an iterative updating procedure for refining and improving an initial model in depth, involving pre-stack depth migration, residual move-out analysis and seismic reflection tomography. The initial model is generally deduced from geologic field surveys, or derived by adopting other techniques. In the case of this study, it was used a velocity-depth model obtained using the CAT3D (OGS, 2014) software. At every iteration both velocity and reflector geometries are updated, until the two set of parameters reach a good degree of stability and consistency.

4.4.1 Overview of the imaging approach

Seismic representation of an earth model in depth usually is described by two sets of parameters: layer velocities and depth of interfaces. Difficulties in estimating these parameters with a required level of accuracy make the earth model estimation a challenging task for the seismic exploration. The concept of depth model is very useful in seismic exploration, by which the earth velocity field can be constructed and optimised. Subsurface Imaging is finally realised by pre-stack depth migration, which using the velocity field converts the seismic data in an image of the earth. The more reliable is the velocity field we supplied to the migration, the more realistic will be the imaging. Nearly all of the practical modelling methods are based on ray theory, and more specifically, on inversion of seismic traveltimes. In the following section the procedure adopted in this work it is described.

4.4.1.1 The residual move-out analysis

Residual move-out analysis is a velocity analysis performed after applying an imperfect initial velocity function to the data, in order to find the remaining error to the velocity field. If the initial velocity field has been estimated with sufficient accuracy, then the common image gathers (CIGs) derived from pre-stack depth migration using this model should exhibit flat events. Any errors in layer velocities and/or reflector geometry, on the other hand, should give rise to a residual move-out along those events on the CIGs, which are non-flat in these cases. In other words, The degree of non-flatness of the reflection events on the CIGs is a measurement of the error in the model, and residual move-out analysis identifies the correction required to flatten reflection events (Yilmaz, 2001).
The residual move-out is a measurement of non-flatness, defined by the difference between the location of the reflection event on the near and far offset traces. Generally, a fixed offset value known as *reference offset* is used for far offset. As shown in Fig. 58, a positive residual indicates that the local velocity used for the depth migration is too high, while a negative residual is associated with a too low velocity. The method of performing residual move-out analysis utilises semblance sections, obtained by scanning various residuals, and is similar to that of standard stacking velocity analysis. This method, implemented in some commercial software packages, computes a semblance value for every residual and creates a semblance section.

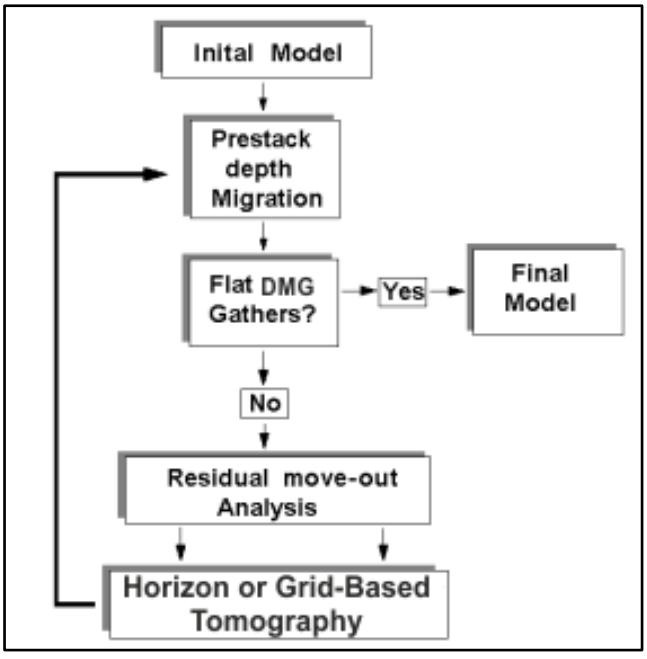

Fig. 71 - Flow-chart of a typical iterative depth imaging procedure, adopted by the Geodepth software (Paradigm, 2016). It encompasses, in sequence, pre-stack depth migration (performed starting from an initial sesimic velocity field), residual move out analysis on depth migrated gathers (DMG) and the Horizon or Grid-based tomographic approaches. (Paradigm, 2016).

A vertical function that represents the depth-dependent residual move-out can be picked from the semblance sections. This function can then be used to correct for the residual move-out, and so to improve the velocity field in order to obtain a better depth migrated section.

4.4.1.2 Horizon-Based and Grid Tomography

Tomography of depth migrated gathers is a method of refining the velocity-depth model when pre-stack depth migration is performed with an incorrect velocity field. The degree of non-flatness of the reflection events on the CIGs is a measurement of the error in the model. Therefore, since residual move-out is a measurement of non-flatness, Horizon-Based Tomography (HBT) uses residuals as input and attempts to find an alternative model which will minimise the error; i.e. produce flatter gathers (Yilmaz, 2001).
The first step in HBT is to scale the residuals to time using the initial model. A difference in time Δt, obtained scaling a specific residual, represent an error in travel-time measured at a specific Common Mid Point (CMP) location. The tomographic approach attributes the value of Δt to an accumulation of errors Δt_i within each layer were the ray has travelled. In other words, the error Δt can be the result of an error in the model at any point along the ray. Moreover, an error in the model can be an error in velocity Δv_i or depth Δz_i. So, the objective is to obtain Δt_i, the error in travel-time within each layer, and derive from Δt_i the error in velocity, Δv_i, and the error in depth Δz_i.
A basic part of the tomography algorithm is the Common Reflection Point (CRP) ray tracing. One equation is written for each *k*-ray:

$$\Delta t_k = \sum_{i=1}^{n} \Delta t_{ki} \tag{1}$$

The resulting system of equation can be written in the matrix form:

$$\Delta t = L \Delta p \tag{2}$$

where Δt denotes the column vector that represents the residual move-out times measured from the image gathers, and Δp is tomographic update column vector that comprise the changes in the slowness and depths to layer boundaries. *L* is a sparse matrix: its elements are in terms of the slowness and depth parameters associated with the initial model.
The system of equations is then solved using last-squares and the tomographic update Δp is given by the Generalised Linear Inversion (GLI) solution:

where *T* denotes matrix transposition.

$$\Delta p = (L^T L)^{-1} L^T \Delta t \tag{3}$$

Grid-based tomography is similar to horizon-based tomography except that only error in velocity is assumed (there is no Δz_i, only Δv_i), and the grid of unknowns spans the whole section, not only the horizon. Similarly to horizon-based tomography, the rays are shot only from the horizons.
1.3-Earth modelling in depth
Considering an initial model, made up of horizontal layers with laterally invariant velocities, or partially refined adopting other techniques. It has to be made an attempt to update this initial estimate using the modelling procedure described by the flow-chart shown in Fig. 71. This is an

iterative updating procedure involving pre-stack depth migration, residual move-out analysis and seismic reflection tomography.
It can be summarised as follows:
Generation of a set of CIGs from pre-stack depth migration, by using the velocity field derived from the initial model.
If the CIGs exhibit flat events, then the model is good and the procedure stops giving the final model and the imaging performed by the pre-stack depth migration. If the events are not flat, the model is not sufficiently accurate yet, and the procedure goes on.
Computation the horizon-consistent residual move-out for all offsets along events on the CIGs that corresponds to layer boundaries included in the model, obtaining the semblance sections.
Picking on the residual move-out profiles for all the horizons, by tracking the semblance peaks.
Building of the travel-time error vector Δt using the picked residual move-out in depth.
Definition of the initial model by a set of slowness and depth parameters and construction of the coefficient matrix L in equation (2).
Estimation of the change in parameters vector Δp, by means of the GLI solution given by equation (3).
Update of the parameter vector $p+\Delta p$. By combining the update interval velocity profiles with the new depth horizons, the updated model is obtained.
Extraction of the velocity field from the new model and perform the pre-stack depth migration.
Return to the point 2.
This procedure goes on until the quality of pre-stack depth migration is not sufficient. Generally, this point is reached when the events on the CIGs become flat (Yilmaz, 2001).

4.4.1.3 Modelling and Imaging of the Data: Construction of the initial model

The 3D Imaging was carried out in two sessions: in the first it was reached a first estimation of the velocity-depth model using CAT3D (OGS, 2014) software. In the second, the model was refined and it was performed the 2D pre-stack depth migration by using the Geodepth (Paradigm, 2016) commercial package.
According to the modelling procedure shown in Fig. 71, it was used the initial velocity field to perform a first pre-stack depth migration of the seismic data. The result shows that the image quality is not very good yet, because the seismic energy is not well focused. This is because the CIGs derived from pre-stack depth migration exhibit non-flat events. Geodepth (Paradigm, 2016) provides an Interpretation Module by which is possible to pick on the migrated section the main horizons, in order to perform the residual move-out analysis and tomography.

4.4.1.4 Modelling and Imaging of the Data: Refinement of the model.

A residual move-out analysis was performed by using the Velocity Navigator Module of Geodepth (Paradigm, 2016) (Fig. 72). The horizontal axis of this semblance plane represents the depth error which corresponds to either positive or negative residual move-out.

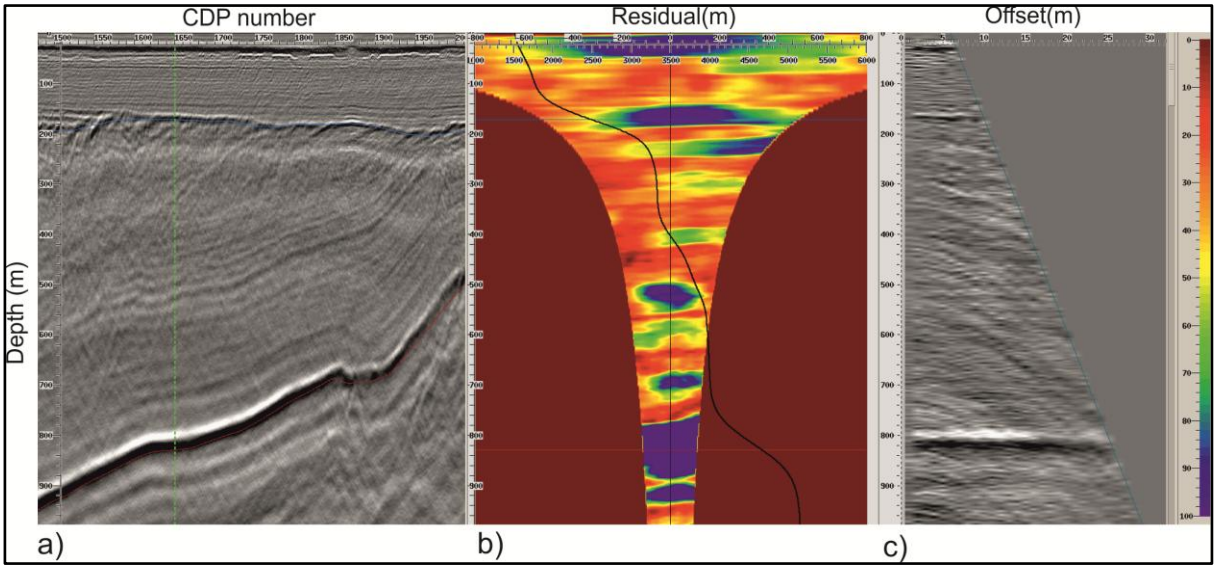

Fig. 72 - a) Zoom of the PSDM; b) residual semblance of the CIG indicated by the green dashed line in a), and represented in c). The black line in b) represents the local velocity function.

The vertical residual move-out analysis was carried out for a number of CIGs, by picking the coherences on the semblance profiles. For each semblance panel picked, a residual move-out function is defined. Obviously, it is not necessary to pick all the CIGs, because the residual move-out functions can be interpolated, in order to make a residual move-out map for all the section. The residual map and the interval velocity section are the input data for the tomographic update.
Following the update, the new model needs to be checked for consistency with the input seismic data (Yilmaz, 2001). According with the modelling flow-chart in Fig. 71, a second pre-stack depth migration was performed, by using the velocity field derived from the new model. The main consistency checks are the following:
Overlay the depth horizons from the updated model onto the image section derived from pre-stack depth migration and note if they coincide with the reflectors associated with the layer boundaries included in the model.
Computation of the residual move-out semblance spectra from the image gathers at selected locations after the model update and perform the comparison with those obtained before the update.
The residual move-out analysis of image gathers and the update of velocity-dept model should be performed iteratively until the velocity-depth model and the depth image are consistent.

4.5 Geophysical and Geological Dataset

4.5.1 Geophysical Dataset

The subsurface of the Gulf of Trieste (GT) remained widely undiscovered until recent time, although in this offshore area it was executed the very first Italian geophysical marine experiment of active seismic. In 1955, the Osservatorio Geofisico (Geophysical Observatory), the former name of the National Institute of Oceanography and Experimental Geophysics – OGS, conducted a multichannel seismic (MCS) refraction acquisition (source SIE GA11) in the GT, onboard the Italian Navy Vessel Abete (Morelli & Mosetti, 1955), (Cappelli, et al., 2008). Ten years later, onboard the OGS M/V Vercelli, OGS acquired the "Grado-Miramare" multichannel seismic (MCS) refraction profile covering the same area of the 1955 line and extending further SW-ward in the gulf, with a SW-NE direction, for a total distance of 13 km (Finetti, 1965). Moreover, in the same year, OGS acquired a seismic refraction profile, running 19.5 km that (Finetti, 1967) studied to understand the structural relationship between the onland Karst. 9.5 km were collected onland, in a NE-SW direction, between Doberdò del Lago and Duino; the remaining 10 km were recorded, at sea (by means of the OGS M/V Vercelli) towards SW, from Duino to a point in the gulf located 6 km W respect to Trieste. In 1968, an extensive high resolution singlechannel seismic survey (Sparker) was collected in the GT, near the coast of Miramare and in correspondence of the Timavo outlet (Mosetti & Morelli, 1968).

In 1995, a deep penetration MCS reflection profile, the CROP-M18 was recorded by the R/V OGS Explora in 1995, within the framework of the CROP (CROsta Profonda) Italian project (Scrocca, et al., 2003)(Finetti & Del Ben, 2005). The line CROP-M18 extends for 97 km in the Northern Adriatic Sea and, of these, 20 km are located in the western area of the GT (Fig. 73).

During the last decade, OGS carried out three geophysical surveys in the Gulf of Trieste (GT), onboard the R/V OGS Explora. Two-dimensional (2D) MCS lines (position in Fig. 73) along with sub-bottom profiler (Boomer and Chirp) and Multibeam data have been acquired. In total, the MCS profiles cover a distance of about 600 km and are located in the Italian and Slovenian waters of the gulf. Although the surveys were conducted in different years (2005, 2009, and 2013), the acquisition parameters are similar and the resulting dataset network has an average spacing between lines of around 1.5 km; the nearest distance from the Eastern and Southern coastline is about 1.5 km and 0.7 km, respectively. The MCS lines provide an horizontal resolution of about 5 m, that is comparable to the vertical resolution for the shallower layers (Ramella, et al., 2005) (Zgur, et al., 2010) (Zgur, et al., 2013).

As concerns others very high resolution seismic data, singlechannel and multichannel seismic (Boomer) along with Chirp profiles were collected in various parts of the gulf (near the coastline) in several geophysical surveys, since 2003 (Fig. 74).

All the available geophysical data have been uploaded in the digital database of the Kingdom® (IHS, 2014) interpretation software.

During the OGS survey of 2005 and 2013, the R/V OGS Explora was also equipped for the measurement of gravity field (Ramella, et al., 2005) (Zgur, et al., 2013).

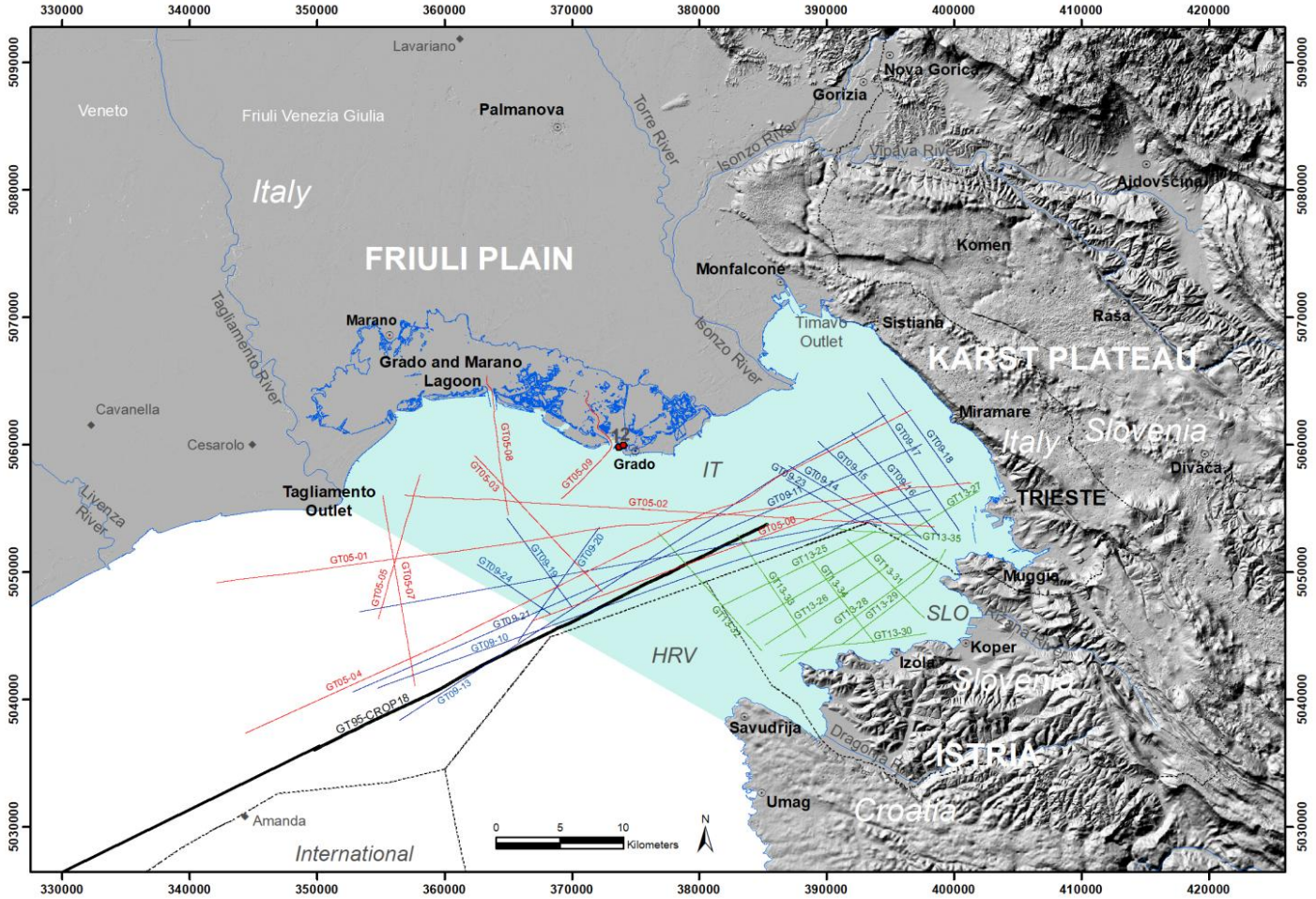

Fig. 73 - Map of the geophysical dataset used in this study. The dataset was made available by OGS and it is located in the Gulf of Trieste (azure area of the offshore, enclosed by the coastline connecting the Tagliamento River Outlet and Savudrija). The R/V OGS Explora acquired a total of about 600 km of 2D MCS reflection profiles (extending in Italian and Slovenian waters), in the framework of three surveys (2005 in red lines, 2009 in blue lines, 2013 in green lines). The CROsta Profonda CROP-M18 MCS reflection profile (black line) was also recorded by the R/V OGS Explora in 1995. Grey squares and red circles indicate the position of the AGIP exploration wells and the Grado 1 and Grado 2 geothermal wells, respectively. Map compiled by using ArcGis® (ESRI, 2017) software; datum WGS84, projection UTM33. Digital Elevation Model from: (IRDAT-FVG, 2017) for the Italian area, 10 m cell resolution; (EU-DEM, 2017) for the Slovenian and Croatian areas, 20 m cell resolution.

4.5.1.1 OGS Survey of 2005

The geophysical exploration survey of the 2005 was conducted by OGS, in the framework for the redaction of the geological-technical chart of the geothermal resource and the definition of the guide-lines for its exploitation ("Risorsa Geotermica RA-FVG" project; agreement "Rep. 8493, dd. 24/11/2004"), in the lower part of the Friuli plain. The work has been funded by the Italian Autonomous Region Friuli Venezia Giulia (Servizio Geologico, Direzione Centrale Ambiente e Lavori Pubblici) with the purpose of developing a previous study ("Studio preliminare degli acquiferi profondi della pianura friulana" project, agreement "Rep. 7170, dd. 09/12/1999") that defined the main underground geological units along with the deep hydrological resources of the Region's flood plain. OGS, the. Depts. of Civil Engineering (DIC) and of Geological, Environmental and Marine Sciences (DiSGAM) of the University of Trieste (UniTS) recovered, integrated and analysed pre-existing data. New data acquisitions were planned to define the shelf extension of the Mesozoic-Paleogene Friuli-Dinaric Carbonate Platform, in the offshore area. According to (Calore, et al., 1995) (Della Vedova, et al., 2001)(Nicolich, et al., 2004), in the Friuli Plain the shelf margin represents a structural high that lies about 700-800 m below the sea level and corresponds to a positive geothermal anomaly (60-70 mW m^{-2}), that has been identified by onshore wells measurements (e.g. Amanda, Cavanella and Cesarolo, see section Exploration Wells). The map of the top of the carbonates proposed by (Nicolich, et al., 2004) shows that the south-western edge of the shelf is, onshore, alternatively oriented NW and NE with a very high steepening angle. Offshore, the inferred NW-SW orientation was the basis on which the acquisition of the 2005 MCS profiles was planned, almost entirely, along the E-W and the NE-SW direction (Ramella, et al., 2005).

Between the 15th and the 22th June 2005, the R/V OGS Explora collected seven 2D MCS reflection profiles (listed in Tab. 5), with a total length of 233 km in the Gulf of Trieste (location in Fig. 73).

Line Name		Initial Coordinates (GMS)	Final Coordinates (GMS)	Length (km)
G05-01	Lat.	45°39'33.8980"N	45°34'40.6149"N	60.127
	Lon.	13°43'58.1725"E	12°58'32.7619"E	
G05-02 (NW)	Lat.	45°38'36.1041"N	45°38'11.7016"N	19.313
	Lon.	13°09'51.1261"E	13°24'54.3265"E	
G05-02B (SE)	Lat.	45°38'14.5585"N	45°37'42.7034"N	23.536
	Lon.	13°24'02.7614"E	13°41'53.7889"E	
G05-03	Lat.	45°33'21.5736"N	45°39'32.6862"N	15.054
	Lon.	13°08'24.1494"E	13°10'42.7810"E	
G05-04	Lat.	45°28'04.1778"N	45°42'39.0943"N	55.936
	Lon.	13°00'49.6355"E	13°40'23.2365"E	
G05-05	Lat.	45°40'19.6157"N	45°34'14.8816"N	12.100

	Lon.	13°13'58.6663"E	13°22'28.6903"E	
G05-06	Lat.	45°39'33.4930"N	45°33'21.5406"N	32.000
	Lon.	13°40'20.9515"E	13°17'36.4101"E	
G05-07	Lat.	45°30'32.4784"N	45°38'36.3329"N	15.488
	Lon.	13°10'40.5056"E	13°08'28.6688"E	
			Total Length (km)	**233.554**

Tab. 5 - Name, coordinates and length of the seven MCS reflection lines acquired by the R/V OGS Explora in the Gulf of Trieste, during the geophysical survey of the 2005 in the framework of the "Risorsa Geotermica RA-FVG" project (Ramella, et al., 2005).

The boat Castorino2 acquired 32 km of very high resolution seismic profiles in the Grado-Marano Lagoon. The survey took place in the period 2nd - 6th May 2005 inside the lagoon and it extended outside the lagoon mouths, with the aim of joining with the MCS seismic lines collected in the gulf. Two lines were acquired, among the three originally planned, due to climate conditions and maritime traffic. In Tab. 6 are listed the positions of the acquired profiles.

Line Name		Initial Coordinates (GMS)	Final Coordinates (GMS)	Length (km)
G05-08	Lat.	45°46'09.34"N	45°42'36.41"N	19.954
	Lon.	13°14'42.53"E	13°15'02.32"E	
G05-09	Lat.	45°38'30.98"N	45°43'13.90"N	12.051
	Lon.	13°19'09.41"E	13°20'43.84"E	
			Total Length (km)	**32.005**

Tab. 6 - Name, coordinates and length of the two MCS reflection lines acquired by the boat Castorino 2 in the Grado-Marano Lagoon, during the geophysical survey of the 2005 in the framework of the "Risorsa Geotermica RA-FVG" project (Ramella, et al., 2005).

The parameters of the 2005 seismic acquisition in the Gulf of Trieste and in the Grado-Marano Lagoon are listed in Tab. 7.

Acquisition Area	Trieste Gulf	Grado-Marano Lagoon
Line Name	G05-01 to G05-07	G05-08, G05-09
Vessel	R/V OGS EXPLORA	Castorino 2 boat
Recording date	June 2005	May 2005
Recording system	OYO DAS-1	BISON Jupiter 20 bit
Sample rate	0.5 ms resampled 1 ms	0.25 ms resampled 1 ms
Filters	Low 3 Hz, high Anti-Alias	Low 3 Hz, high Anti-Alias
Max coverage	24	8
Source energy	GI-gun Sleeve	Air gun
Source array	2 x 355 cu.in.	1 X 80 cu.in.
Source depth	3 m	1.5 m
Streamer length	600 m	120 m
Trace number	48	24
Group interval	12.5 m	5 m
Source interval	12.5 m	7.5 m
Streamer Depth	3 m	0.5 m

Tab. 7 - Acquisition parameters of the seismic survey conducted in 2005 in the Gulf of Trieste, onboard the R/V OGS Explora, and in the Grado-Marano Lagoon, onboard the Castorino 2 boat (Ramella, et al., 2005).

The entire dataset is available in SEGD and SEGY format and is processed in time domain.

4.5.1.2 OGS Survey of 2009

The geophysical investigation survey took place between the 1st and the 6th October 2009, onboard the R/V OGS Explora, and was conducted by OGS with the aim of integrating the pre-existing geophysical data, in order to enhance the understanding of the geological structure of the Gulf of Trieste. Thirteen 2D MCS reflection profiles (listed in Tab. 8) were acquired, with a total length of 281 km in the gulf (location in Fig. 73). The acquisition parameters are reported in Tab. 9 (Zgur, et al., 2010).
The entire dataset is available in SEGD and SEGY format and was processed in time domain; some profiles were also converted into depth.

Line Name *streamer 1200m °streamer 600m		Initial Coordinates (GMS)	Final Coordinates (GMS)	Length (km)
G09-10*	Lat.	45°30'32"N	45°39'16"N	45,591
	Lon.	13°08'54"E	13°41'39"E	
G09-11*	Lat.	45°41'02"N	45°30'10"N	48,217
	Lon.	13°40'33"E	13°06'52"E	
G09-13*	Lat.	45°29'14"N	45°42'25"N	50.129
	Lon.	13°10'13"E	13°38'47"E	
G09-14°	Lat.	45°40'05"N	45°36'42"N	12.497
	Lon.	13°33'10"E	13°41'29"E	
G09-15°	Lat.	45°37'19"N	45°41'15"N	10.869
	Lon.	13°40'51"E	13°34'39"E	
G09-16°	Lat.	45°41'29"N	45°37'16"N	10.338
	Lon.	13°36'55"E	13°42'08"E	
G09-17°	Lat.	45°37'43"N	45°43'22"N	12.734
	Lon.	13°43'10"E	13°37'37"E	
G09-18°	Lat.	45°39'23"N	45°43'59"N	10.610
	Lon.	13°43'20"E	13°38'27"E	
G09-19*	Lat.	45°34'15"N	45°37'44"N	8.124
	Lon.	13°19'46"E	13°15'58"E	
G09-20*	Lat.	45°37'07"N	45°32'26"N	10.473
	Lon.	13°21'18"E	13°16'47"E	

G09-21*	Lat.	45°38'22"N	45°33'36"N	44.992
	Lon.	13°41'05"E	13°07'09"E	
G09-23°	Lat.	45°39'31"N	45°37'11"N	9.999
	Lon.	13°33'00"E	13°39'51"E	
G09-24*	Lat.	45°35'33"N	45°33'39"N	6.399
	Lon.	13°14'43"E	13°18'50"E	
			Total Length (km)	**280.970**

Tab. 8 - Name, coordinates and length of the thirteen MCS reflection lines acquired by the R/V OGS Explora in the Gulf of Trieste, during the OGS geophysical survey of 2009 (Zgur, et al., 2010).

Acquisition Area	**Trieste Gulf** (Lines NE-SW oriented)	**Trieste Gulf** (Lines NW-SE oriented)
Line Name	G09-10, 11, 13, 19, 20, 21, 24	G09-14, 15, 16, 17, 18, 23
Vessel	R/V OGS EXPLORA	R/V OGS EXPLORA
Recording date	October 2009	October 2009
Recording system	Sercel Seal	Sercel Seal
Sample rate	1 ms	1 ms
Filters	Low 3 Hz, high Anti-Alias	Low 3 Hz, high Anti-Alias
Max Coverage	48	24
Source energy	Sleeve guns	Sleeve guns
Source frequency	150 Hz	150 Hz
Source array	1 x 1180 cu.in.	1 x 1180 cu.in.
Source depth	5 m	5 m
Streamer length	**1200 m**	**600 m**
Trace number	96	48
Group interval	12.5 m	12.5 m
Source interval	12.5 m	12.5 m
Streamer depth	3 m	3 m
Near offset	25 m	25 m

Tab. 9 - Acquisition parameters of the OGS seismic campaign conducted in 2009 in the Gulf of Trieste, onboard the R/V OGS Explora (Zgur, et al., 2010).

At the same time of acquisition of the MCS lines, acoustic profiles from sub-bottom profiler / chirp were also recorded and provide a decimetre vertical resolution for the shallower layers. The CAP-6600 Chirp II Workstation (Benthos, Chirp II) was employed as signal generator, operating with a sweep frequency ranging between 2 and 7 kHz.
Furthermore, bathymetric data were collected by the SeaBat 8111 multibeam system operating at a frequency of 100 kHz and generating 101 beams with a coverage angle of 150° and 1.5° across and along the Vessel track, respectively.

4.5.1.3 OGS Survey of 2013

The geophysical survey of the 2013 was conducted and funded by the OGS, under the aegis of the Ministero Italiano dell'Istruzione, dell'Università e della Ricerca. The project, named SLOMARTEC, was developed in collaboration with the University of Ljubljana and Harpha Sea d.o.o of Koper (Slovenia). The main objective of the project was the integration of the geophysical data previously collected within the Italian waters of the Gulf of Trieste with new data from the Slovenian part of the gulf. The aim was a further investigation of the geological and structural setting, along with the identification of the neo-tectonic evidences in a wider area of the gulf (Zgur, et al., 2013).
Between the 18th and the 21st March 2013, the R/V OGS Explora acquired, in the Slovenian waters of the Gulf of Trieste, eleven MCS reflection profiles (listed in Tab. 10) for a total length of 131 km (location in Fig. 73). The acquisition parameters are reported in Tab. 11.
The entire dataset is available in SEGD e SEGY format and was processed in time domain.

Line Name		Initial Coordinates (GMS)	Final Coordinates (GMS)	Length (km)
GT13-25	Lat.	45°37'28"N	45°34'11"N	15.610
	Lon.	13°38'19"E	13°29'04"E	
GT13-26	Lat.	45°36'00"N	45°32'33"N	11.530
	Lon.	13°39'04"E	13°31'42"E	
GT13-27	Lat.	45°33'23"N	45°39'15"N	21.109
	Lon.	13°30'35"E	13°44'30"E	
GT13-28	Lat.	45°36'22"N	45°31'27"N	15.224
	Lon.	13°42'01"E	13°32'39"E	
GT13-29	Lat.	45°32'38"N	13°42'33"E	11.229
	Lon.	13°36'22"E	45°36'45"N	
GT13-30	Lat.	45°32'07"N	45°33'10"N	11.679
	Lon.	13°32'40"E	13°41'30"E	
GT13-31	Lat.	45°33'50"N	45°37'06"N	8.647
	Lon.	13°41'18"E	13°36'34"E	
GT13-32	Lat.	45°32'18"N	13°25'09"E	12.363
	Lon.	13°31'32"E	45°37'15"N	
GT13-33	Lat.	45°37'12"N	45°32'53"N	8.691
	Lon.	13°29'58"E	013°34'13"E	
GT13-34	Lat.	45°36'09"N	45°32'43"N	8.091
	Lon.	13°34'29"E	13°38'20"E	
GT13-35	Lat.	45°37'18"N	45°37'34"N	7.005
	Lon.	13°41'03"E	13°35'40"E	
			Total Length (km)	**131.178**

Tab. 10 - Name, coordinates and length of the eleven MCS reflection lines acquired by the R/V OGS Explora in the Slovenian part of the Gulf of Trieste, during the SLOMARTEC geophysical survey of 2013 (Zgur, et al., 2013).

Acquisition area	Trieste Gulf
Line name	GT13-25, 26, 27, 28, 29, 30, 31, 32, 33, 34, 35
Vessel	R/V OGS EXPLORA
Recording date	Marzo 2013
Recording system	Sercel Seal
Sampling rate	1 ms
Filters	Low 3 Hz, high Anti-Alias
Max Coverage	48
Source energy	GI- gun Sercel
Source frequency	187.5 Hz
Source array	4 x 210 cu.in.
Source depth	4 m
Streamer length	1200 m
Trace number	96
Group interval	12.5 m
Source interval	12.5 m
Streamer depth	4 m
Near offset	25 m

Tab. 11 - Acquisition parameters of the SLOMARTEC seismic campaign conducted in 2013 in the Slovenian part of the Gulf of Trieste, onboard the R/V OGS Explora (Zgur, et al., 2013).

Simultaneously with the MCS lines acquisition, acoustic profiles from sub-bottom profiler / chirp were also recorded and provide a decimetre vertical resolution for the shallower layers. The CAP-6600 Chirp II Workstation (Benthos, Chirp II) was employed as signal generator, operating with a sweep frequency ranging between 2 and 7 kHz.
Bathymetric data were collected by the SeaBat 8111 multibeam system operating at a frequency of 100 kHz and generating 101 beams with a coverage angle of 150° and 1.5° across and along the Vessel track, respectively. The configuration parameters were used to fit the best acquisition quality with respect to the average depth of the seafloor. The collected data provided an average bottom resolution of about 3.7 cm.
Moreover, gravity profiles were recorded during the entire survey, by means of the KSS 31 (Bodenseewerk) tool fixed on the proximity of the Vessel gravity centre. The effective accuracy of the measurement ranges between 0.2 and 0.8 mGal RMS.

4.5.1.4 Other MCS Seismic Reflection Data

4.5.1.4.1 CROP Project: 1995

In the Gulf of Trieste, it is also available the eastern part (20 km long) of a MCS profile acquired in 1995 by the R/V OGS Explora. The line belongs to the geophysical dataset of the Italian project CROsta Profonda (CROP) conducted between the 1980s and the 1990s, with the aim of deep crustal investigation (Scrocca, et al., 2003) (Finetti & Del Ben, 2005). The seismic profile CROP-M18 extends along the SW-NE direction in the Northen Adriatic sea for about 97 km (Fig. 73). It is processed in time domain and it is available in SEGY format.

4.5.1.5 Other Very High Resolution Boomer and Chirp Data

In the Gulf of Trieste are available other very high resolution singlechannel and multichannel seismic profiles (Boomer) along with Chirp data acquired in several geophysical surveys (Fig. 74).

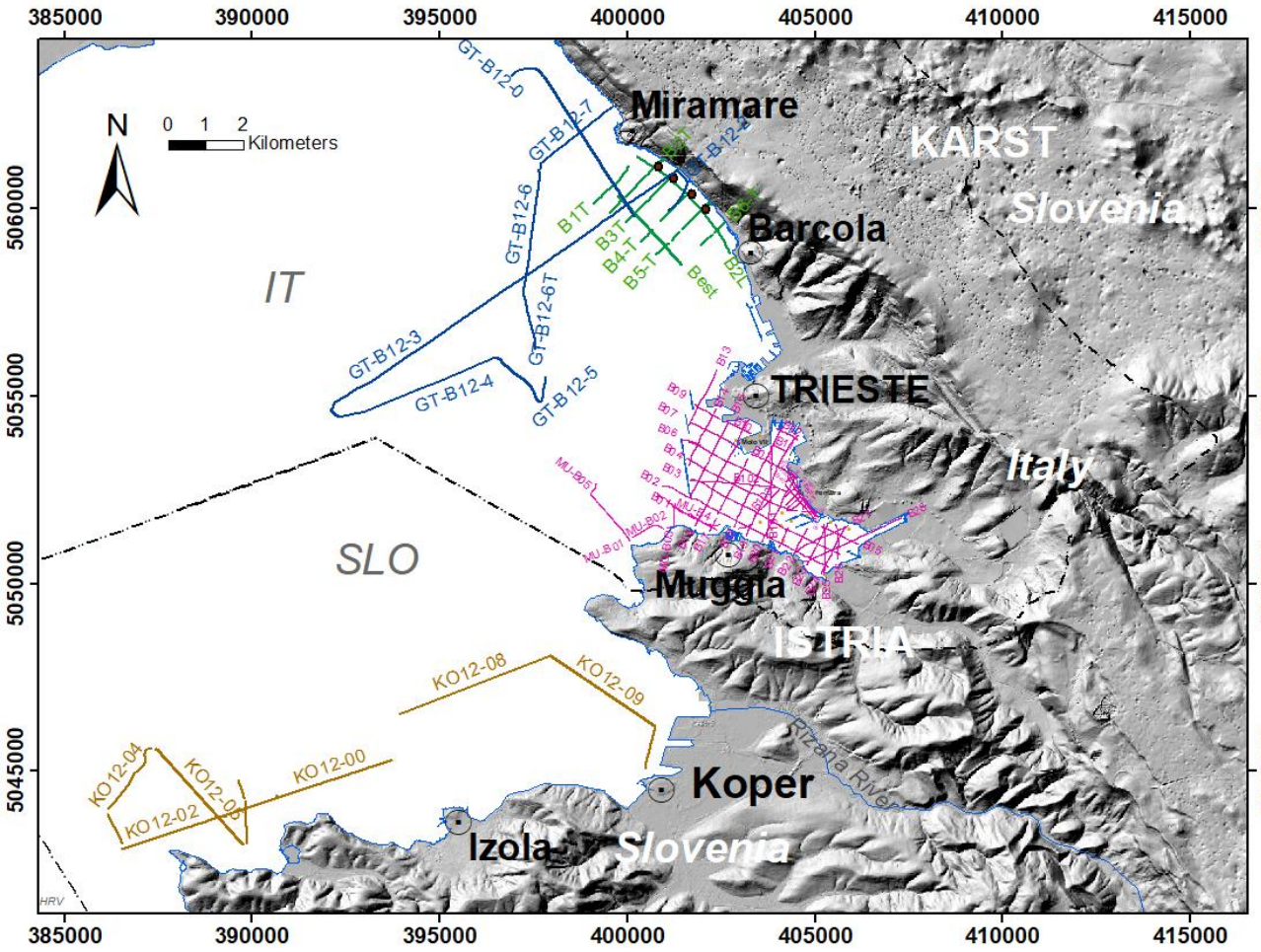

Fig. 74 – Position map of the Boomer profiles acquired in several geophysical campaigns: 2003 Barcola dataset (green, in this case sub-bottom profiler / Chip data were also acquired), 2012 Miramare dataset (blue, in this case data were acquired by both single and multichannel streamers), 2013 Muggia Bay (Vallone di Muggia, Sito di Interesse Nazionale - SIN) dataset (pink, names and position of these profiles are also shown in Fig. 75), 2012 Koper dataset acquired in the offshore near the Koper coastline (ochre). The Miramare 1998 sampling sites are represented in brown circles (named M1 to M4, from S to N). Azure, green, orange circles indicate the sampling positions in Molo VII, Scalo Legnami-Ferriera di Servola (1989 and 2005-2006), and Muggia bay (Vallone di Muggia, 1960s), respectively (details in Fig. 75). Map compiled by using ArcGis® (ESRI, 2017) software; datum WGS84, projection UTM33. Digital Elevation Model from: (IRDAT-FVG, 2017) for the Italian area, 10 m cell resolution; (EU-DEM, 2017) for the Slovenian and Croatian areas, 20 m cell resolution.

4.5.1.5.1 Very High Resolution Boomer and Chirp Data: Barcola 2003

In May 2003, on board the Castorino 2 boat, singlechannel seismic data with Boomer Uniboom-like source (UWAK 05, PULSAR 2002) and sub-bottom profiler / chirp profiles were acquired in the offshore of the Barcola coastline (Romeo, 2009). The geophysical investigation was conducted for the characterisation of coastal marine sediments and the rocky basement. The Boomer dataset (total length of 16 km) is composed by eight profiles. Of these, two are longitudinal and six are perpendicular respect to the shoreline. Their position is shown in Fig. 74, while their singular name and length are listed in Tab. 12. Moreover, the acquisition parameters of the survey are reported in Tab. 13. The entire dataset was processed with the aim of enhancing the signal-to-noise ratio and is available in SEGY format.

Line Name	Orientation respect to the shoreline	Length (m)
B1T	Perpendicular	1393
B2T	Perpendicular	1979
B3T	Perpendicular	2003
B4T	Perpendicular	1605
B5T	Perpendicular	1767
B6T	Perpendicular	1216
Best	Parallel	2533
B2L	Parallel	3645
	Total length (m)	16141

Tab. 12 – Name, orientation respect to the shoreline and length of the eight Boomer profiles acquired in 2003 by the Castorino 2 boat, offshore the coast of Barcola.

Acquisition area	Barcola offshore
Line Name	B1T, B2T, B3T, B4T, B5T, B6T e B2L, BestL
Boat	Castorino2
Recording date	2003
Recording system	Delph II Triniton Elics Int., SA
Sampling rate	0.05 ms
Recording length	150 ms
Streamer	8 hydrophones EG&G mod.265 – 320 cm
Source	UWAK 05 plate, PULSAR 2002
Source interval	0.64 m
Streamer depth	30 cm
Source-streamer offset	5 m
Source Power	300 J (100J x 3 pulses per second)
Source pulse length	0.1 ms
Dominant Frequency	2 kHz

Tab. 13 – Acquisition parameters of the Boomer profiles collected by the Castorino 2 boat in 2003, offshore the coast of Barcola.

In the framework of the same campaign, in the same area and onboard the Castorino 2 boat, a sub-bottom profiler / chirp acquisition was conducted, by means of Datasonics, CHIRP II acoustic profiling system (tow vehicle TTV 190). It consists of six profiles, two longitudinal and four perpendicular to the shoreline, for a total length of 13 km. There were collected the chirp profiles C2T, C3T, C4T, C5T and C2L, along the same path of the Boomer profiles B2T, B3T, B4T, B5T and B2L, respectively (position in Fig. 74). Furthermore, the C1L line was acquired parallel to the B2L, but nearer to the coast. Name and length of each profile are listed in Tab. 14.
The data were collected with an sampling interval of 0.122 ms, a source interval of 0.250 ms; their recording length is 0.14 s (acquisition parameters listed in Tab. 15). The entire dataset was processed with the aim of enhancing the signal-to-noise ratio and is available in SEGY format.

Line Name	Orientation respect to the shoreline	Lunghezza (m)
C1L	Parallel	2582
C2L	Parallel	2248
C2T	Perpendicular	2038
C3T	Perpendicular	2069
C4T	Perpendicular	1955
C5T	Perpendicular	2350
	Total Length (m)	13242

Tab. 14 - Name, orientation respect to the shoreline and length of the six sub-bottom / chirp profiles acquired in 2003 by the Castorino 2 boat, offshore the coast of Barcola.

Acquisition area	**Barcola offshore**
Line Name	C2T, C3T, C4T, C5T, C1L, C2L
Boat	Castorino2
Recording date	2003
Recording system	TTV 190, 8 hydrophones
Sampling rate	0.122 ms
Recording length	140 ms
Source	Datasonics, CHIRP II
Source interval	0.250 m
System depth	3.5 m
Source pulse length	5 ms
Dominant Frequency	2-23 kHz

Tab. 15 - Acquisition parameters of the sub-bottom / chirp profiles collected by the Castorino 2 boat in 2003, offshore the coast of Barcola.

4.5.1.5.2 Very High Resolution Boomer : Koper 2012

In 2012, Boomer seismic data were collected offshore the coastline of Koper, in Slovenian waters. The survey consists of nine profiles (location in Fig. 74) with a total length of 23 km. Name and length of each line are listed in Tab. 16. The entire dataset was processed with the aim of enhancing the signal-to-noise ratio and is available in SEGY format.

Line Name	Length (m)
KO12-00	3282
KO12-02	2923
KO12-03	854
KO12-04	2094
KO12-05	3475

Line Name	Length (m)
KO12-06	1680
KO12-08	4311
KO12-09	3379
KO12-10	1093
Total length (m)	23091

Tab. 16 – Name and length of the Boomer lines acquired in the offshore of Koper (Slovenia), in 2012.

4.5.1.5.3 Very High Resolution Boomer: Miramare 2012

In March 2012, offshore the Miramare coastline single and multichannel Boomer profiles were acquired onboard the Castorino 2 boat (Romeo, et al., 2012). The aim of the survey was the technical evaluation of the high resolution Boomer seismic source CSP-S1250 seismic source (S-Boom, a system of 3 high power electromechanical plates AA202, installed on the CAT300 Catamaran) provided by the Applied Acoustic Company. The acquisition consists of a single and multichannel seismic reflection profile, made up of nine transects for a total length of 32 km (position in Fig. 74). Name and length of the singlechannel and multichannel sections are listed in Tab. 17. In Tab. 18 and Tab. 19 are reported the acquisition parameters for the single and multichannel measurements, respectively. The entire dataset was processed with the aim of enhancing the signal-to-noise ratio and is available in SEGY format.

Line Name	Length (m)
GT-B12-0	1083
GT-B12-1	4463
GT-B12-2	838
GT-B12-3	11724
GT-B12-4	4501

Line Name	Length (m)
GT-B12-5	2574
GT-B12-6	1035
GT-B12-7	1547
GT-B12-T	4584
Total Length (m)	32349

Tab. 17 – Name and length of the nine single and multichannel Boomer transects acquired in 2012 by the Castorino 2 boat, in the offshore of the Miramare coastline.

Acquisition Area	Trieste Gulf - Miramare offshore, singlechannel Boomer
Line name	GT-B12-0,1,2,3,4,5,6,7,T
Boat	Castorino2
Recording date	2012
Recorder	Triton SB-Logger
Sampling rate	0.05 ms
Recording length	500 ms
Streamer	8 hydrophones, 4.5 m
Source	S-Boom system, CSP-S1250 seismic source - AA202 plates, on CAT300 Catamaran
Source interval	0.5 s – 1m
Streamer depth	0 cm
Source-streamer offset	3 m
Source Power	750 J per pulse
Source pulse length	0.5 ms

Tab. 18 - Acquisition parameters of the singlechannel Boomer profiles collected in 2012 by the Castorino 2 boat, in the offshore of the Miramare coastline.

Acquisition Area	Trieste Gulf - Miramare offshore, multichannel Boomer
Line name	GT-B12-0,1,2,3,4,5,6,7,T
Boat	Castorino2
Recording date	2012
Recorder	DAQlink-III, Seismic Source
Sampling rate	5 ms
Recording length	500 ms
Streamer	10 hydrophones, 7.5m - 24 channels
Source	S-Boom system, CSP-S1250 seismic source - AA202 plates, on CAT300 Catamaran
Source interval	0.5 s – 1m
Streamer depth	0 cm
Source-streamer offset	6 m
Source Power	750 J per pulse
Source pulse length	0.5 ms

Tab. 19 - Acquisition parameters of the multichannel Boomer profiles collected in 2012 by the Castorino 2 boat, in the offshore of the Miramare coastline.

4.5.1.5.4 Very High Resolution Boomer: Vallone di Muggia (Sito di Interesse Nazionale - SIN) 2013

Between the 29th and the 5th January 2013, a very high resolution Boomer seismic survey was conducted in the Sito di Interesse Nazionale (SIN) of Trieste, Vallone di Muggia (Muggia Bay), Gulf of Trieste (Baradello, et al., 2013). The position is shown in Fig. 74 and Fig. 75. The client of geophysical investigation was the Multiproject S.r.l. Company of Gorizia. The aim of the investigation was the definition of the thickness of the marine and atrophic sediments in the SIN area.

The Boomer survey was executed onboard the Quicksilver Pilothouse 580 (PL-DELAR307C909) and consists of forty-eight singlechannel seismic profiles with a total length of 76 km (name and length of each line are listed in Tab. 20, while the acquisition parameters are shown in Tab. 21. It was employed a Boomer source UWAK 05 Nautiknord, PULSAR 2002. The entire dataset was processed with the aim of enhancing the signal-to-noise ratio and is available in SEGY format.

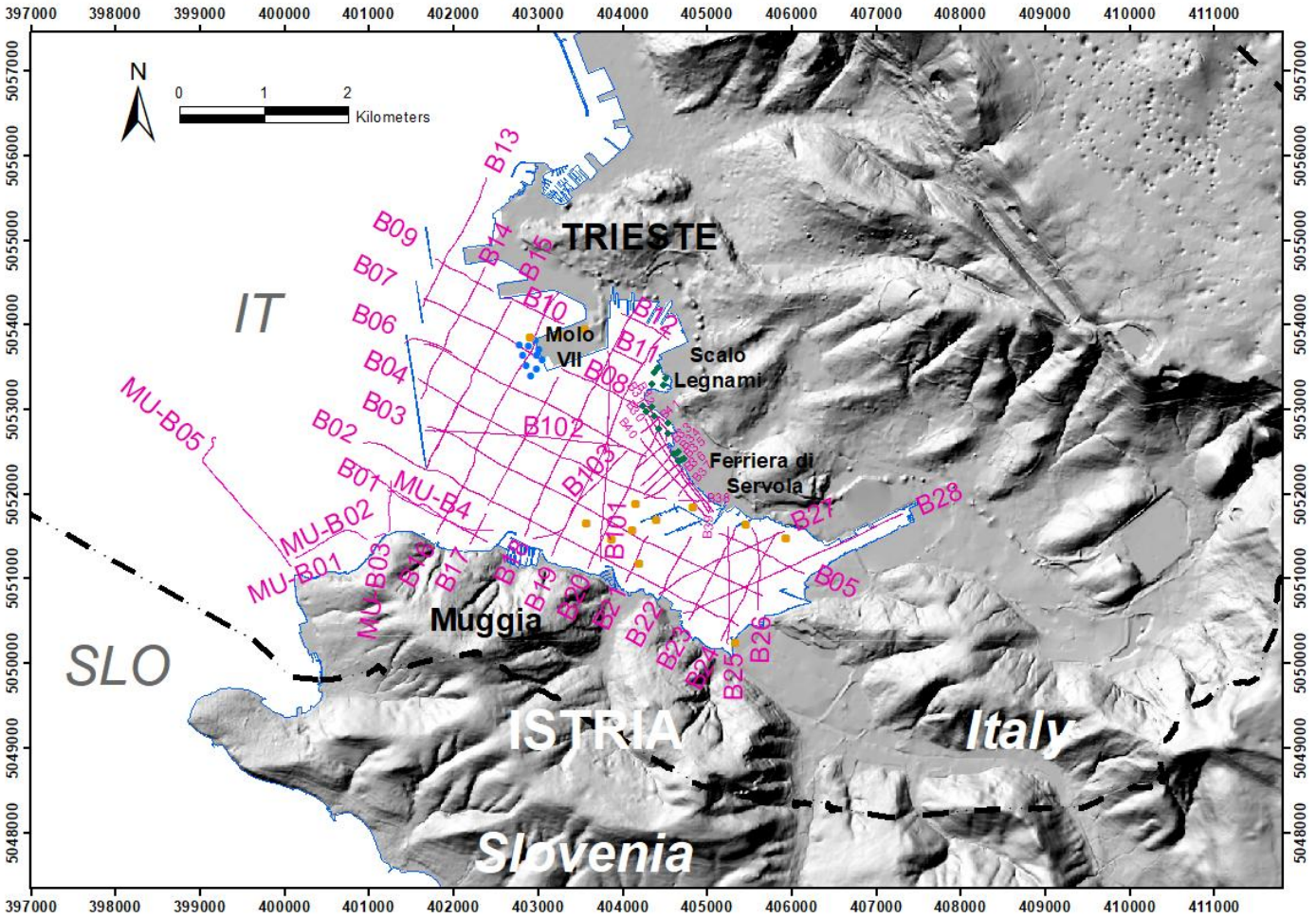

Fig. 75 - Position map the 2013 single channel Boomer profiles acquired by the OGS Quicksilver Pilothouse 580, in the Sito di Interesse Nazionale (SIN) of Trieste, Vallone di Muggia (Muggia Bay, Gulf of Trieste), in 2013. Circles represent the cores recovered: cores recovered (in 1989 and 2005-2006) near the Molo VII of the Trieste Harbour (azure circles) and in the area between the Scalo Legnami and the Ferriera di Servola (green circles), and the ochre circles represent the position of the marine drillings executed in the 1960s (Mosetti & Morelli, 1968). Map compiled by using ArcGis® (ESRI, 2017) software; datum WGS84, projection UTM33. Digital Elevation Model from: (IRDAT-FVG, 2017) for the Italian area, 10 m cell resolution; (EU-DEM, 2017) for the Slovenian and Croatian areas, 20 m cell resolution.

Line Name	Length (m)
GT13-B01	1347
GT13-B02	5075
GT13-B03	4502
GT13-B04	3326
GT13-B05	1164
GT13-B06	3521
GT13-B07	1644
GT13-B08	1420
GT13-B09	820
GT13-B10	799
GT13-B11	448
GT13-B12	662

Line Name	Length (m)
GT13-B13	1727
GT13-B14	1758
GT13-B15	3149
GT13-B16	3257
GT13-B17	2192
GT13-B18	3057
GT13-B19	3077
GT13-B20	2052
GT13-B21	648
GT13-B22	777
GT13-B23	1265
GT13-B24	1513
GT13-B25	1413

Line Name	Length (m)
GT13-B26	1001
GT13-B27	1708
GT13-B28	2879
GT13-B101	2552
GT13-B102	2400
GT13-B103	1627
GT13-B30	1354
GT13-B31	1477
GT13-B32	506
GT13-B33	467
GT13-B34	541
GT13-B35	722
GT13-B36	560

Line Name	Length (m)
GT13-B37	206
GT13-B38	303
GT13-B39	131
GT13-B40	1239
GT13-B41	275
MU13-B1	963
MU13-B2	137
MU13-B3	613
MU13-B4	1939
MU13-B5	2003
Total length (m)	**76116**

Tab. 20 - Name and length of the singlechannel seismic Boomer profiles collected by the OGS Quicksilver Pilothouse 580, in the Sito di Interesse Nazionale (SIN) of Trieste, Vallone di Muggia (Muggia Bay, Gulf of Trieste), in 2013.

Acquisition Area	**SIN Vallone di Muggia**
Line name	GT13- from B01 to B28; GT13- from B101 to B103
Boat	OGS Quicksilver Pilothouse 580 (PL-DELAR307C909)
Recording date	2013
Recorder	Triton SB-Logger
Sampling rate	0.05 ms
Recording length	100 ms
Streamer	8 hydrophones EG&G mod.265 – 320 cm
Source	UWAK 05 plate Nautiknord, PULSAR 2002
Source interval	3/sec
Streamer depth	40 cm
Source-streamer offset	3 m
Source Power	450 J per pulse
Source pulse length	0.1 ms
Dominant Source Frequency	2 kHz

Tab. 21 - Acquisition parameters of the singlechannel seismic Boomer profiles collected by the OGS Quicksilver Pilothouse 580, in the Sito di Interesse Nazionale (SIN) of Trieste, Vallone di Muggia (Muggia Bay, Gulf of Trieste), in 2013.

4.5.2 Geological Data

4.5.2.1 Exploration Wells

In the Gulf of Trieste, two exploration wells are present in the northern part (Grado-Marano Lagoon). Several others were realized, by the industry, between the 1960s and the 1980s throughout the Friuli Venezia Giulia Region and in the neighbouring Veneto; none of these, however, is positioned inside the area of the Gulf of Trieste. They reach a bottom depth that ranges between 800 m and 7200 m. Information, such as well logs, cores and cuttings, are available in a variety of format and combinations (e.g. analogical or digital), depending on the period of the acquisition. These geophysical and geological data are useful for the calibration of the available seismic profiles, especially those providing medium-high resolution. Furthermore, they represent a valid constraint for the reconstruction of the geological setting of the investigated area.

4.5.2.1.1 Industrial Wells: Friuli Plain 1960s and Northern Adriatic 1979

Exploration wells by AGIP (Italian hydrocarbon Company, now ENI) and related geological-geophysical data exist and are located some tens of kilometres far from the study area. In particular, the Cesarolo well was realised in 1960 and the Cavanella well was drilled an year later; they are located in the onshore adjacent to the north-western boundary of the gulf. The first has a maximum depth of 4236 m below seabed and it intercepts the top of the Carbonate Platform at 700 m below seabed. The Cavanella well is 1482 m deep and reaches the top of the carbonates at 1100 m below seabed (AGIP, 1972) (AGIP, 1977)(AGIP, 1994). Among the Northern-Adriatic offshore industrial wells, the Amanda (Amanda 1bis) is the closest (20 km SW) to the Gulf of Trieste and it was drilled in 1979. Its maximum depth is 7280 m below seabed and it drilled the top of the Meso-Cenozoic Carbonate platform at 1800 m below seabed (Cati, et al., 1987b). The geographical position of these mentioned wells in reported in Fig. 73.

4.5.2.1.2 Geothermal Wells: Grado 2008 and 2015

In the study area (Grado Island) two geothermal wells were drilled: Grado-1 e Grado-2 (Fig. 73). They were realised for the exploitation of the low-enthalpy geothermal energy (closed system) and their geological (cores and cuttings) and geophysical (log data) information are useful for the calibration of the seismic profiles available in the area (e.g. the 2005 MCS reflection lines). The Grado-1 well (realised in 2008, 1110 m deep) and the Grado-2 well (realised in 2015, 1200 m deep) reached the Meso-Cenozoic Friuli-Dinaric Carbonate Platform affected by systems of fractures containing brackish waters at 42°C and 49.5°, respectively. Furthermore, The Grado-1 and Grado-2 wells intersect the top of the platform at a depth of 616 m and 630 m below sea level, respectively (Cimolino, et al., 2010) (Della Vedova, et al., 2014).

4.5.2.2 Cores

In the Gulf of Trieste, samples were collected from the seabed and the first tens of meters of sediments just below. These direct data are useful for the calibration of the available seismic profiles, especially those providing very high resolution (e.g. Boomer and sub-bottom profiles / Chirp).

4.5.2.2.1 Cores: Trieste Harbour 1989 and 2005-2006

Eleven sampling sites are located the marine area adjacent to edge of the Molo VII of the Trieste Harbour, that was interested by an expansion plan. The cores reached the top surface of the Flysch unit at a depth between 16 and 32 m below the seabed (Masoli, et al., 2015). Sixteen cores were also collected in the area within the Scalo Legnami and the Ferriera di Servola. The location of all the sampling sites (executed in 1989 and in 2005-2006 by the Imprefond and GeoSyntech Companies, respectively) is shown in Fig. 74 and Fig. 75.

4.5.2.2.2 Cores: Miramare 1998

A group of four cores was recovered along the coastline connecting Barcola and Miramare, in the framework of the "Piano Regolatore Generale del Comune di Trieste" in 1998 for the extension of the shoreline (Fig. 74). The cores reach a maximum depth between 10 and 21 m and the top of the Flysch was found at depths between 2 and 20 m below seabed. The Unit lies underneath Late Pleistocene-Holocene marine and continental sediments (Romeo, 2009).

4.5.2.2.3 Cores: Vallone di Muggia/Muggia Bay 1960s

Thirteen drillings were realised in the 1960s within the Vallone di Muggia (Muggia Bay, Fig. 74 and Fig. 75) and revealed the depth of the top of the Flysch at a depth of 44-86 m below seabed (Mosetti & Morelli, 1968).

5 RESULTS

5.1 Foreword

In this chapter it is described the sequence of the procedure that allowed to obtain a reliable 3D velocity depth model of the main units and surfaces characterising the geology of the Gulf of Trieste (GT). The CAT3D (OGS, 2014) and Geodepth (Paradigm, 2016) softwares were used to perform the inversion. The Kingdom (IHS, 2014) software was used to perform the seismic interpretation of the time stacked and migrated profiles located within the area of the Gulf of Trieste that was selected to build the model. This area extends for 154 km^2 in the eastern part of the gulf (Fig. 76). Along NW-SE direction it is 14 km long, while in the NE-SW direction it is 11 km long. It was chosen for the following reasons. According to (Busetti, et al., 2008) (Busetti, et al., 2010a)(Busetti, et al., 2010b), in this area the Meso-Cenozoic Friuli-Dinaric Carbonate Platform is flexured towards NE, near the influence of the Dinaric Karst thrust system. This is mainly expressed by the Karst Thrust, extending along the north-eastern rocky coast of the GT, with an accomodation belt located just 2-3 km offshore. It gives an important vertical displacement between the carbonates outcropping in the Karst and those lying in the easternmost area of the gulf. The main aim of the analysis is to provide a reliable value of the depth at which the carbonates lie near the coast and, in turn, the vertical displacement given by the thrust. Another reason is that the area here is covered quite uniformly by a network of 9 MCS seismic profiles belonging to the 2009 OGS survey (GT09-23, GT09-18, GT09-17, GT09-16, GT09-15, GT09-14, GT09-13, GT09-11, GT09-10) and the north-eastern part of the GT13-27 (from kilometres 10th to 21st). Furthermore it can be constrained on its south-western part by the GT13-35 line, the NE extremes of the GT13-25, GT-13-26, GT13-28 and the central part of the GT13-31. They have an average spacing, one from the other, of 1.5 km; the nearest distance from the north-eastern and south-eastern coastline is 1.7 km and 1.5 km, respectively. The distance between the north-western bound of the analysed area and the north-western coast (connecting the Timavo Outlet and Grado) is about 5 km. In total, the MCS cover a distance of 132 km.

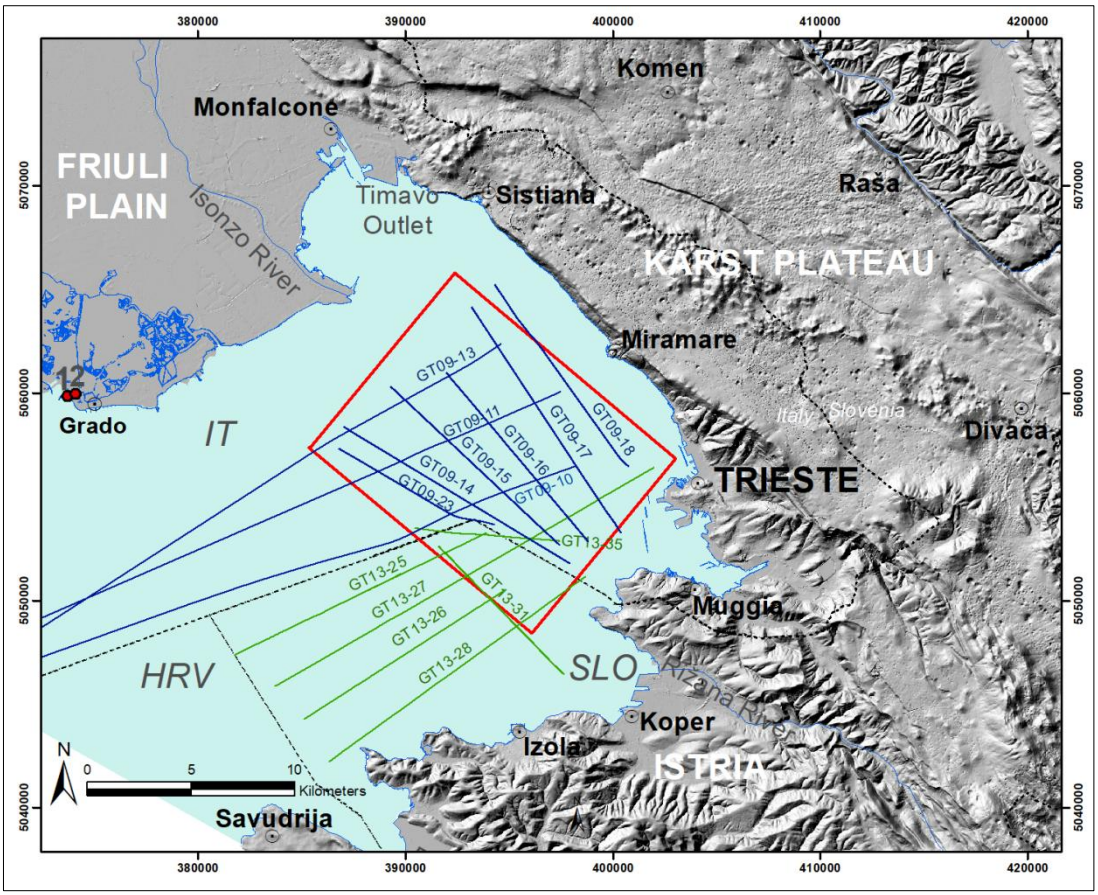

Fig. 76 - Map of the area (red rectangle) that was selected to build the 3D velocity depth model within the Gulf of Trieste (azure area). The multichannel seismic reflection profiles used for the tomographic analysis belong to the 2009 survey (blue lines) and 2013 survey (green lines), collected onboard the R/V OGS Explora. Red circles indicate the position of the Grado 1 and 2 geothermal wells. Map compiled by using ArcGis® (ESRI, 2017) software; datum WGS84, projection UTM33. Digital Elevation Model from: (IRDAT-FVG, 2017) for the Italian area, 10 m cell resolution; (EU-DEM, 2017) for the Slovenian and Croatian areas, 20 m cell resolution.

5.2 The Observed Traveltimes

Starting from raw data sorted by common shot gathers, the reflections related to the seabed and to the top of the flysch, were picked (Fig. 77, Fig. 78). The refractions from the top of the flysch were detected as well. Common trace sections were used to help the interpretation. The shot interval of the acquisition is 12.5 m, with a number of traces per shot of 96 for all the lines, except for those NW-SE oriented of the 2009 survey (48 traces, Fig. 77b). The sampling interval of the picking was, when possible, of one shot gather every ten. Anyhow, the number of the picked traces, was variable. For example, the hyperbola of the reflected seabed is represented by only few traces where the seabed particularly shallow (about less than 20 m). Moreover, the reflection from the top of the carbonates was identifiable only along the 2013 lines, in the parts where it is shallower than about 600 milliseconds (ms) two way time (twt), e.g. Fig. 78.

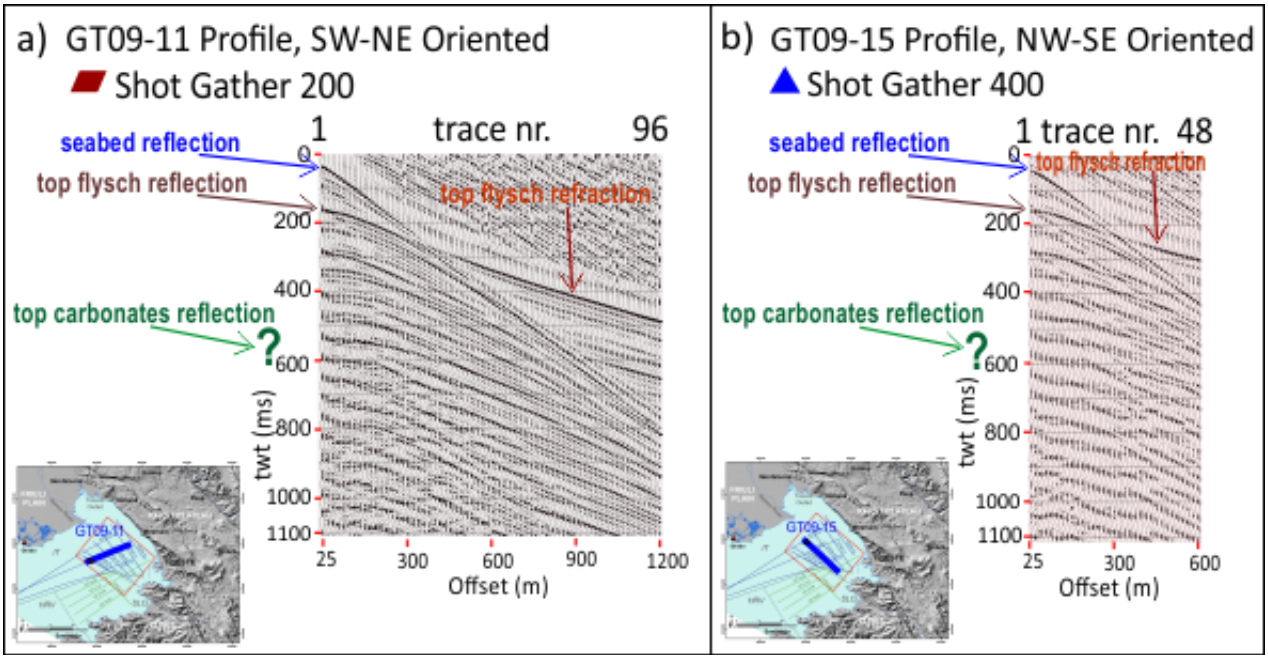

Fig. 77 – Examples of raw data sorted by common shot gathers, for the SW-NE oriented GT09-11 (a) and the NW-SE oriented GT09-15 (b) lines (acquired with a streamer length of 1200 and 600 m, respectively). On these data, the hyperbolas related to the reflection from the seabed and the top flysch (indicated by the blue and brown arrows, respectively) could be identified through the entire dataset with good certainty. The refraction from the top flysch (red arrow) could be detected as well. Whereas, the event related to the reflection from the top carbonates (green arrow) is undetectable through the entire raw data of the 2009 survey. Location maps, of the lines within the analysed area (red rectangle), are shown on the bottom right of both panels (a) and (b).

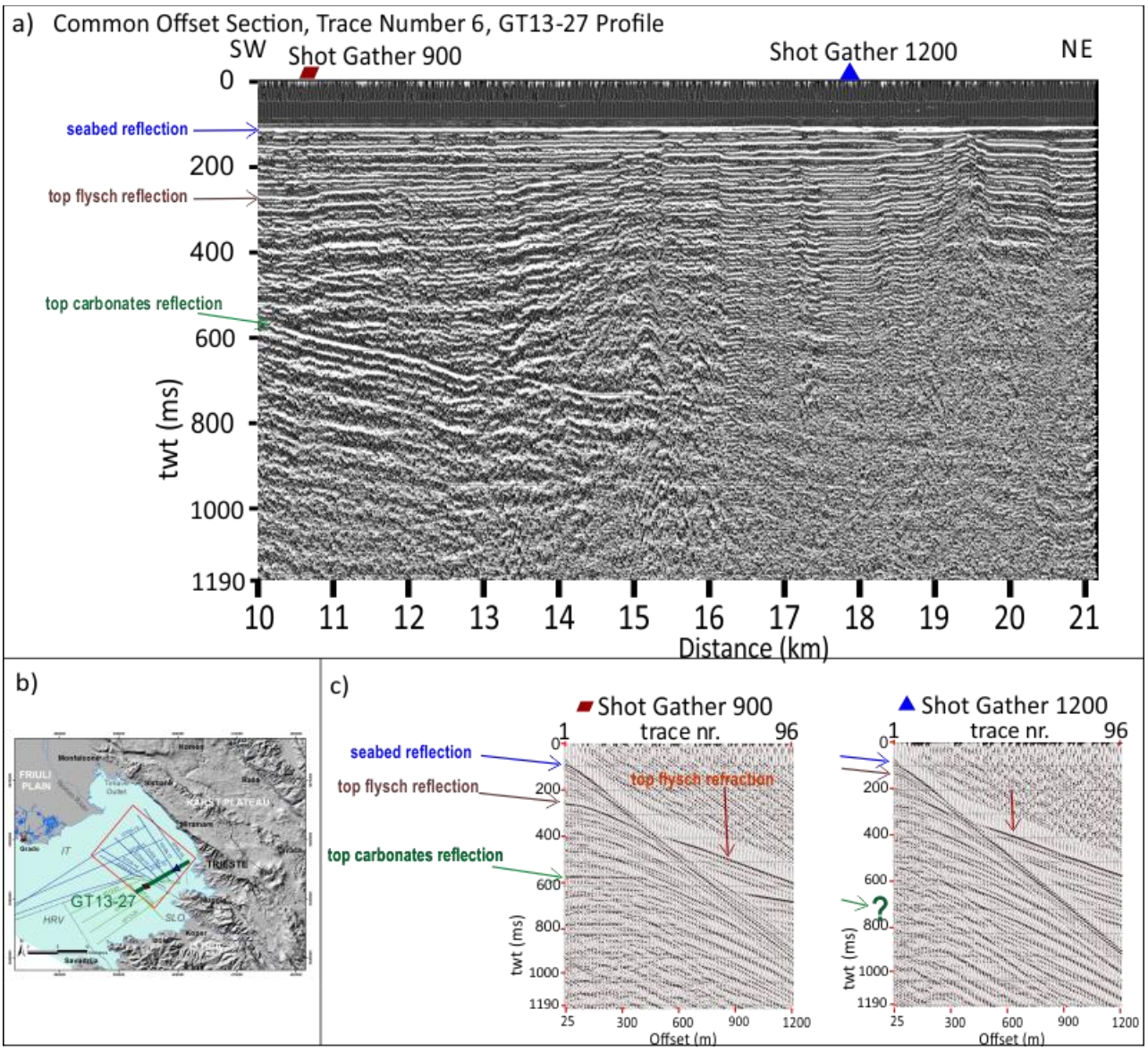

Fig. 78 - Examples of raw data from the GT13-27 profile, acquired with a streamer length of 1200 m. Gathers sorted by common offset (a), trace number 6, along the north-eastern part of the line (from kilometre 10th to 21st). Examples of common shot gathers (c) in correspondence of the top carbonates reflection shallower and deeper than 600 ms (gathers number 900 and 1200, respectively). On these data, the reflections from the seabed and the top flysch (indicated by the blue and brown arrows, respectively) could be identified through the entire dataset with good certainty. The refraction from the top flysch (red arrow) could be detected as well. Whereas, the event related to the reflection from the top carbonates (green arrow) is evident in the area where it is shallower than about 600 ms, while it becomes gradually undetectable (unfocused energy) as it deepens, towards the eastern side of the line. Location map, of the line within the analysed area (red rectangle), is shown in panel (b).

5.3 - 3D Velocity Depth Model A

The first obtained 3D velocity depth model is relative to the top of the flysch and its overburden. The reflected traveltimes of the seabed and the top of the flysch were used for the tomographic inversion. The initial 3D model was defined by a regular grid made up of 2 horizontal interfaces and 3 homogeneous velocity layers. Velocities given as a guess were (from top to bottom) 1500, 2000, 2500 m/s. Each layer, representing the velocity field, was discretized by a series of 14 voxels along the X axis (NW-SE oriented) and 11 voxels along the Y axis (NE-SW).
The tomographic inversion was performed with the CAT3D (OGS, 2014), by applying the procedure described in the section 4.3.1 and the layer stripping method. This latter consists of the inversion of each layer of the model, one by one, from the shallower to the deepest. During the inversion of a layer, the velocity and geometry of the upper layers estimated in the previous steps are constrained.
After having obtained the velocity of the seawater and the geometry of the seabed, the reflected traveltimes of the top flysch were inverted to define the velocity of the Quaternary sediments and update the top flysch surface geometry. For this latter, the inversion procedure was stopped after 80 iterations, with resulting mean acceptable traveltime residual of 1.5% and 0.003 s, Fig. 79.
The resulting 3D tomographic model (Model A) is shown in Fig. 80 and Fig. 81. In Fig. 80, the estimated reflection points in depth, along the top flysch surface, are represented. Their dispersion exhibit acceptable low values along all the profiles.
The resulting average velocity of the seawater and underlying layer are 1510 m/s and 1720 m/s, respectively. The estimated depths range between 22 m and 25 m bsl for the seabed and 24-230 m bsl for the top flysch. The former displays an almost flat surface, with highest depths located in the central part, and trending NE-SW of the modelled area. The latter is characterised by irregular morphology, superimposed on a gradual deepening towards NW. The shallowest area of the surface is located in the south-easternmost part of the model (along profile GT13-27), about 3 km offshore the Trieste coastline.

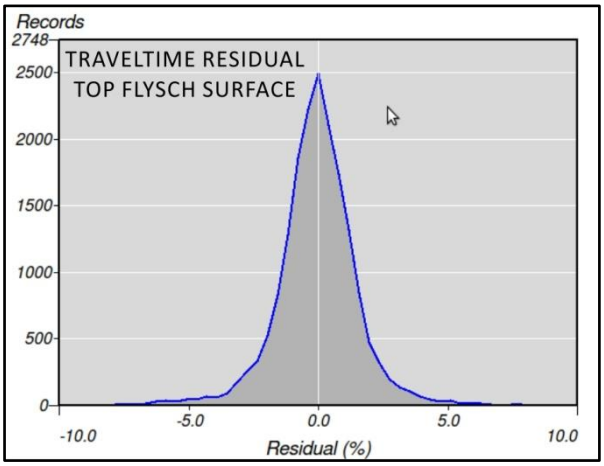

Fig. 79 – Gauss distribution of the traveltime residuals at the end of the tomographic inversion for the top flysch surface.

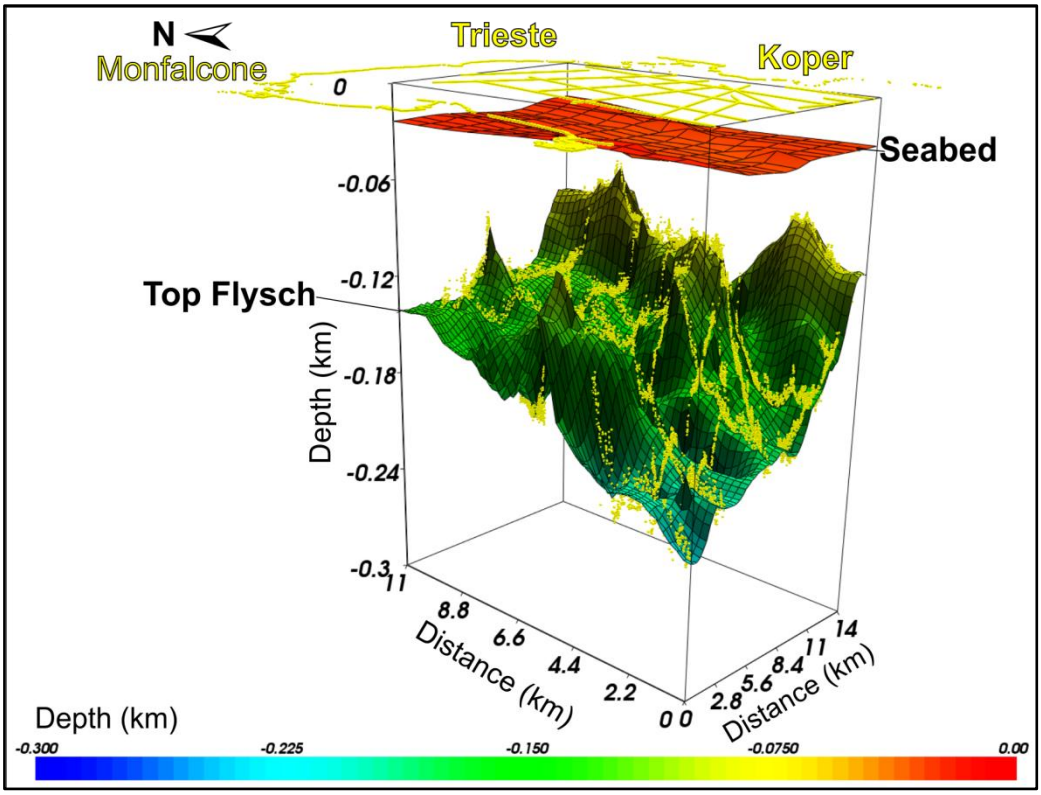

Fig. 80 – Model A. 3D depth model of the seabed and the top flysch surface obtained from tomographic inversion. The yellow points represent the estimated reflection point along the top flysch surface, in correspondence of the analysed 2D profiles.

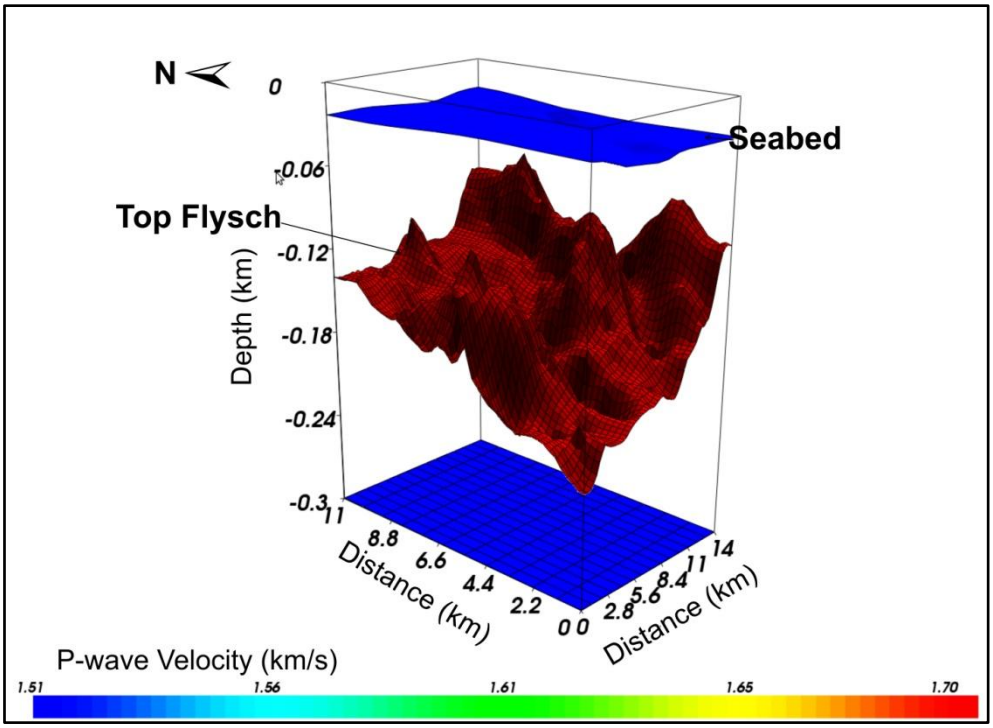

Fig. 81 – Model A. 3D velocity depth model of the seabed and the top flysch surface obtained from tomographic inversion. The Quaternary sediments, bounded by these two surfaces, have an average P-wave velocity of 1.72 km/s.

5.4 - 2D Velocity Depth Model of the GT13-27 Profile

The reflection related to the top carbonate surface is not visible on the 2009 survey profiles, while along the raw profiles of the 2013 it is identifiable, with higher certainty, up to about 600 ms twt and on short offsets (maximum 100 m, 4th trace) when it exceeds this value. Therefore, the 3D tomographic inversion was not possible. It was tentatively performed on the western part of the GT13-27 profile. It trends NE-SW, near, and almost parallel, to the coast of Slovenia. The initial 2D model was constructed similarly to that of Model A, but with a two-dimensional grid (regular) having 3 interfaces and 4 layers. Velocity given as a guess were (from top to bottom) 1500, 2000, 3500, 4000 m/s. Each layer, representing the velocity field, was discretized by a series of 30 pixels along the X axis and 1 pixel along the Y axis.
The tomographic inversion was performed with the CAT3D (OGS, 2014) software, by applying the procedure described in the section 4.3.1 and the layer stripping method.
After having obtained the velocity and geometry of the overlaying layers (sea water, Quaternary sediments) and surfaces (seabed, top flysch), the reflected traveltimes of the top carbonates were inverted to detect the velocity of the flysch unit and update the top carbonate surface geometry.
Time residuals (Fig. 82d) resulted to be acceptable for mean values of 0.006 s, in the south-western part of the section, where the estimated surface lies at 500-800 m bsl. P-wave velocity values for the flysch unit here range between 3250 and 3750 m/s (Fig. 82a). Moreover, Fig. 82c displays dispersion of the reflection points along the distance of the profile: at shallower depth of the surface, points show lower dispersion for both short and long offsets. As the depth of the horizon increases (towards NW), the dispersion of reflected points (picked only at short offsets) increases and the correspondent traveltime residuals (computed for the 4th traces of the common shot gathers) reach peaks of 0.02 seconds, indicating that results are not reliable.
On raw data, the deeper is the reflection, the higher will be the dispersion of the seismic energy. This creates difficulties in the identification of the correspondent event within the pre-stack traces. Moreover, the availability of signals limited to short offsets, hampers in general the possibility to obtain reliable solution in this methodology that attempt to define seismic velocity field (Böhm et al., 1999,2000; Vesnaver and Böhm, 2000) from the picking of pre-stack data.
It was decided then, to try to upgrade and refine the velocity field for the flysch unit, through an iterative imaging technique. Pre-stack depth migration, residual move-out analysis and horizon based tomography, were performed by using the Geodepth (Paradigm, 2016) software. Differently from the tomographic method applied up to now, the imaging technique provides the definition of both lateral and vertical velocity gradients within layers, at higher resolution. This allows, in turn, further detailed reconstruction of the geological elements.

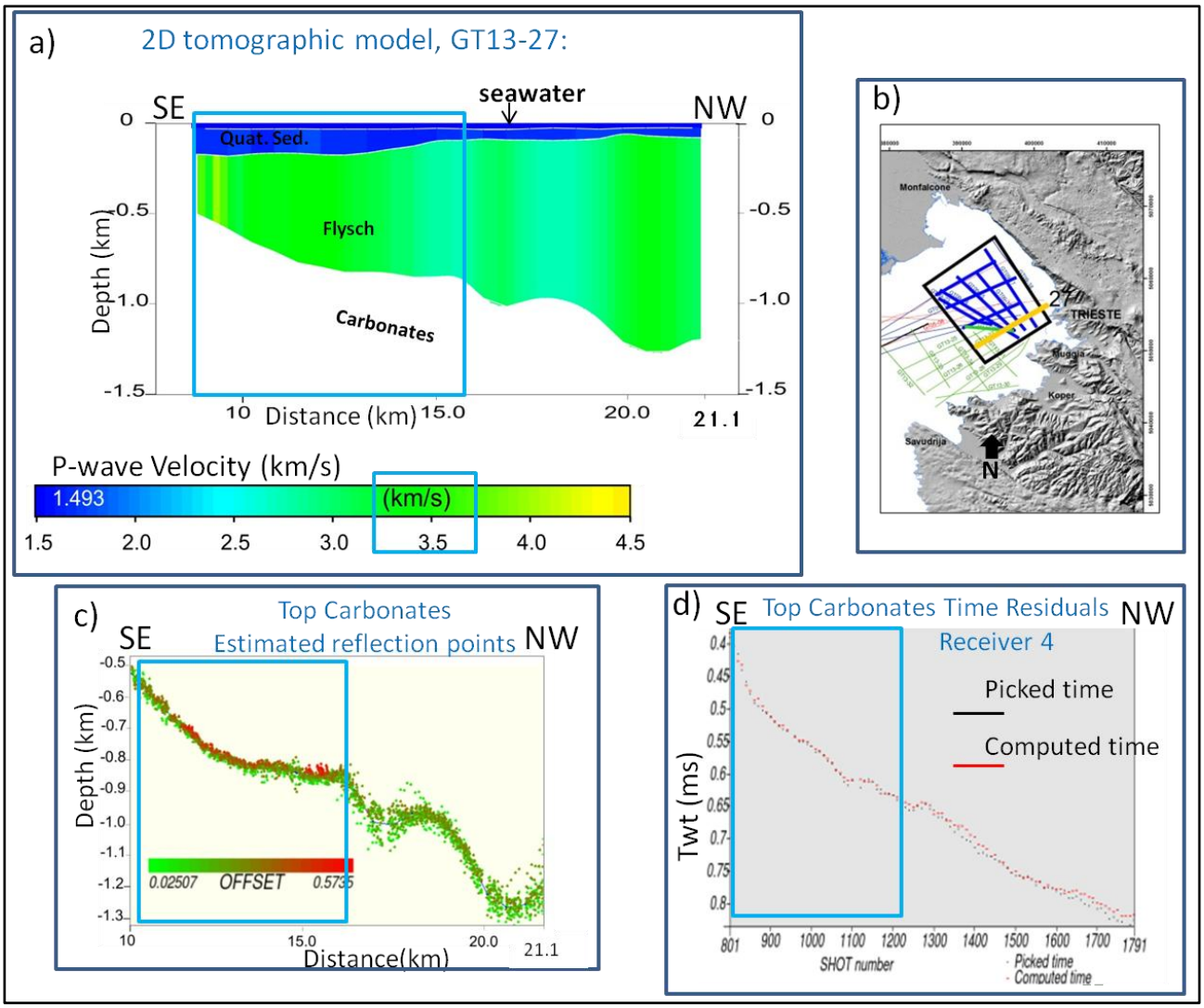

Fig. 82 – a) 2D tomographic model of the north-western line GT13-27, with its location in b) plot of estimated reflection points along the distance of the profile; red and green points refer to longer and shorter offsets, respectively. d) plot of the estimated and observed traveltimes (for the 4th traces, offset of 100 m), along the spatial distribution of the shot gathers along the profile.

5.5 Earth modelling in depth of the 2D GT13-27 Profile

In order to further refine the obtained velocity model, it was employed an iterative imaging technique involving pre-stack depth migration, residual move-out analysis and horizon based tomography, by using the Geodepth (Paradigm, 2016) commercial software (see section Imaging in Depth).
The procedure was applied to the GT13-27 line, 21.1 km long. It represents a key profile of the entire available dataset, as it is almost perpendicular to the north-eastern coastline, ending at NE just 1.7 km offshore the city of Trieste. This is the most proximal area to the Karst Thrust of the Dinaric Karst system, covered by MCS data. The Karst Thrust, running along the coast, displaces the carbonates, lying in the gulf, from those of the hangingwall outcropping on the Karst Plateau anticline. Moreover, the GT13-27 profile trends SW-NE (N60°E) across the south-eastern part of the Gulf of Trieste (Slovenian and Italian waters). Its average distance from the south-eastern GT shoreline is about 5 km. This line was therefore chosen as sample for the detection of the maximum depth, beneath sea level, of the top of the carbonate platform, that deepens towards NE (due to the weight effect of the neighbouring External Dinarides and Southern Alps) and represents part of footwall of the Karst Thrust system.

The final pre-stack depth migrated (PSDM) profile is shown, in Fig. 83. Moreover, the imaging is displayed through its trace amplitude on which it is superimposed the resulting updated interval velocity field. It was obtained after three iterations and by using the Grid-Tomography approach, which allows the determination of the vertical velocity gradients within layers. This is very important because the thickness of the flysch layer becomes very large towards the east.

Different ranges of interval velocities characterise the sedimentary units, with well defined vertical gradients: 1600 to 2100 m/s for the Quaternary sediments, 2200 to 4600 m/s for the Eocene flysch unit, and 4600 to 4800 m/s for the Meso-Cenozoic carbonates.
At its north-easternmost side, the profile reveals the top of carbonate platform at a maximum depth of around 1600 m below the sea level (bsl). Between kilometres 10 and 21, the horizon dips gradually towards NE, with a mean real angle of 5° along the profile's direction. If the depth of the top of the carbonates is linearly extrapolated using this average inclination, then it reaches 1740 m bsl in correspondence of the coast of Trieste.

Other interesting features are also well imaged by PSDM. The main are:

- in the SW part, between kilometres 3.5 and 10 (Fig. 83), the carbonates are structured as an anticline. Its top has an irregular surface and rises up to a depth of 120 m bsl. It is covered by a seismic package 100 to 210 m thick, representing the shallowest unit of the entire sedimentary sequence of the gulf (Quaternary marine and continental sediments).

- The flysch unit, on the south-western side of the carbonate anticline, between kilometres 0 and 4, is about 200 m thick (Fig. 83). It has a dome shape rising up to 70 m bsl, with an irregular top surface showing pervasive vertical offsets up to 25-30 m. On the north-eastern part of the line, at kilometre 21, the unit shows its maximum thickness, that is almost 1500 m, gradually decreasing towards SW. At kilometre 7, the flysch pinches out on the top of the carbonate anticline. The top flysch surface in this part deepens from NE (minimum depth of 50 m bsl), to SE (maximum depth of 120 m). Also along this sector, the horizon is overall depicted by irregular shape (Fig. 83 and Fig. 84).

- More into detail, the acoustic response of the reflection package between the top of the flysch and the seabed, locally changes in correspondence of DMG2080 (Depth Migrated Gather) at kilometre 8 (Fig. 84): on the western part of the seismogram, the layers lye above an almost flat top flysch horizon and have a good lateral continuity; while on the eastern part, the reflections cover a discontinuous top surface of the flysch and are affected by diffuse acoustic disturbance. This could suggest the presence of fractures and fluids.

- Toplap stratifications are present within the flysch unit and terminate against the top flysch unconformity (Fig. 83, Fig. 84, Fig. 85). Considering the local vertical velocity field around DMG1805 (Fig. 85), a low interval velocity trend is present at depths between 200 and 400 m. This suggests occurrence of fluids. These migrate towards the shallower sediments, probably along the porous and permeable sandstone layers of the flysch.

- At 4.8 km depth, a quite well focused reflection is highlighted (Fig. 86). At this depth, the average interval velocity reaches 4800 m/s.

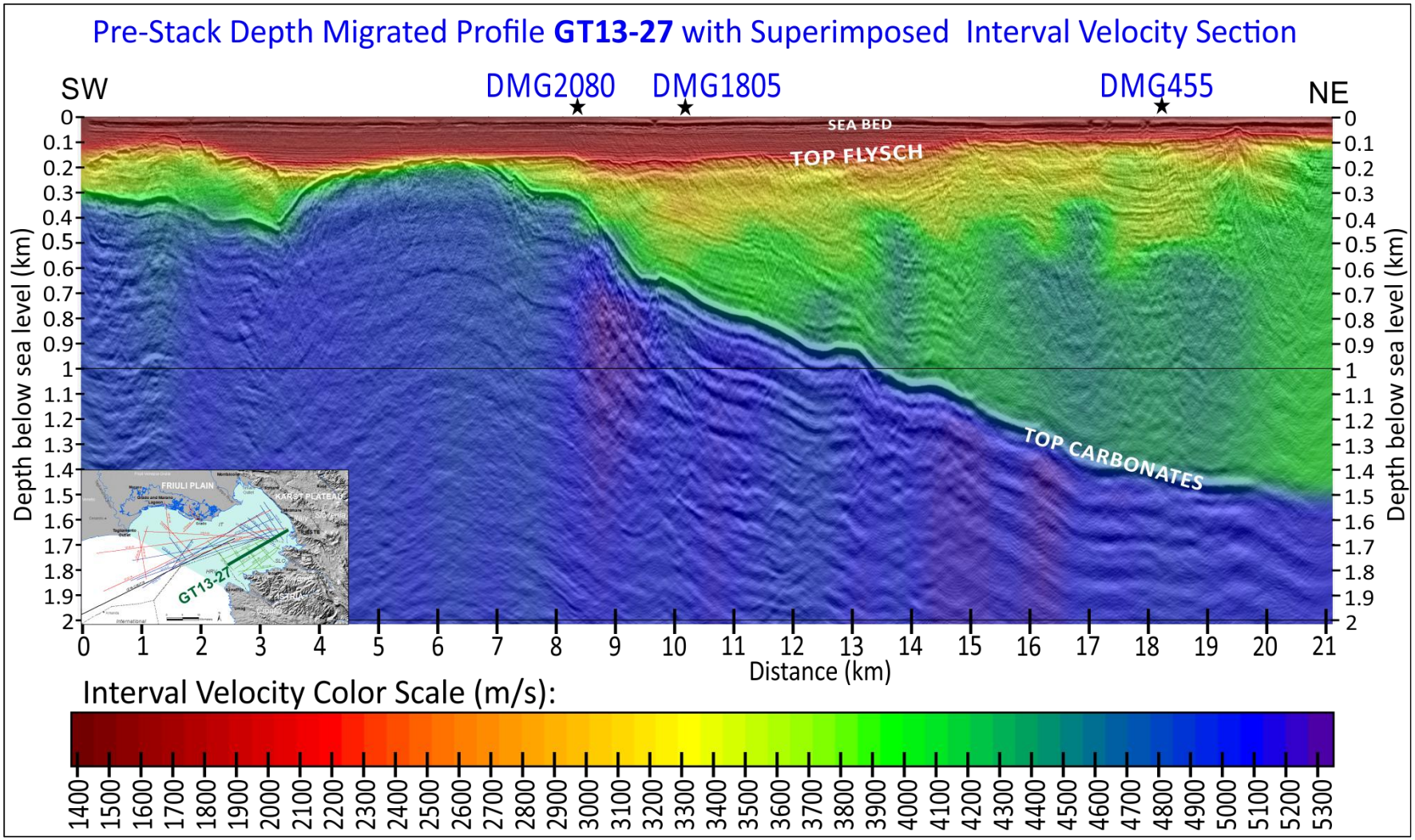

Fig. 83 - Result of the Pre-Stack Depth Migration (PSDM) of the profile GT13-27, amplitude attribute (gray colour scale), with superimposed the refined velocity field (m/s). Black stars indicate position of three samples of the depth image gathers (DMG) analysed during imaging. Vertical exaggeration: x5. Performed by using Geodepth (Paradigm, 2016) software.

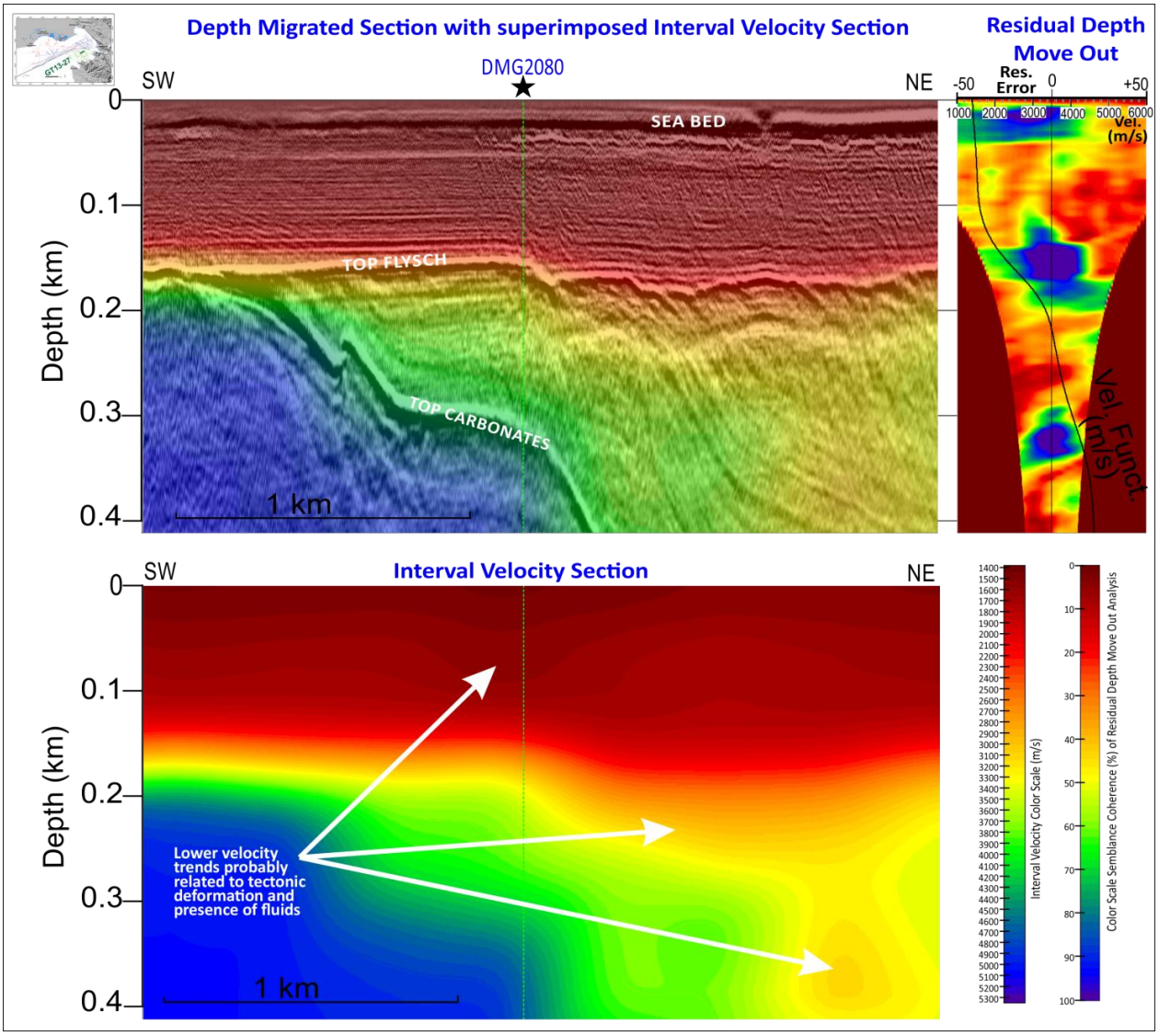

Fig. 84 - Top: blow-up of the PSDM of line GT13-27 with superimposed Interval velocity section (left), the residual move out (right) centred almost on the maximum semblance coherence (minimum error), computed from the DMG2080. Bottom: interval velocity section of the PSDM. The position of the DMG2080 on the seismic line is shown by a dashed green line (black star in Fig. 83). The vertical black line on the residual panel represents the local velocity function at DMG2080. Performed by using Geodepth (Paradigm, 2016) software.

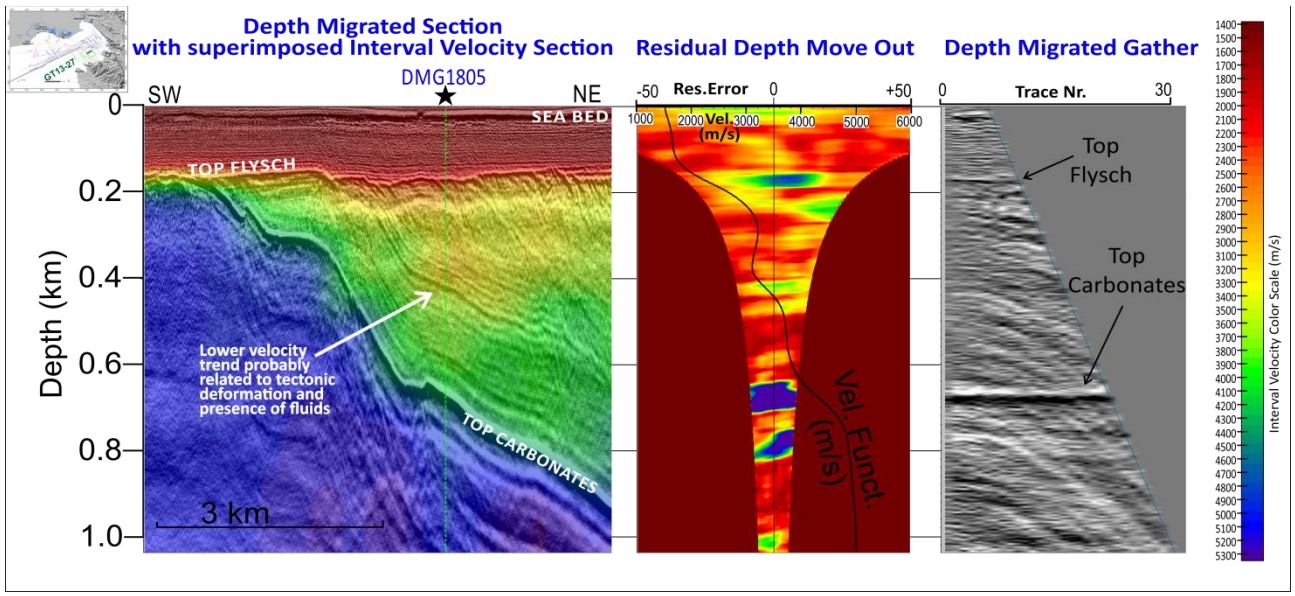

Fig. 85 - Panels representing (from left to right) a blow-up of the PSDM of line GT13-27 with superimposed interval velocity section, the residual move out and a flat sequence of events on the corresponding DMG1805. The residual move out panels, centred almost on the maximum semblance coherence (minimum error), is derived from the displayed DMG, whose position on the seismic line are shown by a vertical dashed green line (black stars in Fig. 83). The vertical black line on the residual panels represents the local velocity function. Performed by using Geodepth (Paradigm, 2016) software.

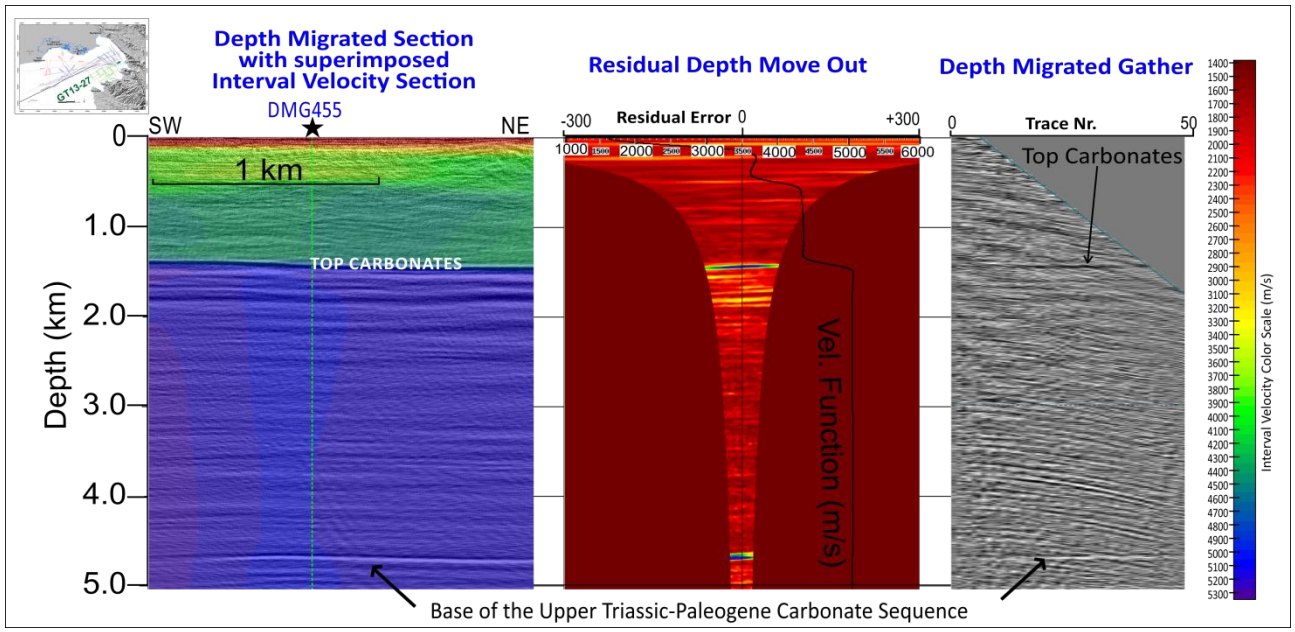

Fig. 86 - Panels representing (from left to right) a blow-up of the PSDM of line GT13-27 with superimposed interval velocity section, the residual move out and a flat sequence of events on the corresponding DMG 455. The residual move out panel, centred almost on the maximum semblance coherence (minimum error), is derived from the displayed DMG, whose position on the seismic line is shown by a vertical dashed green line (black stars in Fig. 83). The vertical black line on the residual panel represent the local velocity. Performed by using Geodepth (Paradigm, 2016) software.

5.5.1 Reliability of Estimated Velocities and Depths in the Pre-Stack Depth Migration

The estimated error, related to the top flysch and top carbonates depth surfaces, is displayed in Fig. 87 and Fig. 88, respectively. As regards the normalised amplitude coherence for the top flysch surface, the chosen reference offset is 250 m. This is a compromise between the shallower and the deeper part of the horizon. The amplitudes result more variable where the depth of the surface rises towards the sea bed, due to the fact that the wavelet stretching is higher and therefore the mute is heavier. Despite this, considering an amplitude coherence of 70%, the maximum average error in the estimation of the depth is ±15 m. Similarly, the semblance of the coherence amplitude for the top carbonate surface is obtained for the distance between 8 and 21 kilometres. The reference offset is 800 m, chosen as compromise for the shallower and deeper part of the horizon. The amplitudes are more variable from kilometre 13 towards the north-eastern part of the profile. This is due to the fact that the carbonates top surface exhibits a marked slope. Moreover, the reference offset should be reduced because the surface becomes shallower. Despite this, considering an amplitude coherence of 70%, the maximum average error in the estimation of the depth is ±25 m. In the south-western part of the section, the carbonates are shallower and encounter the top flysch horizon. Therefore, the error for the top of the carbonates becomes the same of that of the top of the flysch.

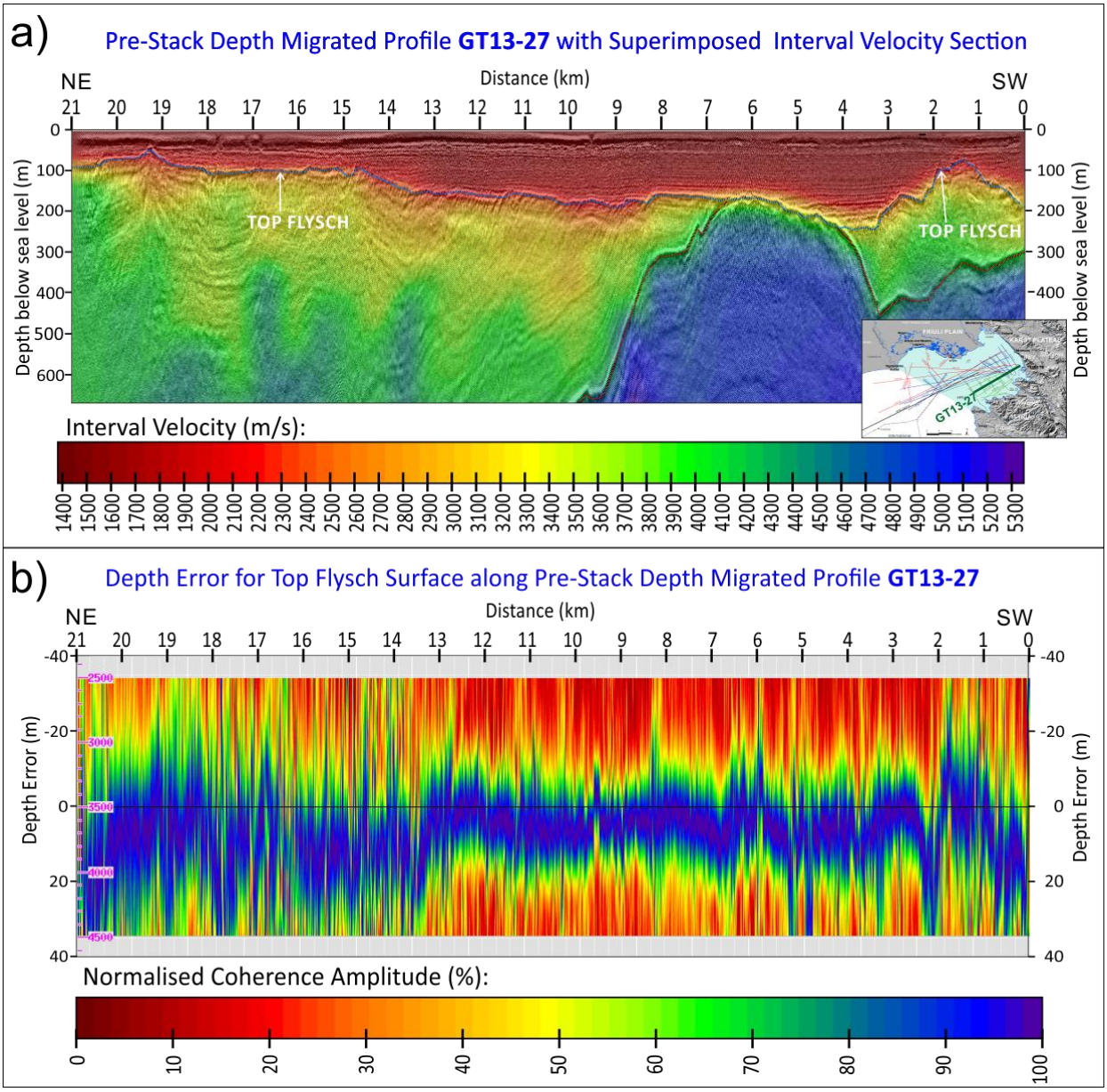

Fig. 87 – The figure gives a comparison of the entire depth migrated section GT13-27, displayed with interval velocity field superimposed on seismic amplitude (a), with the normalised coherence amplitude along the entire top flysch surface (b). The average maximum error in the estimated depth of the surface results to be about ±15 m (for a coherence amplitude of 70%). Performed by using Geodepth (Paradigm, 2016) software.

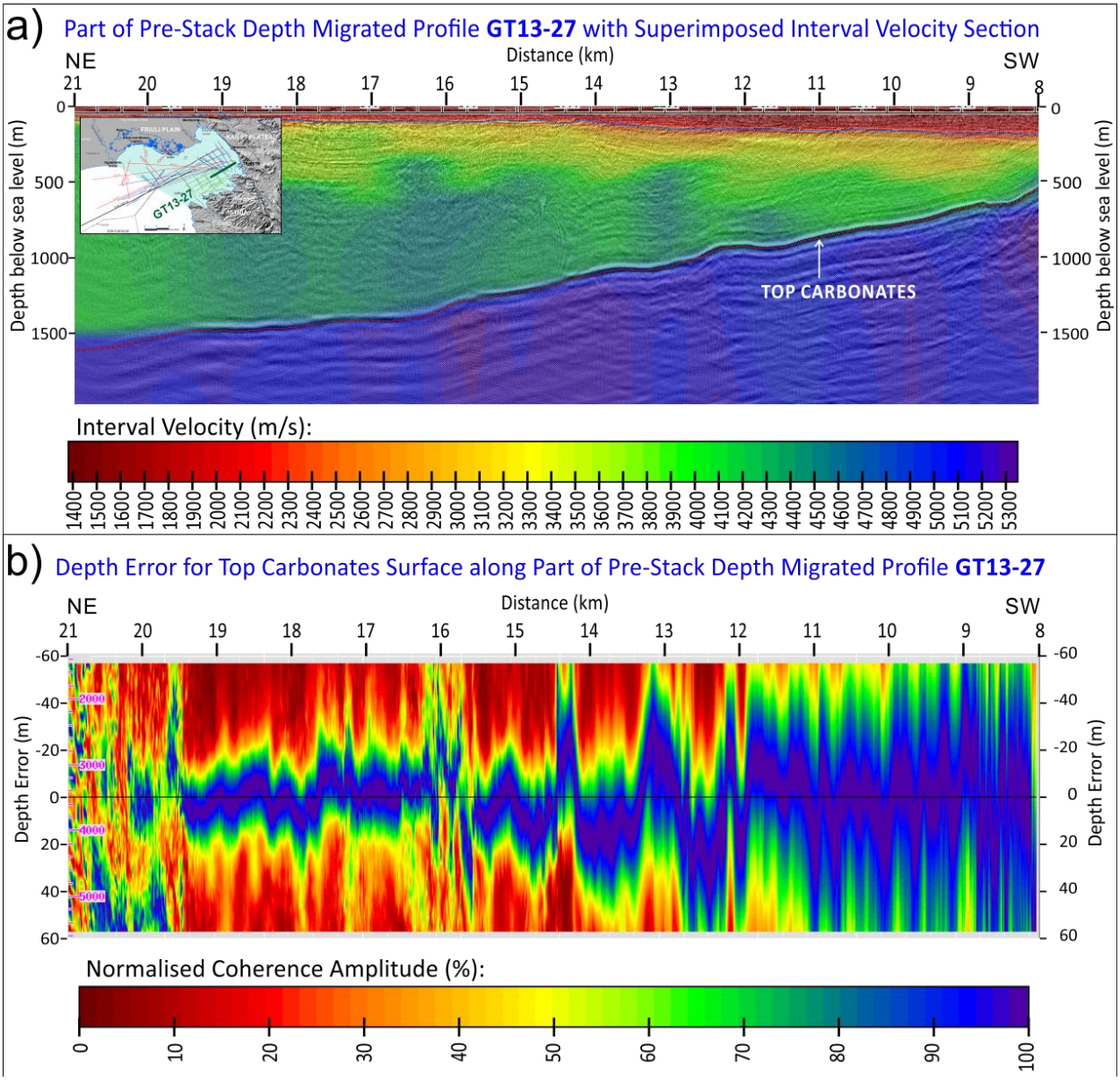

Fig. 88 - The figure gives a comparison of part of depth migrated section of line GT13-27 (from the 8th to 21st km), displayed as interval velocity field superimposed on the seismic amplitude (a), with the normalised coherence amplitude along the top carbonate surface (b). The average maximum error in the estimated depth of the surface, in the deeper part, results to be about ±30 m.

5.6 - 3D Time Model

A 3D time model was built, starting from the interpretation on all the time migrated lines belonging to the investigated area. The recognised surfaces are: seabed, top of the flysch, an inner surface within the flysch and the top of the carbonates (e.g., Fig. 90b and Fig. 91b). The interpretation was executed on the Kingdom (IHS, 2014) software. The inner flysch horizon is generally detected at around 300-500 ms twt, with a relative higher amplitude response than that characterising the upper and lower flysch packages (here named upper and lower flysch, respectively). The reflections of the seabed, top flysch and top carbonates show an even higher acoustic impedance along the post-stack time migrated data. Migration, in fact, refocuses the seismic energy along the reflector, enhancing the signal response.
The model was constructed with the main aim of exploitation all the available information obtained from the time data interpretation (e.g. inner flysch) and the refraction velocities calculated from the picked top flysch refracted event on raw data (see section Flysch Anisotropy Analysis5.7). The subsequent step (model B), was that of the conversion into depth of the surfaces, created by the interpolation of the picked data in time domain. The conversion used mean velocities from the tomographic result of the model A (Quaternary sediments), from the flysch anisotropy analysis (upper flysch) and from the velocity gradient of the flysch detected by the iterative imaging technique.
The 2D picked surfaces were gridded along the three dimension by a dedicated algorithm available in the CAT3D (OGS, 2014) software. The resulting 3D time model is shown in (Fig. 89). It consists of the top flysch, inner flysch and top carbonates surfaces, reconstructed through the same area covered by the 3D velocity depth model A, and the subsequent B.
In particular, the top flysch reflects its general deepening towards NW, detected by the Model A. It ranges between 0.03 s twt, in the south-eastern sector, and 0.3 s twt in the opposite north-western side. The flexured top carbonates shows that its NE deepening, detected on the 2D velocity depth model and 2D pre-stack depth migrated GT13-27 profile, is a characteristic for the entire investigated area. The inner flysch surface, mimics the above lying top flysch, but it shows smoother irregularities. Furthermore, it bends towards opposite depth direction along the south-eastern border the modelled volume.

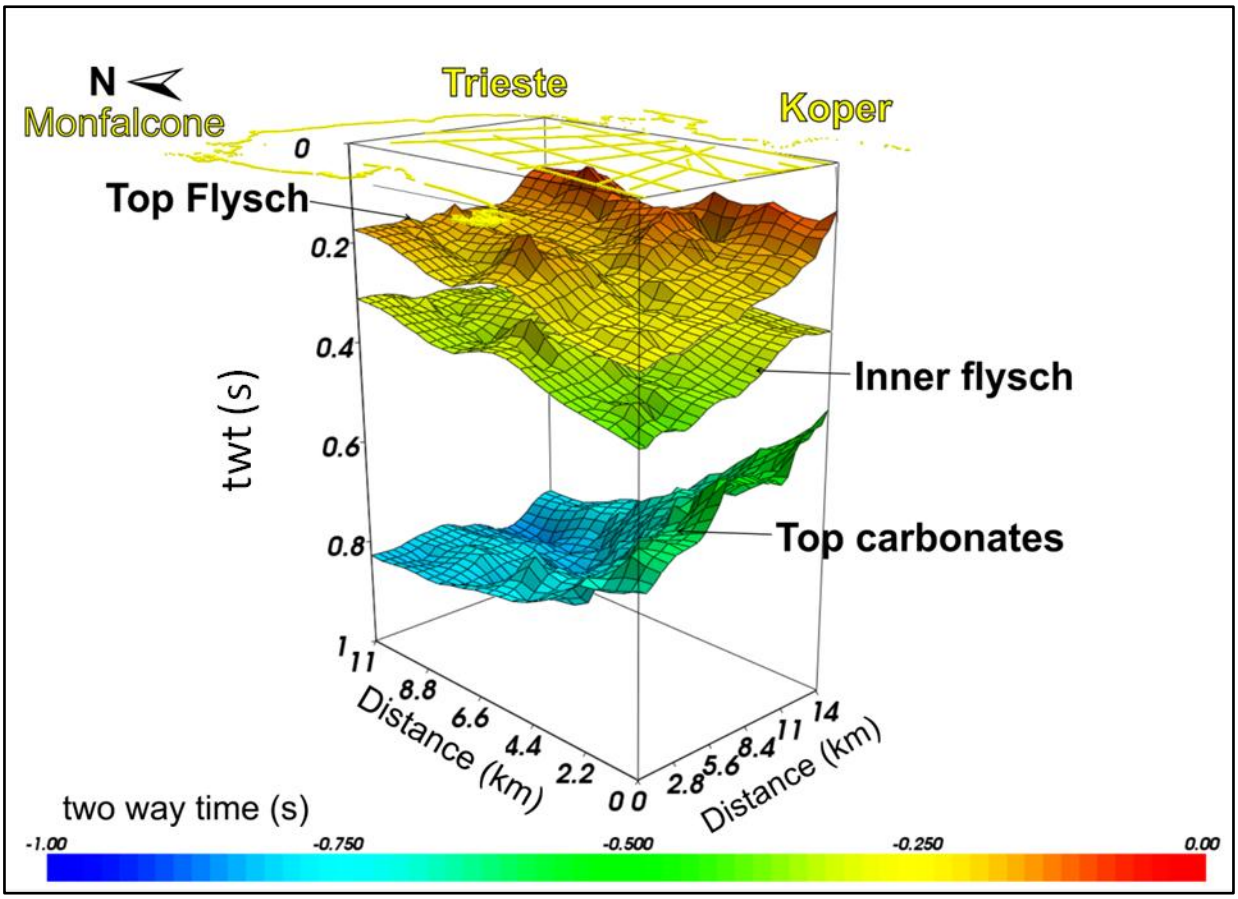

Fig. 89 – 3D time model of the investigated area, showing twt (s) surfaces of the top flysch, inner flysch and top carbonate. The gridding was performed by the CAT3D (OGS, 2014) software, after the interpretation of the horizon on 2D time migrated profiles.

5.7 Flysch Anisotropy Analysis

The iterative imaging procedure applied to the GT13-27 seismic line allowed to recover in detail the vertical P-wave velocity gradient characterizing the whole flysch layer (Fig. 83).

Furthermore, the traveltimes of the refracted P-waves at the top flysch were analyzed (e.g. Fig. 90, Fig. 91). The input traveltimes were picked on common shot gathers of raw data, that show the straight event related to the refraction from the top flysch surface (e.g. Fig. 77, Fig. 78c). The resulting horizontal P-wave velocities, for the upper part of the flysch unit, vary from 3100 and 4200 m/s, with an average value of about 3700 m/s for the entire analysed dataset.

The analysis evidences a marked discrepancy between the average vertical and horizontal P-wave velocities characterizing the upper part of the flysch unit, which are about 2900 m/s and 3700 m/s, respectively.

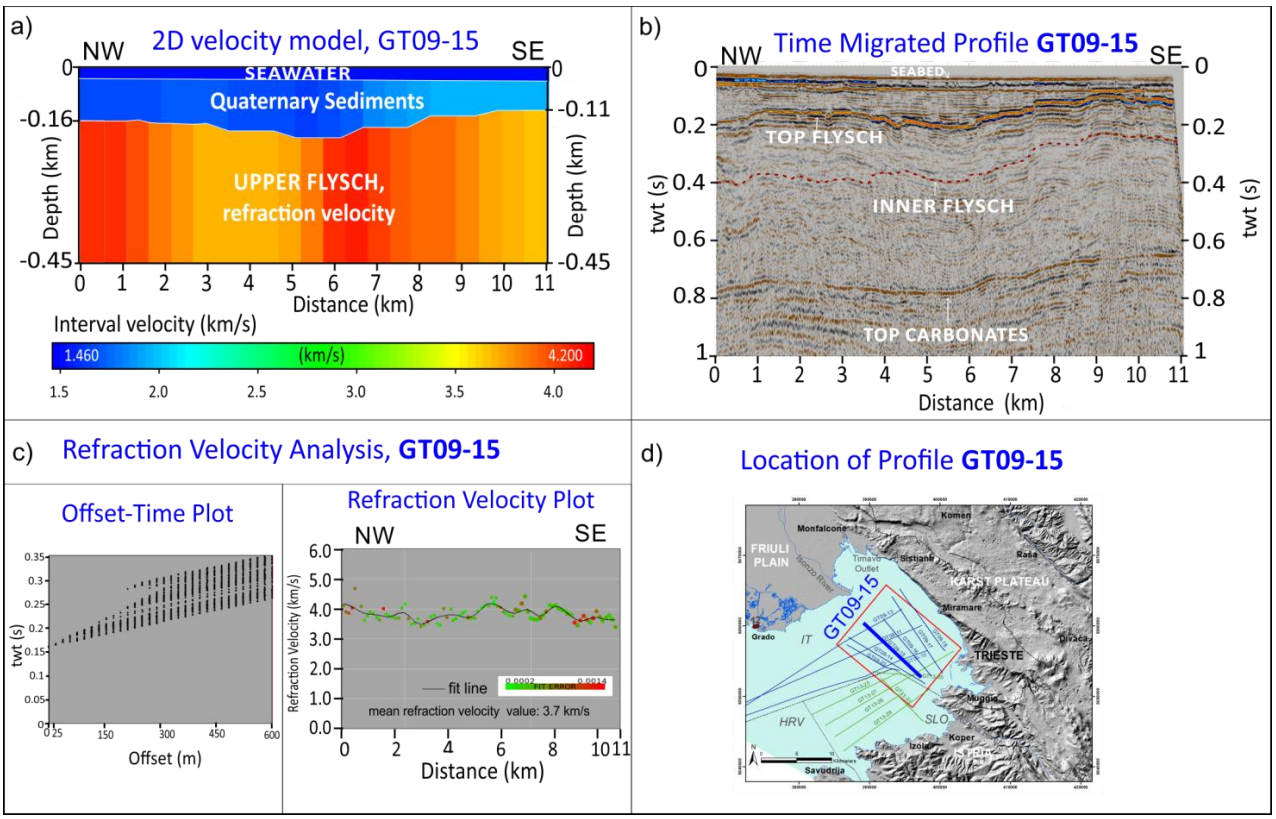

Fig. 90 – 2D velocity depth model for the NW-SE oriented GT09-15 profile (a), performed by CAT3D software (OGS, 2014). The seabed and the top flysch reflection traveltimes were used as input for the tomographic inversion to detect depth geometries of the seabed and top flysch surfaces, along with the velocities of the seawater of the Quaternary sediments. The horizontally varying velocity field of the shallower flysch unit was estimated by refraction analysis, form travel time picking on raw data sorted by common shot gathers (e.g. Fig. 77, Fig. 78c). Along this line, the refracted P-waves velocities range between 3.5 and 4.2 km/s, with a mean value of 3.7 km/s (a, c). Moreover, panel (c, left) represents the distribution of the picked twt reflected events along the streamer (600 m long); panel (c, right) shows the calculated refraction velocity values along the distance of the profile, with the best fit interpolation (black line). Time migrated section of line GT09-15 (b) on which the seabed, top flysch, inner flysch (dashed red line) and top carbonates horizons were interpreted, by using the Kingdom software(IHS, 2014), to construct the subsequent 3D time and 3D velocity depth-B models. Location of the profile, within the analysed area (red rectangle), is shown in (d).

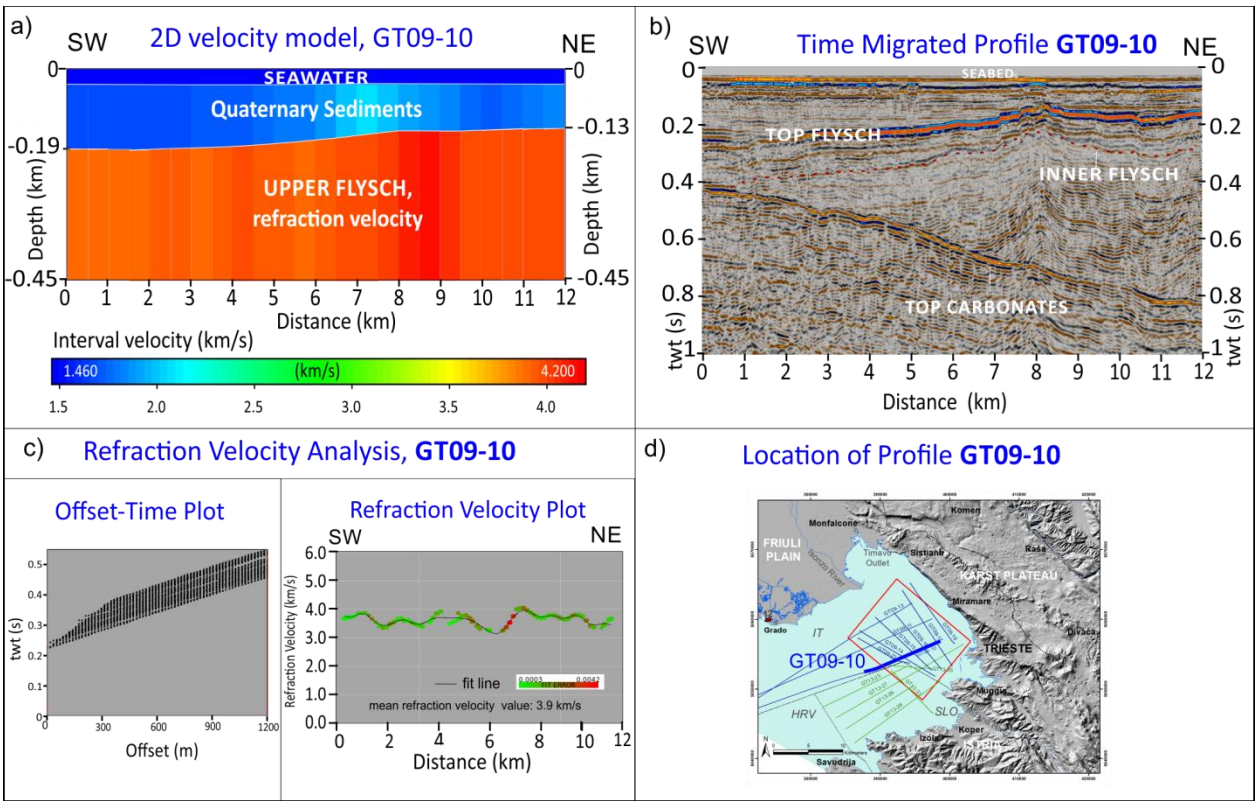

Fig. 91 - 2D velocity depth model for the SW-NE oriented GT09-10 profile (a), performed by CAT3D software (OGS, 2014). The seabed and the top flysch reflection traveltimes were used as input for the tomographic inversion to detect depth geometries of the seabed and top flysch surfaces, along with the velocities of the seawater of the Quaternary sediments. The horizontally varying velocity field of the shallower flysch unit was estimated by refraction analysis, form travel time picking on raw data sorted by common shot gathers (e.g. Fig. 77, Fig. 78c). Along this line, the refracted P-waves velocities range between 3.1 and 4.2 km/s, with a mean value of 3.9 km/s (a, c). Moreover, panel (c, left) represents the distribution of the picked twt reflected events along the streamer (1200 m long); panel (c, right) shows the calculated refraction velocity values along the distance of the profile, with the best fit interpolation (black line). Time migrated section of line GT09-10 (b) on which the seabed, top flysch, inner flysch (dashed red line) and top carbonates horizons were interpreted, by using the Kingdom software(IHS, 2014), to construct the subsequent 3D time and 3D velocity depth-B models. Location of the profile, within the analysed area (red rectangle), is shown in (d).

At this step it is attempted to explain this difference in terms of seismic anisotropy due to fine layering, in the frame of Backus (1962) averaging theory (described in Appendix 1).
Let's consider a periodic laminated sequence of silty marls and cemented sandstone constituting the flysch. The properties of each isotropic viscoelastic material are given in Tab. 22, the elastic high-frequency limit compressional (C_P) and shear-wave (C_S) velocities, densities (ρ) and quality factors (Q_{01}, Q_{02}).

Material	c_P (m/s)	c_S (m/s)	ρ (kg/m^3)	Q_{01}	Q_{02}
Sandstones	4500	2800	2400	60	40
Silty marls	2100	900	2250	20	10

Tab. 22 - Material properties composing a typical flysch sequence (Shön, 2011).

Let the time constants in equation (7) be τ1 = 0.16 s and τ2 = 0.3 ms, so that the quality factor of each single isotropic layer is nearly constant over the exploration seismic band. Fig. 92 shows a polar representation of the qP-wave phase velocity vector at the dominant frequency of 80 Hz, which is the average dominant frequency of the seismic signal at the flysch top. This plot denotes a pronounced anisotropic effect due to fine layering in this kind of medium. Moreover, the vertical and horizontal qP-wave velocities are very similar to the observed values.

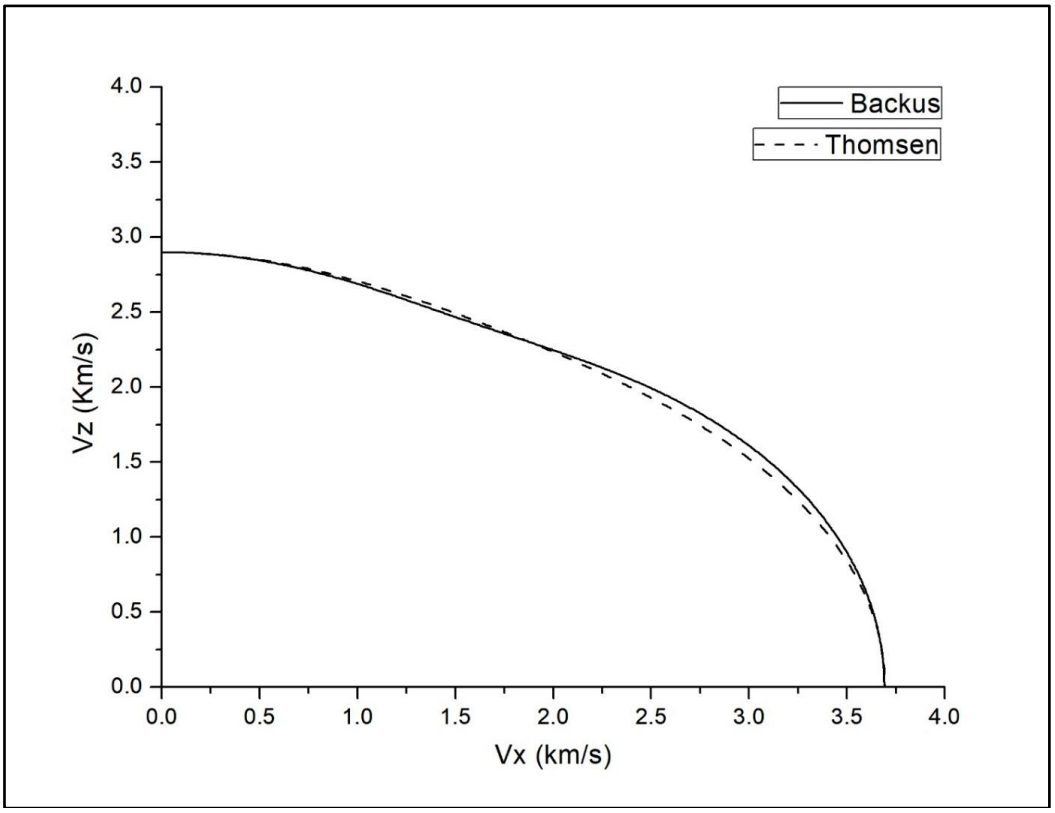

Fig. 92 - Polar representation of the qP-wave phase velocity vector at the dominant frequency of 80 Hz (solid line). The Thomsen (1986) approximation is also represented (dashed line).

The average tomographic velocity value obtained from the upper flysch layer using the iterative imaging procedure is very close to the vertical qP-wave velocity provided by this model. Similarly, the agreement between the velocity values obtained by analyzing the traveltimes of the P-waves refracted at the top of the flysch layer and the horizontal qP-wave velocity provided by this model

is also excellent. The large discrepancy between the two tomographic velocity values is therefore here justified using the generalized Backus theory.

Fitting the qP-wave velocity provided by the Backus model using equation (10), the following Thomsen (1986) parameters are obtained: ε=0.275 and δ=-0.08. The approximated qP-wave velocity polar plot is represented in Fig. 92.

5.8 - 3D Velocity Depth Model B

The 3D depth velocity model B was constructed with the intention of characterising the top carbonate surface over the entire space occupied by the analysed volume in the Gulf of Trieste. It was built inserting the seabed and top flysch surfaces obtained by the velocity depth model A. The velocity field, attributed to the upper flysch layer, was estimated by the flysch anisotropy analysis. The ε=0.275 Thomsen parameter was used to convert horizontal into vertical P-wave velocities. The results were then obtained by performing the conversion into depth of the inner flysch surface. Moreover, the top of the carbonates was converted into depth by attributing the average velocity, detected by the iterative imaging technique, to the lower sequence of the flysch (lower flysch unit).
Therefore the surfaces and the P-wave velocity values used to construct the 3D depth velocity model B are, from top to bottom:
- P-wave velocity of about 1510 m/s for the seawater, obtained from the traveltime tomographic inversion related to the Model A;
- seabed surface obtained from the traveltime tomographic inversion related to the Model A;
- P-wave velocity of the Quaternary sediments, obtained from the traveltime tomographic inversion related to the Model A;
- top flysch surface obtained from the traveltime tomographic inversion related to the Model A;
- vertically varying P-wave vertical velocity ranging between about 2800 and 3100 m/s for the upper flysch unit, obtained from horizontally varying P-wave velocity by the flysch anisotropy analysis;
- inner flysch surface obtained from the 3D time model and converted into depth by using the average velocity attributed to the upper flysch unit;
- average P-wave velocity of 4500 for the lower flysch units, obtained from the pre-stack depth migration of the GT13-27 profile.
- top carbonate surface, obtained from the 3D time model and converted into depth by using the velocity of all the overlaying units.
The model was constructed by the CAT3D (OGS, 2014) software providing in input all this information.
In Fig. 93 and Fig. 94 are shown the 3D velocity depth and 3D depth model B, respectively. The general NE deepening of the top carbonates, observed in the previous models is confirmed. The surface shows a pattern of high and low morphologies, whose longitudinal axis is NW-SE oriented. Its depth ranges between 1450 and 1550 m bsl, along the north-eastern side of the model B, close to the coast. It gradually rises up to 800 m and 1000 m in the south-western and north-western edges of the model.
The top carbonate horizon, interpreted along the pre-stack depth migrated line GT13-27, is reported in the figures (yellow line). This 2D horizon and the 3D modelled top carbonate surface fit together with a good degree of approximation (considering the large depth of this surface), except from some local discrepancies (up to ±90 m), Fig. 95. In correspondence of the north-easternmost part of the PSDM profile, the local difference is about ±75 m.

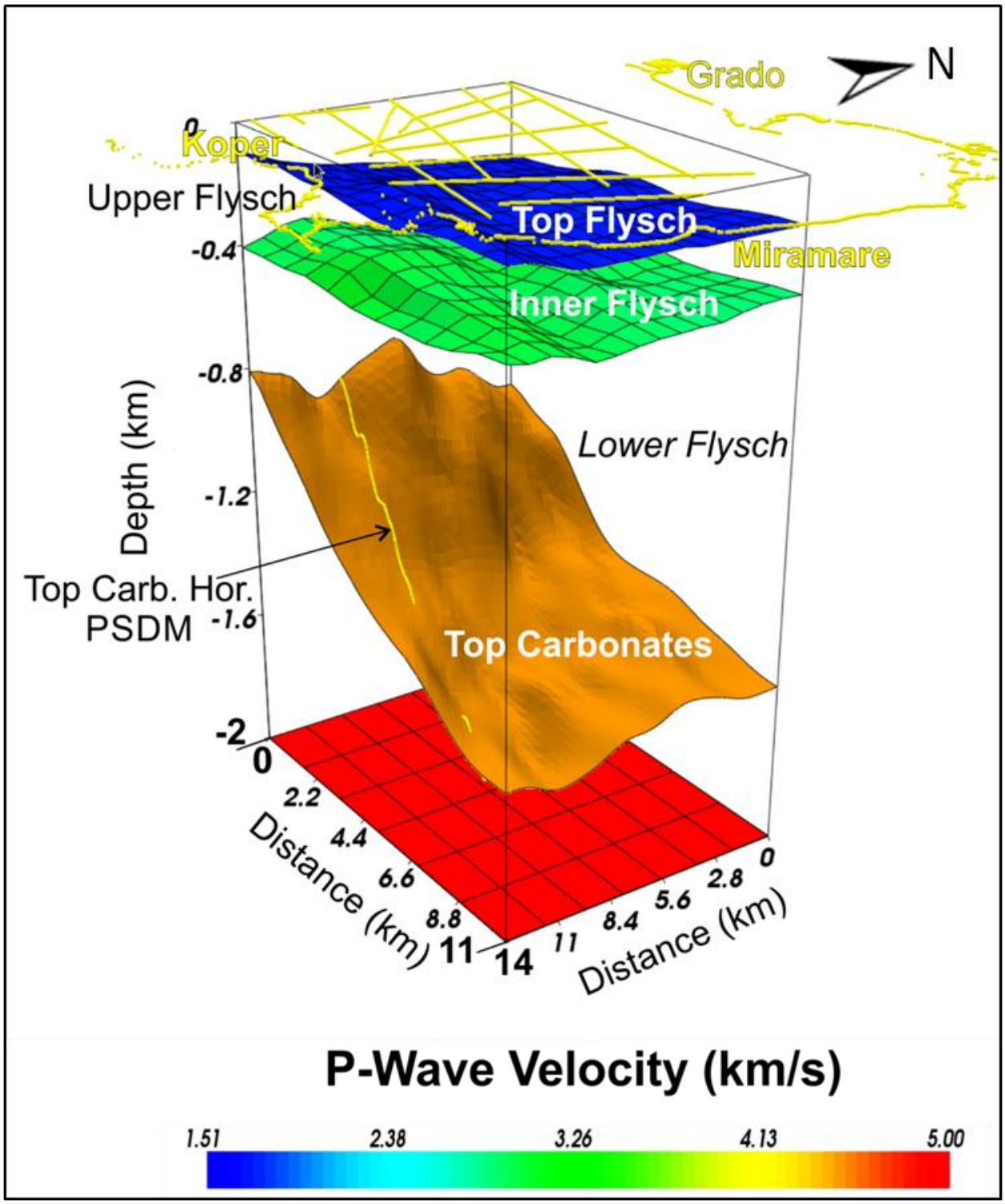

Fig. 93 - 3D velocity depth model B for the investigated volume in the Gulf of Trieste. From top to bottom are shown: the top flysch depth surface, with velocity for the sediments of the Quaternary layer; the inner surface of the flysch, with horizontally varying velocity for the upper flysch unit; the top carbonates surface, with velocity for the lower flysch unit. Model construction into depth, by using parameters derived from different methods, performed by the CAT3D (OGS, 2014) software. The yellow line, along the top carbonate surface, represents the picked top carbonate horizon along the pre-stack depth migrated line GT13-27.

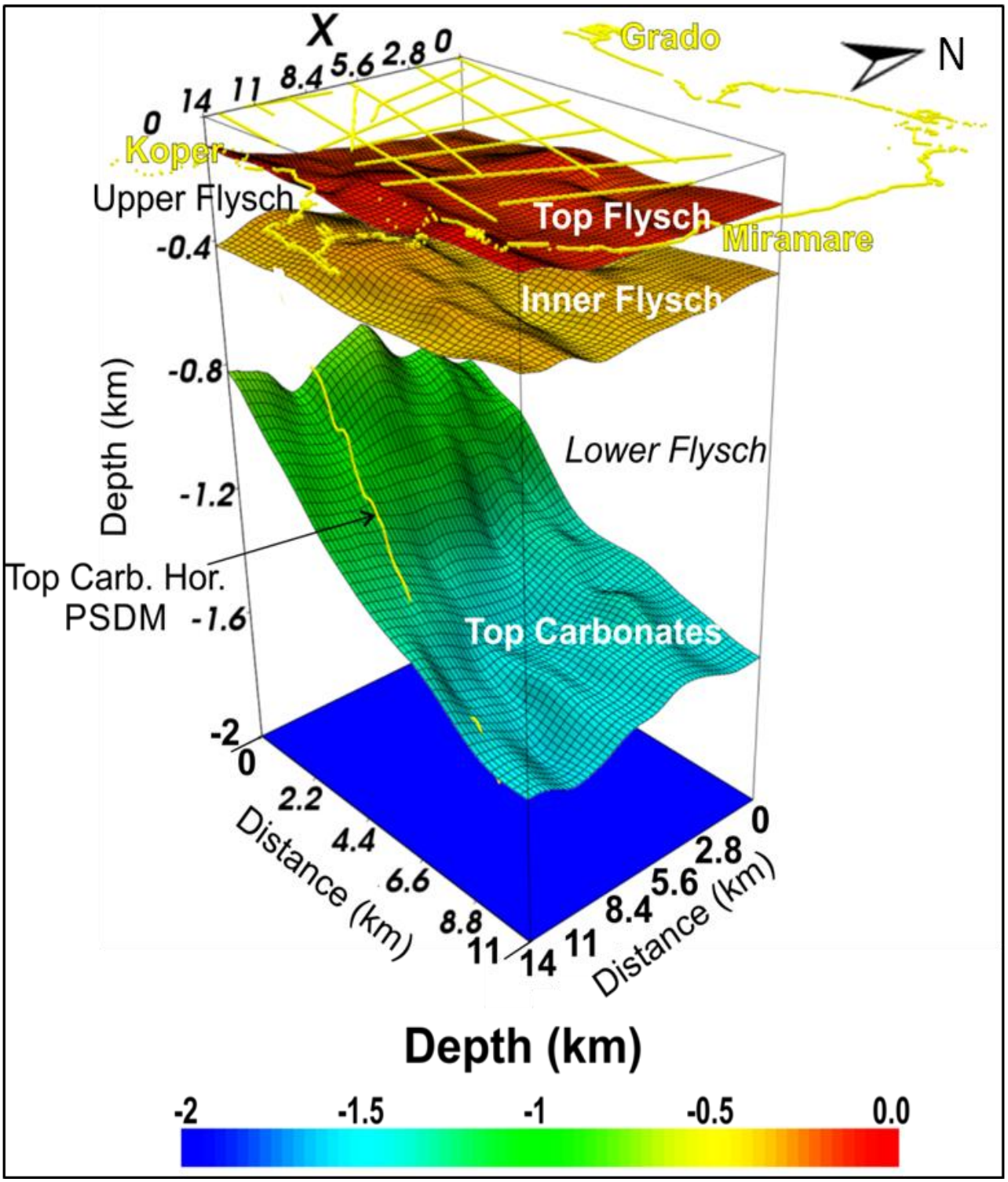

Fig. 94 - 3D depth model B for the investigated volume in the Gulf of Trieste. From top to bottom are shown: the top flysch, inner flysch and top carbonates 3D depth surfaces. Model construction, by using parameters derived from different methods, performed by the CAT3D (OGS, 2014) software. The yellow line along the top carbonate surface represents the picked top carbonate horizon along the pre-stack depth migrated line GT13-27.

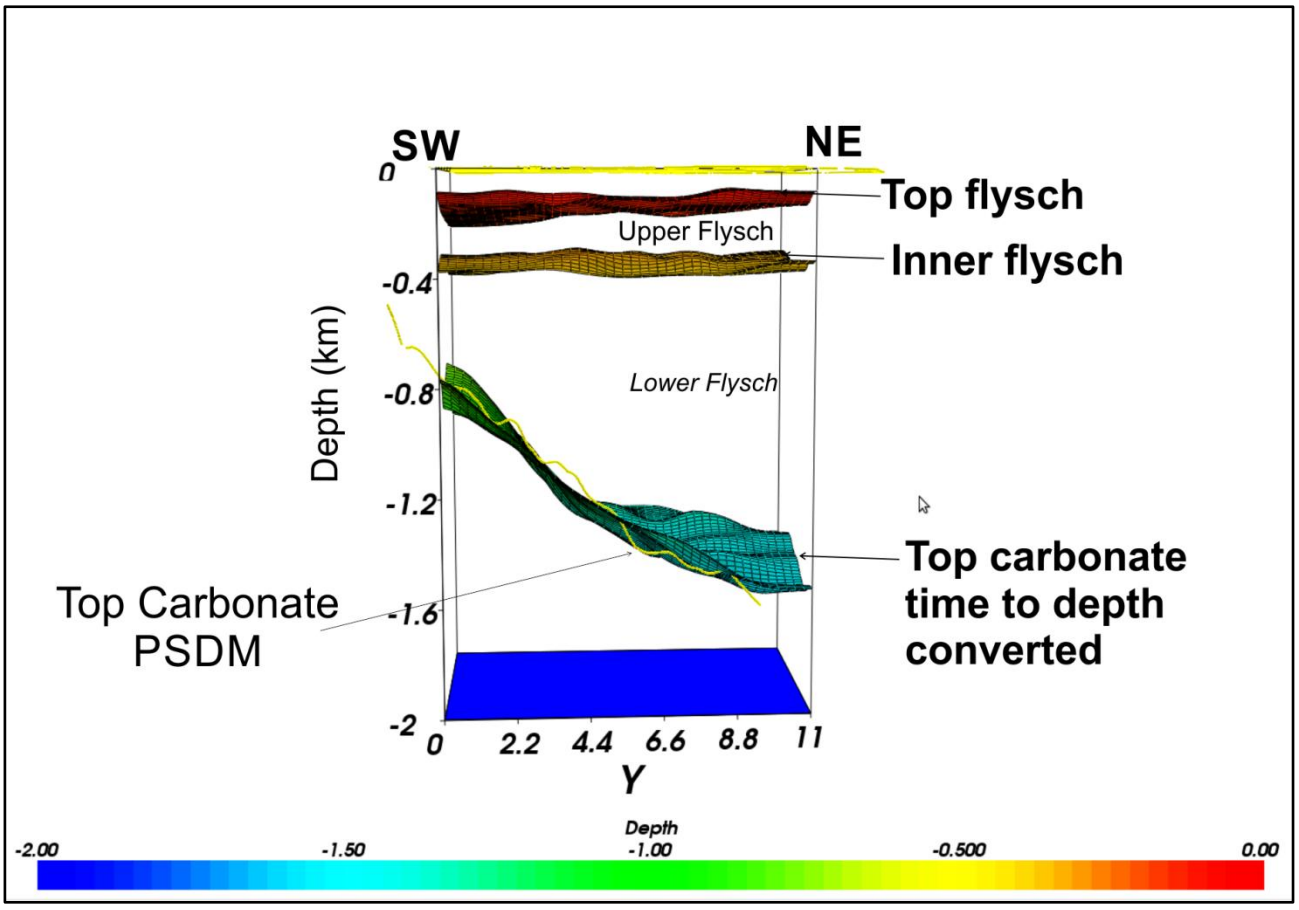

Fig. 95 – SW-NE section of the 3D depth model B, for the investigated volume in the Gulf of Trieste. From top to bottom are shown the profiles of the top flysch, inner flysch and top carbonates 3D depth surfaces. Moreover, the SW-NE profile (yellow line) of the top carbonate horizon, picked along the pre-stack depth migrated (PSDM) line GT13-27, is reported for comparison. The misfit between the two estimated surfaces is local and results a maximum of ±90 m and a local difference of ±75 m at the NE side of the PSDM profile.

In the following images (Fig. 96, Fig. 97, Fig. 98, Fig. 99, Fig. 100, Fig. 101, Fig. 102, Fig. 103, Fig. 104, Fig. 105, Fig. 106) are reported the 2D velocity depth tomographic models (panel a), obtained from the cut of the resulting 3D tomographic model B. These lines (GT09-10, 11, 13, 14, 15, 16, 17, 18, 23; GT13-27, 35) are the most significant among the dataset used for the inversion. The corresponding (time stack or migrated) multichannel seismic profile is represented (panel b). Note that the velocities within the Quaternary sediments layer and the upper flysch vary along each section (an so in the 3D model B): the correspondent velocity intervals are reported in the histogram (panel c). The position in map of the displayed lines is shown in panel (d).

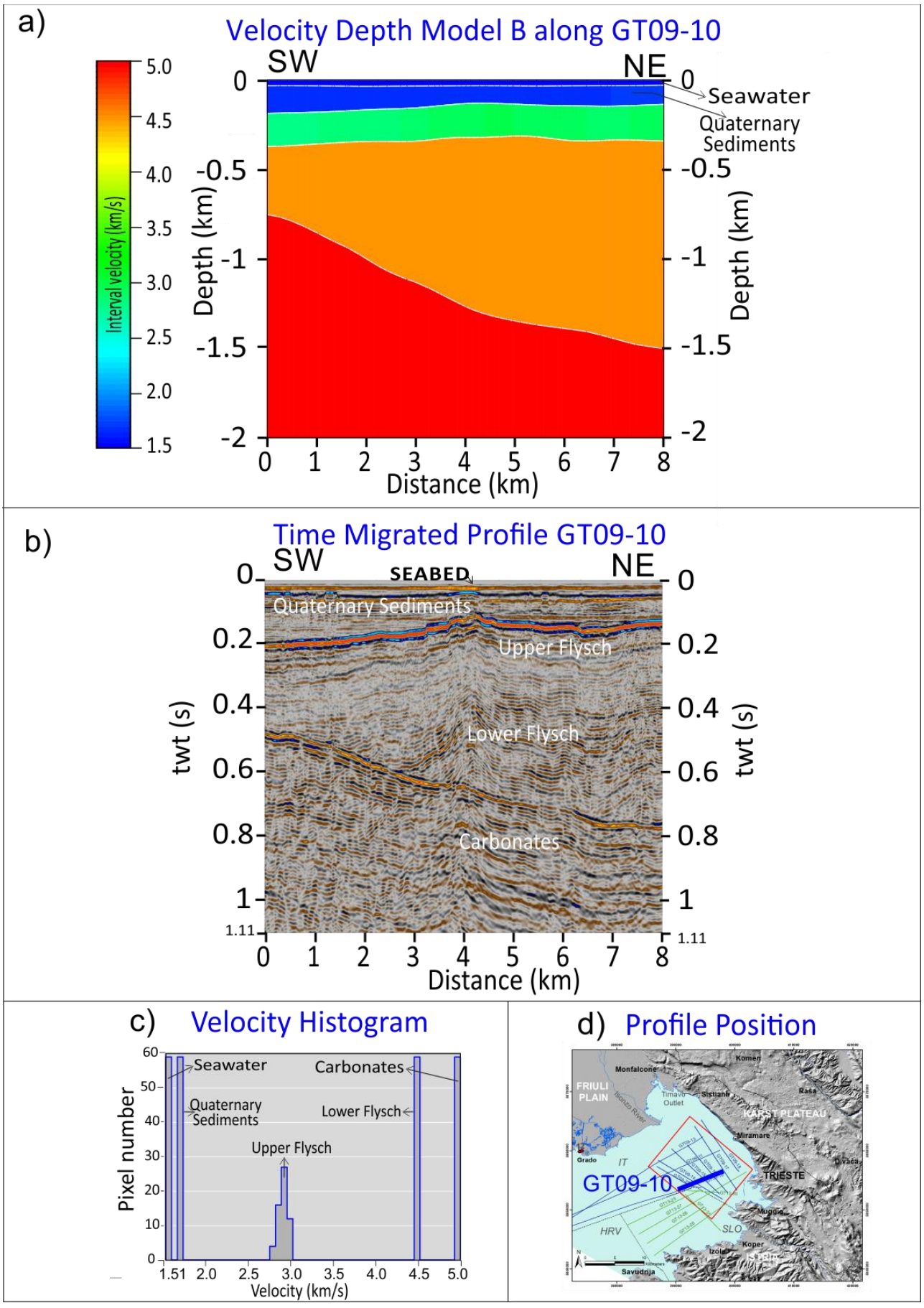
a)
Velocity Depth Model B along GT09-10
SW
NE
Interval velocity (km/s)
5.0
4.5
4.0
3.5
3.0
2.5
2.0
1.5
Depth (km)
0
-0.5
-1
-1.5
-2
Seawater
Quaternary Sediments
0 1 2 3 4 5 6 7 8
Distance (km)
b)
Time Migrated Profile GT09-10
SW
NE
SEABED
Quaternary Sediments
Upper Flysch
Lower Flysch
Carbonates
twt (s)
0
0.2
0.4
0.6
0.8
1
1.11
0 1 2 3 4 5 6 7 8
Distance (km)
c)
Velocity Histogram
Pixel number
60
50
40
30
20
10
0
Seawater
Carbonates
Quaternary Sediments
Lower Flysch
Upper Flysch
1.51 2.0 2.5 3.0 3.5 4.0 4.5 5.0
Velocity (km/s)
d)
Profile Position
FRIULI PLAIN
Monfalcone
Komen
Sistiana
Timavo Outlet
Isonzo River
Rasa
KARST PLATEAU
Miramare
Grado
IT
TRIESTE
Divača
GT09-10
Muggia
HRV
SLO
Koper
Izola
ISTRIA
Savudrija

Fig. 96

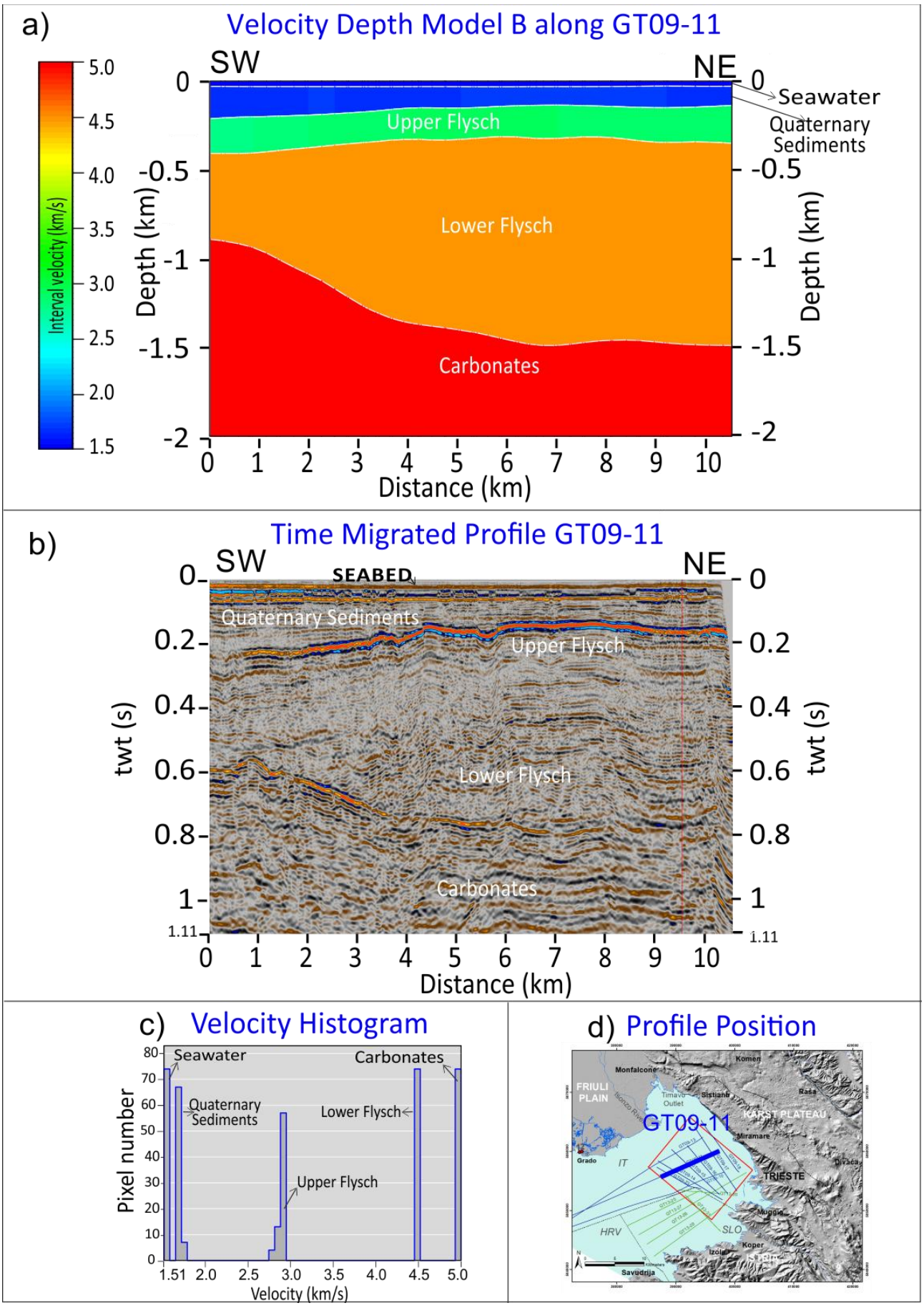
a)
Velocity Depth Model B along GT09-11
SW
NE
Interval velocity (km/s)
5.0
4.5
4.0
3.5
3.0
2.5
2.0
1.5
Upper Flysch
Lower Flysch
Carbonates
Seawater
Quaternary Sediments
Depth (km)
Distance (km)
b)
Time Migrated Profile GT09-11
SW
NE
SEABED
Quaternary Sediments
Upper Flysch
Lower Flysch
Carbonates
twt (s)
Distance (km)
c)
Velocity Histogram
Seawater
Carbonates
Quaternary Sediments
Lower Flysch
Upper Flysch
Pixel number
Velocity (km/s)
d)
Profile Position
GT09-11
FRIULI PLAIN
KARST PLATEAU
TRIESTE
Monfalcone
Grado
Sistiana
Miramare
Muggia
Koper
Izola
Savudrija
IT
SLO
HRV

Fig. 97

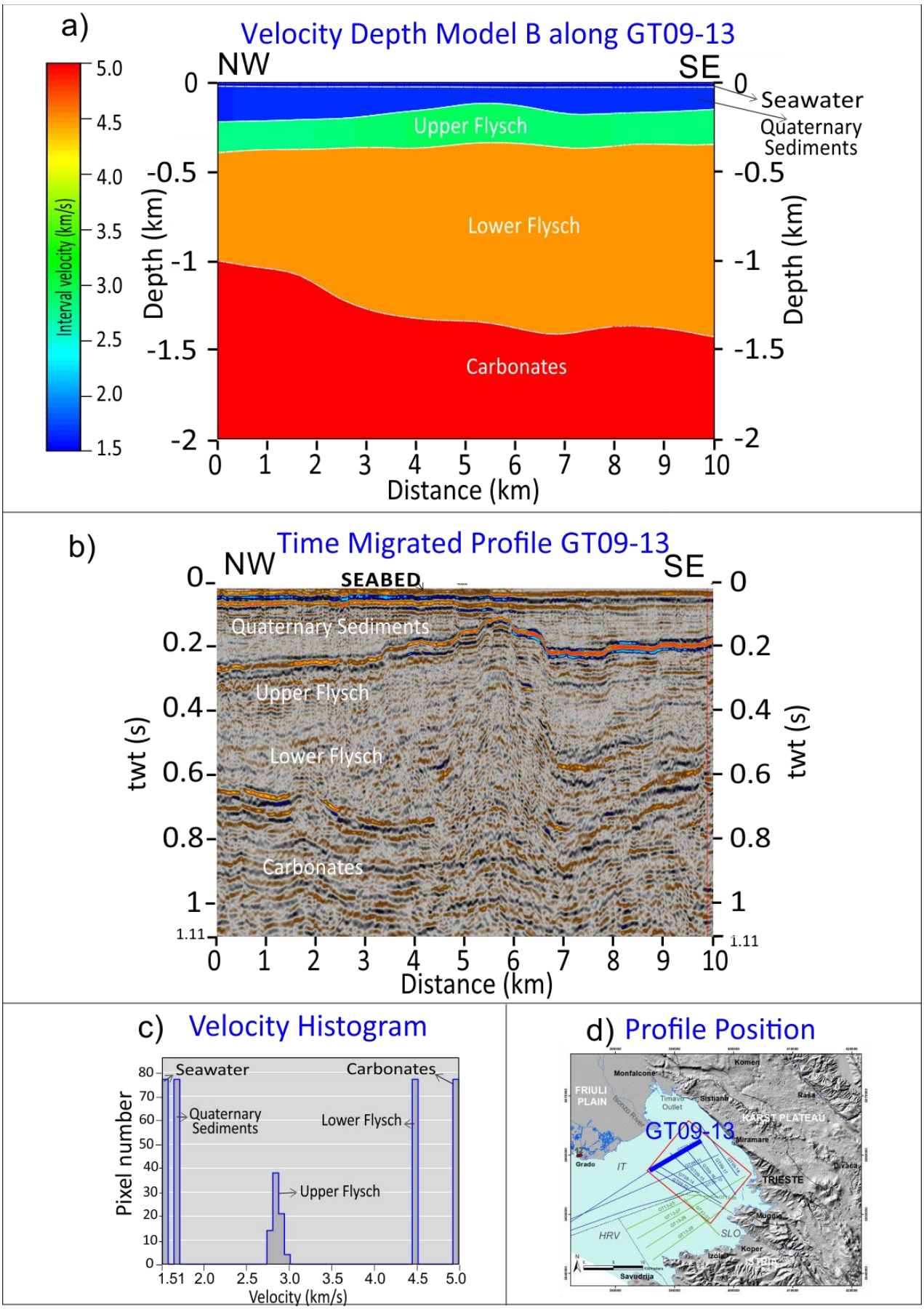
a)
Velocity Depth Model B along GT09-13
NW
SE
Seawater
Quaternary Sediments
Upper Flysch
Lower Flysch
Carbonates
Interval velocity (km/s)
Depth (km)
Distance (km)
b)
Time Migrated Profile GT09-13
SEABED
Quaternary Sediments
Upper Flysch
Lower Flysch
Carbonates
twt (s)
Distance (km)
c) Velocity Histogram
Seawater
Carbonates
Quaternary Sediments
Lower Flysch
Upper Flysch
Pixel number
Velocity (km/s)
d) Profile Position
GT09-13
FRIULI PLAIN
KARST PLATEAU
TRIESTE
Monfalcone
Grado
Miramare
Sistiana
Rasa
Divača
Muggia
Koper
Izola
Savudrija
HRV
SLO
IT

Fig. 98

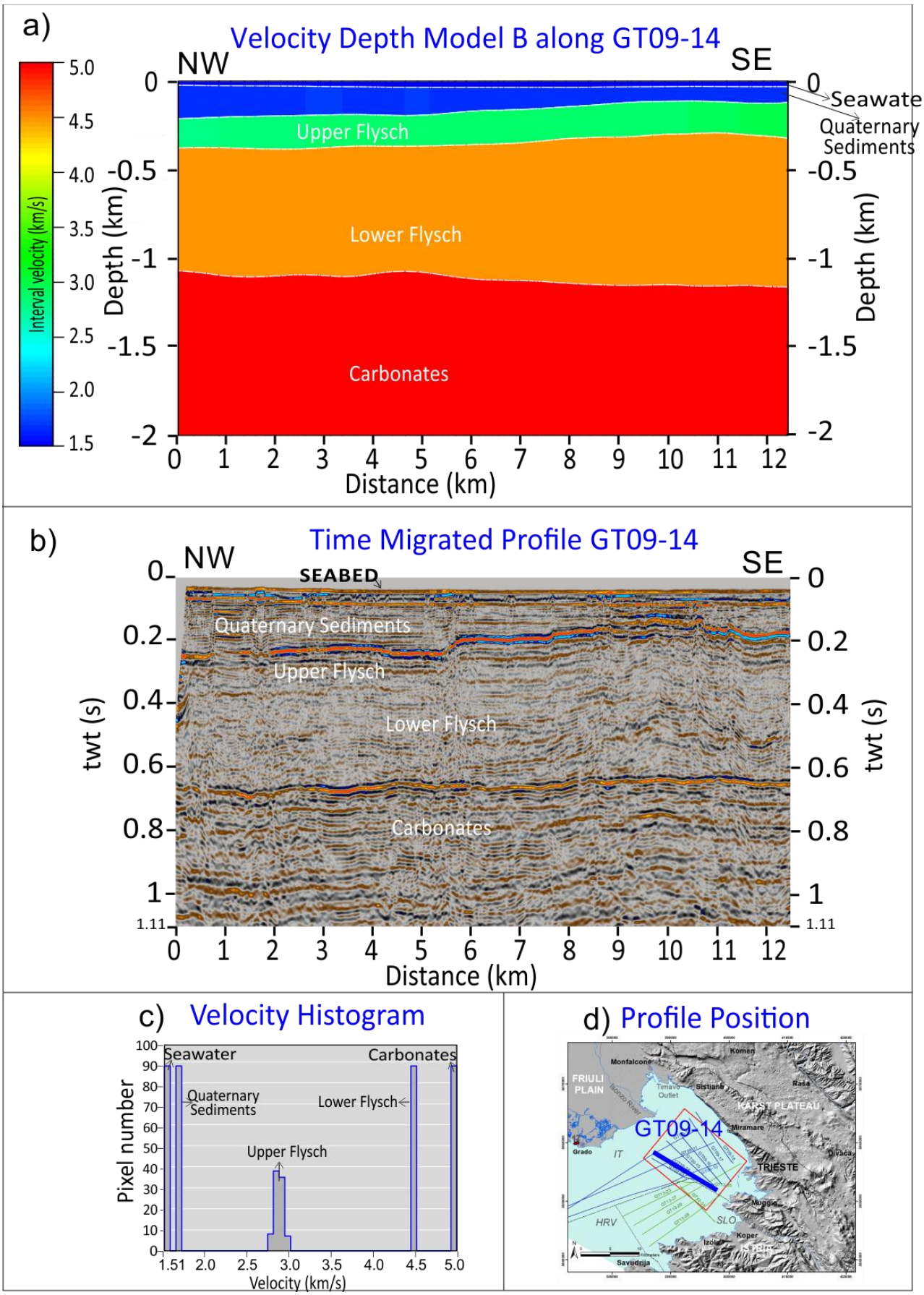
a)
Velocity Depth Model B along GT09-14
NW
SE
Interval velocity (km/s)
Seawater
Quaternary Sediments
Upper Flysch
Lower Flysch
Carbonates
Depth (km)
Distance (km)
b)
Time Migrated Profile GT09-14
SEABED
twt (s)
c)
Velocity Histogram
Pixel number
Velocity (km/s)
d)
Profile Position
GT09-14
FRIULI PLAIN
KARST PLATEAU
TRIESTE
Monfalcone
Grado
Miramare
Muggia
Koper
Izola
Savudrija
HRV
SLO
IT

Fig. 99

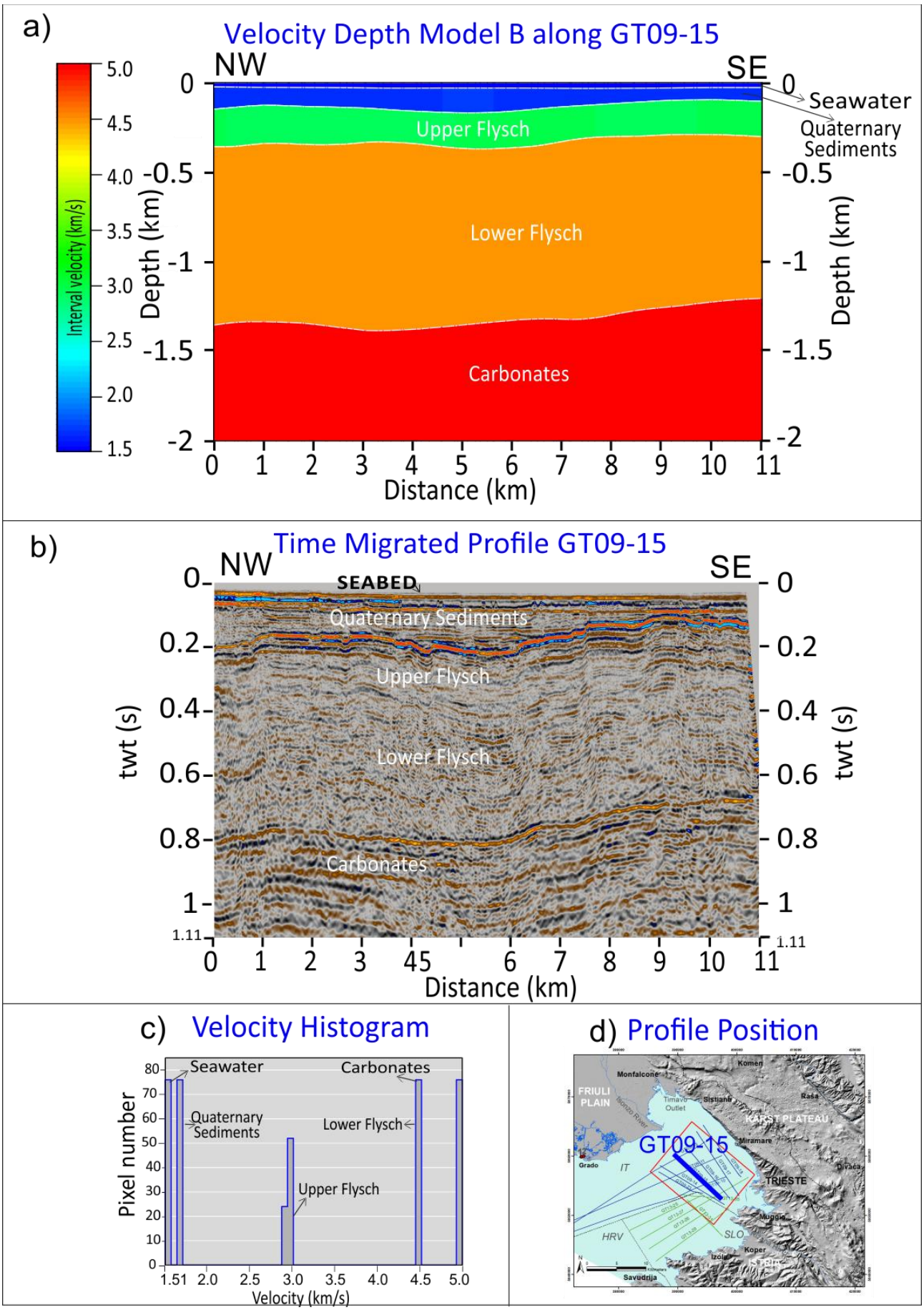
a)
Velocity Depth Model B along GT09-15
NW
SE
Seawater
Quaternary Sediments
Upper Flysch
Lower Flysch
Carbonates
Interval velocity (km/s)
Depth (km)
Distance (km)
b)
Time Migrated Profile GT09-15
SEABED
Quaternary Sediments
Upper Flysch
Lower Flysch
Carbonates
twt (s)
Distance (km)
c) Velocity Histogram
Seawater
Carbonates
Quaternary Sediments
Lower Flysch
Upper Flysch
Pixel number
Velocity (km/s)
d) Profile Position
GT09-15
FRIULI PLAIN
KARST PLATEAU
TRIESTE
Monfalcone
Grado
Sistiana
Miramare
Muggia
Koper
Izola
Savudrija
HRV
SLO
IT

Fig. 100

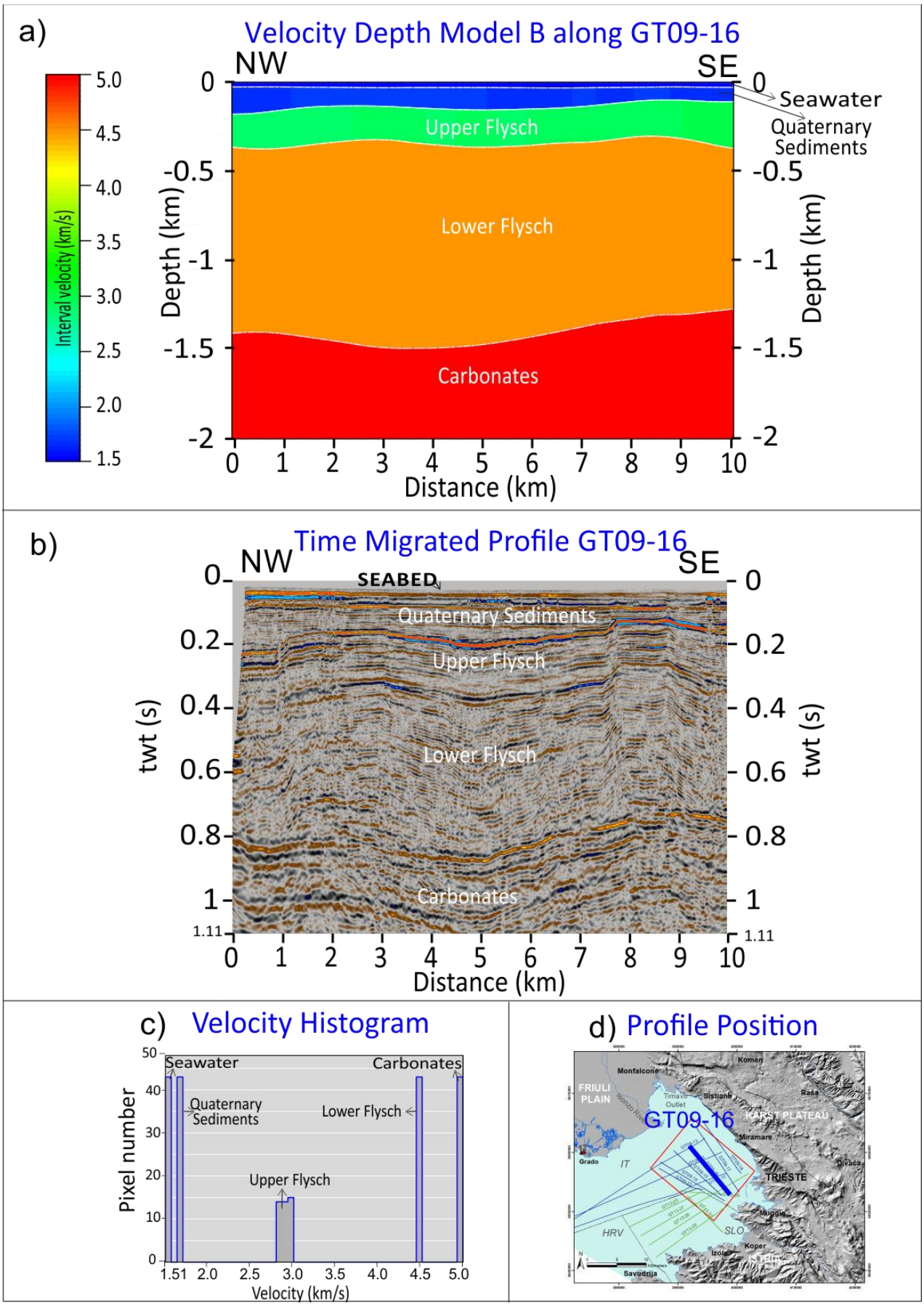
a)
Velocity Depth Model B along GT09-16
NW
SE
Interval velocity (km/s)
5.0
4.5
4.0
3.5
3.0
2.5
2.0
1.5
Seawater
Quaternary Sediments
Upper Flysch
Lower Flysch
Carbonates
Depth (km)
Distance (km)
b)
Time Migrated Profile GT09-16
NW
SE
SEABED
Quaternary Sediments
Upper Flysch
Lower Flysch
Carbonates
twt (s)
Distance (km)
c) Velocity Histogram
Seawater
Carbonates
Quaternary Sediments
Lower Flysch
Upper Flysch
Pixel number
Velocity (km/s)
d) Profile Position
GT09-16
FRIULI PLAIN
Monfalcone
Komen
Sistiana
Rasa
KARST PLATEAU
Miramare
Grado
IT
Divaca
TRIESTE
Muggia
HRV
SLO
Koper
Izola
Savudrija

Fig. 101

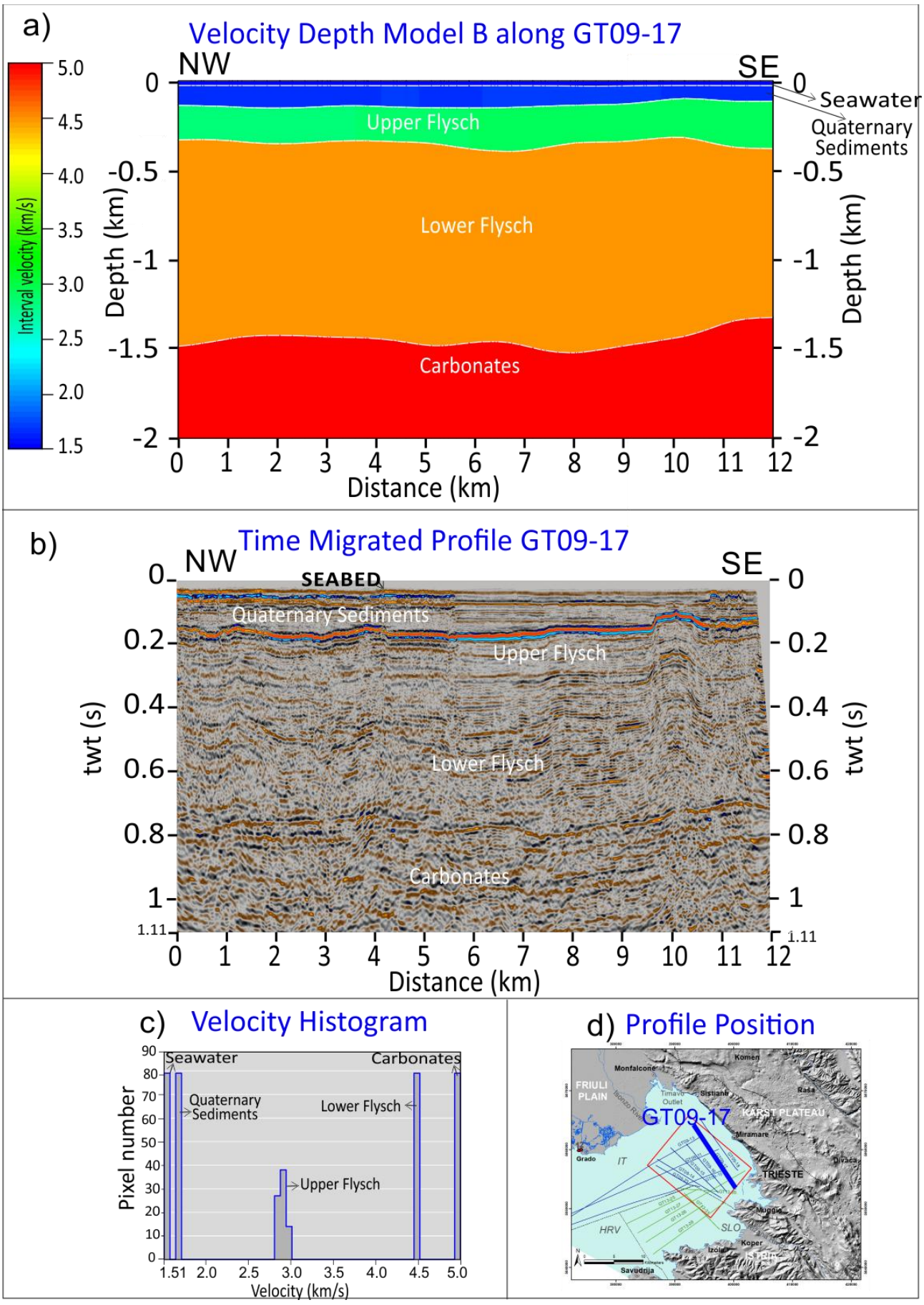
a)
Velocity Depth Model B along GT09-17
NW
SE
Interval velocity (km/s)
5.0
4.5
4.0
3.5
3.0
2.5
2.0
1.5
Seawater
Quaternary Sediments
Upper Flysch
Lower Flysch
Carbonates
Depth (km)
Distance (km)
b)
Time Migrated Profile GT09-17
NW
SE
SEABED
Quaternary Sediments
Upper Flysch
Lower Flysch
Carbonates
twt (s)
Distance (km)
c)
Velocity Histogram
Seawater
Carbonates
Quaternary Sediments
Lower Flysch
Upper Flysch
Pixel number
Velocity (km/s)
d)
Profile Position
GT09-17
FRIULI PLAIN
KARST PLATEAU
Monfalcone
Komen
Sistiana
Miramare
Grado
IT
TRIESTE
Divaca
Muggia
HRV
SLO
Koper
Izola
Savudrija

Fig. 102

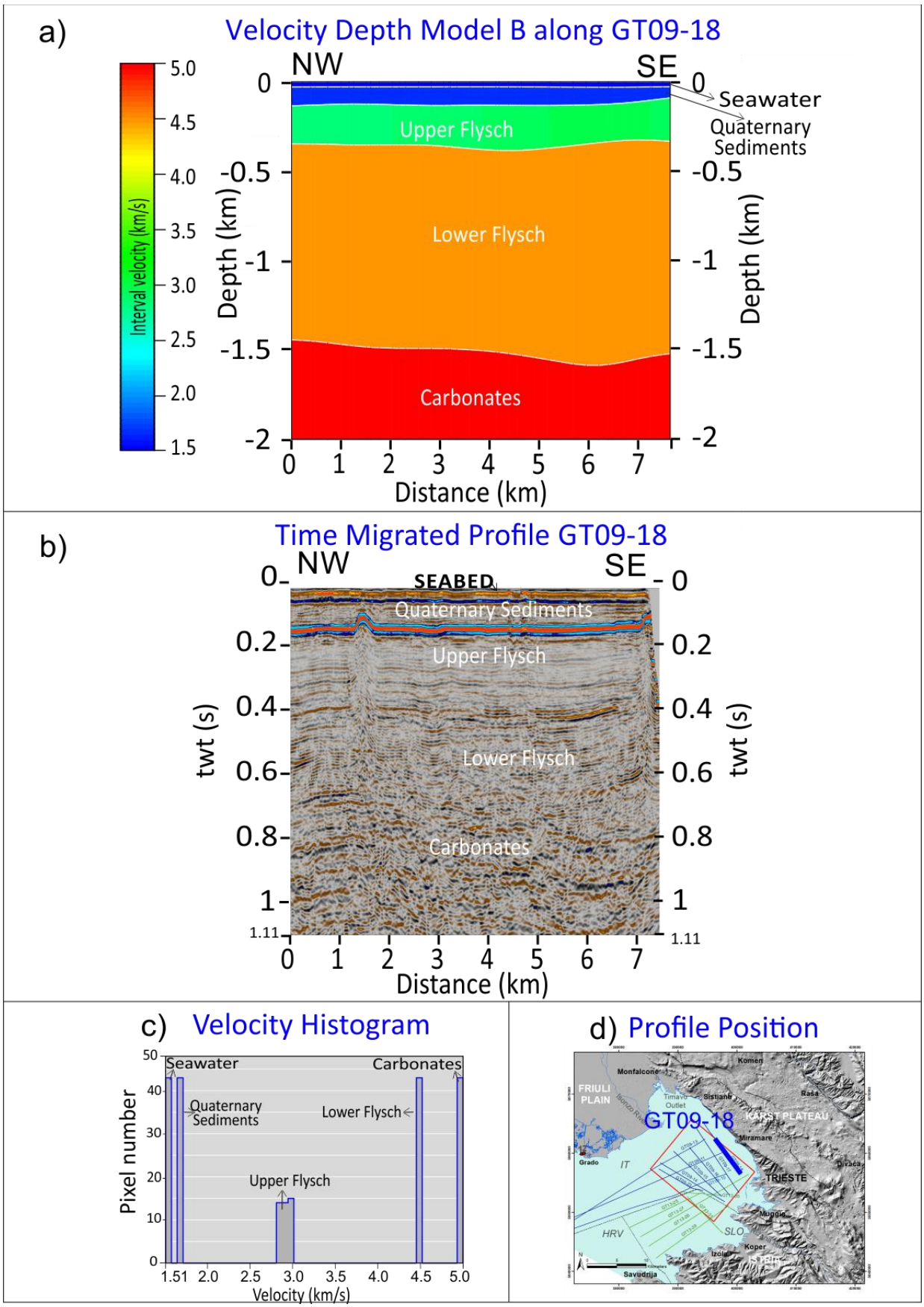
a)
Velocity Depth Model B along GT09-18
NW
SE
Seawater
Quaternary Sediments
Upper Flysch
Lower Flysch
Carbonates
Interval velocity (km/s)
Depth (km)
Distance (km)
b)
Time Migrated Profile GT09-18
SEABED
Quaternary Sediments
Upper Flysch
Lower Flysch
Carbonates
twt (s)
Distance (km)
c) Velocity Histogram
Seawater
Carbonates
Quaternary Sediments
Lower Flysch
Upper Flysch
Pixel number
Velocity (km/s)
d) Profile Position
GT09-18
FRIULI PLAIN
KARST PLATEAU
TRIESTE
Monfalcone
Grado
Sistiana
Miramare
Duino
Muggia
Koper
Izola
Savudrija
IT
HRV
SLO

Fig. 103

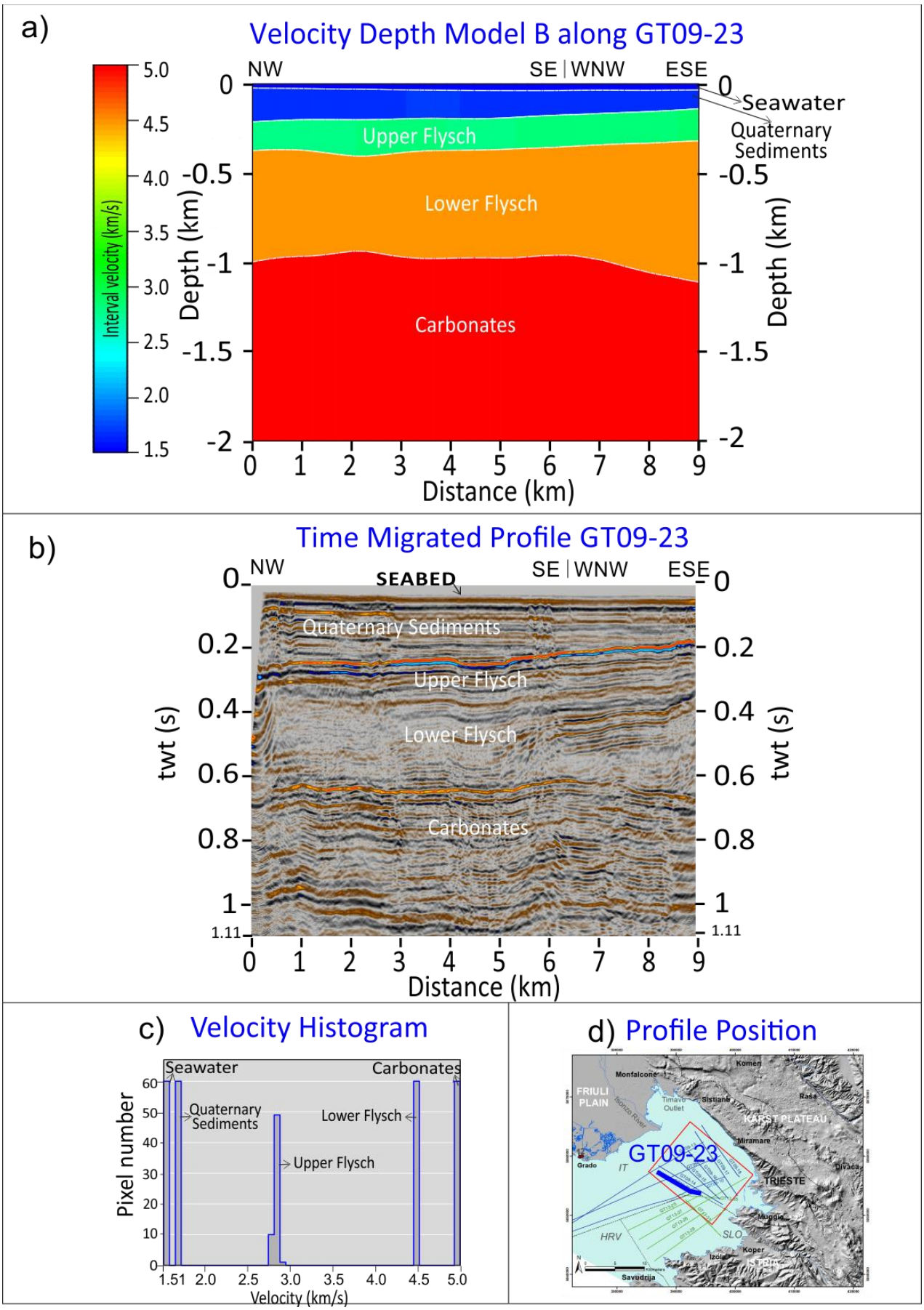
a)
Velocity Depth Model B along GT09-23
NW
SE | WNW
ESE
Seawater
Quaternary Sediments
Upper Flysch
Lower Flysch
Carbonates
Interval velocity (km/s)
Depth (km)
Distance (km)
b)
Time Migrated Profile GT09-23
SEABED
Quaternary Sediments
Upper Flysch
Lower Flysch
Carbonates
twt (s)
Distance (km)
c) Velocity Histogram
Seawater
Carbonates
Quaternary Sediments
Upper Flysch
Lower Flysch
Pixel number
Velocity (km/s)
d) Profile Position
GT09-23
FRIULI PLAIN
KARST PLATEAU
TRIESTE
Monfalcone
Grado
Sistiana
Miramare
Muggia
Koper
Izola
Savudrija
IT
HRV
SLO

Fig. 104

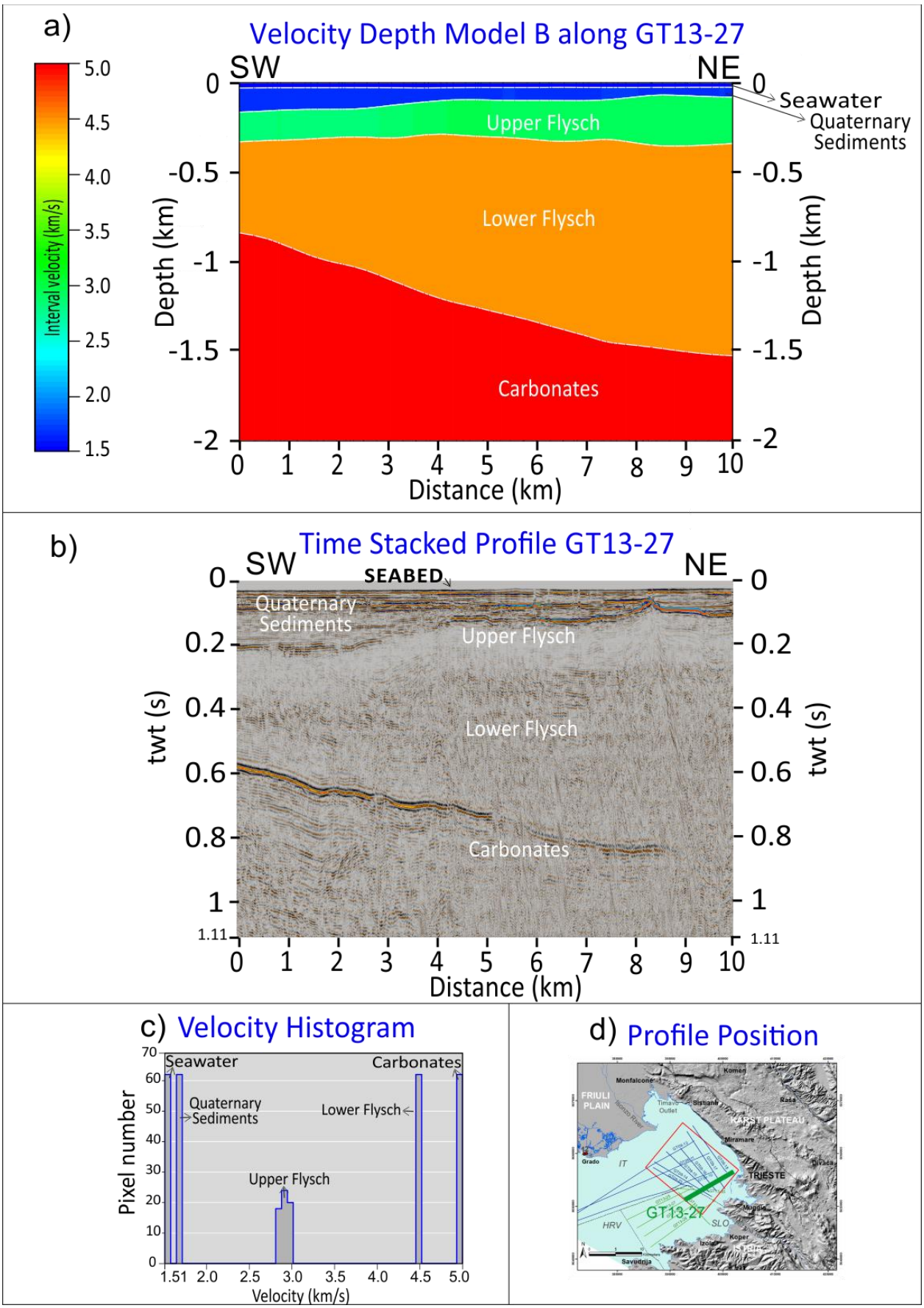
a)
Velocity Depth Model B along GT13-27
SW
NE
Interval velocity (km/s)
5.0
4.5
4.0
3.5
3.0
2.5
2.0
1.5
Seawater
Quaternary Sediments
Upper Flysch
Lower Flysch
Carbonates
Depth (km)
Distance (km)
b)
Time Stacked Profile GT13-27
SEABED
Quaternary Sediments
Upper Flysch
Lower Flysch
Carbonates
twt (s)
Distance (km)
c) Velocity Histogram
Seawater
Carbonates
Quaternary Sediments
Lower Flysch
Upper Flysch
Pixel number
Velocity (km/s)
d) Profile Position
FRIULI PLAIN
KARST PLATEAU
TRIESTE
GT13-27
IT
SLO
HRV

Fig. 105

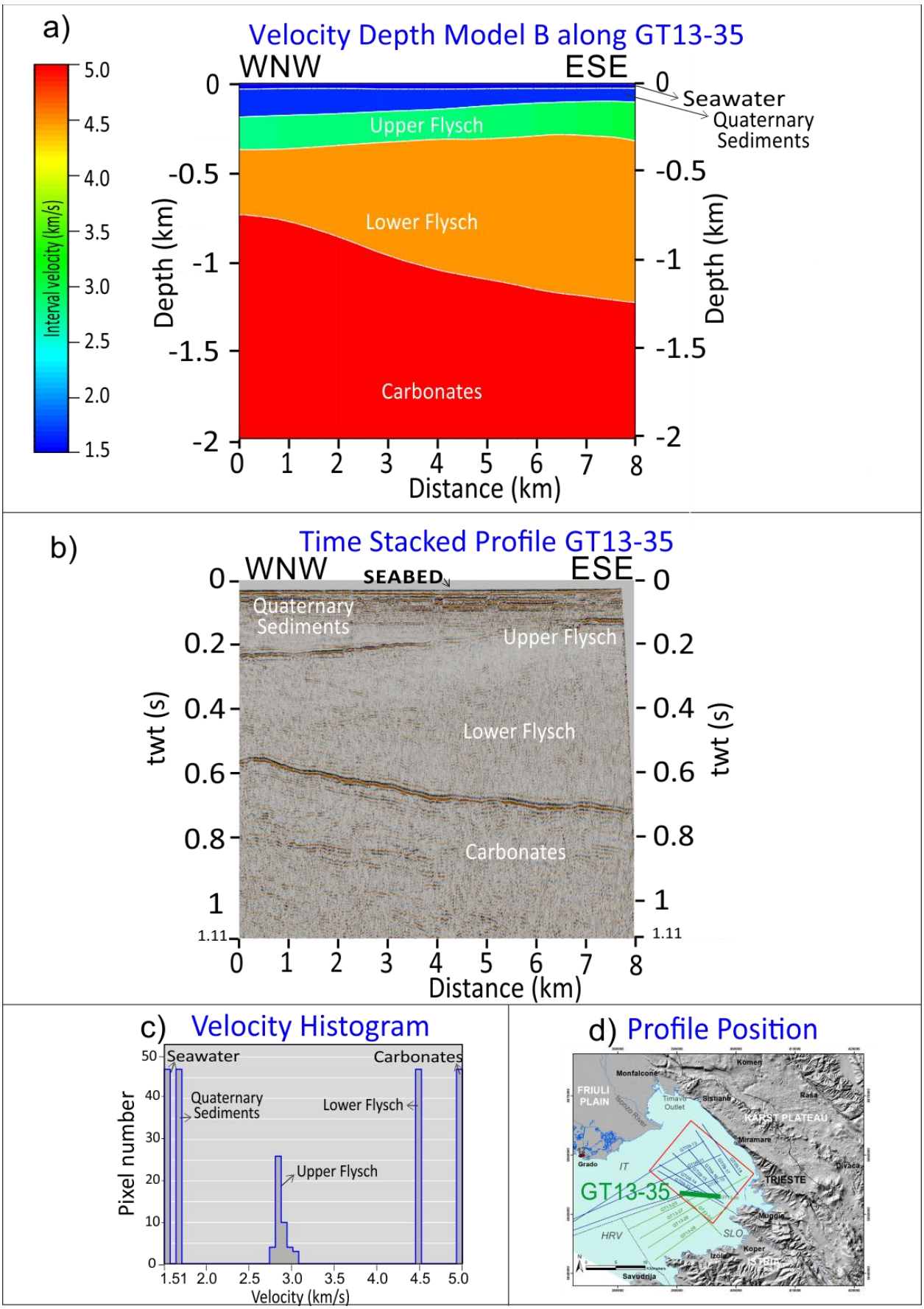
a)
Velocity Depth Model B along GT13-35
WNW
ESE
Interval velocity (km/s)
5.0
4.5
4.0
3.5
3.0
2.5
2.0
1.5
Seawater
Quaternary Sediments
Upper Flysch
Lower Flysch
Carbonates
Depth (km)
Distance (km)
b)
Time Stacked Profile GT13-35
WNW
ESE
SEABED
Quaternary Sediments
Upper Flysch
Lower Flysch
Carbonates
twt (s)
Distance (km)
c) Velocity Histogram
Seawater
Carbonates
Quaternary Sediments
Lower Flysch
Upper Flysch
Pixel number
Velocity (km/s)
d) Profile Position
FRIULI PLAIN
KARST PLATEAU
Monfalcone
Sistiana
Miramare
Grado
IT
TRIESTE
GT13-35
HRV
SLO
Koper
Izola
Savudrija

Fig. 106

6 DISCUSSION

Four main surfaces and three sedimentary units, characterising the sedimentary sequence buried under the Gulf of Trieste, have been reconstructed in depth domain. Therefore, their spatial variability and geometrical relationship can be assessed. Moreover, comparison on the different applied geophysical methodologies, that allowed the detection of these features, can be done.
The analysis was conducted on several available multichannel seismic reflection lines (from the 2009 and 2013 geophysical surveys), located over an area of 154 km^2 in the eastern part of the gulf (Fig. 76).
Starting from the interpretation of the reflected events on the seismic data organised by common shot gathers (Fig. 77, Fig. 78), a reliable 3D velocity depth model (A) is reconstructed for the sea bed and the top of the flysch surfaces (Fig. 80, Fig. 81), by means of traveltime tomography (CAT3D (OGS, 2014)).
Since the top of the carbonate could not be picked continuously along the analysed seismic lines of the 2009 survey, a 2D tomographic inversion for the only GT13-27 line (SE-NW oriented) was performed using the traveltime tomographic procedure (Fig. 82). This worked well on the reconstruction of the shallower layers and interfaces, while, at depths higher than 800 m it loses reliability. This is due to the fact that the raw data could not show seismic response at offsets larger than about 100 m. In addition, on pre-stack data, seismic energy is highly dispersed as depth increases (Yilmaz, 2001). Processing of the raw data improves the visibility of the signal on the pre-stack data, but actually it is not sufficient to gain reliability at depths larger than 800 m.
Another geophysical technique was then used, to try to recover this missing information on GT13-27 profile. The iterative procedure that went through residual analysis on depth migrated gathers (DMG), by using as input the previously obtained tomographic velocity field, allowed to refine it and to resolve the deeper part of the top carbonates. The updated velocities are then used to migrate the data and produce a refined depth migrated imaging, providing reliable geometries and depths up to 1600 m bsl (Fig. 83).
Since other type of information could be recovered from data in time domain, a 3D time model was built (Fig. 89). It bears the two way time (twt) surfaces picked on post-stack time migrated lines (Fig. 90b, Fig. 91b), such as the highly reflective horizons of the seabed, the top flysch, the top carbonates and that of the inner flysch. This latter bounds the base of the upper flysch unit, that in turns lies under the top flysch.
Further information come from the refracted event related to the top of the flysch; it could be detected on pre-stack raw data, that almost homogeneously display it (e.g., Fig. 77a,b and Fig. 78c). It was then possible to define, for the upper flysch unit, its characteristic refracted seismic velocities. These turned out to be much higher than that of the P-waves propagating vertically in the upper flysch (e.g., Fig. 90a and Fig. 91aFig. 92). Therefore, in order to explain this behaviour in terms of its fine layering (sandstone and marls, according to the literature description of this unit analysed on the Karst; e.g. GeoCGT-FVG, 2013), it was applied the averaging theory by Backus (1962). Vertical P-wave velocity values were defined also for the upper part of the flysch.
Finally, a 3D velocity depth model (B) was constructed (Fig. 93, Fig. 94, Fig. 95), by gathering all the information obtained up to this point. These are the tomographic depth horizons of the seabed and top flysch, along with the twt time surfaces of the inner flysch and top carbonates picked on time migrated profiles. The inner flysch surface was converted into depth by using the vertical P-wave velocities obtained from refracted P-waves and the Thomsen's anisotropic parameters. The conversion of the top carbonates was performed by using the velocities of the upper units,

considering also the average interval velocity computed from the model of the flysch along the 2D pre-stack depth migrated (PSDM) line GT13-27.
The resulting depth of the top carbonates in model B fits, with a good degree of approximation, the depth of the same horizon picked on the PSDM (maximum misfit: ± 90 m). Local discrepancies are anyhow due to the fact that the interval velocity function, detected by the PSDM within the flysch unit, is vertically and horizontally detailed with higher accuracy through DMG residual analysis, while in the 3D model the lower flysch unit has constant velocity. An example related to this difference can be seen near to the Trieste coast: here the top carbonates surface reaches a depth 1525 m bsl on the 3D surface of model B, while it is about 75 m deeper according to the PSDM result.
Considering the resulting 2D and 3D depth models, the seabed shows on average an almost flat surface lying between 22 and 25 m bsl, slightly deepening in the central part of the investigated area. This configuration corresponds to that reconstructed by the works that, through time, studied the morphology of the seafloor in the Gulf of Trieste (e.g. (Brambati & Catani, 1988) (Gordini, et al., 2004)(Trobec, et al., submitted)).
The resulting top flysch depth surface, deepens from 70 m to 220 m bsl towards the NW (e.g. Fig. 80, Fig. 81, Fig. 93, Fig. 94, Fig. 107), within the eastern side of the Gulf of Trieste.
Moreover, the offshore surface is depicted by local irregularities, some hundreds of meters wide, that locally rise up to few tens of meters from the seabed. They bound a 2.5-3 km wide area, longitudinally extending from NE to SW, that is some tens of meters depressed. These probably result from of the Messinian-Pliocene erosional phase, whose active drainage system depicted the top flysch in valleys and ridges (Fantoni, et al., 2002) (Busetti, et al., 2010a)(Busetti, et al., 2010b). These patterns were then empathised by the Pleistocene-Holocene transgressive-regressive cycles that affected the gulf and led to the formation of marine terraces (Romeo, 2009) (Zampa, 2014).
Moreover, details on PSDM GT13-27 (Fig. 83, Fig. 84, Fig. 85) show that these terraces are emphasised by tectonically driven vertical offsets up to 25-30 m. The figures show toplap stratification characterising the upper flysch unit just beneath the top flysch surface. Low trends in the vertical velocity functions, indicate tectonic disturbance and presence of fluids. These latter probably migrate from the most permeable (e.g. sandstones) upper flysch sub-vertical layers, through the thin Quaternary sediment package, up to the sea bed. Fluid accumulation just beneath the sea-floor, was also detected on others MCS and high resolution acoustic profiles of the available dataset. These elements can be considered as indicators of neotectonic activity, related to the ongoing N-ward moving of the Adria plate and consequent Alpine convergence (Busetti, et al., 2013).
The thickness values of the marine and continental Quaternary sediments reach a minimum in the eastern part while they increase towards W-NW, in accordance with (Busetti, et al., 2010a)(Busetti, et al., 2010b). Thickness values range from a minimum of 50 m in the south-eastern most part of the analysed area, and a maximum of 190 m in the opposite side (Fig. 80, Fig. 81).
The flysch unit shows its maximum thickness of 1500 m in the eastern side of the modelled area (Fig. 89, Fig. 93, Fig. 94), while it thins towards W where it is about 600 m thick. Further W, it pinches out on the top carbonate surface (Fig. 83, Fig. 84, Fig. 85). In its upper part, it is characterised by internal layering that bend upwards from sub-horizontal to sub-vertical dip. This configuration can be interpreted as the effect of compressive deformation SW-wards vergent. Moreover, the upper flysch unit results to be about 250 m thick. Its base is represented by the inner flysch surface that mimics the top flysch surface, but with less prominent irregularities (Fig.

93). This may reflect tectonic phases with different deformation intensities, during the deposition of the unit.
As concerns the top carbonates, this deepens towards NE. At about 2 km from the Trieste shoreline, it reaches a maximum depth of 1600 ± 30 m below sea level (bsl), according to the PSDM result (e.g. Fig. 88). The horizon depth increases gradually, and if extrapolated using the average inclination of 5°, it reaches about 1740 m bsl in correspondence of the Trieste shoreline.
Previous studies (e.g. Finetti, 1967; Busetti et al., 2010b) analysed the top carbonates surface on multichannel seismic refraction and reflection data, by means of conventional velocity detection. These provided a maximum surface depth, in the same area of the eastern gulf, of about 1200-1400 m bsl.
The new outcomes, herein described, were obtained through advanced seismic tomographic and imaging procedures, that permitted the definition of an higher detailed velocity field. The higher is the resolution of the velocity field, the higher will be, therefore, the reliability of the depth recontruction of the geological features. For this reason, the results of the present work can be considered a further refinement of the former estimations.
Outside the modelled area, towards W, the carbonates are bended in an anticline (Fig. 83). This, on PSDM GT13-27 profile, is about 6.5 km wide on the SW-NE direction. As suggested by (Busetti, et al., 2013), this represents the north-western continuation of the outcropping Izola anticline (Fig. 107 and Fig. 108). This latter was mapped at the Izola Peninsula (Slovenian Istria). Here Paleogene carbonates (Poljak, et al., 2010) outcrop in correspondence of the Simon Thrust system tectonic window (Placer, et al., 2010).

In particular, the Fig. 107 and Fig. 108 show a synthesis of the offshore depth and geometries of the top flysch and carbonates surfaces (from the 3D velocity depth models A and B), with the neighbouring onshore geology of Istria, Karst Plateau and Friuli Plain (compiled from (Placer, et al., 2010) (GeoCGT-FVG, 2013) (Jurkovšek, et al., 2016)).
The flysch unit outcrops in Istria, with elevations above sea level ranging between 0 m (along the coast) to 500 m above sea level (asl) in the hinterland areas. It is affected by the Istrian thrust front of the External Dinarides with NW-SE orientation (the main are from E to W: Petrinje, Črni Kal, Hravstrovlje, Sočerga, Buzet Thrust). Whereas, in the near offshore few kilometres from the coast, the top flysch depth surface lies at some tens of meters bsl (from 70 to 110 m) along the south-eastern border of the modelled area. It has a general deepening trend towards the north-western edge of the area, where it reaches maximum values of 200-220 m bsl. Similarly, the surface deepens from 90 m to 140 m bsl along the north-eastern border of the area, parallel to the rocky coast connecting Trieste to Sistiana.
Moreover, in Fig. 109 it is represented the offshore surface extending over a wider area respect to that of the 3D velocity depth model B. It derives from the conversion from time to dept of the horizon interpreted on the available OGS geophysical dataset (positions in Fig. 73, Fig. 74, Fig. 75): GT2009 and 2013 multichannel seismic reflection data (in the central and eastern part of the gulf); Barcola 2003, Miramare 2012, Muggia 2013 single and multichannel boomer and core data (Muggia 1960s). The resulting depth values are in agreement with those obtained from the tomographic inversion (e.g. Fig. 107), proving that the reconstructed velocity is estimated with high accurancy. The surface shows also irregular morphologies, expecially evident in the proximity of the eastern coast. These correspond to those systems of escarpements and terraces (e.g. Romeo, 2009) related not only to neotectonics but also to the recent sea level changes in the Gulf of Trieste. Towards the central part of the gulf, the grid highlights the fact that the flysch unit

pinches out on the top of the peripheral bulge of the carbonate platform. Furthermore, the prosecution of the Izola anticline, into the gulf, is evidenced in this reconstruction.

The Meso-Cenozoic units of the Friuli-Dinaric Carbonate Platform are structured in a Dinaric anticline (NW-SE axis) and outcrop on the Karst Plateau. This elevates up to about 600 m asl (with a general lowering trend NW-wards) and it represents the hangingwall of the Karst Thrust system, NW-SE oriented and SW vergent. This latter is mainly expressed by the Karst Thrust, that extends along the rocky coast and continues south-east-wards as the Črni Kal (in Istria) and north-west-wards as the Panzano line (in the northern gulf and southern Friuli Plain). Moreover, at sea, the Sistiana left transtensive Fault offsets the tectonic lineament few kilometres west-wards. The Karst Thrust brings the carbonate units above the younger Eocene Flysch. Its footwall is settled in the eastern gulf. The top of the carbonates is settled at depths of about 740-900 m bsl in the western part of the modelled area, while it deepens towards NE up to about 1500-1590 m. Moreover, the top carbonates surface, buried in the gulf, exhibits smooth ridges and valleys SW-NE elongated and few meters wide.
Considering also the GT13-27 depth imaging result, a local maximum depth of about 1600 m bsl is reached by the surface at about 1.7 km from the Trieste coast. Along the shoreline and in the correspondent hinterland, the units of the Meso-Cenozoic Carbonate Platform are settled in folds almost vertical dipping layers. These crop-out, along the eroded topographic surface, between about 0 and 600 m asl. On the basis of these evidences, it can be estimated that the vertical displacement given by the Karst Thrust ranges values of around, minimum, 1600-1800 m. The geological profile of Fig. 110 confirms this estimation. It was reconstructed along the alignement of the SW-NE prestack depth migrated profile GT13-27 and its imaginary linear prosecution across the entire Karst Plateau (up to the Vipava Fault). The onshore section is based on the geological maps provided by (GeoCGT-FVG, 2013) (Jurkovšek, et al., 2016).
The thickness of the Meso-Cenozoic Friuli-Dinaric Carbonate Platform, in the offshore, can be inferred by looking at the DMG analysed during the imaging procedure (Fig. 86). A 4.8 km deep event probably represents the base of the Dolomia Principale. Therefore, it can be estimated that the thickness of these carbonates is around 3200-3400 m, in the north-eastern side of the GT13-27 line. This demonstrates the good compromise between resolution and penetration provided by the analysed MCS reflection lines. They allow the imaging of the main features related to the Meso-Cenozoic geological evolution of the Gulf of Trieste.

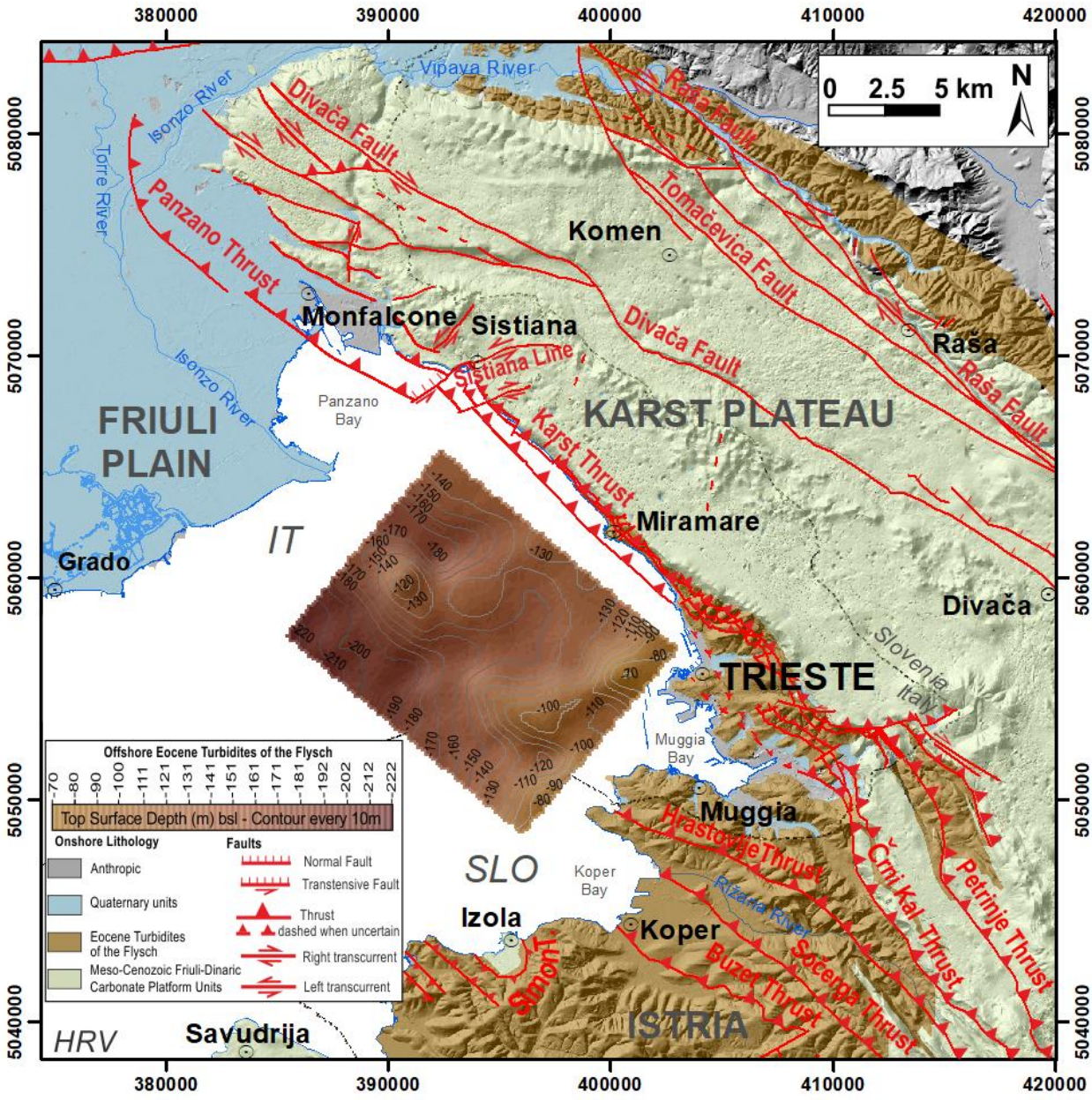

Fig. 107 – Map of the top flysch surface, obtained from the 3D depth models A and B (Fig. 80, Fig. 81, Fig. 93, Fig. 94), within the eastern side of the Gulf of Trieste. Its offshore depth is represented by the graded brown colour scale (contours every 10 m). The neighbouring onshore geology (lithologies and main tectonic lineaments) is also represented. This latter was compiled from (Placer, et al., 2010) as concerns Istria; from (GeoCGT-FVG, 2013) as concerns the Italian Karst and the Friuli Plain; from (Jurkovšek, et al., 2016) as concerns the Slovenian Karst. The Meso-Cenozoic units of the Friuli-Dinaric Carbonate Platform and the Eocene turbidites of the Flysch are represented onland by uniform colours (light green and medium brown, respectively). They are superimposed on the Digital Elevation Models by (IRDAT-FVG, 2017) for the Italian area (10 m cell resolution) and by (EU-DEM, 2017) for the Slovenian and Croatian areas (20 m cell resolution). The map represents the synthesis between the offshore geometry and depth of top flysch surface, with the neighbouring geology. The flysch unit outcrops in the south-eastern onshore between about 0 and 500 m above sea level and is involved by the NW-SE oriented Dinaric Thrusts bounding the eastern edge of the Karst Plateau (e.g. Karst and Črni Kal Thrusts) and those of the north-eastern Istria (e.g. Hrastovlje and Buzet Thrusts). Whereas, the top of the unit lies at depths between 70 and 222 m below sea level in the adjacent offshore, with a general deepening trend from SE towards NW. Moreover, the surface, buried in the gulf, is depicted by a few hundred of meters wide ridges surrounded by valleys (the wider is NE-SW oriented in the central part). Map compiled by using ArcGis® (ESRI, 2017) software; datum WGS84, projection UTM33.

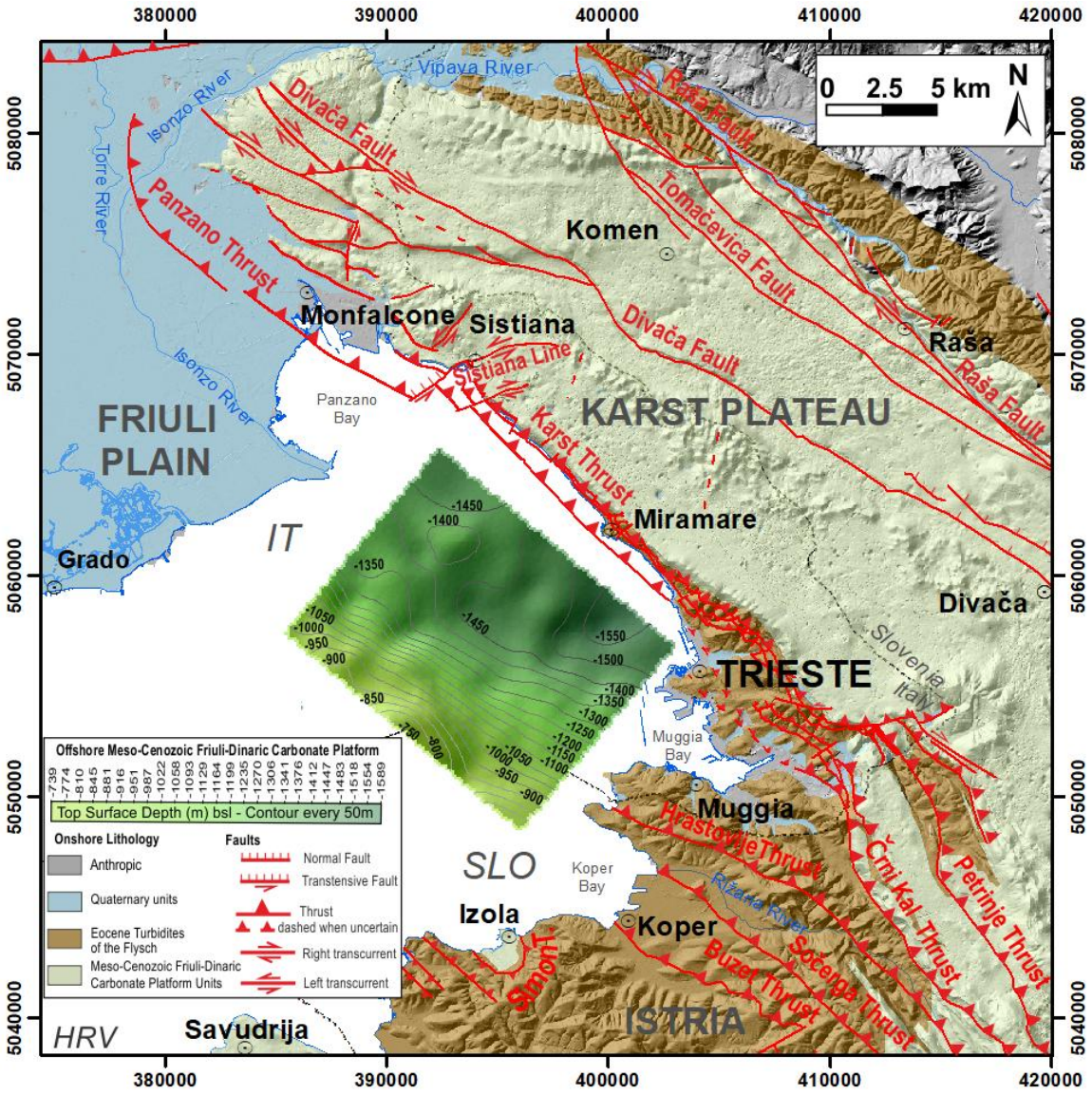

Fig. 108 - Map of the top carbonates surface, obtained from the 3D depth model B (Fig. 93, Fig. 94), within the eastern side of the Gulf of Trieste. Its offshore depth is represented by the graded green colour scale (contours every 50 m). The neighbouring onshore geology (lithologies and main tectonic lineaments) is also represented. This latter was compiled from (Placer, et al., 2010) as concerns Istria; from (GeoCGT-FVG, 2013) as concerns the Italian Karst and the Friuli Plain; from (Jurkovšek, et al., 2016) as concerns the Slovenian Karst. The Meso-Cenozoic units of the Friuli-Dinaric Carbonate Platform and the Eocene turbidites of the Flysch are represented onshore by uniform colours (light green and medium brown, respectively). They are superimposed on the Digital Elevation Models by (IRDAT-FVG, 2017) for the Italian area (10 m cell resolution) and by (EU-DEM, 2017) for the Slovenian and Croatian areas (20 m cell resolution). The map represents the synthesis between the offshore geometry and depth of top carbonates surface, with the neighbouring geology. The carbonate units, outcrop in the Karst Plateau between about 0 and 600 m above sea level (with a general lowering trend NW-wards). They are structured in an anticline, representing the hangingwall of the NW-SE oriented Dinaric Thrusts. These bound the eastern edge of the Karst Plateau (e.g. Karst and Črni Kal Thrusts), continuing as the Panzano Thrust towards NW (displaced few kilometres W-wards by the left transtensive Sistiana Line). Whereas, the top of the units lies at depths between 739 and 1589 m below sea level (bsl), in the adjacent offshore, with a general deepening trend from SW towards NE. Note that at about 1.7 km from the Trieste coast, the surface reaches 1600±30 m bsl, according to the 2D pre-stack depth migrated GT13-27 profile (Fig. 83, Fig. 93, Fig. 94), that is not represented here. Moreover, the deepening surface, buried in the gulf, is not flat but results to be shaped by few meters wide ridges, surrounded by valleys elongated in the SW-NE direction. Map compiled by using ArcGis® (ESRI, 2017) software; datum WGS84, projection UTM33.

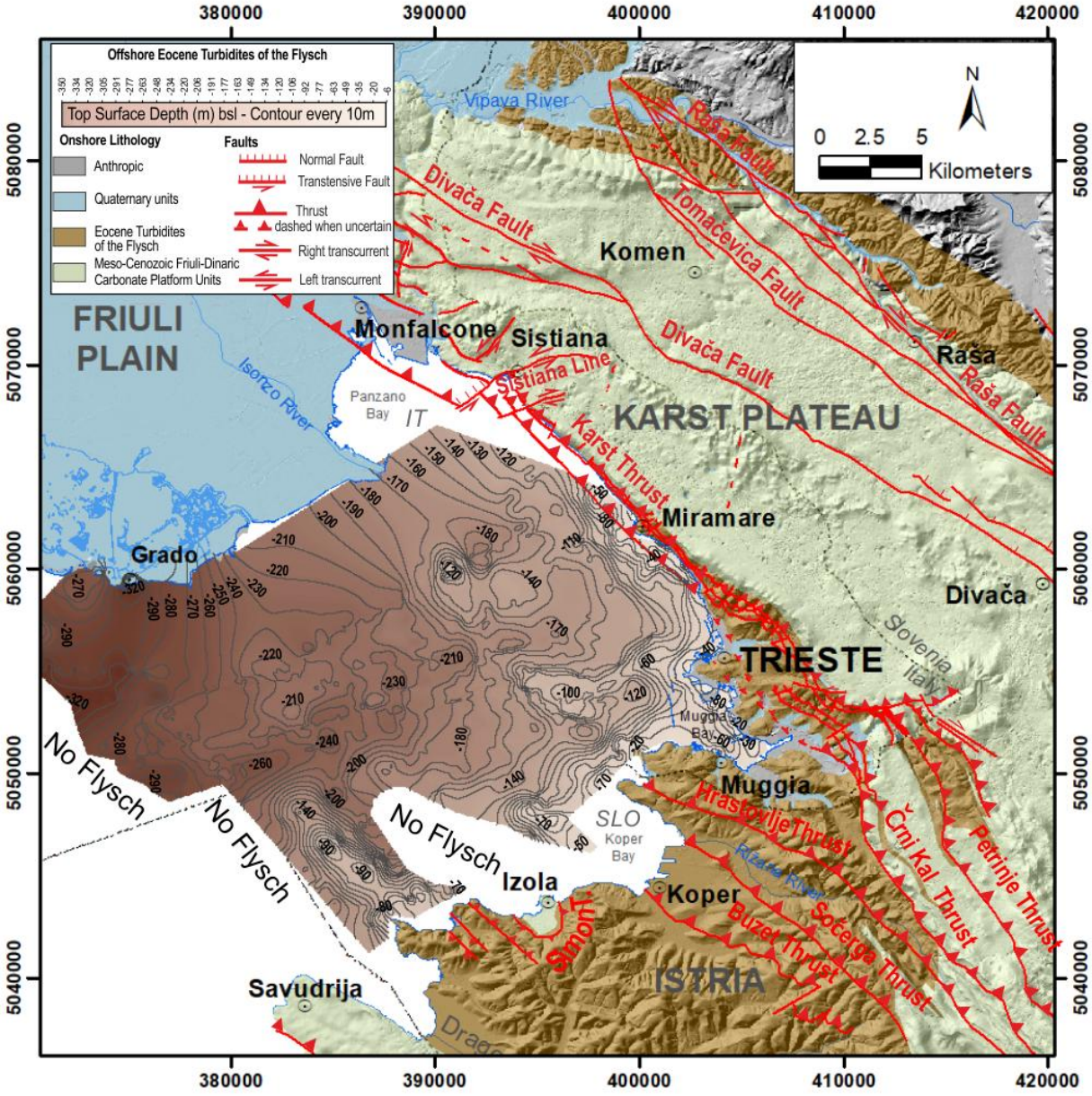

Fig. 109 - Depth map of the top flysch surface extending towards the gulf coastline, over a wider area respect to that covered by the 3D velocity depth model reconstructed through the tomographic analysis. It was obtained by converting into depth (by using mean tomographic velocity of 1700 m/s for the Quaternary sediments) the interpreted horizon on the available 2D, two way time, multichannel seismic reflection data (GT2009 and 2013 OGS surveys) in the central and eastern part of the gulf, boomer (Barcola 2003, Miramare 2012, Muggia 2013 OGS surveys) and core data (Muggia 1960s) along the southern and north-eastern coastlines (section Geophysical and Geological Dataset for position details). The detected tomographic velocity turn out to be adequate since the reconstructed depths in the area of the 3D model are in good agreement with those of the inverted tomographic depth surface. The blank area, on the SW, reflects the pinching out of the unit, that closes in correspondence of the carbonate peripheral bulge. Similarly, this occurs in the marine area where the Izola anticline outcrops. The neighbouring onshore geology (lithologies and main tectonic lineaments) is also represented. This latter was compiled from (Placer, et al., 2010) as concerns Istria; from (GeoCGT-FVG, 2013) as concerns the Italian Karst and the Friuli Plain; from (Jurkovšek, et al., 2016) as concerns the Slovenian Karst. The Meso-Cenozoic units of the Friuli-Dinaric Carbonate Platform and the Eocene turbidites of the Flysch are represented onshore by uniform colours (light green and medium brown, respectively). They are superimposed on the Digital Elevation Models by (IRDAT-FVG, 2017) for the Italian area (10 m cell resolution) and by (EU-DEM, 2017) for the Slovenian and Croatian areas (20 m cell resolution). Map compiled by using ArcGis® (ESRI, 2017) software; datum WGS84, projection UTM33.

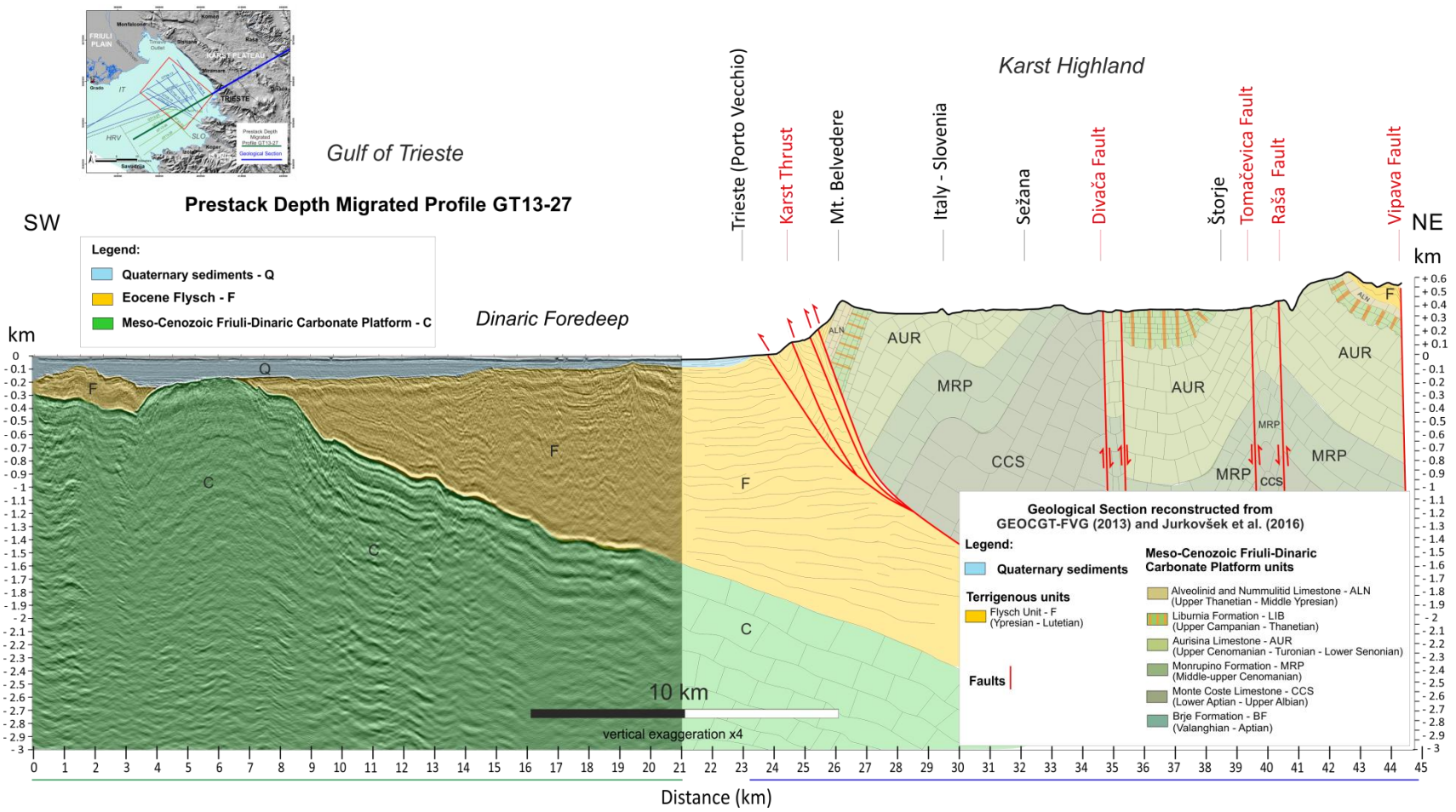

Fig. 110 - Offshore-onland geological section crossing the Gulf of Trieste and the entire Karst Plateau along SW-NE direction. It was reconstructed thanks to the juxtaposition of the prestack depth migrated profile GT13-27, obtained in the present work, and a classical geological section derived from the analysis of the onshore geological maps ((GeoCGT-FVG, 2013) (Jurkovšek, et al., 2016)). It highlights the depth of about 1.7 km (below sea level) of the top of the Meso-Cenozoic Friuli-Dinaric Platform under the city of Trieste. The carbonate units are structured in the Karst anticline that outcrops up to an elevation of 600 m (above sea level). This reveals a vertical displacement related to the Karst Thrust of, at least, about 1.8 km.

7 CONCLUSION

The Gulf of Trieste is settled in the north-easternmost part of the Adriatic Sea, south of the intersection between the NW-SE trending External Dinarides and the E-W oriented South-Eastern Alps. It represents the foredeep of both the chains. Its sedimentary sequence consists of the Mesozoic-Paleogene Friuli-Dinaric Carbonate Platform, the Eocene turbiditic deposits of the flysch, the Plio-Quaternary continental and marine sediments (Nicolich et al., 2004a,b; Busetti et al., 2010a,b). According to Fantoni et al. (2002) and Busetti et al. (2010a,b), the area underwent a multiphase tectonic activity that started in the Mesozoic, when an extensional regime, with NE-SW oriented normal faults, allowed the aggradation of the carbonate platform. In the Late Cretaceous-Paleogene, the Dinaric fold-thrust system gradually migrated towards SW, deflecting the carbonate platform E-ward. The main frontal ramp of the External Dinarides is the Karst Thrust that extends along the north-eastern and rocky coastline of the gulf and separates the hanging-wall, topographically expressed by the Karst highland, from the footwall lying in the gulf. In the Oligocene-Miocene, the convergence that generated the S-ward vergent Southern Alpine orogen, caused a N-ward deepening of the platform and reactivated the inherited Meso-Cenozoic structures, of the gulf, with a dextral transcurrent kinematics. They show neotectonic activity and they are often the preferential way along which fluids migrate from the carbonates to the seafloor (Busetti, et al., 2013).

A dense geophysical dataset has been acquired in the gulf, in the years 2005, 2009, 2013. It consists of 630 km of multichannel seismic reflection profiles, collected by the R/V OGS Explora.

Part of this dataset was used in the present work, to build a 3D velocity depth model in the eastern portion of the gulf. The model gives information on the main surfaces and units up to a depth of 1600 m below sea level. It was obtained by means of advanced seismic tomography techniques. Seismic tomography provides a versatile tool for the velocity estimation from surface reflection data (Yilmaz, 2001). Traveltime tomography allows resolution of vertical as well as lateral velocity gradients, hence obtaining a better definition of the correct geometries with respect to conventional techniques (Böhm et al., 1999; 2000; Vesnaver and Böhm, 2000). Basically, most of the tomographic algorithms are based on ray tracing and on iterative procedures that minimize the difference between the modeled and measured traveltimes. Two main tomographic methods were applied in this work. The first one (CAT3D - OGS, 2014) is based on the simultaneous iterative reconstruction technique (SIRT) method (Van der Sluis and Van der Vorst 1987) and the principle of minimum dispersion of the reflected points (Carrion et al., 1993).

The second (Geodepth - Paradigm, 2016) is an iterative imaging technique encompassing pre-stack depth migration, residual move-out analysis and grid tomography. The former method is very useful to handle complex 3D acquisition geometries but requires the interpretation of the reflected events of interest directly on the pre-stack seismic data. This interpretation session is generally very time-consuming, in terms of a geophysicists effort, since the pre-stack seismic data are often affected by a low signal-to-noise ratio. Moreover, the signal to be picked in the pre-stack data is unfocused and therefore very difficult to identify when the target is very deep and the strength of the adopted seismic source not sufficient. The latter tomographic method is more suitable in these difficult situations, because pre-stack depth migration, even when performed using a preliminary velocity model, allows to focalize the seismic energy enabling for a easier identification of deeper structures or weak impedance contrasts (Yilmaz, 2001). Therefore, the first method was applied to obtain a 3D velocity depth model until about 1 km depth, while the second method was employed to refine the preliminary tomographic model and recover information from the deeper geological features.

Two main reflectors were considered: the top surface of the flysch and that of the carbonates. Their reflected and refracted events were picked on the pre-stack seismic data and used as input

for the first traveltime tomographic algorithm. Moreover, the analysis of the refracted events provided a reliable 3D velocity depth model for the top flysch surface. A seismic velocity section, on a key profile, was then selected and refined by using the second iterative imaging technique. A well-focused 2D pre-stack depth migrated image was obtained. In order to better characterize the flysch unit, an internal reflected event (inner flysch) was also picked on time migrated data. The comparison between the results from reflection tomography and refraction analysis allowed to gain information on the anisotropy of the upper flysch, due to fine layering. The velocities in the upper part of the flysch have been therefore well characterized. The 3D inner flysch and top carbonates surfaces were then mapped into depth. The former was converted from time to depth by using P-wave vertical velocities obtained from the anisotropy analysis. The second was converted by using an average interval lower flysch velocity, obtained from the refined velocity field of the iterative imaging analysis.

The results provide an adequate 3D elastic velocity model in depth, of the flysch and carbonate units and of their top surfaces. It resulted that the top of the Meso-Cenozoic Friuli-Dinaric Carbonate Platform lies at a maximum depth of 1600 ± 30 m below sea level, about 2 km offshore the city of Trieste. If linearly extrapolated up to the north-eastern coast, the horizon depth reaches about 1740 m below sea level (bsl). This indicates that Karst Thrust is responsible for a vertical displacement of about 1600 and 1800 m.

This new result updates the previous estimations. A depth for the top carbonates in the gulf of about 1200 m was evaluated through an investigation that used a seismic refraction survey (Finetti, 1967). Busetti et al. (2010b), evaluated a depth of 1400 m, by using the conventional velocity analysis performed on the multichannel seismic reflection data acquired in the offshore in 2005 and 2009.

Moreover, the 3D velocity depth model and the depth migrated imaging result reveal that the thickness of the flysch, in the eastern side of the gulf, is about 1400-1500 m. The unit thins SW-wards until it pinches out on an anticline involving the carbonates. The anticline is about 6.5 km wide along the SW-NE direction and it rises up to about 200 m bsl. According with Busetti, et al. (2013), this represents the north-western continuation of the Izola anticline, outcropping onshore along the south-eastern coast of the gulf. The upper part of the flysch unit is characterised by sub-vertical strata, that end into the Messinian-Pliocene unconformity. This latter is covered by a thin (from 50 to 190 m, values increase W-wards) package of Quaternary sediments affected by pervasive tectonic disturbance. Local low seismic velocity trends suggest the presence of fluids, that flow through the porous layers of the upper flysch, towards the shallowest unit and the seabed. This represents a further hint about the neotectonic activity of the area.

The obtained information constitute a valuable basis for a construction of a 3D geological and structural depth model of the Gulf of Trieste. The top carbonate surface can be better characterized by applying the velocity refining technique to all the 2D seismic lines available in the gulf. This would allow to reconstruct the spatial variability of the seismic velocity within the deeper part of the flysch. Moreover, advanced processing methods can be further applied to the pre-stack seismic data to enhance the reflected signals from the top carbonates to the deeper parts, in order to improve the whole 3D tomographic model.

This type of analysis would provide a helpful enhanced to further understand the relationship with the geological and tectonic elements characterizing the neighboring onshore region. The reconstruction of a wider and more detailed geological framework would help to better asses also the neotectonic evolution of the area.

Appendix 1

P-Wave Anisotropy of Finely Layered Medium by Using the Generalized Backus Theory

Most geological systems can be modeled as fine layering, which refers to the case where the dominant wavelength of the pulse is much larger than the thicknesses of the single layers. When this occurs, the medium is effectively anisotropic with a transversely isotropic symmetry. Many authors studied this problem, whose references can be found in Carcione (2014). Backus (1962) obtained the average elasticity constants in the case when the single layers are transversely isotropic with the symmetry axis perpendicular to the layering plane. Moreover, the Author assumed stationary, in a given length of composite medium much smaller than the wavelength, the proportion of each material is constant (periodicity is not required). The equations were further generalized by Schoenberg and Muir (1989) for anisotropic single constituents. Backus averaging for the lossless case has been verified numerically by Carcione et al. (1991). They found that the minimum ratio between the P-wave dominant pulse wavelength and the spatial period of the layering depends on the contrast between the constituents. For instance, for a periodic sequence of epoxy-glass it is around 8, and for sandstone-limestone (which has a lower reflection coefficient) it is between 5 and 6. In any case, an optimal ratio can be found for which the equivalence between a finely layered medium and a homogeneous transversely isotropic medium is valid. Carcione (1992) generalized Backus averaging to the anelastic case, obtaining the first model for Q-anisotropy (e.g. Carcione, 2014). Analyses on sequences of sandstone-limestone and shale-limestone with different degrees of anisotropy indicate that the quality factors (Q) of the shear modes are more anisotropic than the corresponding phase velocities, cusps of the qSV mode are more pronounced for low frequencies and midrange proportions, and in general, attenuation is higher in the direction perpendicular to layering or close to it, provided that the material with lower velocity is the more dissipative.
In two recent works, Picotti et al. (2010) and Picotti et al. (2012) verified the generalized Backus theory for the anelastic (lossy) case of Q-anisotropy. They introduced a new numerical method based on a finite element solution of the equations of motion in the space-frequency domain to simulate harmonic compressibility and shear tests. The methodology allows to obtain the complex and frequency-dependent stiffnesses to compute the wave velocities and quality factors as a function of frequency and propagation angle. The Authors found that attenuation anisotropy is more pronounced than velocity anisotropy. Hence, measurements of Q-anisotropy may provide more reliable information about the orientation of layering and fractures, and fluid properties of hydrocarbon reservoirs. Shear wave experiments can provide useful information, since it is seen that attenuation anisotropy due to fine-layering is more pronounced for shear waves than for compressional waves. A brief description of all these models can be found in Carcione (2014).

Fine layering on a scale much finer than the dominant wavelength of the signal yields effective anisotropy, whose elasticity constants are given by Backus averaging (Backus, 1962). Here, it is considered that each medium is isotropic and anelastic with complex Lamé constants given by

$$\lambda(\omega) = \rho\left(c_P^2 - \frac{4}{3}c_S^2\right)M_1(\omega) - \frac{2}{3}\rho c_S^2 M_2(\omega) \quad (4)$$

$$\mu(\omega) = \rho c_S^2 M_2(\omega),$$

where *w* is the angular frequency, M_1 and M_2 are the dilatational and shear complex moduli, respectively, c_P and c_S are the elastic high-frequency limit compressional- and shear wave velocities, and ρ is the density.
Omitting the angular-frequency (*w*) dependency for brevity, the dilatational modulus *k* and the P-wave modulus *E* are

$$k = \lambda + \frac{2}{3}\mu = \rho\left(c_P^2 - \frac{4}{3}c_S^2\right)M_1, \qquad E = k + \frac{4}{3}\mu. \tag{5}$$

The equivalent viscoelastic transversely isotropic medium is defined by the following complex stiffnesses (Carcione (1992) and Picotti et al. (2010):

$$\begin{aligned} p_{11} &= \langle E - \lambda^2 E^{-1}\rangle + \langle E^{-1}\rangle^{-1}\langle E^{-1}\lambda\rangle^2, \\ p_{33} &= \langle E^{-1}\rangle^{-1}, \\ p_{13} &= \langle E^{-1}\rangle^{-1}\langle E^{-1}\lambda\rangle, \\ p_{55} &= \langle \mu^{-1}\rangle^{-1}, \\ p_{66} &= \langle \mu\rangle, \end{aligned} \tag{6}$$

where <*> denotes the thickness weighted average. According to Picotti et al. (2010) we assume constant quality factors over the frequency range of interest (until about 100 Hz). Such behavior is modelled by a continuous distribution of relaxation mechanisms based on the standard linear solid. The dimensionless dilatational and shear complex moduli for a specific frequency can be expressed as

$$M_\nu(\omega) = \left(1 + \frac{2}{\pi Q_{0\nu}}\ln\frac{1 + i\omega\tau_2}{1 + i\omega\tau_1}\right)^{-1}, \tag{7}$$

where τ_1 and τ_2 are time constants, with $\tau_1 < \tau_2$, and $Q_{0\nu}$ defines the value of the quality factor which remains nearly constant over the selected frequency range.
We consider homogeneous viscoelastic waves (e.g., Carcione, 2014). The complex velocities are the key quantities to obtain the wave velocities and quality factors of the equivalent anisotropic medium. The quasi-compressional qP-wave velocity is given by

$$v_{qP} = (2\rho)^{-1/2}\sqrt{p_{11}l_1^2 + p_{33}l_3^2 + p_{55} + A}, \qquad A = \sqrt{[(p_{11} - p_{55})l_1^2 + (p_{55} - p_{33})l_3^2]^2 + 4[(p_{13} + p_{55})l_1 l_3]^2}. \tag{8}$$

(Picotti et al., 2010; Carcione, 2014) where l_1 =sinϑ and l_3 = cosϑ are the directions cosines, ϑ is the propagation angle between the wave number vector and the symmetry axis. The modulus of the phase velocity vector is given by

$$v_p = \left[\mathrm{Re}\left(\frac{1}{v}\right)\right]^{-1}, \qquad (9)$$

where *v* represents in this case only the quasi-compressional *qP*-wave velocity given by equation (5).

The most common type of anisotropy is transverse isotropy with a vertical axis of symmetry (VTI media. Thomsen (1986) suggested a convenient notation for VTI media when it is weakly anisotropic. The elastic coefficients are expressed in terms of the *P*-wave and *S*-wave velocities, α and β, respectively, propagating along the symmetry axis plus three additional constants ε, γ and δ. The constant ε describes the fractional difference of the *P*-wave velocities in the vertical and horizontal directions and therefore is referred to as the *P*-wave anisotropy. Similarly, the constant γ describes the fractional difference of the *SH*-wave velocities between vertical and horizontal polarizations of the horizontally propagating *S*-wave. δ is the crucial anisotropy parameter for near vertical *P*-wave propagation. This can be seen from the approximation for phase velocities, which can be written as (Thomsen, 1986):

$$\begin{aligned} V_P &\approx \alpha\left(1+\delta\sin^2\theta\cos^2\theta+\varepsilon\sin^4\theta\right), \\ V_{SV} &\approx \beta\left[1+\frac{\alpha^2}{\beta^2}\left(\varepsilon-\delta\right)\sin^2\theta\cos^2\theta\right], \\ V_{SH} &\approx \beta\left(1+\gamma\sin^2\theta\right). \end{aligned} \qquad (10)$$

where VSH is the wavefront velocity of the pure shear wave which has no component of polarization in the vertical direction, VSV is the pseudo-shear wave polarized normal to the pure shear wave, and VP is the pseudo-longitudinal wave. θ is the phase angle between the wavefront normal and the symmetry axis. Since ε, γ and δ are usually of the same order of magnitude, it is clear from the above equations that at small angles θ, where $\sin\theta$ is small compared to $\sin^2\theta\cos^2\theta$, the third term (with ε) is small compared to the second term (with δ). Therefore since most reflection profiling takes place with small angles θ, δ will dominate most anisotropic effects for P-wave propagation.

Acronym Glossary

CAT3D: Computer Aided Tomography for 3D models

DMG: Depth Migrated Gather

ESFM: Earth Science and Fluid Mechanics

GT: Gulf of Trieste

MCS: Multichannel Seismic

OGS: National Institute of Oceanography and Experimental Geophysics

PSDM: Prestack Depth Migration

References

Accaino, F., Böhm, G. & Tinivella, U., 2005. Tomographic inversion of common image gathers. First Break, Volume 23, pp. 40-44.

AGI (2009). Glossary of geology. *American Geological Institute*, At web page: www.agiweb.org.

AGIP (1972). Acque dolci sotterranee. *Grafica Palombi*, 914.

AGIP (1977). Temperature sotterranee. *Tip. Brugora*, 1390.

AGIP (1994). Acque dolci sotterranee (aggiornamento dati dal 1971 al 1990). *AGIP S.p.A.*, 515.

Amato, A., Barnaba, P., Finetti, I., Groppi, G., Martinis, B., & Muzzin, A. (1977). Geodynamic Outline and Seismicity of Friuli Venezia Julia region. *Bollettino di Geofisica Teorica ed Applicata, 19* (72), 217-256.

Ambert, M. (1978). Le littoral de l'Istrie: premieres observations géomorphologiques. *Méditerranée, 1-2*, 47-56.

Antonioli, F., & Silenzi, S. (2007c). Variazioni relative del livello del mare e vulnerabilità delle pianure costiere italiane. *Quaderni della Societa' Geologica Italiana, 2*, 29.

Antonioli, F., Anzidei, M., Lambeck, K., Auriemma, R., Gaddi, D., Furlani, S., Surace, L. (2007a). Sea level change during Holocene from Sardinia and northeastern Adriatic (Central Mediterranean sea) from archaeological and geomorphological data. *Quaternary Science Reviews, 26*, 2463-2464.

Antonioli, F., Anzidei, M., Lambek, K., Auriemma, R., Gaddi, D., Furlani, S., Surace, L. (2007b). Sea level change in Italy during Holocene from archaeological and geomorphological data. *Qua. Sci. Rev., 26*, 2463-2486.

Antonioli, F., Carulli, G., Furlani, S., Auriemma, R., & Marocco, R. (2004). The enigma of submerged marine notches in northern Adriatic Sea. *Quaternaria, VIII*, 27-36.

Antonioli, F., Ferranti, L., Fontana, A., Amorosi, A., Bondesan, A., Braitenberg, C. D., Stocchi, P. (2009). Holocene relative sea-level changes and vertical movements along the Italian and Istrian coastlines. *Quaternary International, 206*, 102-133.

Ashcroft, W., 2011. *A Petroleum Geologist's Guide to Seismic Reflection.* Oxford: Wiley – Blackwell.

Auriemma, R., & Maggi, P. (2012). L'archeologia sommersa. Vecchie e nuove scoperte nella laguna di Marano. *La Bassa, 65*, 7-24.

Backus, G. E. (1962). Long-wave elastic anisotropy produced by horizontal layering, *Journal of Geophysical Research*, 67, 4427–4440.

Baradello, L., Busetti, M., Nieto Yabar, D., Romeo, R., & Visnovic, G. (2013). Survey VHR Sismico Boomer del Sito di Interesse Nazionale (SIN) di Trieste. *REL. OGS 2013/14 Sez. IRI 2 dd. 25 febbraio 2013*(14), 66 pp., 20 figs., 5 tabs., 36 attms.

Bechtold, M., Battaglia, M., D. C. Tanner, D., & Zuliani, D. (2009). Constraints on the active tectonics of the Friuli/NW Slovenia area from CGPS measurements and three-dimensional kinematic modeling. *Journal of Geophysical Research, 114, B03408*.

Bernardis, G., Poli, M., Snidarcig, A., & A., Z. (2000). Seismotectonic and macroseismic characteristics of the earthquake of Bovec (NW Slovenia: April 12th 1998). *Bollettino di Geofisica Teorica e Applicata, 41*(2), 133-148.

Bindoff, N., Willebrand, J., Artale, V., Cazenave, A., Gregory, J., Gulev, S., Unnikrishnan, A. (2007). Observations: Oceanic Climate Change and Sea Level. In S. Solomon, D. Qin, M. Manning, Z. Chen, M. Marquis, K. Averyt, H. Miller, *Climate Change 2007: The Physical Science Basis. Contribution of Working Group I to the Fourth Assessment Report of the Intergovernmental Panel on Climate Change* (pp. 385-432). Cambridge and New York: Cambridge University Press.

Biolchi, S., Furlani, S., Covelli, S., Busetti, M., & Cucchi, F. (2015). Morphoneotectonics and lithology of the eastern sector of the Gulf of Trieste (NE Italy). *Journal of Maps*, 11.

Bishop, T.N., Bube, K.P., Cutler, R.T., Langan, R.T., Love, P.L., Resnick., J.R., Shuey, R.T., Spindler, D.A., Wyld, H.W. (1985). Tomographic determination of velocity and depth in laterally varying media. Geophysics 50 (6), 903-923.

Böhm, G., Galuppo, P., Vesnaver, A. (2000) 3-D adaptive tomography using Delaunay triangles and Voronoi polygons. Geophysical Prospecting 48 (4), 723-744.

Böhm, G., Rossi, G. Vesnaver, A. (1999). Minimum-time ray-tracing for 3-D irregular grids. Journal of Seismic Exploration 8, 117-131.

Braitenberg, C., Mariani, P., Tunini, L., Grillo, B., & Nagy, I. (2011). Vertical crustal motions from differential tide gauge observations and satellite altimetry in southern Italy. *Journal of Geodynamics, 51*, 233–244.

Braitenberg, C., Nagy, I., Romeo, G., & Taccetti, Q. (2005). The very broad-band data acquisition of the long-base tiltmeters of Grotta Gigante (Trieste, Italy). *Journal of Geodynamics, 41*, 164–174.

Braitenberg, C., Nagy, I., Romeo, G., & Taccetti, Q. (2006). The very broad-band data acquisition of the long-base tiltmeters of Grotta Gigante (Trieste, Italy). *Journal of Geodynamics, 41*, 164–174.

Brambati, A. (1970). Provenienza, trasporto e accumulo dei sedimenti recenti nella laguna di Marano e di Grado e nei litorali tra i fiumi Isonzo e Tagliamento. *Mem. Soc. Geol. It., 9*, 281-329.

Brambati, A., & Catani, G. (1988). Le Coste e i Fondali del Golfo di Trieste dall'Isonzo a Punta Sottile: Aspetti Geologici, Geomorfologici, Sedimentologici e Geotecnici. *Hydrores Information, 5*(6), 13-28.

Burrato, P., Poli, M. E., Vannoli, P., Zanferrari, A., Basili, R., & Galadini, F. (2008). Sources of Mw 5+ earthquakes in northeastern Italy and western Slovenia: An updated view based on geological and seismological evidence. *Tectonophysics, 453*, 157–176.

Buser, S. (1989). Development of the Dinaric and the Julian Carbonate platforms and of the intermediate Slovenian basin (NW Yugoslavia). *Mem. Soc. Geol. It., 40*, 313-320.

Busetti, M., Gordini, E., Baradello, L., Cova, A., Caburlotto, A., Deponte, M., Tomini, I. (2007). The morphological and seismic stratigraphic characterization of the Grado and Marano lagoon (northern Adriatic). *Conegno Nazionale "GeoItalia2007", Rimini 12–14 sett. 2007, 2*, 48–50.

Busetti, M., Volpi, V., Barison, E., Giustiniani, M., Marchi, M., Ramella, R., Zanolla, C. (2010b). Cenozoic seismic stratigraphy and tectonic evolution of the Gulf of Trieste (Northern Adriatic). *Proceedings of the "ADRIA 2006 – International Geological Congress on Adriatic area", GeoActa, Special Publication, 3*, 1-14.

Busetti, M., Volpi, V., Marchi, M., Zanolla, C., Barison, E., Baradello, L., Wardell, N. (2008). Dinaric tectonic features in the Gulf of Trieste (Northern Adriatic). *Proceedings of the 27th Gruppo Nazionale di Geofisica della Terra Solida (GNGTS) Congress, Trieste 6-8 October 2008, 3-Applied Geophysics*, 411–414.

Busetti, M., Volpi, V., Nicolich, R., Barison, E., Romeo, R., Baradello, L., Ramella, R. (2010a). Dinaric tectonic features in the Gulf of Trieste (Northern Adriatic). *In: D. Slejko (Ed.), Novelties in Geophysics, Select paper from the 27th Annual Conference of the Italian Group for Solid Earth Geophysics, Trieste. Bollettino di Geofisica Teorica e Applicata., 51*(2-3), 117-128.

Busetti, M., Zgur, F., Romeo, R., Sormani, L., & Pettenati, F. (2012). Caratteristiche geologico-strutturali del Golfo di Trieste. In: D'Angelo S. e Fiorentino A. (Eds.), *Contributi al Meeting Marino, Roma 25-26 ottobre 2012, Atti Ispra,* 65-70.

Busetti, M., Zgur, F., Vrabec, M., Facchin, L., Pelos, C., Romeo, R., Zerial, A. (2013). Neotectonic reactivation of Meso-Cenozoic structures in the Gulf of Trieste and its relationship with fluid seepings. *Proceedings of the 32nd Gruppo Nazionale di Geofisica della Terra Solida (GNGTS) Congress, Trieste 19-21 November 2013, 3-Applied Geophysics*, 29-34.

Calore, C., Della Vedova, B., Grassi, S., Marson, I., Nicolich, R., & Squarci, P. (1995). A hydrothermal system along the coastal area of Friuli Venezia Giulia Region (NE Italy). *Proceedings of World Geothermal Congress*, *2*, pp. 1269-1274. Florence.

Cappelli, V., Cassano, E., Deluchi, L., Gandino, A., La Torre, P., & Ramella, R. (2008). *La Storia dei Gruppi Geofisici in AGIP.* AGIP.

Carcione, J. M., D. Kosloff, & A. Behle (1991) Long wave anisotropy in stratified media: A numerical test, Geophysics, 56, 245–254.

Carcione, J. M. (1992) Anisotropic Q and velocity dispersion of finely layered media, Geophys. Prospect., 40, 761–783.

Carcione, J. M. (2014) Wave Fields in Real Media. Theory and Numerical Simulation of Wave Propagation in Anisotropic, Anelastic, Porous and Electromagnetic Media, 3rd ed., revised and extended (Elsevier Science, Amsterdam).

Carrion, P., Böhm, G., Marchetti, A., Petteinati, F. & Vesnaver, A. (1993) Reconstruction of lateral gradients from reflection tomography, Journal of seismic exploration, 2, 55-67.

Carulli, G. (2006a). *Carta geologica del Friuli Venezia Giulia, scala 1:150,000.* Regione Autonoma Friuli Venezia Giulia, Direzione Regionale Ambiente e Lavori Pubblici, Servizio Geologico Regionale.

Carulli, G. (2006b). *Note illustrative della Carta geologica del Friuli Venezia Giulia, scala 1:150,000.* Firenze: Regione Autonoma Friuli Venezia Giulia, Direzione RegionaleAmbiente e Lavori Pubblici, Servizio Geologico Regionale.

Carulli, G., & Cucchi, F. (1991). Proposta di interpretazione strutturale del Carso triestino. *Atti Tic. Sc. Terra, 34*, 161–166.

Carulli, G., Carobene, L., Cavallin, A., Martinis, B., & Onofri, R. (1980). Evoluzione strutturale plio-quaternaria del Friuli e della Venezia Giulia. In *Contributi Preliminari Alla Realizzazione Della Carta Neotettonica D'Italia* (pp. 489–545). Geodinamica, C.N.R.

Carulli, G., Cucchi, F., Marocco, R., Masetti, D., Peruzza, L., Ponton, M., & Tunis, G. (2000). Guida alle Escusioni. Trieste: 80° Riunione Estiva - Società Geologica Italiana.

Casero, P., Rigamonti, A., & Iocca, M. (1990). Paleogeographic relationship during Cretaceous between the Northern Adriatic area and the Eastern Southern Alps. *Mem. Soc. geol. It., 45*, 807-814.

Castellarin, A., Nicolich, R., Fantoni, R., Cantelli, L., Sella, M., & Selli, L. (2006). Structure of the lithosphere beneath the Eastern Alps (south sector of the TRANSALP transect). *Tectonophysics, 414*, 259-282.

Cati, A., Fichera, R., & Cappelli, V. (1987a). Northeastern Italy. Integrated processing of geophysical and geological data. *Mem. Soc. Geol It., 40*, 273-288.

Cati, A., Sartorio, D., & Venturini, S. (1987b). Carbonate Platforms in the Subsurface of the Northern Adriatic Area. *Mem. Soc. Geol. It.*, 295-308.

Catuneanu, O. (2002). Sequence Stratigraphy of clastic systems: concepts, merits, and pitfalls. *Journal of African Earth Sciences, 1*, 1-43.

Cavallin, A., Martinis, B., Carobene, L., & Carulli, G. (1979). Dati preliminari sulla neotettonica del fogli 25 (Udine p.p.) e 40A (Gorizia). *In: Contributi preliminari alla realizzazione della Carta Neotettonica d'Italia, CNR, 155*, 489-545.

Christophersen, A., Litchfield, N., Berryman, K., Thomas, R., Basili, R., Wallace, L., & Yeats, R. (2015). Developmnet of the Global Earthquake Model's neotectonic fault database. *Natural Hazards, 79*(1), 111-135.

Church, J., Clark, P., Cazenave, A., J.M., G., S., J., Levermann, A., Unnikrishnan, A. (2013). Sea Level Change. In: T. Stocker, D. Qin, G. Plattner, M. Tignor, S. Allen, J. Boschung, P. Midgleym (Eds.), *Climate Change 2013: The Physical Science Basis. Contribution of Working Group I to the Fifth Assessment Report of the Intergovernmental Panel on Climate Change* (pp. 1137-1216). Cambridge and New York: Cambridge University Press.

Cimolino, A. (2010). *Caratterizzazione delle risorse geotermiche della Bassa Pianura Friulana (Regione FVG).* University of Trieste: PhD Thesis in Civil and Environmental Engineering.

Cimolino, A., Della Vedova, B., Nicolich, R., Barison, E., & Brancatelli, E. (2010). New evidence of the outer Dinaric deformation front in the Grado area (NE - Italy). *Rendiconti Lincei, 21*(suppl. 1), 167 – 179.

Clark, P., Dyke, A., Shakun, J., Carlson, A., Clark, J., Wohlfarth, B., McCabe, A. (2009). The Last Glacial Maximum. *Science, 325*, 710-714.

Clayton, R., 1984. Seismic Tomography. *Eos, Trans. Am. Geophys. Union,* Volume 65, p. 236.

Coe, A. (2002). The Sedimentary Record of Sea-Level Change. *Cambridge University Press*, 57–98.

Cornalia, E., & Chiozza, L. (1851a). *Carta geologica dell'Istria tracciata nell'autunno del 1850, scala 1:400.000.* I.R. Istituto Lombardo di Scienze, Lettere ed Arti del giorno 9 gennajo 1851.

Cornalia, E., & Chiozza, L. (1851b). *Cenni geologici sull'Istria.* letti nell'adunanza dell'I.R. Istituto Lombardo di Scienze, Lettere ed Arti del giorno 9 gennajo 1851.

Covelli, S., Fontolan, G., Faganelli, J., & Ogrinc, N. (2006). Anthropogenic markers Anthropogenic markers Anthropogenic markers Anthropogenic markers Anthropogenic markers Anthropogenic markers Anthropogenic markers Anthropogenic markers in the Holocene stratigraphic sequence of Gulf Trieste (northern Adriatic Sea). *Marine Geology, 230*, 29-51.

Cucchi, F., & Forti, F. (1983). Primi risultati dello studio di alcune sorgenti carsiche marine presso San Giovanni di Duino (TS). *Atti del 6° Convegno Regionale di Speleologia del Friuli-Venezia Giulia, 2*, 67-75.

Cucchi, F., Finocchiaro, F., & Muscio, G. (2009). Geositi del Friuli Venezia Giulia. *Dipartimento di Scienze Geologiche, Ambientali, Marine dell'Universita' di Trieste; Direzione Centrale Ambiente e Lavoi Pubblici, Servizio Geologico, RAFVG*, 383.

Cucchi, F., Pirini Radrizzani, C., & Pugliese, N. (1989). The carbonate stratigraphic sequence of the Karst of Trieste (Italy). *Mem. Soc. Geol. Ital. In: Proceedings of "International Symposium on Evolution of the karstic carbonate platform" (1987), XL*, 35–44.

Cucchi, F., Pugliese, N., Covelli, S., Fanzutti, G., Fanucci, F., Fontana, A., Marocco, R. (2008b). Carta geologica di sintesi GEO-CGT alla scala 1:10.000, foglio 131-Caresana. Regione Autonoma Friuli Venezia Giulia, Università di Udine, Università di Trieste*; convenzione n. 8504 del 25 febbraio 2005*.

Cucchi, R., Pugliese, N., Covelli, S., Fanzutti, G., Fanucci, F., Fontana, A., Marocco, R. (2008a). Carta geologica di sintesi GEO-CGT alla scala 1:10.000, foglio 110-Trieste. Regione Autonoma

Friuli Venezia Giulia, Università di Udine, Università di Trieste; *convenzione n. 8504 del 25 febbraio 2005*.

De Waele, J., & Furlani, S. (2012). Seawater and biokarst effects on coastal limestones. In J. Shroder, & A. Frumkin (Eds.), *Treatise on Geomorphology* (Vol. 9). San Diego, CA: Academic Press.

De Waele, J., Mucedda, M., & Montanaro, L. (2009). Morphology and origin of coastal karst landforms in Miocene and Quaternary carbonate rocks along the central-western coast of Sardinia (Italy). *Geomorphology, 106*(1-2), 26-34.

Degrassi, V., Furlani, S., Scotti, F., Melis, R., Antonioli, F., & Fonda, G. (2008). Strutture portuali di Via dei Cavazzeni (Trieste): indicazioni sul livello del mare. Terre di mare. L'archeologia dei paesaggi costieri e le variazioni climatiche. In R. Auriemma, & S. Karinja (Eds.), *Atti del Convegno Interreg Internazionale di Studi, Trieste, 8-10 novembre 2007* (pp. 275-281). Udine.

Del Ben, A., Finetti, I., Rebez, A., & Slejko, D. (1991). Seismicity and seismotectonics at the Alps-Dinarides contact. *Bollettino di Geofisica Teorica e Applicata, 32*, 155-176.

Della Vedova, B., Bellani, S., Pellis, G., & Squarci, P. (2001). Deep temperatures and surface heat flow density distribution. In G. Vai, & P. Martini (Eds.), *Anatomy of an orogen: the Appennines and adjacent Mediterranean Basins* (pp. 65-76). Dordrecht, Netherlands: Kluwer academic Publishers.

Della Vedova, B., Castelli, E., Cimolino, A., Vecellio, C., Nicolich, R., & Barison, E. (2008). La valutazione e lo sfruttamento delle acque geotermiche per il riscaldamento degli edifici pubblici . *Rassegna Tecnica del Friuli Venezia Giulia, 6*, 16 - 19.

Della Vedova, B., Cimolino, A., Castelli, E., & Brancatelli, G. (2014). Geothermal Heating and Cooling in the FVG Region: the Grado District Heating and the Pontebba Ice Rink Plants. Status and future in the Peri – Adriatic Area - Veli Lošinj (Croatia): Proceedings of the Workshop on Geothermal Energy.

Dobrin, M. & Savit, C., 1988. Introduction to geophysical prospecting. McGraw-Hill Book Co., Volume 4 th ed., 867 pp.

Dobroka, M., Dresen, L., Gelbke, C. & Ruter H, (1992) Tomographic inversion of normalized data: double trace tomography algorithms, Geophysical Prospecting, 40, 114.

Doglioni, C., & Carminati, E. (2008). Structural styles and Dolomites field trip. *Mem. Descr. Carta Geol. It., 82*, 299.

Douglas, B. (2001). An introduction to sea level change in the era of the recording tide gauge. In B. Douglas, M. Kearney, & S. Leatherman (Eds.), *Sea Level Rise* (pp. 1-233). San Diego: Academic Press.

Embry, A., & Johannessen, E. (1992). T–R sequence stratigraphy, facies analysis and reservoir distribution in the uppermost Triassic- Lower Jurassic succession, western Sverdrup Basin,

Arctic Canada. In T. Vorren, E. Bergsager, O. Dahl-Stamnes, E. Holter, B. Johansen, E. Lie, & T. Lund (Eds.), *Arctic Geology and Petroleum Potential* (pp. 121–146). Norwegian Petroleum Society (NPF), 2 Special Publ.

ESRI. (2017). ArcGIS Desktop 10.5.

EU-DEM. (2017). *Copernicus Land Monitoring Service*. Website: https://www.eea.europa.eu/data-and-maps/data/copernicus-land-monitoring-service-eu-dem

Fantoni, R., Catellani, D., Merlini, S., Rogledi, S., & Venturini, S. (2002). La registrazione degli eventi deformativi cenozoici nell'avampaese Veneto-Friulano. *Mem. Soc. Geol. It. , 57*, 301–313.

Fantoni, R., Della Vedova, B., Giustiniani, M., Nicolich, R., Barbieri, C., Del Ben, A., Castellarin, A. (2003). Deep seismic profiles through the Venetian and Adriatic foreland (Northern Italy). *Mem. Sc. Geologiche, 54*, 131-134.

Ferranti, L., Antonioli, F., Mauz, B., Amorosi, A., Dai Pra, G., Mastronuzzi, G., Verrubbi, B. (2006). Markers of the last interglacial sea level highstand along the coast of Italy: tectonic implications. *Quaternary International, 145-146*, 30–54.

Finetti, I. (1965). Ricerche sismiche marine nel Golfo di Trieste (profilo a rifrazione). *Boll. Geof. Teor. Appl., 7*(27), 201-217.

Finetti, I. (1967). Ricerche sismiche a rifrazione sui rapporti strutturali fra il Carso e il Golfo di Trieste. *Boll. Geof. Teor. Appl., 9*, 214-225.

Finetti, I., & Del Ben, A. (2005). Crustal tectono-stratigraphic setting of the Adriatic Sea from new CROP seismic data. In I. Finetti, & I. Finetti (Ed.), *CROP Project: Deep Seismic Exploration of the Central Mediterranean and Italy* (pp. 519-547). Elsevier.

Fitzko, F., Suhadolc, P., Aoudia, A., & Panza, G. (2005). Constraints on the location and mechanism of the 1511 Western-Slovenia earthquake from active tectonics and modeling of macroseismic data. *Tectonophysics, 404*, 77-90.

Fontana, A., Mozzi, P., & Bondesan, A. (2008). Alluvial megafans in the Venetian-Friulian Plain(North-eastern Italy): evidence of aggrading and erosive phases during Late Pleistocene and Holocene. *Quaternary International, 189*, 71–90.

Frank, G., Križ, J., & Vlašić, B. (1983). Results and directions in hydrocarbon exploration of the Adriatic offshore. *Nafta, 34*(7-8), 387-396.

Fulani, S., Cucchi, F., Biolchi, S., & Odorico, R. (2011c). Notches in the Northern Adriatic Sea: Genesis and development. *Quaternary International, 232*, 158e168.

Furlani, S. (2003a). Shore Platforms along the North-Western Istria Coast: an overview. *Annales Ser. Hist. Nat., 13*(2), 247-256.

Furlani, S. (2003b). Morphologic Features of shore platform between Punta Sottile (Italia) and Punta Grossa (Debelj Rti-Slovenija) and its sustainable development. Puglia: Final Conference IGCP Project N. 437.

Furlani, S., Biolchi, S., Cucchi, F., Antonioli, F., Busetti, M., & Melis, R. (2011a). Tectonic effects on Late Holocene sea level changes in the Gulf of Trieste (NE Adriatic Sea, Italy). *Quaternary International, 232*, 144-157.

Furlani, S., Biolchi, S., Cucchi, F., Bensi, S., & Burelli, G. (2009a). Surveying of a submerged Flysch outcrop at Sistiana-Duino (Gulf of Trieste, Italy). *Atti e Memorie della Commissione Grotte "E. Boegan", 42*, 85-94.

Furlani, S., Biolchi, S., Cucchi, F., Bensi, S., & Burelli, G. (2009a). SURVEYING OF A SUBMERGED FLYSCH OUTCROP AT SISTIANA-DUINO (GULF OF TRIESTE, ITALY). *Atti e Memorie della Commissione Grotte "E. Boegan", 42*, 85-94.

Furlani, S., Chersicla, D., Bressan, G., Biolchi, S., & Cucchi, F. (2011d). Shore Grykes along the Western Istrian Coast. *Acta Carsologica, 40*(1), 29-42.

Furlani, S., Cucchi, F., & Biolchi, S. (2011b). Morfologie carsiche costiere intertidali lungo le coste del Golfo di Trieste. *Atti e Memorie della Commissione Grotte "E. Boegan", 43*, 151-168.

Furlani, S., Cucchi, F., & Biolchi, S. (2011b). MORFOLOGIE CARSICHE COSTIERE INTERTIDALI LUNGO LE COSTE DEL GOLFO DI TRIESTE. *Atti e Memorie della Commissione Grotte "E. Boegan", 43*, 151-168.

Furlani, S., Cucchi, F., Forti, F., & Rossi, A. (2009b). Comparison between coastal and inland Karst limestone lowering rates in the northeastern Adriatic Region (Italy and Croatia). *Geomorphology, 104*, 73-81.

Furlani, S., Pappalardo, M., Gomez-Pujol, L., & Chelli, A. (2014). The rock coast of theMediterranean and Black Seas. In D. Kennedy, W. Stephenson, N. L.A., D. Kennedy, W. Stephenson, & L. Naylor (Eds.), *Rock coast geomorphology: A global synthesis* (Vol. 40, pp. 89-123). Memoirs Geologica Society of London.

Galadini, F., Poli, M., & Zanferrari, A. (2005). Seismogenic sources potentially responsible for earthquakes with M ≥ 6 in the eastern Southern Alps (Thiene-Udine sector, NE Italy). *Geophys. J. Int., 161*, 739-762.

Generalic, E. (2011). *Climate change: do follow us global warming, cooling or pollution?* From https://www.periodni.com/climate_change.html

GeoCGT-FVG. (2013). *Carta geologica del Carso Classico (tratta dalla Carta di sintesi geologica alla scala 1:10.000 – Progetto GEO-CGT) e Brevi Note Illustrative della Carta Geologica del Carso Classico Italiano.* Trieste: Direzione centrale ambiente energia e politiche per la montagna, Servizio Geologico, Regione Autonoma Friuli Venezia Giulia.

GeositiFVG. (2010a). *Banchi sommersi della Mula di Muggia - Trezza Grande - Trezza Piccola.* From http://www.geositi.units.it/vedigeo1.php?ID_GEO=154

GeositiFVG. (2010b). *Grebani del Golfo di Trieste*. From http://www.geositi.units.it/vedigeo1.php?ID_GEO=163

GeoZS, (2017) - Bavec, M., Novak, M.; Poljak, M.; Trajanova, M., & Skaberne, D. Harmonized geological map of Slovenia, scale 1:1.000.000. OneGeology-Europe project. Web site: http://peridot.geo-zs.si/GeoZS_Superficial_Geology/ows?

Giorgetti, F., Mosetti, F., & Macchi, G. (1968). Caratteristiche Morfologiche, Fisiche e Chimiche del Fondo Marino del Golfo di Trieste nell'area compresa entro la congiungente Pinta Grossa-Bocche di Primero. *Boll. Soc. Adriatica di Scienze, LVI*(1), 3-21.

Google. (2017). Google Earth Pro. Google Inc.

Gordini, E., Caressa, S., & Marocco, R. (2003). Nuova carta morfo-sedimentologica del Golfo di Trieste (da Punta Tagliamento alla foce dell'Isonzo). *Gortania, 25*, 5-29.

Gordini, E., Ciriaco, S., Borme, D., Cibic, T., Falace, A., Faresi, L., S., K. (2010). *Trezze o "Grebeni": biotopi e geotopi dell'Alto Adriatico.* Trieste: OGS.

Gordini, E., Marocco, R., & Vio, E. (2002). Stratigrafia del sottosuolo della "Trezza Grande" (Golfo di Trieste, Adriatico Settentrionale). *Gortania, 24*, 31-63.

Gordini, E., Marocco, R., Tunis, G., & Ramella, R. (2004). I depositi cementati del Golfo diTrieste (Adriatico Settentrionale): Distribuzione areale, caratteri geomorfologici e indagini acustiche ad alta risoluzione. *Il Quaternario - Italian Journal of Quaternary Sciences, 17*(2), 555-563.

Gortani, M. (1959). Carta della glaciazione würmiana in Friuli. *Rend. Atti Acc. Sc. Ist. Bologna, 6*, 1-11.

Gosar, A. (2007). Monitoring of micro-deformations along Idrija and Raša faults in W Slovenia. *Geologija , 50*(1), 45-54.

Gušić, I., & Jelaska, V. (1993). Upper Cenomanian-Lower Turonian sea-level rise and its consequences on the Adriatic-Dinaric carbonate platform. *Geol. Rundsch., 82*(4), 676-686.

Hallam, A., & Cohen, J. (1989). The Case for Sea-Level Change as a Dominant Causal Factor in Mass Extinction of Marine Invertebrates. *Philosophical Transactions of the Royal Society of London. Biological Sciences, Series B*(325), 437-455.

Haq, B. U., & Schutter, S. (2008). A Chronology of Paleozoic Sea-Level Changes. *Science, 322*, 64-68.

Holland, S. (2016). *UGS Stratigraphy Lab, the data in the strata.* From https://strata.uga.edu/sequence/types.html

IHS. (2014). Kingdom Suite (v. 8.8) - Software for seismic interpretation.

IRDAT-FVG. (2017). *Infrastruttura Regionale di Dati Ambientali e Territoriali per il Friuli Venezia Giulia*. Tratto da http://www.regione.fvg.it/rafvg/cms/RAFVG/ambiente-territorio/conoscere-ambiente-territorio/FOGLIA7/

Jurkovšek, B. (2008). Geološka karta severnega dela Tržaško-Komenske planote 1:25.000 = Geological Map of the of Trieste-Komen Plateau 1:25.000. *Geološki zavod Slovenije*.

Jurkovšek, B. (2010). Geološka karta severnega dela Tržaško-Komenske planote 1:25.000 = Geological Map of the of Trieste-Komen Plateau 1:25.000, explanatory book. *Geološki zavod Slovenije*, 72.

Jurkovšek, B., Biolchi, S., Furlani, S., Kolar-Jurkovšek, T., Zini, L., Jež, J., Cucchi, F. (2016). Geology of the Classical Karst Region (SW Slovenia–NE Italy). *Journal of Maps*, 1–12.

Jurkovšek, B., Toman, M., Ogorelec, B., Šribar, L., Drobne, K., Poljak, M., & Šribar, L. (1996). Formacijska Geološka karta Južnega dela Tržaško-Komenske planote 1:50.000 = Geological Map of the southern part of Trieste-Komen Plateau 1:50.000. *Institut za geologijo, geotehniko in geofiziko*, 144 pp., 1 map.

Kearey, P. M., Brooks, I. & Hill, I., 2002. An Introduction to Geophysical Exploration. Blackwell Science, Oxford, Issue 3th edition, p. 262.

Kastelic, V., Vannoli, P., Burrato, P., Fracassi, U., & Tiberti, M. (2012). Seismogenic sources in the Adriatic Domain. *Marine and Petroleum Geology, 42*, 191-213.

Kastelic, V., Vrabec, M., Cunningam, D., & Gosar, A. (2008). Neoalpine structural evolution and present day tectonic activity of the eastern Southern Alps: the case of the Ravne fault, NW Slovenia. *J. Structural Geol., 30*, 963-965.

Kopp, R. E., Simons, F., Mitrovica, J., Maloof, A., & Oppenheimer, M. (2013). A probabilistic assessment of sea level variations within the last interglacial stage. *Geophys. J. Int., 193*, 711-716.

Lambeck, K., Antonioli, F., Anzidei, M., Ferranti, L., Leoni, G., Scicchitano, G., & Silenzi, S. (2011). Sea level change along the Italian coast during the Holocene and projections for the future. *Quaternary International, 232*, 250-257.

Lee, J., & Cleveland, J. (2017). *Milancovitch, Biography.* From https://editors.eol.org/eoearth/wiki/Milankovitch,_Milutin_(Climate_Change)

Marocco, R. (1989a). Evoluzione Quaternaria della Laguna di Marano (Friuli-Venezia Giulia). *Il Quaternario, 2*(2), 125-137.

Marocco, R. (1989b). Considerazioni sedimentologiche sui sondaggi S19 e S20 (Delta del Fiume Tagliamento). *Gortania - Atti Museo Friul. Storia Nat., 10*(88), 101-120.

Marocco, R. (1991). Evoluzione Tardo Pleistocenica-Olocenica del Delta del Fiume Tagliamento e delle Lagune di Marano e Grado (Golfo di Trieste). *Il Quaternario, 4*(1b), 223-232.

Marocco, R., & Melis, R. (2009). Stratigrafia e paleogeografia del "Lacus Timavi" (Friuli Venezia Giulia). *Il Quaternario, 22*(2), 157-170.

Marocco, R., Covelli, S., Fanucci, F., Fontana, A., & Tunis, G. (2008). Carta geologica di sintesi GEO-CGT alla scala 1:10.000, foglio 109-Grado. Regione Autonoma Friuli Venezia Giulia, Università di Udine, Università di Trieste*; convenzione n. 8504 del 25 febbraio 2005*.

Marocco, R., Pugliese, N., & Stolfa, D. (1984). Some Remarks on the origin and Evolution of the Grado Lagoon (Northern Adriatic Sea). *Boll. Oceanologia Teorica e Applicata, II*(1), 11-17.

Márton, E., Ćosović, V., Moro, A., & Zvocak, S. (2008). The motion of Adria during the Late Jurassic and Cretaceous: new paleomagnetic results from stable Istria. *Tectonophysics, 454*, 44-53.

Masoli, C., Petronio, L., Gordini, E., Deponte, M., Cotterle, D., Romeo, R., Meneghini, F. (2015). Marine geophysical and geological investigations in support to the construction of new harbour infrastructures: the Trieste Marine Terminal extension. *Proceedings of the 34th GNGTS 2015, Trieste 17-19 Novenber 2015, 3-Applyed Geophysics*, 63-70.

Merlini, S., Doglioni, C., Fantoni, R., & Ponton, M. (2002). Analisi strutturale lungo un profilo geologico tra la linea Fella-Sava e l'avampaese adriatico (Friuli Venezia Giulia – Italia). *Memorie Società Geologica Italiana, 57*, 293-300.

Michelini, A., Živčič, M., & Suhadolc, P. (1998). Simultaneous inversion for velocity structure and hypocenters in Slovenia. *Journal of Seismology, 2*, 257–265.

Milankovitch, M. (1941). *Canon of Insolation and the Ice-Age Problem (Kanon der Erdbestrahlungen und seine Anwendung auf das).* Jerusalem (1969): Israel Program for Scientific Translations.

Mitchum, R. j., & Vail, P. (1977). Seismic stratigraphy and global changes of sea level; Part 7, Seismic stratigraphic interpretation procedure. *AAPG Memoir, 135-143*, 26.

Morelli, C., & Mosetti, F. (1955). Rilievo Gravimetrico e sismico sperimentale nel Golfo di Trieste. *Metano, IX*, 9.

Morelli, C., & Mosetti, F. (1968). Rilievo sismico nel Golfo di Trieste. Andamento della formazione arenacea (Flysch) sotto il fondo marino nella zona tra Trieste, Monfalcone e Grado. *Boll. Soc. Adriat. Scienze, LVI*(1), 42-57.

Mosetti, F. (1966). Morfologia dell'Adriatico Settentrionale. *Boll. Geofis. Teor. Appl., 8*, 138-150.

Mosetti, F., & Morelli, C. (1968). Rilievo sismico continuo nel Golfo di Trieste. *Boll. Soc. Adriat. Scienze, LVI*(1), 42-57.

NASA. (2017). *Ocean Surface Topography from Space.* From https://sealevel.jpl.nasa.gov/missions/

Nicolich, R., & Dal Piaz, R. (1990). Moho Isobaths. *CNR PF geodinamica, structural model of Italy, SELCA, Firenze*.

Nicolich, R., Della Vedova, B., Barison, E., Vecellio, C., Rizzetto, D., Masetti, D., Marocco, R. (2008). *Le acque calde della Pianura Friulana. Realizzazione della Carta Geologico-Tecnica della Risorsa Geotermica Regionale e definizione delle Linee Guida per il suo Utilizzo.* Serv. Geol.

Nicolich, R., Della Vedova, B., Giustiniani, M., & Fantoni, R. (2004a). *Carta del Sottosuolo della Pianura Friulana.* Regione Autonoma Friuli Venezia Giulia e Università degli Studi di Trieste.

Nicolich, R., Della Vedova, B., Giustiniani, M., & Fantoni, R. (2004b). Note Illustrative della Carta del Sottosuolo della Pianura Friulana. *Regione Autonoma Friuli Venezia Giulia e Università di Trieste*, 32.

Odorico, R. (2010). *Olistoloti di Miramare.* From Geositi del Friuli Venezia Giulia: http://www.geositi.units.it/vedigeo_foto.php?ID_GEO=487

OGS. (2014). CAT3D software (v6.0). Computer Aided Tomography for 3D models, User manual.

OGS. (2017). *Bollettino della Rete Sismometrica del Friuli Venezia Giulia*. From http://www.crs.inogs.it/bollettino/RSFVG/

Pamič, J., Gušić, I., & Jelaska, V. (1998). Geodynamic evolution of the Central Dinarides. *Tectonophysics*, 251-268.

Paradigm. (2016). Geodepth v.15.

Pavlides, S. (1989). Looking for a definition of neotectonics. *Terra Nova, 1*, 233-235.

Pavšič, J., & Peckmann, J. (1996). Stratigraphy and Sedimentology of the Piran Flysch Area (Slovenia). *Annales, Ser. hist. nat., 6*(1), 123-138.

Peruzza, L., Poli, M., Rebez, A., Renner, G., Rogledi, S., Slejko, D., & Zanferrari, A. (2002a). The 1976-1977 seismic sequence in Friuli: new seismotectonic aspects. *Mem. Soc. Geol. It., 57*, 391-400.

Peruzza, L., Renner, G., & Slejko, D. (2002b). Stress field along the eastern Adriatic coast from earthquake fault plane solutions. *Mem. Soc. Geol. It., 57*, 409-418.

Picotti, S., Carcione, J. M., Santos, J. E., & Gei, D. (2010) Q-anisotropy in finely-layered media. *Geophysical Research Letters*, 37(6), L06302.

Picotti, S., Carcione, J. M., Santos, J. E. (2012) Oscillatory numerical experiments in finely layered anisotropic viscoelastic media. *Computers & Geosciences* 43, 83-89. doi:10.1016/j.cageo.2012.02.026

Piffer, G., Rinaldi, M., & della Vedova, B. (2015). Well Logging for the Geothermal Reservoir Characterisation: the Grado Geothermal Project (Gorizia, Italy) - Part 2. *Geo Alp Kongress - Geologie und Hydrogeologie der Alpen - Geologia e Idrogeologia delle Alpi, 5-7 novembre 2015*, 2.

Placer, L. (2008). Principles of the tectonic subdivision of Slovenia. *Geologija, 51*(2), 205–217.

Placer, L. (2015). Simplified structural map of Kras; Kras (Slovene), Carso (Italian) = Geographical unit. *Geologija, 58*(1), 89-93.

Placer, L., Košir, A., Popit, T., Šmuc, A., & Juvan, G. (2004). The Buzet Thrust Fault in Istria and overturned carbonate megabeds in the Eocene flysch of the Dragonja Valley (Slovenia). *Geologjia, 47*(2), 193-198.

Placer, L., Vrabec, M., & Celarc, B. (2010). The bases for understanding of the NW Dinarides and Istria Peninsula tectonics. *Geologija, 53*(1), 55–86.

Plint, A., & Nummedal, D. (2000). The falling stage systems tract: recognition and importance in sequence stratigraphic analysis. In D. Hunt, & R. Gawthorpe (Eds.), *Sedimentary Response to forced regression* (pp. 1-17). Geol. Soc. London Speci. Publ, 172.

Poli, E., & Zanferrari, A. (2008). Inquadramento geologico e lineamenti strutturali. *Note illustrative della carta geologica d'Italia, scala 1:50.000, Foglio 66, Udine*, 23-34.

Poli, M. (1996). Analisi strutturale del Monte di Medea (Friuli): tettonica polifasica nell'avampaese sudalpino orientale. *Atti Ticinensi di Scienze della Terra, 4*(special series), 103-113.

Poli, M., Monegato, G., Zanferrari, A., Falcucci, E., Marchesini, A., Grimaz, S., Del Pin, E. (2015). *D6/a2.1 - Seismotectonic characterization of the western Carnic pre-alpine area between Caneva and Meduno (NE Italy, Friuli).* Base-knowledge improvement for assessing the seismogenic potential of Italy. DPC-INGV-S1 Project.

Poli, M., Zanferrari, A., & Monegato, G. (2009). Geometria, cinematica e attività pliocenico-quaternaria del sistema di sovrascorrimenti Arba-Ragogna (Alpi Meridionali orientali, Italia NE). *Rendiconti Società Geologica Italiana, 5*, 172-175.

Poljak, M., Gosar, A., & Živčič, M. (2010). Active tectonics in Slovenia. *Geology of Adriatic Area, Geo Acta Special Pubblication, 3*, 15-24.

Poljak, M., Živčič, M., & Zupačič, P. (2000). The seismotectonic characteristics of Slovenia. *Pure and Applied Geophysics, 157*, 37-55.

Ponton, M. (2010). Architettura delle alpi Friulane. *Museo Friulano di Storia Naturale, Udine, 52*, 79.

Posamentier, H., & Allen, G. (1999). *Siliciclastic Sequence Stratigraphy: concepts and applications* (7 ed.). SEPM Concepts in Sedimentology and Paleontology .

Posamentier, H., & Vail, P. R. (1988b). Eustatic controls on clastic deposition II-sequence and systems tract models. In C. Wilgus, B. Hastings, C. Kendall, H. Posamentier, C. Ross, & J. Van Wagoner (Eds.). SEPM Special Publication.

Posamentier, H., Jervey, M., & Vail, P. (1988a). Eustatic controls on clastic deposition. I. Conceptual framework. In C. Wilgus, B. Hastings, C. Kendall, H. Posamentier, C. Ross, & J. Van Wagoner (Eds.), *Sea Level Changes-An Integrated Approach* (Vol. 42, pp. 110– 124). SEPM Special Publication, 42.

Ramella, R., Barison, E., Busetti, M., Cova, A., Caressa, S., Cotterle, D., Zgur, F. (2005). Realizzazione della carta geologico-tecnica della risorsa geotermica regionale. *Risorsa Geotermica RA-FVG 8493, dd. 24.11.2004, REL. 80/2005 - RIMA-9*(80), 47 pp., 39 figs, 17 tabs.

Ravnik, D. (1991). Geothermal investigation in Slovenia. *Geologija, 34*, 265-303.

Rebez, A., Slejko, D., & Suhadolc, P. (1987). Seismic behaivour at the Alps-Dinaric contact. *Mem. Soc. Geol, It., 40*, 321-326.

Ribarič, V. (1982). Seismicity of Slovenia Catalogue of Earthquakes (792 AD- 1981). *Seismological Survey of the Republic of Slovenia, A*(1-1), 650.

Romeo, R. (2009). *Studio geofisico integrato ad alta risoluzionedei depositi marini e della struttura del substrato della riviera di miramare (Gorfo di Trieste)* (Doctoral Thesis, XX cycle ed.). Trieste: University of Trieste.

Romeo, R., Zgur, F., Baradello, L., Petronio, L., & Deponte, M. (2012). Valutazione tecnica di una sorgente sismica ad alta risoluzione S-Boomer nel Golfo di Trieste. *REL. OGS 2012/61 RIMA 10 GEA dd. 13 luglio 2012*(61), 21 pp., 20 figs., 6 tabs., 1 attms.

Rovida, A., Locati, M., Camassi, R., Loolli, B., & Gasperini, P. (2016). CPTI15, the 2015 version of the Parametric Catalogue of Italian Earthquakes. *Istituto Nazionale di Geofisica e Vulcanologia, doi:http://doi.org/10.6092/INGV.IT-CPTI15* .

Scrocca, D., Doglioni, C., Innocenti, F., Manetti, P., Mazzotti, A., Bertelli, L., D'Offizi, S. (2003). Atlante CROP – Profili Sismici a rifelssione della crosta italiana. *Memorie descrittive della Carta Geologica d'Italia, 62*, 194.

SEPM. (2017). *SEPM Strata, Sequence Stratigraphy*. Tratto da http://www.sepmstrata.org/Terminology.aspx?id=size%20of%20sea%20level%20excursions

Schoenberg, M. & Muir F. (1989) A calculus for finely layered media. *Geophysics*, 54, 581–589.

Schön, J. H. (1996) Physical properties of rocks: fundamentals and principles of petrophysics. *Handbook of Geophysical Exploration*, vol. 18, Pergamon.

Sheriff, R. & Geldart, L., 1995. Exploration seismology. Cambridge Uniersity Press, 592 pp.

Silenzi, S., Devoti, S., Gabellini, M., Magaletti, E., Nisi, M., Pisapia, M., Zarattini, A. (2004). Le variazioni del clima nel Quaternario. *Geo-Archeologia, 1*, 15-50.

Slavec, P. (2014). *Analiza morfologije morskega dna slovenskega morja.* Koper: Harpha sea, d.o.o..

Sleep, N. & Fujita, K., 1997. *Principles of geophysics.* Blackwell Science, 586 pp.

Slejko, D., Carulli, G., Nicolich, R., Rebez, A., Zanferrari, A., Cavallin, A., Zanolla, C. (1989). Seismotectonics of the eastern Southern-Alps: a review. *Boll. Geof. Teor. Appl., 31*, 109-136.

Stache. (1889). *Geologiche übersichts Karte der Küstenländer von Osterreich Ungran 1:1.008.000.*

Stewart, R.R. (1991). Exploration seismic tomography: Fundamentals. Society of Exploration Geophysicists, Tulsa (USA), 196.

Suess, E. (1906). *The Face of the Earth.* (W. J. Sollas, Trans.) Oxford: Clarendon.

Sunamura, T. (1992). *Geomorphology of Rocky Coasts* (302 ed.). Chichester: Wiley.

Tari, K. (2002). Evolution of the northern and western Dinarides: a tectonostratigraphic approach. EGU Special Pubblication Series, 1, 223-236.

Telford, W., Geldart, L. & Sheriff, L., 1990. Applied Geophysics. Cambridge University Press, 771 pp.

Tentor, A., Tunis, G., & Venturini, S. (1994). Schema stratigrafico e tettonico del Carso Isontino. *Natura Nascosta, 9*, 1-32.

Thomsen, L. (1986). Weak elastic anisotropy. *Geophysics* 51, 1954-1966.

Tišljar, J., Vlahović, I., & Velić I., S. B. (2002). Carbonate Platform Megafacies of the Jurassic and Cretaceous Deposits of the Karst Dinarides. *Geologia Croatica, 55*(2), 139-170.

Tišljar, J., Vlahovic, I., Velić, I., Matičec, D., & Robson, J. (1998). Carbonate facies evolution from the late albian to Middle Cenomanian in Southern Istria (Croatia): influence of synsedimentary tectonics and extensive organic carbonate production. *Facies, 38*, 137-151.

Trenhaile, A. (1987). *The Geomorphology of Rock Coasts.* Oxford: Claredon Press.

Trenhaile, A. (2001). Modeling the quaternary evolution of shore platforms and erosional continental shelves. *Earth Surf. Process. Landf., 26*, 1103-1128.

Triches, A., Pillon, S., Bezzi, A., Lipizer, M., & Gordini, E. (2011a). *Carta batimetrica della Laguna di Marano e Grado. Note illustrative.* Udine: Autorità di bacino regionale del Friuli Venezia Giulia - Arti Grafiche Friulane / Imoco spa (Ud).

Triches, A., Pillon, S., Bezzi, A., Lipizer, M., & Gordini, E. (2011a). *Carta batimetrica della Laguna di Marano e Grado. Note illustrative.* Autorità di bacino regionale del Friuli Venezia Giulia, Commissario Delegato per l'emergenza socio-economico ambientale determinatasi nella Laguna di Marano Lagunare e Grado, Dipartimento di Geoscienze dell'Università di Trieste, Istituto Nazionale di Oceanografia e di Geofisica Sperimentale - OGS, Arti Grafiche Friulane / Imoco spa (Udine).

Triches, A., Pillon, S., Bezzi, A., Lipizer, M., & Gordini, E. (2011b). *Carta batimetrica della Laguna di Marano e Grado - Regione Autonoma Friuli Venezia Giulia.* Autorità di bacino regionale del Friuli Venezia Giulia, Commissario Delegato per l'emergenza socio-economico ambientale determinatasi nella Laguna di Marano Lagunare e Grado, Dipartimento di Geoscienze dell'Università di Trieste, Istituto Nazionale di Oceanografia e di Geofisica Sperimentale - OGS, Arti Grafiche Friulane / Imoco spa (Udine).

Trincardi, F., Argnani, A., Correggiari, A., Foglini, F., Rovere, M., Angeletti, L., Taviani, M. (2011a). *Carta Geologica dei mari italiani alla scala 1:250.000 foglio NL 33-7 Venezia.* Firenze: Istituto di Scienze Marine, Consiglio Nazionale delle Ricerche, ISPRA.

Trincardi, F., Argnani, A., Correggiari, A., Foglini, F., Rovere, M., Angeletti, L., Taviani, M. (2011b). *Note illustrative della Carta Geologica dei mari italiani alla scala 1:250.000 foglio NL 33-7 Venezia.* Firenze: Istituto di Scienze Marine, Consiglio Nazionale delle Ricerche, ISPRA, 151 pp.

Trobec, A., Busetti, M., Zgur, F., Baradello, L., Babich, A., Cova, A., Vrabec, M. (submitted). Thickness of marine Holocene sediment in the Gulf of Trieste (Northern Adriatic Sea). *Earth Science System Data*, 23 pp.

Trobec, A., Šmuc, A., Poglajen, S., & Vrabec, M. (2017). Submerged and buried Pleistocene river channels in the Gulf of Trieste (Northern Adriatic Sea): Geomorphic, stratigraphic and tectonic inferences. *Geomorphology, 286*, 110-120.

Tunis, G., & Venturini, S. (1985). Flysch of Eastern Friuli: a preliminary approach to paleoenvironmental recontruction. *Rudarsko-Metalurski Zbornik (Mining and Metallurgy Quarterly), 32*(1-2), 7.

Tunis, G., & Venturini, S. (1992). Evolution of the Southern Margin of the Julian Basin with Emphasis on the Megabeds and Turbidites Seqence of the Southern Julian Prealps (NE Italy). *Geologia Croatica, 45*, 127 - 150.

Tunis, G., Marocco, R., Poli, M., Ponton, M., & Pugliese, N. (2008). Carta geologica di sintesi GEO-CGT alla scala 1:10.000, foglio 088-Gorizia. Regione Autonoma Friuli Venezia Giulia, Università di Udine, Università di Trieste*; convenzione n. 8504 del 25 febbraio 2005*.

Vai, G., Venturini, C., Carulli, G., & Zanferrari, A. (2002). *Alpi e Prealpi Carniche e Giulie (Friuli Venzia Giulia)* (9 - Itinerari ed.). Roma: Società Geologica Italiana.

Vail, P. (1977). Seismic stratigraphy and global changes of sea level. In C. Payton (Ed.), Seismic stratigraphy – Application to Hydrocarbon Exploration (Vol. 26, pp. 49-212.). A.A.P.G. Memoir, 26.

Van der Sluis, A. & Van der Vorst, H.A. (1987). Numerical solutions of large, sparse linear algebraic systems arising from tomographic problems, in: Nolet, G., (Ed), Seismic Tomography, D. Reidel Publishing Co., Dordrecht, Holland. 49-83.

Van Wagoner, J., Posamentier, H., Mitchum, R., Vail, P., Sarg, J., Loutit, T., & Hardenbol, J. (1988). An overview of sequence stratigraphy and key definitions. In C. Wilgus, B. Hastings, C. Kendall, H. Posamentier, C. Ross, & J. Van Wagoner (Eds.), *Sea Level Changes-An Integrated Approach* (42 ed., pp. 39–45). SEPM Special Publication, 42.

Velić, I., & Vlahović, I. (1994). Foraminiferal assemblages in the Cenomanian of the Buzet-Savudrija Area (Northwestern Istria, Croatia). *Geologia Croatica, 47*(1), 25-43.

Velić, I., Tišljar, J., Matičec, D., & Vlahović, I. (1995). A review of the Geology of Istria. *Field Trip Guide Book The first Croatian Geol. Cong.*, 21-30.

Venturini, C. (2006). Evoluzione geologica delle Alpi Carniche. Un viaggio attraverso il tempo. *Museo Friulano di Storia Naturale, Udine, 48*, 207.

Vesnaver, A., Böhm, G. (2000). Staggered or adapted grids for seismic tomography?. The Leading Edge 19 (9), 944-950.

Vesnaver A., Böhm G., Madrussani G., Petersen S. and Rossi G.; 1999: Tomographic imaging by reflected and refracted arrivals at the North Sea*. Geophysics, 64,* 1852-1862.

Vesnaver, A., Böhm, G., Madrussani, G., Rossi, G., & Granser, H. (2000). Depth imaging and velocity calibration by 3D adaptive tomography. *First Break*, 303-312.

Vesnaver, A. (1994) Towards the uniqueness of tomographic inversion solutions. Journal of Seismic Exploration 3, 323-334.

Vlahović, I., Tišljar, J., Velić, I., & Matičec, D. (2002). The Karst Dinarides are Composed of Relics of a Single Mesozoic Platform: Facts and Consequences. *Geologia Croatica, 55*(2), 171-183.

Vlahović, I., Tišljar, J., Velić, I., & Matičec, D. (2005). Evolution of the Adriatic Carbonate Platform: Paleogeography main events and depositional dynamics. *Paleogeography, Paleoclimatology, Paleoecolog, 220*, 333-360.

Vrabec, M., & Fodor, L. (2006). Late Cenozoic tectonics of Slovenia: Structural Styles at the Northeastern corner of the Adriatic Microplate. *Springer*, 151–168.

Weber, J., Vrabec, M., Pavlovčič-Prešeren, P., Dixon, T., Jiang, Y., & Stopar, B. (2010). GPS-derived motion of the Adriatic microplate from Istria Peninsula and Po Plain sites, and geodynamic implications. *Tectonophysics, 483*, 214–222.

Wilgus, C., Hastings, B., Kendall, C., Posamentier, H., Ross, C., & Van Wagoner, J. (1988). *Sea Level Changes–An Integrated Approach* (42 ed.). SEPM Special Publication.

Yilmaz, O. (2001). *Seismic Data Analysis: Processing, Inversion and Interpretation of Seismic Data.* Tulsa: Stephen M. Doherty - SEG.

Zampa, L. (2014). *Evidenze di Subsidenza Tettonica nel Sistema di Scarpata e Terrazzi Tardo-Pleistocenici nel Golfo Di Trieste.* University of Trieste: Bachelor Thesis in Geology and Geomorphology.

Zanferrari, A. (1978). Aspetti Geologici dei terremoti del 1976 in Friuli. *Museo St. Nat. Trieste, 10*.

Zanferrari, A., Avigliano, R., Monegato, G., Paiero, G., Poli, M. E., Barbieri, S., Zanolla, S. (2008). Note Illustrative della Carta Geologica d'Italia alla scala 1:50.000, foglio 066 Udine. *Servizio Geologico; ISPRA - Servizio Geologico d'Italia*, 176.

Zanferrari, A., Bollettinari, G., Carobene, L., Carton, A., Carulli, G., Castaldini, D., Sauro, U. (1982). Evoluzione neotettonica dell'Italia nord-orientale. *Mem. Sci. Geol., 35*, 355-376.

Zanferrari, A., Masetti, D., Monegato, G., Poli, M., Avigliano, R., Carraro, F., Stefani, C. (2013). Carta geologica d'Italia alla scala 1:50.000 – Foglio 049 Gemona del Friuli – Note Illustrative. *Regione Friuli Venezia Giulia - Servizio Geologico; ISPRA - Servizio Geologico d'Italia*, 262.

Zecchin, M., Donda, F., & Forlin, E. (2017). Genesis of the Northern Adriatic Sea (Northern Italy) since early Pliocene. *Marine and Petroleum Geology, 79*, 108-130.

Zecchin, M., Gordini, E., & Ramella, R. (2015). Recognition of a drowned delta in the northern Adriatic Sea, Italy: Stratigraphic characteristics and its significance in the frame of the early Holocene sea-level rise. *The Holocene, 25*(6), 1027–1038.

Zelt, C. A. and Smith, R. B. (1992) Seismic traveltime inversion for 2-D crustal velocity structure, *Geophysical Journal International*, 108, 16-34.

Zgur, F., Codiglia, R., Busetti, M., Petronio, L., De Vittor, R., Loreto, M., Romeo, R. (2010). Studio dell'evoluzione geologica e tettonica del Golfo di Trieste (Adriatico Settentrionale). *RELAZIONE OGS 2010/24 RIMA 6 ADEST dd. 18-03-2010*(24), 50 pp., 9 figs., 6 tabs., 6 attms.

Zgur, F., Facchin, L., Busetti, M., Vrabec, M., Slavec, ,. P., Romeo, R., Pelos, C. (2013). Correlation of tectonic structures occurring onland in the Istria Peninsula and in the Gulf of Trieste (Northern Adriatic), and investigation of their neotectonic Activity. *Rel. 2013/64 Sez. IRI 9 ADEST dd. 02/07/2013*(64), 51 pp., 18 figs., 6 tabs., 8 attms.

Žumer, J. (2004). Odkritje podmorskih termalnih izvirov. *Geografski Obzornik, 51*(2), 11-17.